

New Therapies Targeting the PI3K Pathway for the Failing Heart: Characterising the Role and Safety of Cardiac PI3K (p110 α)

Sebastian Bass-Stringer

Bachelor of Science (Degree with Honours)

Thesis submitted in total fulfilment of the requirements for the degree of
Doctor of Philosophy

Department of Physiology, Anatomy and Microbiology

School of Life Sciences

College of Science, Health and Engineering

La Trobe University

Victoria, Australia

October 2021

Table of Contents

Abstract	1
Statement of authorship	2
Acknowledgements	3
Publications arising from this thesis	4
Abstracts arising from this thesis	5
List of abbreviations	6
1. Chapter 1. Introduction	9
1.1. Chapter 1 (preface)	10
1.2. Chapter 1, Part 1: IGF1-PI3K-induced physiological cardiac hypertrophy: Implications for new heart failure therapies, biomarkers, and predicting cardiotoxicity	11
Abstract.....	12
1.2.1. Introduction and background.....	12
1.2.2. Delineating key molecular pathways by understanding differences between the athlete’s heart and the diseased heart.....	13
1.2.3. The IGF1-PI3K signaling pathway: A key mediator of physiological hypertrophy and cardioprotection.....	13
1.2.4. PI3K-based therapies as an approach for improving function of the failing heart—Overview.....	15
1.2.5. Gene therapy as an approach for treating heart failure.....	15
1.2.6. Cardiac pathology and cardiotoxicity in settings of reduced PI3K.....	18
1.2.7. Identifying molecular distinctions in the healthy and diseased heart—New drug targets and biomarkers.....	19
1.2.8. Concluding remarks.....	20
1.2.9. References.....	21
1.3. Chapter 1, Part 2: Adeno-Associated Virus Gene Therapy: Translational Progress and Future Prospects in the Treatment of Heart Failure.....	23
Abstract.....	24
1.3.1. Introduction.....	24
1.3.2. AAV as a Vector for Gene Therapy.....	25
1.3.3. AAV Vector Selection and Design.....	25

1.3.4. Overcoming Challenges Associated with AAV Gene Therapy.....	27
1.3.5. AAV Gene Therapy Studies in Large Animal Models of Heart Failure...	27
1.3.6. Clinical Studies Using AAV for the Treatment of HF.....	36
1.3.7. Future Directions and Challenges.....	36
1.3.8. References.....	37

2. Chapter 2. Advancing knowledge of the PI3K signalling pathway, and its protective role in the heart.....40

2.1. Chapter 2 (preface).....	41
2.2. Chapter 2. PI3K is critical for protection against atrial and ventricular pathology: Implications for the reverse J-shaped relationship between physical activity and cardiac risk	42
Abstract.....	45
Translational perspective.....	46
2.2.1. Introduction.....	47
2.2.2. Methods.....	49
2.2.3. Results.....	49
2.2.3.1. caPI3K Tg mice display cardiac hypertrophy in a dose-dependent manner, and have preserved or enhanced systolic function.....	49
2.2.3.2. Homozygote dnPI3K Tg mice display cardiac dysfunction, arrhythmia and atrial pathology.....	53
2.2.3.3. Distinct histological and molecular profiles in caPI3K Tg and dnPI3K Tg mice.....	56
2.2.3.4. PI3K and exercise can induce hypertrophy and protection independent of Akt.....	58
2.2.3.5. Contribution of inflammatory signalling, GM3, and defective physiological signalling in mediating pathology in a model of extreme endurance swim exercise and dnPI3K Tg(+/+) mice.....	63
2.2.3.6. Evidence of dysregulation of GM3 and PI3K signalling in veteran athletes with AF.....	64
2.2.4. Discussion.....	69
2.2.4.1. No evidence that PI3K activity within physiological levels leads to cardiac dysfunction, pathology or arrhythmia.....	69
2.2.4.2. Reduced PI3K activity contributes to cardiac dysfunction, cardiac fibrosis, arrhythmia and increased susceptibility to atrial thrombi.....	71

2.2.4.3.	Reduced PI3K activity contributes to cardiac dysfunction, cardiac fibrosis, arrhythmia and increased susceptibility to atrial thrombi.....	72
2.2.4.4.	Potential role of defective IGF1R-PI3K signalling contributing to intense exercise-induced cardiac complications, and increased risk with physical inactivity.....	74
2.2.4.5.	Overview of IGF1-PI3K signalling with regular versus intense extreme exercise.....	75
2.2.4.6.	Conclusion.....	78
2.2.5.	References.....	80
2.2.6.	Supplementary data.....	87

3.	Chapter 3. A step-by-step method to detect neutralizing antibodies against AAV using a colorimetric cell-based assay.....	116
3.1.	Chapter 3 (preface)	117
	Abstract.....	120
3.2.	Introduction.....	121
3.3.	Protocol.....	122
3.3.1.	Initial preparation.....	124
3.3.2.	Day 1. Plating cells.....	124
3.3.3.	Day 2. Infecting Cells.....	125
3.3.4.	Day 3. Fixing and adding substrate to cells.....	128
3.3.5.	Quantitation to determine neutralizing activity using ImageJ.....	128
3.3.6.	Determination of Transduction Inhibition (TI ₅₀) titer.....	131
3.3.7.	Determination of neutralized AAV particles.....	131
3.4.	Representative results.....	132
3.5.	Discussion.....	136
3.6.	References.....	139
3.7.	Supplementary data.....	142
4.	Chapter 4. Generation of an AAV encoding a truncated-PI3K with enhanced cardiac expression capabilities for use in the mouse and sheep heart.....	145
4.1.	Chapter 4 (preface).....	146
	Abstract.....	149
4.2.	Introduction.....	150
4.3.	Methods.....	151

4.4. Results.....	159
4.4.1. Successful generation of new PI3K-AAV constructs.....	159
4.4.2. Validation and characterisation of iSH2 AAVs in the healthy mouse heart.....	160
4.4.3. AAV6-cTnT-IVS2-iSH2 did not increase heart size in healthy adult mice.....	163
4.4.4. AAV6-cTnT-IVS2-iSH2 increased the phosphorylation of Akt but did not improve systolic function following ischemia/reperfusion injury.....	164
4.4.5. AAV6-iSH2 transduces the healthy sheep heart and activates PI3K by phosphorylating PIP.....	167
4.5. Discussion.....	170
4.6. References.....	174
4.7. Tables and Supplementary data.....	177
5. Chapter 5, Clusterin is regulated by IGF1–PI3K signaling in the heart: implications for biomarker and drug target discovery, and cardiotoxicity	208
5.1. Chapter 5.1 (preface)	209
Abstract.....	211
5.2. Introduction.....	211
5.3. Materials and methods.....	212
5.4. Results.....	212
5.5. Discussion.....	214
5.6. References.....	215
6. General discussion and concluding remarks.....	216
6.1. Summary of key findings.....	217
6.2. Advancing knowledge of the PI3K signalling pathway, and its protective role in the heart.	218
6.3. Translation of fundamental PI3K cardiac research into therapeutic design and development.....	220
6.4. Detection of drug targets likely to cause cardiotoxicity using cardiac profiling data.....	223
6.5. Concluding remarks and future perspectives.....	224
6.6. References.....	225

Abstract

Heart failure is the final clinical presentation of various cardiovascular diseases. An inverse relationship exists between moderate exercise and likelihood of adverse cardiovascular events. Phosphoinositide 3-kinase (PI3K-p110 α) is a master regulator of exercise-induced heart growth and protection, and increased cardiac PI3K activity provides protection in cardiac stress settings. PI3K-based therapeutics demonstrate promise to treat heart disease, but a thorough understanding of the safety profile of increasing/decreasing PI3K is imperative as there is potential for adverse outcomes in settings of extreme exercise. The first study examined the impact of increasing/decreasing PI3K in the heart using newly generated cardiac-specific transgenic PI3K mice. Reduced PI3K directly contributed to increased cardiac pathology, whilst increased PI3K displayed no cardiac pathology. Having demonstrated the safety of PI3K, novel PI3K-based gene therapies and tools were developed. Adeno-associated virus (AAV) PI3K-based therapies represent a promising approach to treating heart failure, however significant optimisation is necessary for clinical translation. In the second study, a neutralising-antibody assay was developed to screen for neutralising particles against AAV. This assay was validated in serum from sheep before/after AAV administration. In the third study an optimised PI3K-based gene therapy was developed. Optimised PI3K-AAVs transduced the mouse and sheep heart, and this was accompanied by increased PI3K activity. The PI3K-AAV construct was tested in a mouse model of ischemia-reperfusion injury. The final study highlights the potential of mining pre-existing cardiac profiling data sets from PI3K mouse models to assess whether regulating new drug targets is likely to lead to cardiac damage/toxicity. Collectively this thesis has 1) advanced understanding of the role of PI3K in the heart with implications for the safety and therapeutic window of drugs targeting PI3K for cardiac disease and cancer, 2) described the development and optimisation of a PI3K-AAV gene therapy and neutralising-antibody assay with broad applications in the AAV field.

Statement of Authorship

This thesis includes work by the author that has been published, submitted or soon to be submitted for publication as described in the text. Except where reference is made in the text of thesis, this thesis contains no other material published elsewhere or extracted in whole or in part from a thesis accepted for the award of any other degree or diploma. No other person's work has been used without due acknowledgment in the main text of the thesis. This thesis has not been submitted for the award of any degree or diploma in any other tertiary institution.

Signature:

Date: 22/10/2021

Acknowledgements

First and foremost, I would like to extend my deepest appreciation and gratitude to my primary supervisor Professor Julie McMullen. I am extremely thankful for the guidance and support Julie has provided over the past four years. Julie's diligence, passion, work ethic and dedication in what she does is admirable and a genuine inspiration to those around her. Julie has been an excellent role model and has always been understanding and supportive during the numerous hurdles and challenges that have arisen throughout this PhD. I would also like offer an enormous thank you to Dr Kate Weeks who has been a crutch to lean on in the most challenging times, has always checked up on me and gone above and beyond to help those in need. She has been an incredible mentor both on a professional and personal level. A big thank you to my two additional supervisors Associate Professor Colleen Thomas and Dr Bianca Bernardo, you have both been excellent mentors and your support throughout my PhD has been invaluable.

To everyone in the Cardiac Hypertrophy lab, thank you for the fun times, it has been great getting to know everyone and learning so much with you. You have all been so supportive over the last four years and have made this journey so enjoyable. A special thank you to Suzan Yildiz and Dr Yow Keat Tham. Suzan for always being a friend, looking out for me and making me laugh. Yow Keat for assistance with lipidomics, always taking the time to answer my questions and being a great mentor. A big thank you to Helen Kiriazis for performing all of the echocardiography's throughout my thesis, Daniel Donner for performing the I/R surgeries and assisting with analyses and Aascha Brown for analysing the PV loop and echo data from the I/R cohort, you have all been incredibly helpful. I would also like to acknowledge and thank external collaborators, Professor Clive May for helping with sheep studies, Associate Professor Paul Gregorevic for generating the AAV's and Associate Professor Andre La Gerche for providing patient samples.

Big thanks to my family and friends for being so supportive throughout these four years, and a special thanks to my grandfather Professor Ludvik Bass, without your support and encouragement I would not be who I am or where I am today.

Lastly, I would like to acknowledge and thank La Trobe University and the Baker Heart and Diabetes Institute for their financial support. This research was supported by a Joint Baker-La Trobe Postgraduate Scholarship and a Baker Bright Sparks Scholarship top up. This research was also supported by an Australian Government Research Training Program Scholarship.

Publications arising from this thesis

- **Bass-Stringer S**, Bernardo BC, May CN, Thomas CJ, Weeks KL, McMullen JR. Adeno-Associated Virus Gene Therapy: Translational Progress and Future Prospects in the Treatment of Heart Failure. *Heart Lung Circ.* 27(11):1285-1300 (2018).
- **Bass-Stringer S**, Ooi JYY. & McMullen JR. Clusterin is regulated by IGF1–PI3K signaling in the heart: implications for biomarker and drug target discovery, and cardiotoxicity. *Arch Toxicol* 94, 1763–1768 (2020).
- **Bass-Stringer S**, Tai CM, McMullen JR. IGF1–PI3K-induced physiological cardiac hypertrophy: Implications for new heart failure therapies, biomarkers, and predicting cardiotoxicity, *Journal of Sport and Health Science*, In Press (2020): J Sport Health Sci. 2020 Nov 24:S2095-2546(20)30160-5. doi: 10.1016/j.jshs.2020.11.009. Online ahead of print.
- **Bass-Stringer S**, Yildiz GS, Tham YK, Matsumoto A, Kiriazis H, Harmawan CA, Tai CM, Bottrell L, Ezeani M, Donner DG, Ooi JYY, Mellett NA, Luo J, Janssens K, Howden EJ, Hagemeyer CE, Meikle PJ, Lin RCY, Thomas CJ, Weeks KL, La Gerche A, Bernardo BC, McMullen JR. PI3K is critical for protection against atrial and ventricular pathology: Implications for the reverse J-shaped relationship between physical activity and cardiac risk. Currently under review with *Nature Communications*.
- **Bass-Stringer S**, Thomas CJ, May CN, Gregorevic P, Weeks KL, McMullen JR. A step-by-step method to detect neutralizing antibodies against AAV using a colorimetric cell-based assay. Currently under review with *Journal of Visualized Experiments*.
- **Bass-Stringer S**, Thomas CJ, May CN, H Qian, Gregorevic P, Brown A, Kiriazis H, Bernardo BC, Donner DG, Weeks KL, McMullen JR. Generation of an AAV encoding a truncated-PI3K with enhanced cardiac expression capabilities for use in the mouse and sheep heart. To be submitted shortly after PhD submission.*

*Minor delay in submission due to COVID-19 related setbacks.

Abstracts arising from conference presentations

- **Bass-Stringer S**, Yildiz GS, Tham YK, Matsumoto A, Kiriazis H, Harmawan CA, Tai CM, Bottrell, Ezeani M, Donner DG, Ooi JYY, Mellett NA, Luo J, Janssens K, Howden EJ, Hagemeyer CE, Meikle PJ, Lin RCY, Thomas CJ, Weeks KL, La Gerche A, Bernardo BC, McMullen JR. Physical activity and cardiac risk: Role of PI3K(p110 α) and clinical implications. Cardiometabolic Health Symposium, University of Melbourne, 2021 (Virtual mini oral).
- **Bass-Stringer S**, Thomas CJ, May CN, Hongwei Q, Gregorevic P, Brown A, Kiriazis H, Donner DG, Bernardo BC, Weeks KL, McMullen JR. Generation and characterisation of novel PI3K-based gene therapies for the treatment of heart failure. Cardiac Society of Australia and New Zealand (CSANZ) Annual Scientific Meeting. Adelaide, August 2021. International Society for Heart Research (ISHR) Student Investigator Prize Finalist, <https://doi.org/10.1016/j.hlc.2021.06.034> (Virtual oral).
- **Bass-Stringer S**, Yildiz GS, Kiriazis H, Harmawan CA, Bottrell, Thomas CJ, Weeks KL, Bernardo BC, McMullen JR. Investigating the safety of enhanced cardiac phosphoinositide 3-kinase [PI3K(p110 α)] as a prospective therapeutic gene. Rod Andrew Student Mini Oral, Baker Heart and Diabetes Institute, November 2020 (Virtual oral).
- **Bass-Stringer S**, Yildiz GS, Kiriazis H, Harmawan CA, Bottrell, Thomas CJ, Weeks KL, Bernardo BC, McMullen JR. Investigating the safety of enhanced cardiac phosphoinositide 3-kinase [PI3K(p110 α)] as a prospective therapeutic gene. PAM Research Symposium, La Trobe, December 2019. (Oral).
- **Bass-Stringer S**, Yildiz GS, Kiriazis H, Harmawan CA, Bottrell, Thomas CJ, Weeks KL, Bernardo BC, McMullen JR. Investigating the safety of enhanced cardiac phosphoinositide 3-kinase [PI3K(p110 α)] as a prospective therapeutic gene. Cardiac Society of Australia and New Zealand (CSANZ) Annual Scientific Meeting. Adelaide, August 2019. International Society for Heart Research (ISHR) Student Investigator Prize Finalist <https://doi.org/10.1016/j.hlc.2019.06.034> (Oral).

List of Abbreviations

AAV	Adeno-Associated Virus
AB	Antibody
AF	Atrial Fibrillation
Akt	Protein Kinase B
ANOVA	Analysis of Variance
ANP	Atrial Natriuretic Peptide
AW	Atrial Weight
BNP	B-type Natriuretic Peptide
BW	Body Weight
Ca ²⁺	Calcium
caPI3K	Constitutively Active Phosphoinositide 3-Kinase
CASQ1	Calsequestrin 1
CMV	Cytomegalovirus
cTnT	Cardiac Troponin-T
DCM	Dilated Cardiomyopathy
dnPI3K	Dominant Negative Phosphoinositide 3-Kinase
ECG	Electrocardiography
EDPVR	End-diastolic Pressure Volume Relationship
EF	Ejection Fraction
ESPVR	End-systolic Pressure Volume Relationship
FS	Fractional Shortening
GM3	Monosialodihexosylganglioside
HA	Human Influenza Hemagglutinin
HER	Human Epidermal Growth Factor Receptor
HF	Heart Failure
hPLAP	Human Placental Alkaline Phosphatase
HR	Heart Rate
HSP70	Heat Shock Protein 70
HW	Heart Weight

I/R	Ischemia Reperfusion
IgG	Immunoglobulin G
IVRT	Isovolumic Relaxation Time
IVS	Interventricular Septum
IGF1	Insulin-like Growth Factor 1
IGF1R	Insulin-like Growth Factor 1 Receptor
iSH2	Inter-SH2 Domain
ITR	Inverted Terminal Repeat
IVS2	Intervening Sequence 2
kd	Kinase Dead
KO	Knock Out
LPI	Lysophosphatidylinositol
LV	Left Ventricle
LVEDD	Left Ventricular End Diastolic Dimension
LVESD	Left Ventricular End Systolic Dimension
LVPW	Left Ventricular Posterior Wall
LW	Lung Weight
MCAD	Medium Chain Acyl-coenzyme A Dehydrogenase
MCS	Multiple Cloning Site
MI	Myocardial Infarction
miRNA	MicroRNA
MOI	Multiplicity of Infection
MTORC2	Mammalian Target of Rapamycin Complex 2
MV	Mitral Valve
NAb	Neutralising Antibody
NRVM	Neonatal Rat Ventricular Myocyte
Ntg	Non-transgenic
pAkt	Phosphorylated Akt
PBS	Phosphate Buffered Saline
PFA	Paraformaldehyde
PI	Phosphatidylinositol
PI3K	Phosphoinositide 3-Kinase

PIP ₁ /PIP	Phosphatidylinositol Monophosphate
PIP ₂	Phosphatidylinositol 4,5-biphosphate
PIP ₃	Phosphatidylinositol (3,4,5)-triphosphate
qPCR	Quantitative Polymerase Chain Reaction
RPM	Revolutions Per Minute
RT	Room Temperature
SEM	Standard Error of the Mean
SERCA2a	Sarcoplasmic Reticulum Calcium-ATPase isoform 2a
SpA	Synthetic Poly-A Tail
Tg	Transgenic
Tg(+/-)	Transgenic Heterozygote
Tg(+/+)	Transgenic Homozygote
TL	Tibia Length
TLR4	Toll-like Receptor 4
vg	Vector Genomes

Chapter 1

Introduction

Chapter 1. Preface

Chapter 1, the introductory chapter comprises two parts, which provide an in-depth review of the current literature relating to the primary subject matter of this thesis. Namely, the role of Insulin-like Growth Factor 1-Phosphoinositide 3-Kinase (IGF1-PI3K) signalling in the heart and the present landscape of adeno-associated viral (AAV) mediated cardiac gene therapy. This chapter consists of two separate published articles which, taken together, provides a detailed overview of the critical components of all chapters within this thesis.

Part 1, *IGF1-PI3K-induced physiological cardiac hypertrophy: Implications for new heart failure therapies, biomarkers, and predicting cardiotoxicity* focuses on molecular targets underpinning the scope of this thesis, the PI3K signalling pathway. The review initially introduces the relationship between exercise, physiological cardiac hypertrophy and cardioprotection. Molecular mechanisms involved in PI3K signalling are subsequently described and evidence for the critical role of PI3K in regulating exercise-induced cardiac hypertrophy and protection is presented. Next, the review provides an overview of therapeutic strategies that utilise PI3K to target the failing heart and outlines cardiotoxicity and pathological outcomes that can be attributed to reduced cardiac PI3K. Lastly, the review discusses how identifying molecular distinctions between healthy and diseased hearts can be used as an approach for discovering novel drug targets and biomarkers. This review introduces and discusses key themes presented in chapters two, four and five.

Part 2, *Adeno-Associated Virus Gene Therapy: Translational Progress and Future Prospects in the Treatment of Heart Failure* focuses on the translational and therapeutic component of the thesis. The review describes in detail recent advances in the field of AAV gene therapy for the treatment of heart failure. The benefits and limitations of using AAV as gene therapy vectors are summarised, and strategies under development to overcome current limitations are detailed and evaluated. Translational progress of cardiac AAV gene therapies in large animal models and the clinic are comprehensively summarised. This review introduces and discusses key themes presented in chapters three and four.

Chapter 1. Part 1

IGF1–PI3K-induced physiological cardiac hypertrophy: Implications for new heart failure therapies, biomarkers, and predicting cardiotoxicity

Published in ‘Journal of Sport and Health Science’ November 2020 by S Bass-Stringer, CM Tai and JR McMullen.

Journal of Sport and Health Science gives permission to reproduce this work as an academic thesis by the authors.

As first author, S Bass-Stringer contributed ~75% to this publication. This included contributions to the conception, drafting, design, editing and revisions



Review

IGF1–PI3K-induced physiological cardiac hypertrophy: Implications for new heart failure therapies, biomarkers, and predicting cardiotoxicity

Sebastian Bass-Stringer^{a,b}, Celeste M.K. Tai^a, Julie R. McMullen^{a,b,c,d,*}

^a Baker Heart and Diabetes Institute, Melbourne, VIC 3004, Australia

^b Department of Physiology, Anatomy and Microbiology, La Trobe University, Bundoora, VIC 3086, Australia

^c Department of Diabetes, Central Clinical School, Monash University, Melbourne, VIC 3004, Australia

^d Department of Physiology and Department of Medicine Alfred Hospital, Monash University, Melbourne, VIC 3004, Australia

Received 1 July 2020; revised 28 October 2020; accepted 13 November 2020

2095-2546/© 2021 Published by Elsevier B.V. on behalf of Shanghai University of Sport. This is an open access article under the CC BY-NC-ND license (<http://creativecommons.org/licenses/by-nc-nd/4.0/>)

Abstract

Heart failure represents the end point of a variety of cardiovascular diseases. It is a growing health burden and a leading cause of death worldwide. To date, limited treatment options exist for the treatment of heart failure, but exercise has been well-established as one of the few safe and effective interventions, leading to improved outcomes in patients. However, a lack of patient adherence remains a significant barrier in the implementation of exercise-based therapy for the treatment of heart failure. The insulin-like growth factor 1 (IGF1)–phosphoinositide 3-kinase (PI3K) pathway has been recognized as perhaps the most critical pathway for mediating exercised-induced heart growth and protection. Here, we discuss how modulating activity of the IGF1–PI3K pathway may be a valuable approach for the development of therapies that mimic the protective effects of exercise on the heart. We outline some of the promising approaches being investigated that utilize PI3K-based therapy for the treatment of heart failure. We discuss the implications for cardiac pathology and cardiotoxicity that arise in a setting of reduced PI3K activity. Finally, we discuss the use of animal models of cardiac health and disease, and genetic mice with increased or decreased cardiac PI3K activity for the discovery of novel drug targets and biomarkers of cardiovascular disease.

Keywords: Cardiac protection; Cardiotoxicity; Exercise; Heart failure; IGF1; PI3K; Therapies

1. Introduction and background

In this review, we have focused on a signaling cascade in the heart referred to as the insulin-like growth factor 1 (IGF1)–phosphoinositide 3-kinase (PI3K) pathway, which plays an essential role in mediating the protective actions of regular physical activity or exercise on the heart. Regular exercise is a well-established and accessible intervention that has been demonstrated to provide benefit to multiple organ systems in settings of both health and disease.¹ The benefits are well-established in a setting of cardiac health, in which exercise has been demonstrated to reduce the risk of future cardiac events or diseases and improve outcomes following a cardiac event or diagnosis.^{2,3} This is of particular interest given the rising prevalence of ischemic heart disease, which is currently the

greatest burden of disease globally, both reducing quality of life and increasing overall mortality.⁴

Heart failure represents the end point of a variety of cardiovascular diseases and occurs when the heart is unable to supply adequate blood to the body. It is of particular relevance because of the high mortality rate (5-year mortality greater than 40% following initial diagnosis), high lifetime risk of acquisition (20%–45%),⁵ and the limited effectiveness of treatment options currently available. Aerobic exercise training has proven to be one of the few safe and effective interventions following a diagnosis of stable heart failure, with patients displaying improved cardiac function, aerobic capacity, and attenuation of abnormal cardiac remodeling following 3–6-month training programs.^{6,7} Both a lack of patient adherence and an inability to exercise due to loss of cardiac function from heart failure progression pose barriers for an individual to use exercise training as a method of treatment.

Peer review under responsibility of Shanghai University of Sport.

*Corresponding author.

E-mail address: julie.mcmullen@baker.edu.au (J.R. McMullen).

<https://doi.org/10.1016/j.jshs.2020.11.009>

Understanding the key molecular pathways and mediators involved in exercise-induced heart protection is an exciting approach for treating heart failure. That being said, the development of an exercise-based therapy is far from a simple process. The cardioprotective effects of exercise reflect a complex and multifactorial web of neurohormonal, hemodynamic, molecular, and physiological changes that occur during and following physical activity, both in settings of acute and chronic exercise.¹ Exercise in an acute setting activates the sympathetic nervous system and reduces parasympathetic activity. This, in conjunction with engagement of muscular and respiratory pumps, increases stroke volume and heart rate, which in turn leads to greater cardiac output to compensate for an increased demand for oxygen. Chronic or long-term exercise similarly leads to increased sympathetic activity, but additionally, the stimulation of various hormones and growth factors that facilitate the thickening and enlargement of the heart.¹

2. Delineating key molecular pathways by understanding differences between the athlete's heart and the diseased heart

The athlete's heart is a term coined as far back as 1896 when Henschen⁸ observed cross-country skiers to have enlarged hearts. More recently, this phenomenon has been routinely observed in endurance athletes, who display an increase in heart mass while maintaining preserved or enhanced systolic and diastolic function.^{9–11} Exercise-induced heart growth, also known as physiological cardiac hypertrophy, is a compensatory mechanism that allows for the preservation or enhancement of cardiac function while facilitating the demand for greater cardiac output (increased workload).¹ This type of growth is typically characterized by an increase in cardiomyocyte size, left ventricular chamber size, wall thickness, and mass. These adaptations function to normalize wall stress and tension in a coordinated manner.^{12,13}

In contrast, pathological heart growth can occur in a setting of disease (pressure overload, myocardial infarction (MI), and cardiomyopathy) and can initially be characterized by thickening of ventricular walls and increased mass, but over time this can lead to cell death, fibrotic replacement, impaired cardiac function, and increased risk of heart failure.^{12,13} Of note, it has been documented that extreme amounts of high-intensity endurance exercise can lead to an increased risk of arrhythmia and/or sudden cardiac death.¹⁴ The risks from these extreme levels of exercise are distinct from the beneficial, normal levels of exercise that are discussed within this review. In a setting of moderate exercise, an increased risk of arrhythmia and sudden cardiac death is not apparent.

Our laboratory and others¹ have investigated key mediators responsible for physiological hypertrophy by studying molecular changes in mouse models following chronic exercise (e.g., swim training) or genetic mouse models. Mice have proven to be a powerful tool to assess key mechanisms responsible for exercise-induced hypertrophy and protection because genes can be relatively easily manipulated to generate knock out and

transgenic models, and mice develop significant physiological cardiac hypertrophy after as little as 3–4 weeks with swim training. Moreover, they breed rapidly, are inexpensive to house and functional changes can be assessed through a variety of exercise models (swim, treadmill, and voluntary running).¹⁵ Numerous molecular pathways have been shown to directly contribute or associate with aspects of physiological cardiac hypertrophy and protection. A comprehensive list is detailed in Bernardo et al.¹ and includes IGF1–PI3K signaling, mediators downstream of vascular endothelial growth factor, hepatocyte growth factor, and platelet-derived growth factor, neuregulin 1, transcription factors and microRNAs (miRNAs). We have summarized work related to the IGF1–PI3K pathway and strategies for targeting this pathway in the failing heart.

3. The IGF1–PI3K signaling pathway: A key mediator of physiological hypertrophy and cardioprotection

Activation of the IGF1–PI3K pathway through physical activity has been well-established in playing an important and beneficial role in protecting the heart. However, exercise is an activity involving the whole body, and evidence has indicated that exercise also plays an important role in activation of the IGF1–PI3K pathway in both brain and skeletal muscle^{14,16–20}; the impact of exercise on this pathway in other tissue types is less clear.

In this review, we have focused on the IGF1–PI3K signaling pathway because, to date, this pathway is the most recognized and essential signaling pathway responsible for mediating physiological hypertrophy. Cardiac IGF1 formation has been demonstrated to be elevated in elite athletes (soccer players) with enlarged hearts following exercise training. It is postulated that, in response to increased stroke volume during exercise, cardiac myocytes undergo stretch, and IGF1 is released from cardiac myocytes in preference to other growth factors (angiotensin II and endothelin-1) which are released from myocytes in response to a chronic pathological stimuli.²¹ IGF1 binds to the IGF1 receptor (IGF1R), a plasma membrane receptor from the family of tyrosine kinases, and initiates the activation of 2 well-established, pro-hypertrophic canonical signaling pathways—the PI3K–protein kinase B (Akt) pathway and the extracellular signaling kinase pathway.^{22,23} Interestingly, in the adult mammalian heart, PI3K rather than extracellular signaling kinase, is the critical regulator of physiological heart growth.²⁴ In this review, we primarily focus on the IGF1–PI3K pathway in the heart, with a particular emphasis on PI3K, providing an updated perspective on current knowledge, the development of therapeutic strategies for heart failure, biomarkers, and predictive tools for cardiotoxicity.

3.1. PI3K signaling

PI3Ks are a family of lipid and protein kinases expressed in all tissues and involved in a wide variety of processes such as cell survival, protein synthesis, cell motility, cell polarity, metabolism, and vesicle trafficking.²⁵ Three classes of PI3Ks exist (I, II, and III) that function to catalyze the phosphorylation of phosphatidylinositols to generate class dependent

phosphoinositide forms with differing functions. Class I PI3Ks have been researched and understood in depth; there are 4 class I PI3Ks (p110 α , β , δ , and γ) that can be further divided in subsets Class IA and IB. Class I PI3Ks function primarily to regulate cell growth, survival, proliferation, autophagy, and metabolism. Research into the function of Class II PI3Ks has been less studied, but 3 isoforms exist (PI3KC2 α , PI3KC2 β , and PI3KC2 γ) with increasing evidence suggesting that they have distinct cellular roles, including cell proliferation, survival, and migration. A single Class III PI3K is conserved in eukaryotes, vacuolar protein sorting 34 acts to phosphorylate phosphatidylinositol to produce phosphatidylinositol 3-phosphate, which regulates autophagy and endocytic sorting.^{26–28} Class I PI3Ks are heterodimers consisting of a regulatory subunit and a catalytic subunit. Multiple isoforms or splice variants of each subunit exist which act to serve differing functions in different cell types.²⁹ This review focuses on the p110 α isoform of PI3K, a Class IA PI3K³⁰ that is primarily activated by tyrosine kinase receptors, and expressed in cardiac myocytes to induce physiological myocyte growth. Activation of PI3K requires interaction of the p85 regulatory subunit with the p110 α catalytic subunit, and this catalyzes the conversion of phosphatidylinositol 4,5-bisphosphate to phosphatidylinositol (3,4,5)-trisphosphate. Following this conversion to phosphatidylinositol (3,4,5)-trisphosphate, pleckstrin homology domain-containing proteins including Akt and

phosphoinositide-dependent kinase-1 are recruited to the plasma membrane. This recruitment leads to phosphoinositide-dependent kinase-1 and mammalian target of rapamycin complex 2 phosphorylating Akt, which in turn allows for its activation and the triggering of subsequent downstream signaling pathways³¹ (Fig. 1).

3.2. Role of PI3K in the heart

Initial interest in the role of PI3K in the heart arose from the previous observation that PI3K plays an essential role in regulating wing size in *Drosophila*. The insulin/IGF receptor/PI3K pathway is highly conserved across species. In *Drosophila* with overexpression of wildtype PI3K (Dp110), wing size was significantly larger than wing size from control flies. By contrast, expression of a catalytically inactive PI3K mutant (Dp110^{D954A}) in *Drosophila* wing resulted in reduced wing size.^{32,33} The role of PI3K in the mammalian heart was first discovered through the characterization of transgenic mouse models with increased and decreased cardiac-specific PI3K (p110 α) activity. This research demonstrated that PI3K is a critical mediator of physiological postnatal heart growth. Shioi et al.³⁴ created a mouse model expressing a cardiac-specific constitutively activated mutant of PI3K (caPI3K), and a mouse model expressing a cardiac-specific dominant negative mutant of PI3K (dnPI3K). The caPI3K transgenic mice displayed

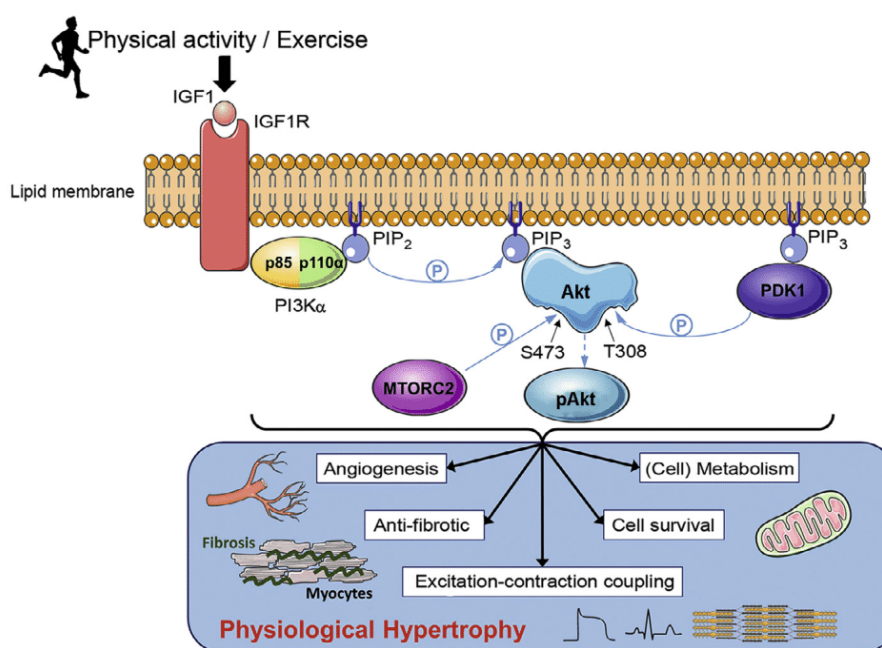


Fig. 1. A schematic diagram displaying the impact of physical activity or exercise on the IGF1–PI3K–Akt signaling pathway and the downstream physiological outcomes in the heart. Following exercise, IGF1 binds to the IGF1R embedded in the plasma membrane of cardiomyocytes, allowing for binding of p85, the regulatory subunit of PI3K α . Once bound, p85 recruits p110 α , the catalytic subunit of PI3K α , forming the fully activated form of PI3K α . Activated PI3K α catalyzes the phosphorylation of PIP₂ to PIP₃, which recruits AKT and PDK1 to the plasma membrane. Binding of Akt to PIP₃ causes a conformational change in Akt, exposing the phosphorylation sites S473 and T308. Phosphorylation of S473 by MTORC2 and T308 by PDK1 activates Akt allowing for numerous downstream protective physiological changes to the heart (via Akt dependent and Akt independent mechanisms). P within the blue circle signifies phosphorylation. Akt = protein kinase B; BTK = Bruton's tyrosine kinase; HER = human epidermal growth factor receptor; IGF1 = insulin-like growth factor 1; IGF1R = insulin-like growth factor receptor; MTORC2 = mammalian target of rapamycin complex 2; NRG1 = neuregulin 1; PDK1 = phosphoinositide-dependent kinase 1, PIP₂ = phosphatidylinositol 4,5-bisphosphate; PIP₃ = phosphatidylinositol (3,4,5)-trisphosphate; PI3K = phosphoinositide 3-kinase; S473 = serine 473; T308 = threonine 308.

increased cardiac PI3K activity, which corresponded to an increase in the size of all chambers and left ventricular (LV) wall thickness, and heart weight to body weight ratio. The dnPI3K transgenic mice had reduced PI3K activity and in turn a reduction in heart weight (Fig. 2). Neither of the models displayed any signs of heart failure following a year of observation.

The role of PI3K(p110 α) for the induction of exercise-induced physiological hypertrophy was later assessed by subjecting dnPI3K mice to chronic swim training. After 4 weeks of chronic swim training the hypertrophic response (heart weight to body weight ratio) of dnPI3K mice was significantly smaller than that of age- and weight-matched non-transgenic (Ntg) controls.³⁵

In addition to its role in regulating heart growth, PI3K has also been demonstrated to mimic the cardioprotective properties of exercise. Exercise training in a genetic model of dilated cardiomyopathy (DCM) from 4 of weeks age, increased lifespan by ~20% and ~16% in male and female mice, respectively. By genetically crossing the DCM model with either dnPI3K or caPI3K mouse models, the impact of altered cardiac PI3K activity on lifespan was also assessed. DCM–caPI3K (increased PI3K) double transgenic mice (without exercise) showed an increase in longevity that was comparable to the increase in lifespan in the DCM model with exercise. In contrast, DCM–dnPI3K (reduced PI3K) mice displayed a drastic reduction in lifespan, highlighting the significance of both exercise and cardiac PI3K activity in the prevention of cardiac disease.³⁶ These findings have been replicated in a variety of settings of cardiac stress, with the caPI3K transgenic mice displaying better cardiac function and less pathology following induction of pressure overload, MI, diabetic cardiomyopathy, and atrial fibrillation. Alternatively, the dnPI3K mice consistently display accelerated heart failure and other pathological complications in the above models of cardiac stress.^{36–41} These studies together highlight (1) the importance of PI3K in

facilitating normal cardiac growth, (2) the role of PI3K in exercise-induced heart growth, and (3) the critical role of PI3K activity providing protection in a variety of settings of cardiac stress.

In keeping with its crucial role in exercise-induced cardiac growth, PI3K signaling and exercise both target and modulate many of the same cell types and cellular processes. These have been extensively described previously and include the regulation of cardiac myocyte growth, excitation and contraction coupling, vascular adaptations, cellular stress response, mitochondrial adaptations, and anti-fibrotic properties¹ (Fig. 1).

4. PI3K-based therapies as an approach for improving function of the failing heart—Overview

Heart transplantation availability is extremely limited, with as few as 4000–4500 heart transplantations occurring worldwide each year.⁴² Current approaches and strategies under investigation are broadly summarized in Fig. 3 and include (1) environmental and dietary approaches, (2) gene-based therapies (e.g., targeting DNA, mRNA, and miRNAs), (3) pharmacological approaches, and (4) surgical approaches (e.g., LV assist devices, valve replacement, and coronary artery bypass surgery). The majority of existing heart failure treatments primarily manage symptoms and delay disease progression, and exercise interventions are not always viable due to the progressive and debilitating nature of the disease.

Given these cardioprotective benefits that PI3K has been demonstrated to provide a therapy that upregulates cardiac PI3K activity may provide a promising approach for improving heart function in individuals with heart failure. Our laboratory has a large interest in investigating the development of a PI3K based therapy as a non-surgical alternative for the treatment of the failing heart. Multiple approaches may be applicable in considering the use of a PI3K therapy, with differing tactics being tailored to particular pathological or clinical settings (Fig. 3). This is an important consideration given that a single approach is unlikely to be a one fix for all. Factors such as the method of administration (surgical vs. dietary), duration of therapeutic effect (short term vs. long term), and dosage of the PI3K therapy provided may differ depending on an individual's age, health status, prognosis, and particular cardiac disease being targeted. Moreover, combined therapeutic approaches to treat cardiovascular diseases are more frequently being utilized and are showing encouraging outcomes in recent times.^{43,44}

Approaches our laboratory are investigating include PI3K therapies that utilize adeno-associated virus (AAV) gene therapy, as well as the identification and utilization of mRNAs, miRNAs, small molecules, and lipids that differ between healthy and diseased hearts. Gene therapy is discussed in Section 5, and other approaches are discussed in Section 7.

5. Gene therapy as an approach for treating heart failure

Gene therapy involves the transfer of an isolated nucleic sequence from a foreign body to a host organism with the

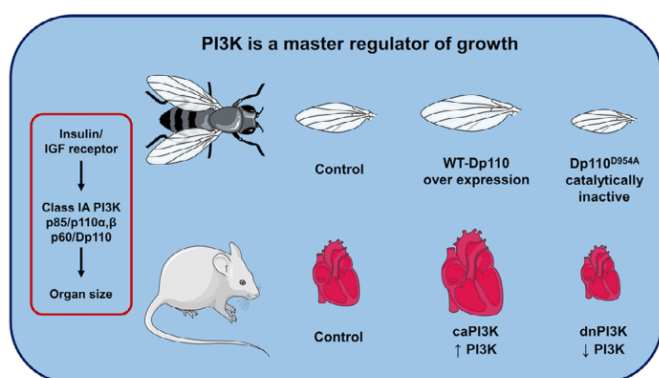


Fig. 2. PI3K is a master regulator of growth. Class IA PI3K(Dp110) overexpression in the wings of drosophila results in enlarged wings while over expression of a mutated inactive PI3K (Dp110^{D954A}) results in smaller wings. Similarly, caPI3K in the hearts of mice results in enlarged hearts, while the presence of a truncated mutated dnPI3K with reduced PI3K activity results in smaller hearts. caPI3K = constitutive activation of PI3K; dnPI3K = dominant negative PI3K; IGF = insulin-like growth factor; PI3K = phosphoinositide 3-kinase; WT = wild type.

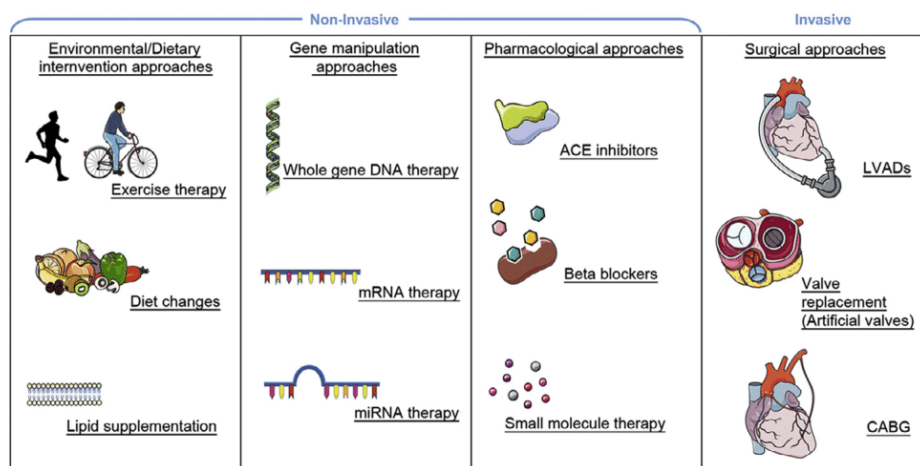


Fig. 3. A summary of current approaches for the failing heart and new promising approaches for improving function in the failing heart (e.g., gene therapy). Approaches are separated into 4 categories based on the type of intervention: environmental and dietary based interventions, approaches involving genetic manipulation, pharmacological interventions, and surgical interventions. Combining multiple approaches may be an optimal strategy to maximize therapeutic outcomes. ACE = angiotensin-converting enzyme; CABG = coronary artery bypass graft; LVAD = left ventricular assist device; miRNA = microRNA.

purpose of altering gene function and/or expression, and in turn, providing a therapeutic outcome.⁴⁵ Numerous factors need to be taken into consideration to maximize clinical viability when developing a cardiac gene therapy. Namely, the choice of vector used to transfer the transgene, the method of delivering the vector to the heart, the vector's capacity to provide efficient transduction of the human heart, the therapeutic potential of the transgene of choice, and the cost/practicality of large-scale manufacturing.⁴⁶

Modified viral vectors have been the primary choice of vectors used for the transfer of genetic material to date; more specifically, AAVs have been demonstrated to be a promising gene therapy vector for the treatment of heart failure with human clinical trials having been undertaken in recent times.^{47–51} AAVs are small, single stranded non-pathogenic viruses with the capacity to transduce both dividing and non-dividing cells. The interest in AAVs as a vector for the use in cardiac gene therapy arises from their high safety profile, non-pathogenicity (invoking a limited host immune response), and

mediating long-term transgene expression that is reported to last several years in human trials.⁵² Moreover, multiple naturally occurring AAV serotypes such as AAV6 and AAV9 have been found to display cardiac-specific tropism, allowing for efficient transduction of cardiomyocytes while minimizing the delivery of transgenes to non-cardiac tissue or cells.⁴⁶

Successful results from a multitude of AAV studies to treat heart failure in clinically relevant small and large animal models paved the way for the 1st AAV heart failure trial in human subjects: The Calcium Upregulation by Percutaneous Administration of Gene Therapy in Cardiac Disease (CUPID) trial. The CUPID trial attempted to increase expression of sarcoplasmic/endoplasmic reticulum Ca^{2+} -ATPase (SERCA2a) activity, which is reduced in the failing heart. Administration of AAV1–SERCA2a in a pilot study in 9 patients with heart failure displayed a positive safety profile and favorable outcomes including improved ejection fraction, end-systolic volume, and maximum rate of oxygen consumption (Table 1).⁴⁹ This trial was replicated in a follow-up placebo controlled, Phase IIa

Table 1
Outcomes from the AAV–SERCA2a CUPID trials.

	CUPID Trial 1/2	CUPID Trial phase IIa	CUPID Trial phase IIb
Patient (n)	9 patients: Treated AAV1/SERCA2a (n = 9)	39 patients: Placebo (n = 14) Treated AAV1/SERCA2a (n = 25)	243 patients: Placebo (n = 122) AAV1/SERCA2a (n = 121)
Dose (vector genomes)	Low: 1.4×10^{11} Mid: 6×10^{11} High: 3×10^{12}	Low: 6×10^{11} Mid: 3×10^{11} High: 1×10^{13}	1×10^{13}
Positive safety profile	Yes	Yes	Yes
Delay/reduction in clinical events	N/A	Yes	No
Improvement in NYHA functional class/quality of life	Yes	Yes	No
Improvement in 6-min walk test	Yes	Yes	No
Improvement in LV function/remodelling	Yes	Yes	No

Abbreviations: AAV = adeno-associated virus; CUPID = The Calcium Upregulation by Percutaneous Administration of Gene Therapy in Cardiac Disease; LV = left ventricular; NYHA = New York Heart Association; N/A = not applicable; SERCA2a = sarcoplasmic/endoplasmic reticulum Ca^{2+} -ATPase.

CUPID trial of 39 patients, in which those that received a high dose of AAV1–SERCA2a (1×10^{13} DNase-resistant particles) demonstrated significantly improved LV end-systolic volume and maximum rate of oxygen consumption, as well as a decreased frequency of cardiovascular events and cardiovascular related hospitalizations (Table 1).⁵⁰ Subsequently, a larger multinational, randomized, double-blinded placebo-controlled CUPID Phase IIb trial with 243 advanced heart failure patients was initiated. The Phase IIb trial did not demonstrate improvement in the primary or secondary end point of recurrent heart failure events or all-cause death, respectively (Table 1). The trial was prematurely terminated, but of importance, no signs of adverse safety outcomes were observed across all studies at any dose following administration of AAV1–SERCA2a.⁵¹ The outcome of the CUPID Phase IIb trial could not conclusively assess whether AAV1–SERCA2a was an appropriate gene target for the treatment of heart failure because efficiency of transduction was considered suboptimal. However, the results have been invaluable in informing future efforts of the use of AAV gene therapy for the treatment of cardiovascular disease.

The poor outcomes from the CUPID Phase IIb trial have not dampened efforts to utilize AAVs as a gene therapy vector, with over 200 clinical trials involving AAVs being registered at Clinicaltrials.gov as of June 2020, ten of which are categorized under the topic of heart disease. The aforementioned caPI3K transgene represents another gene target for the treatment of heart failure. Preliminary studies using an AAV6–caPI3K with a cytomegalovirus (CMV) promoter in both healthy mice and models of cardiac pathology have demonstrated efficacy regarding its potential as a cardioprotective therapeutic agent.⁴⁰ The AAV6 serotype in conjunction with use of a CMV promoter provided cardiac and skeletal muscle-specific transduction. Moreover, administration of AAV6–caPI3K-induced angiogenesis, physiological hypertrophy, and increased phosphorylation of Akt in the hearts of healthy mice. Similarly, promising results have been observed using AAV6–caPI3K in multiple models of established cardiac pathology. In a mouse model with established cardiac dysfunction due to pressure overload (transverse aortic constriction), AAV6–caPI3K was able to restore systolic function (fractional shortening) within 10 weeks of administration.⁴⁰ AAV6–caPI3K administration also provided cardiac protection in mouse models with type 1 or type 2 diabetes. The type 1 diabetic model (low-dose streptozotocin) displayed diastolic dysfunction prior to AAV6–caPI3K, and this was attenuated within 6–8 weeks post-AAV. The type 2 model of diabetes (low-dose streptozotocin in combination with a high-fat diet) displayed systolic dysfunction prior to treatment, and AAV6–caPI3K increased systolic function within 8 weeks. Both type 1 and 2 diabetic models displayed cardiac fibrosis, and fibrosis was lower in AAV6–caPI3K treated mice compared to the corresponding diabetic control mice.^{41,53}

Collectively, these findings have facilitated the continued optimization of AAV6–caPI3K as a gene therapy tool, and its transition into large animal models, a crucial steppingstone between the laboratory and the clinic.

In the process of the development and translation of a gene therapy such as AAV–caPI3K, from a laboratory to a clinical setting, 3 important considerations must be addressed: first, the cardiac specificity of the therapy (ensuring that the transgene is highly expressed in cardiac tissue while simultaneously not displaying expression in non-cardiac tissue); second, the feasibility of mass AAV production to ensure the therapy is financially viable as a treatment option for patients with heart failure; and third, demonstrating safety and efficacy in a large animal model of heart failure.

5.1. Cardiac specificity

Increased PI3K activity is protective and beneficial in cardiac tissue, but PI3K is well-known to be a regulator of tumor growth in other tissues in a variety of cancers.^{54,55} Cardiac myocytes within the adult heart have very little capacity to proliferate. Thus, changes in heart size and mass are typically a consequence of changes in cardiac myocyte size. In response to PI3K activation, cardiac myocytes enlarge and this results in physiological hypertrophy. However, in many forms of cancer, dysregulation and increased activation of the PI3K/Akt pathway in other cell types can lead to uncontrolled cell proliferation and growth, as seen in settings of tumorigenesis.⁵⁶ Ensuring cardiac-specific gene transfer of a PI3K gene therapy is a crucial safety consideration for the prevention of undesirable side effects such as the development of cancer.

Another important consideration is efficient cardiac transduction. If a viral capsid is unable to efficiently transduce cardiac tissue, its capacity as a therapeutic agent is made redundant. One approach to address these concerns involves the selection of AAV serotypes that are naturally cardiotropic. Multiple studies have compared the effectiveness of the most well-established AAV serotypes (AAV1–9), and AAV6 and AAV9 have frequently demonstrated rapid and robust cardiotropic expression with substantial expression in the hearts relative to other organs.^{57–61} As described earlier, the AAV6–CMV–caPI3K vector displays transduction specific to cardiac and skeletal muscle.⁴⁰ Further improvement to cardiac-specific transduction can be established using a cardiotropic AAV serotype in conjunction with a promoter that confers cardiomyocyte-specific gene expression such as a cardiac troponin T promoter. Prasad et al.⁶² compared transduction of AAV6 vectors harboring either a CMV or cardiac troponin T promoter with a luciferase reporter in a variety of tissue types in mice. Luciferase expression driven by the CMV promoter was comparable in the heart, skeletal muscle, and liver, whereas luciferase expression driven by the cardiac troponin T promoter was nearly 100-fold greater in the heart than all other tissue types assessed.⁶² In addition to promoter and serotype selection, further improvements to cardiac specificity may be made through the development of promoters that specifically target diseased tissue, development of chimeric AAV vectors through DNA shuffling, or the use of directed evolution to modify viral capsid sequences and select for cardiotropic variants.⁴⁶

5.2. Feasibility of mass AAV production

The viability of mass scale production of AAV is another necessity to be considered in the process of clinical translation.⁶³ The high global prevalence of heart failure together with the costs of mass producing larger yields of AAV for pre-clinical studies in large animals and for clinically relevant therapeutic interventions would come with a considerable price tag. The limited packaging capacity of AAV (~ 5 kb), makes obtaining sufficient vector yields of larger genes (such as caPI3K) particularly challenging. Reducing the size of gene constructs is an approach to improving yield and in turn reducing cost. Furthermore, other promising approaches to improve large scale production of AAVs have involved modifications to the culture conditions for growing cells with plasmids used for chemical co-transfection of AAVs, as well the investigation of cell lines which display greater transfection efficiency and in turn improved AAV yields.⁶⁴

5.3. Translation to large animal models

Assessment of efficacy and safety in large animal models is important for any new gene therapy approach. Sheep and pigs have typically been the model of choice after small animal studies. This primarily reflects the anatomical and physiological similarities shared between these large animals and humans, which differs in rodents. Moving from small animals to large animals invokes additional challenges, such as determining the optimal method to administer an AAV, identifying if either toxicity or efficacy vary in different animal models, and the optimal dose required to provide a therapeutic effect. This topic is covered in detail by Bass-Stringer et al.⁴⁶

6. Cardiac pathology and cardiotoxicity in settings of reduced PI3K

The earlier part of this review has focused on enhancing PI3K activity in the heart to provide protection in settings of cardiac stress. However, a reduction in PI3K in the heart has the converse effect, that is, making the heart more susceptible to cardiac pathology and heart failure. Factors which can lead to reduced or defective PI3K signaling in the heart include physical inactivity, obesity, diabetes, aging, and drugs (e.g., anti-cancer drugs). The previously mentioned dnPI3K transgenic mouse model has been a valuable tool for understanding the impact of reduced cardiac PI3K activity in a variety of settings of cardiac pathologies. dnPI3K mice displayed cardiac dysfunction in response to pressure overload compared to Ntg controls. This was demonstrated through a significant reduction in fractional shortening, and a marked increase in systolic and diastolic LV dimensions following 1 week of ascending-aortic banding compared to Ntg-banded controls. The animals also displayed an increase in lung weight/body weight ratio, a marker of LV dysfunction.^{35,36} Similarly, in a setting of MI, dnPI3K mice also displayed reduced fractional shortening and increased chamber dimensions.³⁸

PI3K activity has also been shown to affect the progression of heart failure in a setting of DCM. dnPI3K transgenic mice

have been crossed with 2 different cardiac-specific transgenic mouse models of DCM to generate double transgenic mice (dnPI3K–DCM). In the first DCM model, due to very high expression of Cre-recombinase, the dnPI3K transgene drastically shortened life span (~50%) in the dnPI3K–DCM compared to DCM transgenic mice. In a second model of DCM, due to over-expression of mammalian sterile 20-like kinase 1 (Mst1), the dnPI3K–DCM transgenic mice displayed an accelerated heart failure phenotype including more cardiac dysfunction, greater atrial enlargement and cardiac fibrosis than DCM (Mst1) transgenic mice, and developed atrial fibrillation.^{36,37}

In a setting of diabetes, dnPI3K mice have also been shown to develop an exaggerated cardiomyopathy phenotype compared to Ntg diabetic mice.³⁹ Taken together, these studies demonstrate that a reduction in PI3K leads to accelerated cardiac pathology and heart failure in a variety of settings of pathological stress.

The IGF1–PI3K pathway is considered a master regulator of cancer in a variety of non-cardiac tissue types.^{56,65} Thus, extensive efforts have been devoted to developing agents that act to inhibit or modify components of the IGF1–PI3K pathway, and in turn improve survival rates for cancer patients. However, with improvements in survival from cancer, some patients are developing cardiac complications including heart failure and arrhythmias. Given the widespread pathological outcomes seen in mice with reduced PI3K activity, consideration should be taken for potential adverse effects due to cardiotoxicity that may arise when inhibiting this ubiquitously expressed pathway in an already compromised population. Kinase inhibitors for the treatment of cancer, such as trastuzumab,⁶⁶ have been recognized to contribute to cardiac dysfunction.⁶⁷ A Phase III randomized multicenter trial⁶⁸ combined trastuzumab with anthracyclines and cyclophosphamide to treat human epidermal growth factor receptor 2 (HER2)–positive breast cancer patients. Heart failure and cardiac dysfunction was reported in up to 27% of patients receiving the combined therapy. Comparatively, the group that received only anthracyclines and cyclophosphamide had an incident rate of 8%.⁶⁸ A number of mechanisms have been implicated to explain trastuzumab cardiac toxicity but it is noteworthy that this drug also has the potential to inhibit PI3K signaling via HER2 (Fig 4).^{66,69}

Modification of other proteins regulated by the IGF1–PI3K pathway are being targeted for the development of novel anti-cancer drugs. Clusterin has been implicated in the pathogenesis of various cancers, such as prostate cancers, breast cancers, and lung cancer,^{70,71} and has been a target of interest, with multiple recent clinical trials having focused on silencing clusterin with an antisense oligonucleotide (Custirsen) as a therapeutic intervention. We recently reported a potential role of clusterin in physiological cardiac hypertrophy and cardiac protection. Expression of clusterin was increased in hearts of caPI3K mice and decreased in hearts of dnPI3K mice. In addition, we identified increased secretion of clusterin in media from neonatal rat ventricular myocytes stimulated with IGF1.⁷² Given that a link exists between reduced PI3K activity and clusterin expression⁷² (Fig. 4), the possibility for the

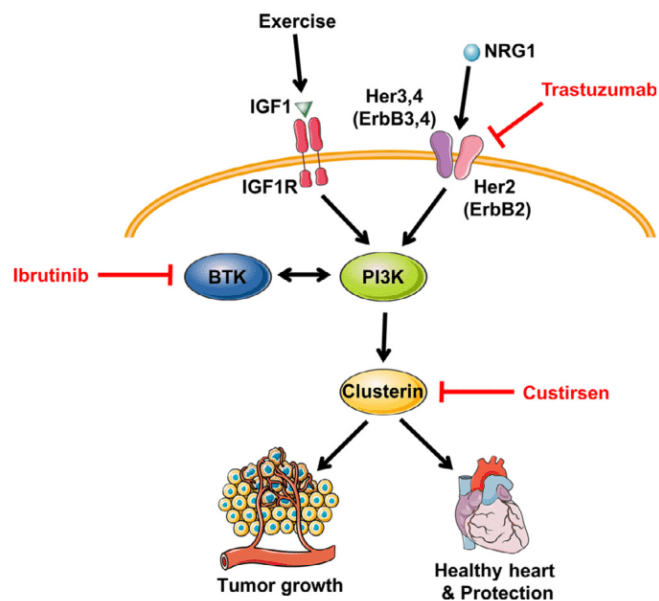


Fig. 4. Anticancer therapeutics with the potential to inhibit the PI3K α pathway. Trastuzumab binds to the extracellular domain of HER2 and triggers mechanisms to downregulate downstream activity. Ibrutinib inhibits BTK expression and is a known regulator of the PI3K–Akt pathway. Custirsen acts to silence clusterin, of which its expression has been correlated with PI3K activity, and may disrupt downstream processes. The mechanisms of anticancer therapies that suppress tumor growth by targeting the PI3K–Akt pathway may simultaneously contribute to an increased susceptibility for the development of cardiac pathologies. Red lines indicate interventions that act to silence, inhibit, or downregulate protein expression. Akt = protein kinase B; BTK = Bruton’s tyrosine kinase; HER (ErbB) = human epidermal growth factor receptor; IGF1 = insulin-like growth factor 1; IGF1R = insulin-like growth factor receptor; NRG1 = neuregulin 1; PI3K = phosphoinositide 3-kinase.

development of cardiac toxicity following its silencing should be considered.

Similarly, a Bruton tyrosine kinase inhibitor called ibrutinib is a targeted cancer therapy used for the treatment of many hematological cancers including chronic lymphocytic leukemia, small lymphocytic lymphoma, mantle cell lymphoma, and Waldenstrom macroglobulinemia. Across multiple trials, 3.5%–6.5% of subjects receiving ibrutinib treatment developed atrial fibrillation.⁷³ There is potential crosstalk between Bruton tyrosine kinase and the PI3K–Akt pathway,⁷⁴ and thus, ibrutinib has the potential to interfere with cardioprotection (Fig. 4). Our laboratory has shown that mice with reduced PI3K activity display greater susceptibility to atrial fibrillation and that PI3K–Akt activity is reduced in human atrial appendages from patients with atrial fibrillation.³⁷ Moreover, reduced PI3K–Akt expression has been observed following the exposure of neonatal rat ventricular myocytes to ibrutinib.⁷³ These observations highlight the importance of taking caution when considering any intervention that may suppress the PI3K–Akt pathway in the heart. The impact of exercise on the IGF1–PI3K signaling pathway in non-cardiac tissue should also be considered when assessing potential toxicities of therapies that act to alter the expression or function of the IGF1–PI3K pathway, as exercise represents a systemic intervention, and has been demonstrated to play a role in activating

the IGF1–PI3K pathway in brain and skeletal muscle tissue.^{16–20} Crosstalk between skeletal muscle and other tissues with the heart has also emerged.¹

7. Identifying molecular distinctions in the healthy and diseased heart—New drug targets and biomarkers

The physiological and pathological hypertrophic heart display distinct and differing functional, metabolic, structural, and molecular features. The use of surgical, genetic, and exercise models representing pathological or physiological cardiac remodeling, together with the profiling of genes, proteins, lipids, and metabolites, has become a valuable research tool to identify potential new drug targets and biomarkers which are distinct in the healthy and diseased heart (Fig. 5). A detailed overview of profiling studies has been summarized previously.¹ This same approach can be used in genetic mouse models which are protected or more susceptible to cardiac stress (e.g., caPI3K and dnPI3K transgenic mice, respectively). Distinguishing a diseased or stress susceptible heart may provide opportunities to assess whether someone is more likely to develop more severe cardiac pathology in response to cardiac stress (e.g., hypertension) or a cancer therapy.

Our laboratory has undertaken gene-profiling studies to attempt to identify candidate therapeutic genes regulated by PI3K. Assessing the profiles of caPI3K, dnPI3K, and Ntg mice subjected to cardiac stress through MI was used to generate a list of genes that were differentially expressed based on PI3K activity.³⁸ Correlating these differentially expressed genes with cardiac function (fractional shortening percentage) and in turn identifying those that are selectively expressed in the heart, provided a shortlist of candidate therapeutic targets. One of the top candidate genes was *Acadm*.

The protein product of *Acadm* is medium chain acyl-coenzyme A dehydrogenase (MCAD), a protein that has not previously been linked with physiological hypertrophy and protection. The therapeutic potential of MCAD in the heart was examined by administering an AAV6 vector encoding MCAD to both healthy mice and mouse models of cardiac dysfunction.⁷⁵ MCAD induced physiological hypertrophy in healthy mice and mitigated characteristics of cardiac remodeling in a setting of cardiac pathology due to pressure overload.⁷⁵ This highlights the potential of how assessing differences in the healthy and diseased heart can identify candidates for novel therapies.

The same approach that led to the identification of *Acadm* was applied to identify miRNAs that are differentially regulated in caPI3K mice, dnPI3K mice, and Ntg mice. Numerous candidates were identified,³⁸ and subsequently, silencing or inhibition of miR-34, miR-652, or miR-154 provided benefit when targeted in settings of cardiac pathology (MI and/or pressure overload).^{76–78}

Our laboratory has also undertaken comprehensive profiling of the lipidome in models of physiological and pathological remodeling. As cardiac myocytes enlarge or change shape in response to a stimulus (e.g., cardiac stress such as hypertension or chronic exercise training), the plasma membrane which

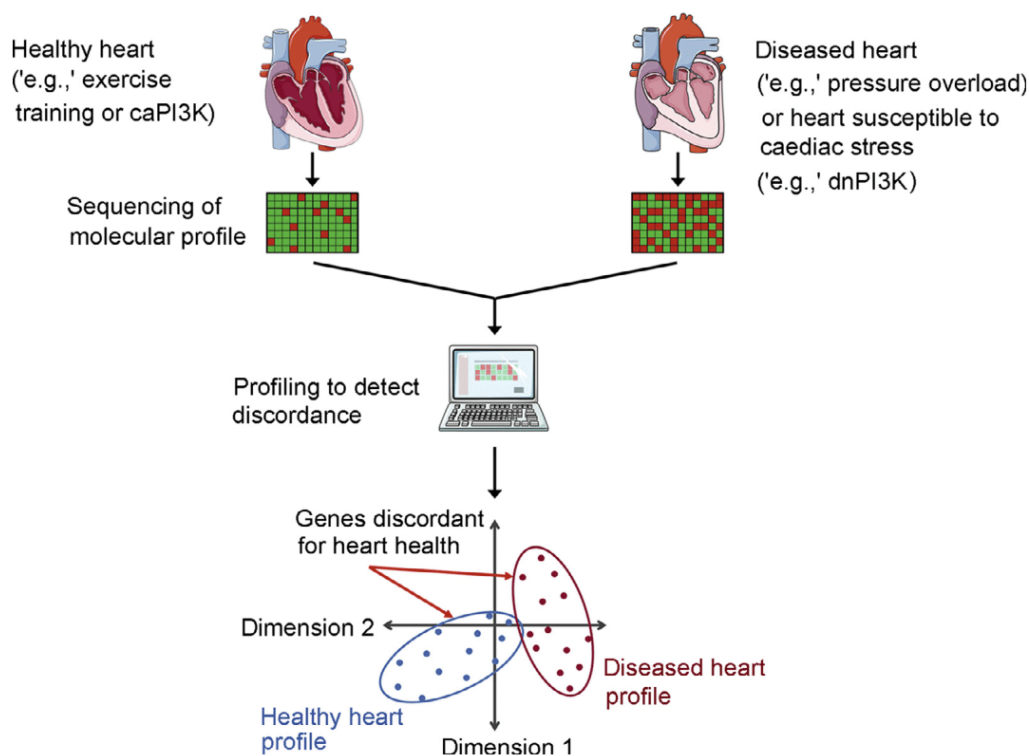


Fig. 5. Identifying molecular distinctions between the healthy and diseased heart. A simplified pipeline demonstrating the process of using sequencing technologies to identify candidate therapeutics and biomarkers of cardiac health and disease. Tissue is collected, pooled, and processed from healthy and diseased hearts. A molecule of interest (e.g., DNA, RNA, protein, lipid) is sequenced and profiled. Expression is compared between groups to identify specific candidates that are discordant for cardiac health, or techniques such as principal component analysis can be used to identify global changes between groups. caPI3K = constitutive activation of PI3K; dnPI3K = dominant negative PI3K; PI3K = phosphoinositide 3-kinase.

includes hundreds of lipid species, undergoes dramatic remodeling. Lipid profiling (>300 lipid species) demonstrated that lipid profiles differ substantially in models of physiological cardiac remodeling (swim training, caPI3K transgenic mice, and IGF1R transgenic mice), models of pathological remodeling (severe pressure overload due to transverse aortic constriction, a transgenic model of DCM, and mice with reduced cardiac PI3K activity and greater susceptibility to cardiac stress, i.e., dnPI3K transgenic).^{79,80} As an example, many sphingolipid species were decreased in the hearts of caPI3K mice and increased in the hearts of dnPI3K mice; by contrast, many phospholipids were increased in the hearts of caPI3K mice but decreased in dnPI3K mice.⁷⁹ Dietary supplementation of lipid species that are depressed in the diseased heart and increased in the healthy heart may offer a non-invasive therapeutic approach for improving heart function (Fig. 3).

Microarray gene profiling and/or protein analyses in physiological models (IGF1R transgenic mice, PI3K transgenic mice, and exercise-trained mice) also led to the observation that heat shock protein 70 (Hsp70) expression is elevated in the heart with cardiac IGF1R–PI3K signaling and exercise training.^{24,40} Hsp70 plays a key role in the cellular stress response.¹ Based on this work, we assessed the therapeutic potential of a small molecule which was a known co-inducer of Hsp70 in a mouse model with heart failure and atrial fibrillation. The small molecule (BGP-15) improved heart

function, reduced arrhythmia and was associated with lower cardiac fibrosis. Unexpectedly, the small molecule appeared to provide benefit via phosphorylation of IGF1R, which was independent of Hsp70.⁸¹

8. Concluding remarks

The benefits of regular physical activity are well-known and represent an accessible intervention that can improve cardiac function and reverse cardiac remodeling in a setting of heart failure. However, patient adherence to exercise is a significant issue. Thus, alternative strategies for recapitulating some of the key benefits of exercise on the heart are of substantial interest. Characterizing mouse models with altered cardiac PI3K activity under basal and disease settings have provided an invaluable tool to identify molecular distinctions between the healthy and diseased heart because PI3K is a critical regulator of physiological cardiac hypertrophy but not pathological hypertrophy. This has allowed for the discovery of novel targets for the treatment of heart failure. Furthermore, the importance of PI3K activity for maintaining cardiac function should be taken into consideration when evaluating the viability of therapies that act to reduce activity of the IGF1–PI3K pathway, as these may cause cardiotoxicity in more vulnerable patients with other conditions such as diabetes and hypertension.

Acknowledgments

All authors are supported by the Victorian Government's Operational Infrastructure Support Program. SBS is supported by a joint Baker Heart and Diabetes Institute–La Trobe University doctoral scholarship. JRM is supported by a National Health and Medical Research Council Senior Research Fellowship (Grant No. 1078985).

Authors' contributions

SBS and JRM drafted the manuscript; CMKT contributed to editing the paper. All authors contributed to the generation of figures. All authors have read and approved the final version of the manuscript, and agree with the order of presentation of the authors.

Competing interests

The authors declare they have no competing interests.

References

- Bernardo BC, Ooi JYY, Weeks KL, Patterson NL, McMullen JR. Understanding key mechanisms of exercise-induced cardiac protection to mitigate disease: current knowledge and emerging concepts. *Physiol Rev* 2018;**98**:419–75.
- Myers J. Cardiology patient pages. Exercise and cardiovascular health. *Circulation* 2003;**107**:e2–5.
- Gielen S, Laughlin MH, O'Conner C, Duncker DJ. Exercise training in patients with heart disease: review of beneficial effects and clinical recommendations. *Prog Cardiovasc Dis* 2015;**57**:347–55.
- Reddy KS. Global Burden of Disease Study 2015 provides GPS for global health 2030. *The Lancet* 2016;**388**:1448–9.
- Virani SS, Alonso A, Benjamin EJ, et al. Heart disease and stroke statistics-2020 update: a report from the American Heart Association. *Circulation* 2020;**141**:e139–596.
- Giannuzzi P, Temporelli PL, Corrà U, Tavazzi L, ELVD-CHF Study Group. Antiremodeling effect of long-term exercise training in patients with stable chronic heart failure: results of the Exercise in Left Ventricular Dysfunction and Chronic Heart Failure (ELVD-CHF) Trial. *Circulation* 2003;**108**:554–9.
- Wisløff U, Støylen A, Loennechen JP, et al. Superior cardiovascular effect of aerobic interval training versus moderate continuous training in heart failure patients: a randomized study. *Circulation* 2007;**115**:3086–94.
- Henschen S. Cross country skiing and ski racing: a medical sports study. (Skilanglauf und Skidwettlauf. Eine medizinische Sporstudie). *Mit Med Klin Upsala* 1899;**2**:15–8. [in German].
- Pluim BM, Zwiderman AH, van der Laarse A, van der Wall EE. The athlete's heart. A meta-analysis of cardiac structure and function. *Circulation* 2000;**101**:336–44.
- Whyte GP, George K, Nevill A, Shave R, Sharma S, McKenna WJ. Left ventricular morphology and function in female athletes: a meta-analysis. *Int J Sports Med* 2004;**25**:380–3.
- Nishimura T, Yamada Y, Kawai C. Echocardiographic evaluation of long-term effects of exercise on left ventricular hypertrophy and function in professional bicyclists. *Circulation* 1980;**61**:832–40.
- Maillet M, van Berlo JH, Molkentin JD. Molecular basis of physiological heart growth: fundamental concepts and new players. *Nat Rev Mol Cell Biol* 2013;**14**:38–48.
- Bernardo BC, Weeks KL, Pretorius L, McMullen JR. Molecular distinction between physiological and pathological cardiac hypertrophy: experimental findings and therapeutic strategies. *Pharmacol Ther* 2010;**128**:191–227.
- Eijsvogels TM, Fernandez AB, Thompson PD. Are there deleterious cardiac effects of acute and chronic endurance exercise. *Physiol Rev* 2016;**96**:99–125.
- Poole DC, Copp SW, Colburn TD, et al. Guidelines for animal exercise and training protocols for cardiovascular studies. *Am J Physiol Heart Circ Physiol* 2020;**318**:H1100–38.
- Egerman MA, Glass DJ. Signaling pathways controlling skeletal muscle mass. *Crit Rev Biochem Mol Biol* 2014;**49**:59–68.
- Ferretti R, Moura EG, Dos Santos VC, et al. High-fat diet suppresses the positive effect of creatine supplementation on skeletal muscle function by reducing protein expression of IGF-PI3K-AKT-mTOR pathway. *PLoS One* 2018;**13**:e0199728. doi:10.1371/journal.pone.0199728.
- Barclay RD, Burd NA, Tyler C, Tillin NA, Mackenzie RW. The role of the IGF-1 signaling cascade in muscle protein synthesis and anabolic resistance in aging skeletal muscle. *Front Nutr* 2019;**6**:146. doi:10.3389/fnut.2019.00146.
- Mysoet J, Canu MH, Cieniewski-Bernard C, Bastide B, Dupont E. Hypoactivity affects IGF-1 level and PI3K/AKT signaling pathway in cerebral structures implied in motor control. *PLoS One* 2014;**9**:e107631. doi:10.1371/journal.pone.0107631.
- Lin JY, Kuo WW, Baskaran R, et al. Swimming exercise stimulates IGF1/PI3K/Akt and AMPK/SIRT1/PGC1alpha survival signaling to suppress apoptosis and inflammation in aging hippocampus. *Aging (Albany NY)* 2020;**12**:6852–64.
- Neri Serneri GG, Boddi M, Modesti PA, et al. Increased cardiac sympathetic activity and insulin-like growth factor-I formation are associated with physiological hypertrophy in athletes. *Circ Res* 2001;**89**:977–82.
- Troncoso R, Ibarra C, Vicencio JM, Jaimovich E, Lavandero S. New insights into IGF-1 signaling in the heart. *Trends Endocrinol Metab* 2014;**25**:128–37.
- Kim J, Wende AR, Sena S, et al. Insulin-like growth factor I receptor signaling is required for exercise-induced cardiac hypertrophy. *Mol Endocrinol* 2008;**22**:2531–43.
- McMullen JR, Shioi T, Huang WY, et al. The insulin-like growth factor I receptor induces physiological heart growth via the phosphoinositide 3-kinase(p110α) pathway. *J Biol Chem* 2004;**279**:4782–93.
- Weeks KL, Bernardo BC, Ooi JYY, Patterson NL, McMullen JR. The IGF1-PI3K-Akt signaling pathway in mediating exercise-induced cardiac hypertrophy and protection. *Adv Exp Med Biol* 2017;**1000**:187–210.
- Fruman DA, Chiu H, Hopkins BD, Bagrodia S, Cantley LC, Abraham RT. The PI3K pathway in human disease. *Cell* 2017;**170**:605–35.
- Gulluni F, De Santis MC, Margaria JP, Martini M, Hirsch E. Class II PI3K functions in cell biology and disease. *Trends Cell Biol* 2019;**29**:339–59.
- Ohashi Y, Tremel S, Williams RL. VPS34 complexes from a structural perspective. *J Lipid Res* 2019;**60**:229–41.
- Jean S, Kiger AA. Classes of phosphoinositide 3-kinases at a glance. *J Cell Sci* 2014;**127**:923–8.
- Sawyer C, Sturge J, Bennett DC, et al. Regulation of breast cancer cell chemotaxis by the phosphoinositide 3-kinase p110δ. *Cancer Res* 2003;**63**:1667–75.
- Ghigo A, Li M. Phosphoinositide 3-kinase: friend and foe in cardiovascular disease. *Front Pharmacol* 2015;**6**:169. doi:10.3389/fphar.2015.00169.
- Leevers SJ, Weinkove D, MacDougall LK, Hafen E, Waterfield MD. The Drosophila phosphoinositide 3-kinase Dp110 promotes cell growth. *EMBO J* 1996;**15**:6584–94.
- Weinkove D, Neufeld TP, Twardzik T, Waterfield MD, Leevers SJ. Regulation of imaginal disc cell size, cell number and organ size by Drosophila class I(A) phosphoinositide 3-kinase and its adaptor. *Curr Biol* 1999;**9**:1019–29.
- Shioi T, Kang PM, Douglas PS, et al. The conserved phosphoinositide 3-kinase pathway determines heart size in mice. *EMBO J* 2000;**19**:2537–48.
- McMullen JR, Shioi T, Zhang L, et al. Phosphoinositide 3-kinase(p110α) plays a critical role for the induction of physiological, but not pathological, cardiac hypertrophy. *Proc Natl Acad Sci U S A* 2003;**100**:12355–60.
- McMullen JR, Amirahmadi F, Woodcock EA, et al. Protective effects of exercise and phosphoinositide 3-kinase(p110α) signaling in dilated and hypertrophic cardiomyopathy. *Proc Natl Acad Sci U S A* 2007;**104**:612–7.
- Pretorius L, Du XJ, Woodcock EA, et al. Reduced phosphoinositide 3-kinase (p110α) activation increases the susceptibility to atrial fibrillation. *Am J Pathol* 2009;**175**:998–1009.

38. Lin RC, Weeks KL, Gao XM, et al. PI3K(p110 α) protects against myocardial infarction-induced heart failure: identification of PI3K-regulated miRNA and mRNA. *Arterioscler Thromb Vasc Biol* 2010;**30**:724–32.
39. Ritchie RH, Love JE, Huynh K, et al. Enhanced phosphoinositide 3-kinase (p110 α) activity prevents diabetes-induced cardiomyopathy and superoxide generation in a mouse model of diabetes. *Diabetologia* 2012;**55**:3369–81.
40. Weeks KL, Gao X, Du XJ, et al. Phosphoinositide 3-kinase p110 α is a master regulator of exercise-induced cardioprotection and PI3K gene therapy rescues cardiac dysfunction. *Circ Heart fail* 2012;**5**:523–34.
41. Prakoso D, De Blasio MJ, Qin C, et al. Phosphoinositide 3-kinase (p110 α) gene delivery limits diabetes-induced cardiac NADPH oxidase and cardiomyopathy in a mouse model with established diastolic dysfunction. *Clin Sci (Lond)* 2017;**131**:1345–60.
42. Cook JA, Shah KB, Quader MA, et al. The total artificial heart. *J Thorac Dis* 2015;**7**:2172–80.
43. Cuffe M. The patient with cardiovascular disease: treatment strategies for preventing major events. *Clin Cardiol* 2006;**29**: II4–12.
44. McMurray JJ, Packer M, Desai AS, et al. Angiotensin-neprilysin inhibition versus enalapril in heart failure. *N Engl J Med* 2014;**371**:993–1004.
45. Wang D, Tai PWL, Gao G. Adeno-associated virus vector as a platform for gene therapy delivery. *Nat Rev Drug Discov* 2019;**18**:358–78.
46. Bass-Stringer S, Bernardo BC, May CN, Thomas CJ, Weeks KL, McMullen JR. Adeno-associated virus gene therapy: translational progress and future prospects in the treatment of heart failure. *Heart Lung Circ* 2018;**27**:1285–300.
47. Clinical Trials US National Library of Medicine. Investigation of the Safety and Feasibility of AAV1/SERCA2a Gene Transfer in Patients With Chronic Heart Failure (SERCA-LVAD). ClinicalTrials.gov Identifier: NCT00534703. First posted: September 26, 2007.
48. Clinical Trials US National Library of Medicine. AAV1-CMV-Serca2a GENE Therapy Trial in Heart Failure (AGENTHF). ClinicalTrials.gov Identifier: NCT01966887. First posted: October 22, 2013.
49. Jaski BE, Jessup ML, Mancini DM, Cappola TP, Pauly DF, Greenberg B, et al. Calcium Upregulation by Percutaneous Administration of Gene Therapy in Cardiac Disease (CUPID Trial), a first-in-human phase 1/2 clinical trial. *J Card Fail* 2009;**15**:171–81.
50. Jessup M, Greenberg B, Mancini D, et al. Calcium Upregulation by Percutaneous Administration of Gene Therapy in Cardiac Disease (CUPID): a phase 2 trial of intracoronary gene therapy of sarcoplasmic reticulum Ca²⁺-ATPase in patients with advanced heart failure. *Circulation* 2011;**124**:304–13.
51. Greenberg B, Butler J, Felker GM, et al. Calcium Upregulation by Percutaneous Administration of Gene Therapy in Patients with Cardiac Disease (CUPID 2): a randomised, multinational, double-blind, placebo-controlled, phase 2b trial. *Lancet* 2016;**387**:1178–86.
52. Wojno AP, Pierce EA, Bennett J. Seeing the light. *Sci Transl Med* 2013;**5**:175fs8. doi:10.1126/scitranslmed.3005798.
53. Prakoso D, De Blasio MJ, Tate M, et al. Gene therapy targeting cardiac phosphoinositide 3-kinase (p110 α) attenuates cardiac remodeling in type 2 diabetes. *Am J Physiol Heart Circ Physiol* 2020;**318**:H840–52.
54. Okkenhaug K, Graupera M, Vanhaesebroeck B. Targeting PI3K in cancer: impact on tumor cells, their protective stroma, angiogenesis, and immunotherapy. *Cancer Discov* 2016;**6**:1090–105.
55. Fruman DA, Rommel C. PI3K and cancer: lessons, challenges and opportunities. *Nat Rev Drug Discov* 2014;**13**:140–56.
56. Yang J, Nie J, Ma X, Wei Y, Peng Y, Wei X. Targeting PI3K in cancer: mechanisms and advances in clinical trials. *Mol Cancer* 2019;**18**:26. doi:10.1186/s12943-019-0954-x.
57. Zincarelli C, Soltys S, Rengo G, Koch WJ, Rabinowitz JE. Comparative cardiac gene delivery of adeno-associated virus serotypes 1–9 reveals that AAV6 mediates the most efficient transduction in mouse heart. *Clin Transl Sci* 2010;**3**:81–9.
58. Palomeque J, Chemaly ER, Colosi P, et al. Efficiency of eight different AAV serotypes in transducing rat myocardium in vivo. *Gene Ther* 2007;**14**:989–97.
59. Wang Z, Zhu T, Qiao C, et al. Adeno-associated virus serotype 8 efficiently delivers genes to muscle and heart. *Nat Biotechnol* 2005;**23**:321–8.
60. Gao G, Bish LT, Sleeper MM, et al. Transendocardial delivery of AAV6 results in highly efficient and global cardiac gene transfer in rhesus macaques. *Hum Gene Ther* 2011;**22**:979–84.
61. Bish LT, Morine K, Sleeper MM, et al. Adeno-associated virus (AAV) serotype 9 provides global cardiac gene transfer superior to AAV1, AAV6, AAV7, and AAV8 in the mouse and rat. *Hum Gene Ther* 2008;**19**:1359–68.
62. Prasad KM, Xu Y, Yang Z, Acton ST, French BA. Robust cardiomyocyte-specific gene expression following systemic injection of AAV: *in vivo* gene delivery follows a Poisson distribution. *Gene Ther* 2011;**18**:43–52.
63. Aucoin MG, Perrier M, Kamen AA. Critical assessment of current adeno-associated viral vector production and quantification methods. *Biotechnol Adv* 2008;**26**:73–88.
64. Kotin RM. Large-scale recombinant adeno-associated virus production. *Hum Mol Genet* 2011;**20**:R2–6.
65. Denduluri SK, Idowu O, Wang Z, Liao Z, Yan Z, Mohammed MK, et al. Insulin-like growth factor (IGF) signaling in tumorigenesis and the development of cancer drug resistance. *Genes Dis* 2015;**2**:13–25.
66. Dubska L, Andera L, Sheard MA. HER2 signaling downregulation by trastuzumab and suppression of the PI3K/Akt pathway: an unexpected effect on TRAIL-induced apoptosis. *FEBS Lett* 2005;**579**:4149–58.
67. Zeglinski M, Ludke A, Jassal DS, Singal PK. Trastuzumab-induced cardiac dysfunction: a “dual-hit”. *Exp Clin Cardiol* 2011;**16**:70–4.
68. Slamon DJ, Leyland-Jones B, Shak S, et al. Use of chemotherapy plus a monoclonal antibody against HER2 for metastatic breast cancer that overexpresses HER2. *N Engl J Med* 2001;**344**:783–92.
69. Mohan N, Jiang J, Dokmanovic M, Wu WJ. Trastuzumab-mediated cardiotoxicity: current understanding, challenges, and frontiers. *Antib Ther* 2018;**1**:13–7.
70. Rizzi F, Bettuzzi S. The clusterin paradigm in prostate and breast carcinogenesis. *Endocr Relat Cancer* 2010;**17**:R1–17.
71. Panico F, Rizzi F, Fabbri LM, Bettuzzi S, Luppi F. Clusterin (CLU) and lung cancer. *Adv Cancer Res* 2009;**105**:63–76.
72. Bass-Stringer S, Ooi JYY, McMullen JR. Clusterin is regulated by IGF1-PI3K signaling in the heart: implications for biomarker and drug target discovery, and cardiotoxicity. *Arch Toxicol* 2020;**94**:1763–8.
73. McMullen JR, Boey EJ, Ooi JY, Seymour JF, Keating MJ, Tam CS. Ibrutinib increases the risk of atrial fibrillation, potentially through inhibition of cardiac PI3K-Akt signaling. *Blood* 2014;**124**:3829–30.
74. Efremov DG, Wiestner A, Laurenti L. Novel agents and emerging strategies for targeting the B-cell receptor pathway in CLL. *Mediterr J Hematol Infect Dis* 2012;**4**: e2012067. doi:10.4084/MJHID.2012.067.
75. Bernardo BC, Weeks KL, Pongsukwechkul T, et al. Gene delivery of medium chain acyl-coenzyme A dehydrogenase induces physiological cardiac hypertrophy and protects against pathological remodeling. *Clin Sci (Lond)* 2018;**132**:381–97.
76. Bernardo BC, Gao XM, Winbanks CE, et al. Therapeutic inhibition of the miR-34 family attenuates pathological cardiac remodeling and improves heart function. *Proc Natl Acad Sci U S A* 2012;**109**:17615–20.
77. Bernardo BC, Nguyen SS, Gao XM, et al. Inhibition of miR-154 protects against cardiac dysfunction and fibrosis in a mouse model of pressure overload. *Sci Rep* 2016;**6**:22442. doi:10.1038/srep22442.
78. Bernardo BC, Nguyen SS, Winbanks CE, et al. Therapeutic silencing of miR-652 restores heart function and attenuates adverse remodeling in a setting of established pathological hypertrophy. *FASEB J* 2014;**28**:5097–110.
79. Tham YK, Huynh K, Mellett NA, et al. Distinct lipidomic profiles in models of physiological and pathological cardiac remodeling, and potential therapeutic strategies. *Biochim Biophys Acta Mol Cell Biol Lipids* 2018;**1863**:219–34.
80. Tham YK, Bernardo BC, Huynh K, et al. Lipidomic profiles of the heart and circulation in response to exercise versus cardiac pathology: a resource of potential biomarkers and drug targets. *Cell Rep* 2018;**24**:2757–72.
81. Sapra G, Tham YK, Cemerlang N, et al. The small-molecule BGP-15 protects against heart failure and atrial fibrillation in mice. *Nat Commun* 2014;**5**:5705. doi:10.1038/ncomms6705.

Chapter 1. Part 2

Adeno-Associated Virus Gene Therapy: Translational Progress and Future Prospects in the Treatment of Heart Failure

Published in 'Heart, Lung and Circulation' March 2018 by S Bass-Stringer, BC Bernardo, CN May, CJ Thomas, KL Weeks and JR McMullen.

Heart, Lung and Circulation gives permission to reproduce this work as an academic thesis by the authors.

As first author, S Bass-Stringer contributed ~70% to this publication. This included contributions to the conception, drafting, design and editing.

Adeno-Associated Virus Gene Therapy: Translational Progress and Future Prospects in the Treatment of Heart Failure



Sebastian Bass-Stringer, BSc (Hons)^{a,b}, Bianca C. Bernardo, PhD^{a,c,d},
Clive N. May, PhD^e, Colleen J. Thomas, PhD^{b,e}, Kate L. Weeks, PhD^{a,d,**},
Julie R. McMullen, PhD^{a,b,d,f*}

^aBaker Heart and Diabetes Institute, Melbourne, Vic, Australia

^bDepartment of Physiology, Anatomy and Microbiology, La Trobe University, Melbourne, Vic, Australia

^cDepartment of Paediatrics, University of Melbourne, Melbourne, Vic, Australia

^dDepartment of Diabetes, Central Clinical School, Monash University, Melbourne, Vic, Australia

^eFlorey Institute of Neuroscience and Mental Health, University of Melbourne, Melbourne, Vic, Australia

^fDepartment of Physiology and Department of Medicine Alfred Hospital, Monash University, Melbourne, Vic, Australia

Received 31 January 2018; accepted 3 March 2018; online published-ahead-of-print 17 March 2018

Despite advances in treatment over the past decade, heart failure remains a significant public health burden and a leading cause of death in the developed world. Gene therapy provides a promising approach for preventing and reversing cardiac abnormalities, however, clinical application has shown limited success to date. A substantial effort is being invested into the development of recombinant adeno-associated viruses (AAVs) for cardiac gene therapy as AAV gene therapy offers a high safety profile and provides sustained and efficient transgene expression following a once-off administration. Due to the physiological, anatomical and genetic similarities between large animals and humans, preclinical studies using large animal models for AAV gene therapy are crucial stepping stones between the laboratory and the clinic. Many molecular targets selected to treat heart failure using AAV gene therapy have been chosen because of their potential to regulate and restore cardiac contractility. Other genes targeted with AAV are involved with regulating angiogenesis, beta-adrenergic sensitivity, inflammation, physiological signalling and metabolism. While significant progress continues to be made in the field of AAV cardiac gene therapy, challenges remain in overcoming host neutralising antibodies, improving AAV vector cardiac-transduction efficiency and selectivity, and optimising the dose, route and method of delivery.

Keywords

Adeno-associated virus • Heart failure • Gene therapy • Large animal models

Introduction

Chronic heart failure (HF) is the final clinical presentation of a variety of cardiovascular diseases and is a leading cause of morbidity and mortality, with a prevalence of over 26 million

individuals afflicted worldwide [1]. HF remains a significant health burden in developed countries with a 5-year survival rate of ~50% following initial diagnosis [2]. Treatment options for HF are limited and existing therapeutic interventions largely delay disease progression and manage

*Corresponding author at: Cardiac Hypertrophy Laboratory, Baker Heart and Diabetes Institute, 75 Commercial Road, Melbourne, Vic 3004, Australia. Tel.: +61 3 8532 1194, Fax: +61 8532 1100., Email: julie.mcmullen@baker.edu.au

**Corresponding author at: Cardiac Hypertrophy Laboratory, Baker Heart and Diabetes Institute, 75 Commercial Road, Melbourne, Vic 3004, Australia. Tel.: +61 3 8532 1205, Fax: +61 8532 1100., Email: kate.weeks@baker.edu.au

© 2018 Australian and New Zealand Society of Cardiac and Thoracic Surgeons (ANZSCTS) and the Cardiac Society of Australia and New Zealand (CSANZ). Published by Elsevier B.V. All rights reserved.

symptoms. In recent years, gene therapy has arisen as a promising therapeutic avenue for the treatment of HF, with numerous studies reporting positive effects on cardiac function in small animal models. However, translating this success to large animal models and to clinical trials has proven to be more challenging. Given the physiological differences between small animals, large animals and humans, translating and optimising gene delivery systems for large animal models, and in turn human subjects, is a crucial step in utilising gene therapy as a therapeutic strategy for the treatment of HF and other cardiovascular diseases. The purpose of this review is to provide an update on current advances in recombinant adeno-associated virus (AAV) gene therapy for the treatment of HF, with emphasis on the progression towards clinical translation, as well as current approaches for optimising efficacy and therapeutic benefit.

AAV as a Vector for Gene Therapy

Gene therapy can broadly be described as the transfer of an isolated nucleic acid sequence to alter gene expression, and, in turn, provide a therapeutic effect, in an individual in a diseased state. Viral particles have been modified to be non-pathogenic and non-replicative. These modified virions have been the primary vectors utilised for gene transfer due to their natural affinity to integrate their genetic material into the cells of a host organism [3]. Adenovirus, lentivirus and AAV have been the viral vectors of choice for gene therapy to date [4,5]. However, plasmid vectors, non-coding RNAs and Cluster Regularly Interspaced Short Palindromic Repeat (CRISPR)-based gene transfer have also shown promise as potential avenues for gene manipulation [6,7]. This review will focus on the use of AAV vectors for gene therapy.

Adeno-associated viruses are small, single-stranded, non-pathogenic viruses with non-enveloped protein capsids that can be used to deliver DNA constructs up to ~5 kb in size [8]. The limited packaging capacity of AAVs presents a disadvantage, although a number of strategies have been devised to deliver transgene products that exceed 5 kb [9]. AAVs can incorporate their genome into both dividing and non-dividing cells; the viral genome primarily exists within the nucleus, independent of chromosomal DNA (Figure 1) [10]. AAVs have gained prominence as one of the leading gene delivery vectors in clinical development. The popularity of AAVs primarily arises from their positive safety profile compared with alternative viral vectors, as AAVs are non-pathogenic in human hosts and cause only a very mild immune response [11,12]. Of relevance for cardiac gene delivery, AAVs are also advantageous because of their potential for mediating longer-term transgene expression in small and large animals (capable of expression for >1 year in non-proliferating cells following a once-off delivery of AAV vector) [13–16]. Comparatively, transgene expression of alternative vectors such as adenoviruses has been shown to return to baseline within 3 to 4 weeks [17]. AAV gene therapy shows

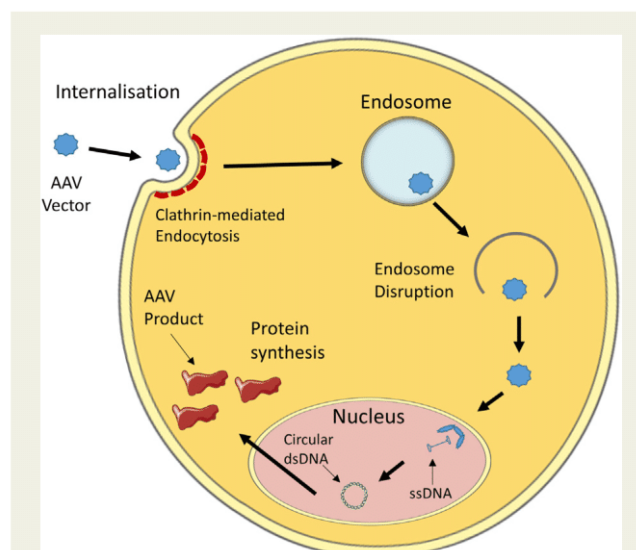


Figure 1 Entry of AAV in cells and transduction of adeno-associated virus (AAV). AAV vectors for gene delivery enter cells through clathrin receptor-mediated endocytosis. Within the cell conformational changes to the AAV capsid can cause the endosome to break, allowing the AAV to enter the cytosol. The AAV inserts its genetic material into the nucleus via nuclear pore complexes, where it is transcribed and then translated into functional protein.

promise as a future treatment for cardiovascular disease; HF has been a primary target to date but treatment of other cardiovascular diseases such as atrial fibrillation are also showing exciting advances [18].

AAV Vector Selection and Design

Numerous AAV serotypes have been discovered, many of which display tissue-specific tropism. AAV serotypes differ in their presentation of AAV capsid protein structures, which in turn influences tissue tropism and transduction efficiency [19]. Cardiac tropism and transduction efficiency are critical aspects of an effective gene delivery system for the treatment of HF, to ensure both efficient cardiac transduction of viral vectors and to minimise undesirable gene delivery to other organs.

To date, more than 100 AAV variants have been identified and isolated [20]. Comparison of the effectiveness of the nine most well-studied AAV serotypes (AAV1-AAV9) to deliver a luciferase reporter in mice revealed that AAV6, AAV2 and AAV9 were the most cardiotropic [20]. AAV6 displayed the best transduction and cardiac tropism, with a 4000-fold increase in luciferase enzyme activity in the heart compared with the liver. In contrast, AAV9 and AAV2 each produced a less than 100-fold increase in cardiac luciferase activity compared with other tissues [20]. Findings by Palomeque *et al.* [21] in rats and by Wang *et al.* [22] in mice were consistent with these results for AAV6. Furthermore, transendocardial delivery of AAV6, 8 and 9 in rhesus monkeys found AAV6 to be the most cardiotropic of the three serotypes [23]. In

contrast, a comparative study in neonatal mice found AAV9 to accomplish superior global cardiac gene transfer to AAVs 1, 6, 7 and 8, for up to 1 year [24]. Thus, AAV6 and AAV9 have emerged as the AAV serotypes of choice for studies in which cardiac-selective expression is desired. AAV pseudotyping is one method which has been used to improve cardiac tropism of AAVs. Muller et al. [25] found that cross-packaging the genome of AAV2 into the AAV6 capsid (rAAV2/6) increased efficiency of cardiac transduction approximately 10-fold in adult mice. Similar improvements in cardiac transduction have been displayed using an AAV 2/9 vector in non-human primates [26].

Chimeric Vectors

Another approach to improve cardiac efficiency and tropism has been the development of chimeric AAV vectors. Asokan et al. [27] created AAV2i8 by replacing a hexapeptide sequence from AAV2 with the homologous sequence from AAV8. The AAV2/AAV8 chimera, designated AAV2i8, displayed greater tropism towards cardiac and skeletal muscle in mice, whilst transduction of the liver was noticeably reduced. Pulicherla et al. [28] used random mutagenesis of capsid protein residues from AAV9 to develop AAV chimeric variants. This method was effective at reducing off-target liver transduction, with variants AAV9.45 and 9.61 showing a 10 to 25-fold reduction in liver transduction, whilst maintaining a cardiac transduction efficiency on par with AAV9. Yang et al. [29] used a directed evolution approach to develop the cardiotropic chimera AAVM41. By shuffling the DNA of capsids from numerous serotypes and selecting for AAV variants that target muscle, AAVM41 was generated and found to be more efficient at transducing the heart than AAV6, whilst having a dramatically reduced affinity for liver transduction in mice [28]. Studies using cardiotropic AAV chimeras suggest that these will be promising due to their improvement of transduction efficiency and cardiac tropism, and ability to circumvent the humoral immune reaction (discussed later), but assessment in large animal models will be a crucial step in determining their translational potential as therapeutic tools for the treatment of HF.

Cardiac-Specific Promoters and Cardiac-Selective Transduction

Cardiac-selective expression can also be achieved through the inclusion of cardiac-specific promoters. The cytomegalovirus (CMV) promoter has been a benchmark promoter for AAV gene therapy due to its capacity to drive robust expression of downstream gene elements, but it may be less suited to clinical applications as it drives expression in a wide range of tissue and cell types [30]. That being said, the CMV promoter may still be favourable for AAV-based transduction as its use in conjunction with a cardiotropic AAV serotype, such as AAV6, can facilitate both cardiac-selective transduction and high levels of recombinant gene expression [20,31,32]. Cardiac-specific promoters, such as

the α -myosin heavy chain (α MHC) promoter, have been shown to provide greater cardiac specificity than the CMV promoter following systemic delivery of rAAV2/9 in mice [33]. However, expression of the delivered reporter gene was significantly lower with these promoters compared with the CMV promoter [30]. A myosin light chain (MLC) promoter in an AAV9 vector promoted expression of the delivered DNA construct exclusively in cardiac tissue [34], and elements of the MLC promoter have been used to enhance the cardiac selectivity of the CMV promoter, resulting in robust protein expression of the transgene exclusively in the heart [35]. Portions of the promoter and enhancer from the human cardiac troponin T (cTnT) gene have been used in an AAV6 vector to increase cardiotropic expression in rodent and swine models [36,37]. The cTnT promoter has also shown promise in an AAV9 vector in mice [38].

Disease-Induced Promoters

Disease-specific promoters may offer an even safer alternative to cardiac-specific promoters, by limiting expression of the therapeutic gene to the particular cells that have changed due to the diseased state. Woitek et al. [39] recently demonstrated this in a canine model of HF induced by left ventricular (LV) pacing. AAV9 was used to deliver vascular endothelial growth factor (VEGF)-B under transcriptional control of the CMV promoter or an atrial natriuretic factor (ANF) promoter. ANF (also known as atrial natriuretic peptide, ANP) is rapidly synthesised and released from cardiac myocytes in response to stretch, and is highly expressed in the failing myocardium [40]. Intracoronary delivery of AAV9-CMV-VEGF-B after 2 weeks of pacing halted the progression from compensated to decompensated HF, attenuated pacing-induced increases in LV end-diastolic pressure and preserved contractile function [39]. In a separate cohort of animals, dogs received AAV9-ANF-VEGF-B 2 days before the start of the pacing protocol. VEGF-B expression and functional improvements were observed in animals subjected to pacing, but not in control animals (no pacing) or in dogs that were allowed to recover for 2 weeks post-pacing, reflecting activity of the ANF promoter. This study provides proof of concept that the use of disease-specific promoters is a powerful strategy for the temporal and spatial regulation of therapeutic genes delivered by AAVs. The capability to exclusively target diseased tissue would provide a safeguard to ensure undesirable transgene expression does not occur in healthy tissue, but would also prevent ongoing expression following the successful treatment of a disease, which may be an important consideration for some therapeutic genes. Although cardiac and disease-specific promoters show a lot of potential to improve specificity of AAV gene therapy, higher doses of AAV may be required than for those containing ubiquitous promoters, to compensate for the reduced transcriptional efficiency of such promoters.

Overcoming Challenges Associated With AAV Gene Therapy

Neutralising Anti-AAV Antibodies

Vector-specific adaptive immune responses have emerged as a critical obstacle in the translation of AAV gene therapy to clinical settings [41]. One of the most favourable qualities of AAV as a gene therapy vector is its lack of immunogenicity [11]. However, the presence of neutralising anti-AAV antibodies (NAbs) results in a reduction of AAV-transduction rates, while CD8⁺ T cells directed to AAV capsid antigens cause rejection of AAV-transduced cells. This humoral immunity associated with previous infection to natural AAVs, or antibodies generated following use of therapeutic AAVs, has been widely accepted as a necessary hurdle to overcome for successful translation of AAV gene therapies [41–44]. Pre-existing NAbs have been found to exist in a large proportion of the human population, with 30–80% of individuals displaying immunity [45–47]; moreover, the highly conserved nature of AAV capsids permits cross-reactivity across numerous serotypes [48]. During the preclinical stages of AAV gene therapy development, the most common strategy to overcome pre-existing AAV-NAbs is to exclude subjects with high serum titres of neutralising antibodies from the study population, i.e., via pre-screening subjects. For research purposes this is effective and acceptable, but given the large proportion of carriers in the human population and the development of immunity following treatment, new strategies are essential prior to commercialising a gene therapy product. Various strategies have been implemented to attempt to overcome this challenging barrier with varying degrees of success. These include administration of immunosuppressants, plasmapheresis, addition of empty capsids, capsid mutagenesis, and, more recently, AAV-containing exosomes (AAVExo) (Table 1 and Figure 2). Liang and colleagues [49] showed that exosomes can envelope AAVs to shield them from NAbs. AAVExo presented resistance to NAbs *in vivo* in mice [49]. Though strategies for tissue-specific delivery will still be important. In summary, while numerous strategies to overcome host immune responses hold promise, a recurring limitation is that individual approaches mostly lead to a reduction, but rarely elimination, of NAbs (Figure 2). Thus, on present indications, multiple and/or new approaches will be required.

AAV Cardiac Gene Delivery Methods

A crucial factor for optimising the efficiency and specificity of cardiac gene therapy is the method used to deliver a transgene. The chosen vector delivery method may impact transduction efficiency; duration of transgene expression; the degree of systemic dispersion of vectors; as well as homogeneity of vectors within myocardial tissue. Moreover, minimising invasiveness and ensuring a high safety profile for the method is critical, particularly given the compromised health condition of individuals in the advanced stages of HF.

Numerous methods of cardiac delivery have been trialled with varying levels of success. These include: intravenous delivery, retrograde delivery, antegrade intracoronary delivery, intramyocardial delivery, pericardial delivery and delivery via cardiac surgery. From a practical perspective, targeting the coronary system through methods such as antegrade intracoronary delivery and retrograde injection through the coronary sinus may both offer safe, efficient delivery methods in a clinical setting following further optimisation [50]. Cardiac gene delivery methods have been extensively reviewed elsewhere [50–54].

Barriers to Overcome for the Large Scale Manufacture of AAV

Reducing the high cost of manufacturing large doses of AAV vectors is a challenging obstacle to overcome in order to make AAV gene therapy viable for large animal studies, and importantly, a financially realistic therapeutic intervention for patients with HF. Currently, the most well-established method for producing AAV vectors is chemical co-transfection of HEK 293 cells with plasmids [55]. This is inefficient for clinical studies, which may require 10¹⁵ viral particles per subject. Using a suspension culture as an alternative to growing adherent cells has been shown to increase the yield of AAV particles five-fold [56]. Adeno-associated virus particle yield may also be increased by developing viral particles in different cell types. Sf9 cells in conjunction with helper baculoviruses have been shown to provide more efficient viral replication of AAV2 compared with HEK 293 cells, which in turn, increases total viral production per cell [57]. One litre of Sf9 cells has been shown to produce the equivalent number of vectors as 500–1000 175 cm² flasks of HEK 293 cells [57].

AAV Gene Therapy Studies in Large Animal Models of Heart Failure

Numerous studies have shown AAV gene therapy to be a feasible strategy for the treatment of HF in small animal models [58]. However, efficient cardiac transduction and expression of gene products has proven more difficult in large animal models and in human trials. The use of large animal models of HF such as sheep, pig, dog or non-human primates is a valuable translational bridge between the laboratory and the clinic to validate the efficacy and safety of novel therapeutic treatments. Importantly, many physiological and anatomical cardiovascular features are shared between humans and large animals that may differ between humans and small animal models (Figure 3).

Cardiac gene therapy studies have been performed using large animal models with varying degrees of success. Table 2 provides a summary of AAV gene therapy studies using clinically relevant large animal models for the treatment of HF. Pig and sheep have been the most commonly used given their shared cardiac resemblance to humans.

Table 1 Strategies implemented to overcome neutralising antibodies for cardiac AAV gene therapy in experimental animals and humans.

Approach	Outcome	Benefit	Limitations	Refs.
Screening for the presence of NABs. Exclusion of subjects positive for NABs.	Has proven successful for isolating NAB negative subjects	<ul style="list-style-type: none"> • NAB assays are simple and relatively cheap to perform 	<ul style="list-style-type: none"> • May limit the possibility of follow-up treatment due to the development of immunity after initial treatment with AAV • Substantially restricts the number of potential candidates for treatment 	[44,96]
Simultaneous use of immunosuppressant	B-cell suppression can lead to a moderate reduction in NAB titre in some subjects	<ul style="list-style-type: none"> • Only a short duration of immunosuppressant required (weeks to months) 	<ul style="list-style-type: none"> • Less effective in high NAB titre • Not effective amongst all subjects • Greater risk of infection for patients who may already have compromised health 	[97,98]
Optimise route and method of AAV administration	Saline flushes can reduce contact between AAVs and NABs present in blood	<ul style="list-style-type: none"> • May reduce systemic exposure to AAVs and immune response 	<ul style="list-style-type: none"> • Invasiveness of delivery may compromise safety of HF patients 	[65,99]
Repeated plasmapheresis (removal, filtration and return of blood plasma)	Has facilitated successful AAV gene transfer in the presence of pre-existing NABs	<ul style="list-style-type: none"> • Safe and commonly performed procedure 	<ul style="list-style-type: none"> • Not effective for all serotypes • Limited effectiveness in patients with high NAB titres 	[100,101]
Altering NAB binding epitopes on AAV capsids (targeted mutagenesis to identify and change NAB recognition sites of AAV capsids)	Some AAV vectors with capsid peptide insertions show a lowered affinity for NABs	<ul style="list-style-type: none"> • Modified AAV vectors can maintain their capacity to transduce targeted tissue 	<ul style="list-style-type: none"> • Limited effectiveness, would need to be done in conjunction with other methods • This approach requires more development to be clinically applicable 	[102,103]
Using directed evolution to generate a mutant capsid library and selecting AAVs that can evade NABs	Has shown success in creating vectors that can evade NABs	<ul style="list-style-type: none"> • May exhibit 10–30 fold greater NAB resistance than wild type AAV 	<ul style="list-style-type: none"> • Labour intensive • This approach requires more development to be clinically applicable 	[96,104]
Addition of empty capsids to adsorb NABs	Addition of empty capsids can circumvent NABs and facilitate successful transduction	<ul style="list-style-type: none"> • Safe and cost effective • Effective at high NAB titres 	<ul style="list-style-type: none"> • Potential for empty capsids to become immunogenic 	[92]
Use of AAV-containing exosomes to resist NABs	AAV-containing exosomes showed greater resistance to NABs	<ul style="list-style-type: none"> • Simultaneously showed enhanced transduction and cardiac function in murine HF models 	<ul style="list-style-type: none"> • This approach is novel and requires further development and assessment 	[49]

Abbreviations: AAV, adeno-associated virus; HF, heart failure; NABs, neutralising antibodies.

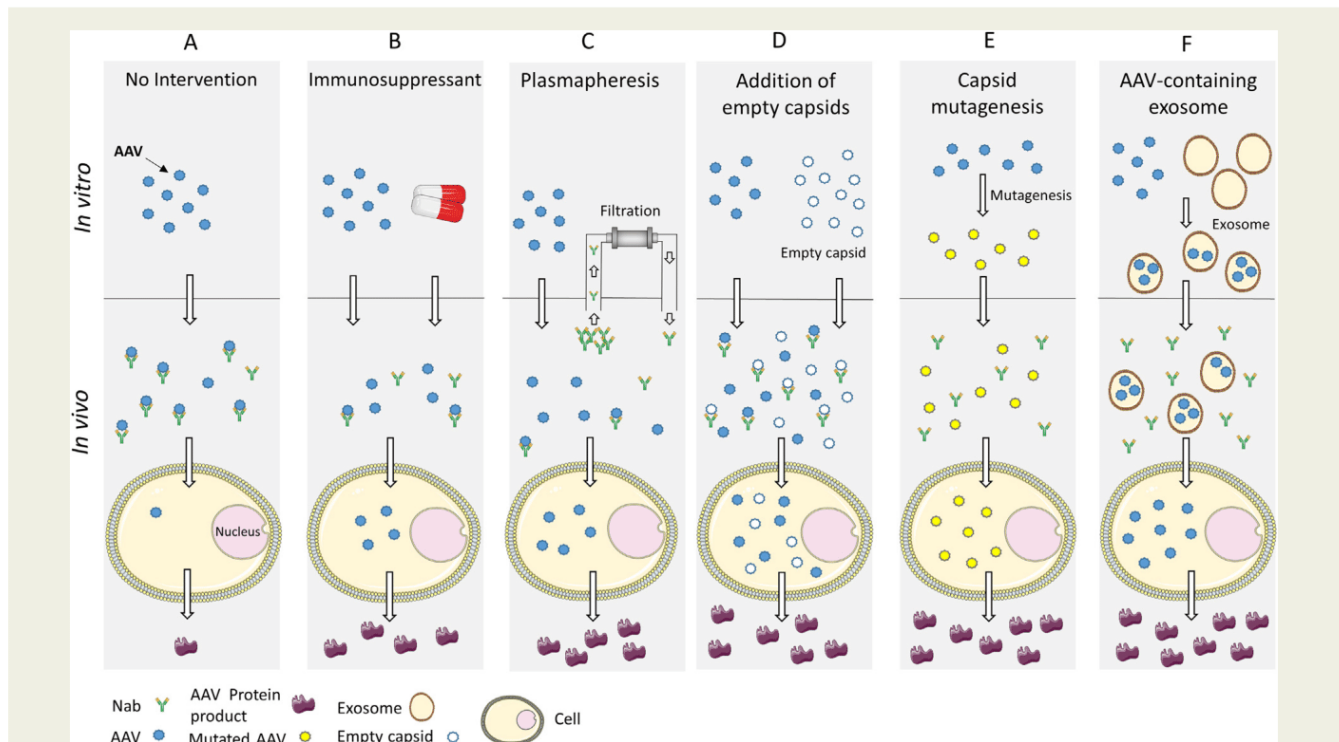


Figure 2 Impact of neutralising antibodies (NAb) on adeno-associated viruses (AAV) vectors and various strategies that have been implemented to overcome neutralisation in AAV sero-positive subjects. (A) In AAV sero-positive subjects, the host humoral immune response neutralises and destroys AAV vectors following administration. This leads to a substantial reduction in AAV transduction leading to limited expression of the AAV protein product. (B) Simultaneous administration of immunosuppressant drugs (e.g. B-cell depletion) with AAV vectors can lead to a reduction in NAb titre and moderately improve transduction leading to more AAV protein. (C) Performing repeated plasmapheresis prior to AAV administration can lead to a reduction in NAb titre and results in a high level of AAV transduction. (D) Simultaneous administration of empty AAV capsids and AAV vectors may act to oversaturate the NAb allowing more vectors to circumvent the NAb and facilitating increased AAV transduction. (E) Altering the immunogenic epitopes on AAV capsids by mutagenesis can result in AAV capsid mutants that have reduced NAb binding affinity. (F) Packaging AAV vectors into exosomes prior to administration may offer a form of transport to import AAV vectors directly into cells without exposure to NAb. N.B. The number of AAV products illustrated represents the potential success of each approach based on current studies. There has been no study directly comparing the five different strategies. The representation is based on multiple references [49,92,97,98,100–103].

Modulation of Molecular Targets With AAV

Here, we describe molecular targets that have been a focus in large animal studies, and introduce some candidates for cardiac AAV gene therapy that have shown promise in mice, with future plans for assessment in large animals (Figure 4). To date, genes related to beta-adrenergic signalling, calcium handling, angiogenesis, physiological signalling, inflammation and metabolism have been targeted (Figure 4 and Table 2).

β -Adrenergic Receptor (β -AR)

Downregulation and desensitisation of β -ARs is a common feature of individuals with HF [59]. β -AR signalling is a critical regulator of cardiac contractility. Disruption or desensitisation of β -ARs leads to upregulation of G-protein-coupled receptor kinases (GRK) [59], which in turn, desensitise β -ARs further through phosphorylation leading to a cycle of

pathological cardiac signalling [60]. β ARKct is an engineered peptide that inhibits GRK-2 via competitive receptor binding, which in turn prevents detrimental phosphorylation. Raake and colleagues [35] inhibited GRK-2 binding using the AAV 6- β ARKct vector to express β ARKct in a pig model of ischaemic HF, which resulted in enhancement of LV haemodynamics and repression of LV remodelling compared to a control [35] (see Table 2 for further details).

Vascular Endothelial Growth Factor (VEGF)

Reduced coronary angiogenesis contributes to the transition of HF [61]. Enhancing angiogenesis by targeting VEGFs (VEGF-A and VEGF-B) has been a candidate for AAV gene therapy in large animal models. Administration of AAV vectors encoding VEGF isoform 165 (VEGF-165) in a canine model induced angiogenesis and arteriogenesis, leading to an enhancement in cardiomyocyte viability compared to controls [62]. Furthermore, AAV gene therapy was used to

Heart rate 500-650 bpm	↑	Heart rate 60-75 bpm	↔	Heart rate 60-90 bpm
Heart weight 100-200 mg	↓	Heart weight 300-400 g	↔	Heart weight 220-400 g
Body weight 20-40 g	↓	Body weight 50-100 kg	↔	Body weight 40-80 kg
Life span 1.5-2 years	↓	Life span 75-90 years	↓	Life span 10-16 years
	↓	Suitability for surgical intervention	↑	
	↓	Genetic heterogeneity	↑	
	↓	Similarity of models to human heart failure	↑	
	↓	Similar cardiac contractile and relaxation kinetics	↑	
	↓	Cost of AAV and required dose	↑	

Figure 3 Comparison of anatomy, physiology and suitability of adeno-associated virus (AAV) gene therapy between mice and humans, and sheep and humans. Arrows on the left compare features of mice to humans and arrows on the right compare features of sheep to humans. Red arrows represent an undesirable difference and green arrows represent a desirable similarity. Presented data is based on multiple references and representative of typical values from adult animals/humans of both sexes [113–124].

administer VEGF in combination with another angiogenic factor, angiopoietin-1, in a pig model of myocardial infarction (MI) [63]. Using the cardiac-specific promoter, MLC, Tao and colleagues [63] showed improvements in cardiac function (Table 2). As discussed previously, AAV9-mediated delivery of VEGF-B isoform 167 attenuated HF progression in dogs subjected to rapid ventricular pacing [39]. This was associated with reduced myocardial apoptosis and the prevention of microvascular rarefaction.

Sarcoplasmic Reticulum Ca^{2+} ATPase2a (SERCA2a)

Decreased activity of SERCA2a contributes to the development of HF [64]. SERCA2a is a calcium pump that causes muscle relaxation and is critical for cardiac contraction [65]. To date, SERCA2a has been the most popular candidate for AAV gene therapy in large animal models for the treatment of HF, with multiple studies in large animal models using a variety of AAV vectors successfully reducing the severity of HF (Table 2). For example, SERCA2a delivery using an AAV6 vector with a CMV promoter in a sheep model of HF [66] led

to better cardiac outcomes in comparison to the control group. Ongoing success in large animal models has led to SERCA2a being one of the first AAV gene therapy molecular targets to be clinically trialled [67–69].

Small Ubiquitin-Related Modifier 1 (SUMO1)

SUMO1 is a post-transcriptional modification protein that acts to stabilise and protect SERCA2a through a process known as SUMOylation [70]. Myocardial SUMO1 is decreased in mouse models of HF [71]. Administration of AAV1-SUMO1 in an ischaemic HF pig model was associated with better LV ejection fraction compared to the control [71] (Table 2).

S100 Calcium-Binding Protein A1 (S100A1)

S100A1 is a calcium binding protein that interacts with numerous calcium regulatory proteins including SERCA2a within cardiomyocytes to enhance calcium homeostasis [72]. It also plays a role in enhancing filament sliding and muscle contraction, reducing apoptosis, as well as inhibiting both

Table 2 AAV gene therapy studies for the treatment of HF in clinically relevant large animal models.

Molecular Target	Animal Model	Disease Model	Promoter/ Dose (vg)	Sex	N ^a	AAV Vector	Delivery Method	Pathway	Outcome	Ref. Year
β ARKKct	Pig	Ischaemic heart failure	CMV- MLC 1×10^{13}	NS	10/10	AAV6- β ARKKct	Retrograde injection into coronary veins	Beta-adrenergic	Time after delivery: 42 days <ul style="list-style-type: none"> Long-term and robust βARKKct expression Amelioration of LV haemodynamics and repressed LV remodelling compared to control Normalisation of neurohormones that are elevated during HF 	[35] 2013
VEGF-B167	Dog	Dilated cardiomyopathy	CMV/ ANF 1×10^{13} 2×10^{13} 5×10^{13}	M	33/20	AAV9-VEGF-B	Intracoronary delivery	Angiogenesis	Time after delivery: 28 days <ul style="list-style-type: none"> Preserved diastolic and contractile function Repressed ventricular chamber remodelling 	[39] 2015
VEGF-A165	Dog	Acute myocardial infarction	CMV 5×10^{12}	M	6/6	AAV2-VEGFA165	Direct injection to intra-myocardium	Angiogenesis	Time after delivery: 28 days <ul style="list-style-type: none"> Enhanced arteriogenesis and cardiomyocyte viability 	[62] 2006
VEGF-A	Pig	Ischaemia	CMV 1×10^{13}	NS	10/7	AAV2/9-VEGF-A/PDGF-B	Retroinfusion into lateral vein	Angiogenesis	Time after delivery: 56 days <ul style="list-style-type: none"> Improved ejection fraction Increased myocardial blood flow reserve 	[105] 2010
VEGF + ANG1	Pig	Myocardial infarction	MLC 1×10^{12}	M	8/16	AAV1 MLC/VEGF + AAV1MLCAng1	Co-injection of both vectors in peri-infarct region	Angiogenesis	Time after delivery: 56 days <ul style="list-style-type: none"> Improved cardiac function and myocardial perfusion Higher cardiac vascular density, proliferating cardiomyocytes and reduced apoptotic cells 	[63] 2011

Table 2. (continued).

Molecular Target	Animal Model	Disease Model	Promoter/ Dose (vg)	Sex	N ^a	AAV Vector	Delivery Method	Pathway	Outcome	Ref. Year
SERCA2a	Pig	Congestive heart failure	CMV 1×10^{12}	F	7/6	AAV1-SERCA2a	Intracoronary injection	Calcium handling	Time after delivery: 56 days <ul style="list-style-type: none"> Increased Ca²⁺ storage capacity Helped restore coronary flow Increased eNOS and eNOS promoter activity in endothelial cells 	[106] 2010
SERCA2a	Sheep	Ischaemic cardiomyopathy	CMV 1×10^{14}	M	6/10	AAV9-SERCA2a	Molecular cardiac surgery with recirculating delivery	Calcium handling	Time after delivery: 56 days <ul style="list-style-type: none"> Treated group had better LV function and reduced markers of oxidative stress Attenuated myocyte hypertrophy 	[107] 2014
SERCA2a	Sheep	Ischaemic cardiomyopathy	CMV 1×10^{13}	M	7/16	AAV1-SERCA2a	Molecular cardiac surgery with recirculating delivery	Calcium handling	Time after delivery: 56 days <ul style="list-style-type: none"> More favourable end diastolic and systolic volumes compared with control Reduction of fibrosis 	[108] 2016
SERCA2a	Sheep	Ischaemic heart failure	CMV 1×10^{13}	NS	7/7	AAV1-SERCA2a	Molecular cardiac surgery with recirculating delivery	Calcium handling	Time after delivery: 56 days <ul style="list-style-type: none"> Ejection fraction was higher in the treated group compared to the control Decreased myocyte apoptosis and myocyte hypertrophy 	[109] 2013
SERCA2a	Sheep	Heart failure	CMV 5×10^{12}	NS	7/7	AAV2/1-SERCA2a	Percutaneous reperfusion circuit	Calcium handling	Time after delivery: 28 days <ul style="list-style-type: none"> Improved LV function despite continued pacing 	[110] 2011

Table 2. (continued).

Molecular Target	Animal Model	Disease Model	Promoter/ Dose (vg)	Sex	N ^a	AAV Vector	Delivery Method	Pathway	Outcome	Ref. Year
SERCA2a	Sheep	Heart failure	CMV 1 × 10 ¹⁰ 1 × 10 ¹² 1 × 10 ¹³	NS	NS	AAV2/1-SERCA2a	Cardiac recirculation delivery	Calcium handling	Time after delivery: 28 and 42 days • Dose-dependent improvement in LV pressure and fractional shortening	[111] 2008
SERCA2a	Sheep	Apical myocardial infarction	CMV 5 × 10 ¹⁴	M	6/6	AAV6-SERCA2a	Percutaneous delivery	Calcium handling	Time after delivery: 28 and 84 days • Better function in treated compared to control • Reduced remodelling • Activation of STAT3 and higher pAKT	[66] 2010
SERCA2a	Pig	Volume overload heart failure	CMV 1 × 10 ¹²	F	10/6	AAV1-SERCA2a	Intracoronary delivery	Calcium handling	Time after delivery: 56 days • Preserved systolic function • Favourable impact on ventricular remodelling	[112] 2008
SUMO1	Pig	Ischaemic heart failure	CMV 5 × 10 ¹² 1 × 10 ¹³	NS	6 + 6/5	AAV1.SUMO1	Antegrade coronary infusion	Calcium handling	Time after delivery: 56 days • LV ejection fraction was higher in treated compared to controls • Prevented significant LV dilation	[71] 2013
S100A1	Pig	Post-ischaemic heart failure	CMV- MLC 1.5 × 10 ¹³	NS	12/18	AAV6-S100A1	Retrograde delivery via anterior cardiac vein	Calcium handling	Time after delivery: 84 days • LV ejection fraction was higher in treated compared to controls • Favourable impact on cardiac remodelling	[76] 2014

Table 2. (continued).

Molecular Target	Animal Model	Disease Model	Promoter/ Dose (vg)	Sex	N ^a	AAV Vector	Delivery Method	Pathway	Outcome	Ref. Year
S100A1	Pig	Heart failure	CMV- MLC 1.5 × 10 ¹³	NS	9/23	AAV9-S100A1	Retrograde coronary venous delivery	Calcium handling	Time after delivery: 84 days • Normalised cardiomyocyte calcium cycling, SR calcium handling and energy homeostasis	[34] 2011
I-1c	Pig	Myocardial infarction	CMV 2.5 × 10 ¹²	F	8/6	AAV9.I-1c	Intracoronary delivery	Calcium handling	Time after delivery: 56 days • Increased cardiac output and preservation of cardiac function • Reduced fibrotic scar size	[80] 2013
I-1c	Pig	Ischaemic heart failure	CMV 3 × 10 ¹² 1 × 10 ¹³	NS	7 + 7/6	BNP116.I-1c	Intracoronary delivery	Calcium handling	Time after delivery: 56 days • Higher stroke volume • Better contractility in treated compared to controls	[81] 2014
HO-1	Pig	Ischaemic heart failure	CMV 1 × 10 ¹³	NS	NS	AAV.hHO-1	Retroidfusion	Inflammation	Time after delivery: 22 days • Reduced myeloperoxidase-positive neutrophils and CD14 ⁺ monocytes • LV displayed a reduced loss of ejection fraction compared to control	[84] 2015

Abbreviations: AAV, adeno-associated virus; ANF, atrial natriuretic factor; Ang1, angiotensin; BNP, bio nano particle; Ca²⁺, calcium ion; CMV, cytomegalovirus; eNOS, endothelial nitric oxide synthase; F, female; hHO-1, human heme oxygenase 1; I-1c, constitutively active inhibitor-1; LV, left ventricular; M, male; MLC, myosin light chain; NS, not specified; S100A1, S100 calcium binding protein A1; SERCA, Sarco/endoplasmic reticulum Ca²⁺-ATPase; SR, sarcoplasmic reticulum; SUMO1, small ubiquitin-related modifier; VEGF, vascular endothelial growth factor; vg, vector genomes.

^aNumber of treated/number of controls (n + n refers to varying doses).

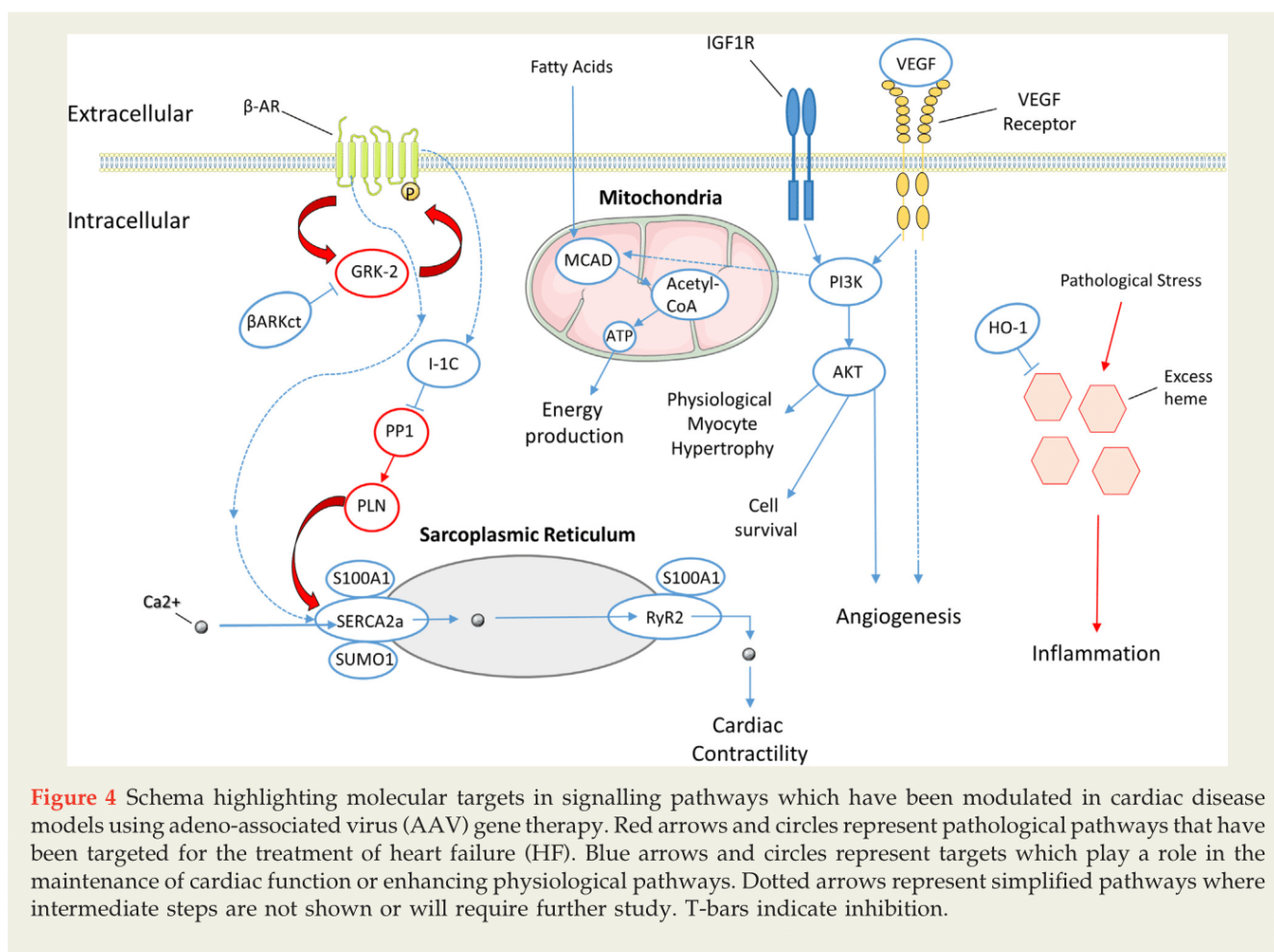


Figure 4 Schema highlighting molecular targets in signalling pathways which have been modulated in cardiac disease models using adeno-associated virus (AAV) gene therapy. Red arrows and circles represent pathological pathways that have been targeted for the treatment of heart failure (HF). Blue arrows and circles represent targets which play a role in the maintenance of cardiac function or enhancing physiological pathways. Dotted arrows represent simplified pathways where intermediate steps are not shown or will require further study. T-bars indicate inhibition.

cardiac remodelling and pathological cardiac hypertrophy [73–75]. The viability for gene therapy of S100A1 in large animals was assessed using both AAV6 and AAV9 CMV-MLC vectors in pig models of HF [34,76]. Both studies reported a favourable outcome on cardiac remodelling with no indication of deleterious side effects (Table 2).

Constitutively Active Inhibitor 1 (I-1c)

I-1c is a constitutively activated form of inhibitor 1, a protein that inhibits the activity of protein phosphatase-1 (PP1). Overexpression of I-1c in the failing heart of transgenic mice led to more favourable SERCA2a Ca^{2+} handling and muscle contractility, and less fibrosis and pathological cardiac hypertrophy [77–79]. Studies have reported preserved cardiac function compared to controls following I-1c gene transfer using AAV9 vectors [80] and BNP116 vectors in pig models [81] (Table 2). BNP116 is a novel AAV 2/8 chimeric vector that is viable for gene transfer and has shown resistance to neutralisation following exposure to anti-AAV2 serum, suggesting it has a unique antigenic profile [81].

Heme Oxygenase (HO-1)

Heme oxygenase (HO-1) is a protein involved in the catabolism of heme. Heme proteins are essential for transportation of oxygen but failing human hearts have increased levels of

heme [82]. Some evidence suggests this induces a pro-inflammatory state that in turn exacerbates the severity of a cardiac injury [83]. Delivery of human HO-1 using a chimeric AAV2/9 vector was trialled in a pig model of ischaemic HF [84]. Increased transgene expression was found to reduce cardiac inflammation and attenuate the decline in LV ejection fraction (Table 2).

Constitutively Active Phosphoinositide 3-kinase (caPI3K) in Mice

caPI3K is a constitutively active form of PI3K(p110 α), a cardioprotective lipid kinase downstream of the insulin-like growth factor 1 receptor (IGF1R). PI3K initiates downstream signalling events such as activation of protein kinase B (AKT) [85] and is activated in cardiac tissue during exercise [86]. PI3K(p110 α) was shown to play a crucial role in mediating exercise-induced physiological cardiac hypertrophy as well as maintaining contractile function in settings of cardiac pathology [32,87,88]. caPI3K has previously been administered to the hearts of mice using an AAV6-CMV vector [32]. Administration of AAV6-caPI3K induced physiological cardiac hypertrophy and angiogenesis in healthy adult mice, restored cardiac function in a mouse model with a failing heart due to pressure overload [32], and limited cardiac pathology in a mouse model of diabetic cardiomyopathy

[88]. Given the potential of caPI3K gene therapy in mice, it will be important to test this in large animal models.

Medium Chain Acyl-coenzyme A Dehydrogenase (MCAD) in Mice

Medium chain acyl-coenzyme A dehydrogenase (MCAD; encoded by *Acadm*) is a mitochondrial enzyme involved in the oxidation of fatty acids, and is considered to play an important role in cardiac metabolism [89]. MCAD was identified as a potential therapeutic target for the treatment of HF, as it was positively correlated with cardiac function and PI3K(p110 α) activity in a mouse model of MI [90]. Administration of MCAD to mice using an AAV6 vector induced physiological hypertrophy in healthy adult animals, and protected against cardiac fibrosis in mice with pressure overload-induced cardiac pathology [91].

Clinical Studies Using AAV for the Treatment of HF

Translating AAV gene therapy from large animal models to clinical trials has proven to be a challenging task. The Calcium Upregulation by Percutaneous Administration of Gene Therapy in Cardiac Disease (CUPID) trial was the first attempt to use AAV gene therapy to treat HF in human subjects. The CUPID trial involved a single intracoronary infusion of varying doses of the AAV1.SERCA2a vector to investigate the potential therapeutic benefit of increasing expression of SERCA2a in nine individuals with advanced HF (New York Heart Association [NYHA] Class III/IV) [67]. AAV1.SERCA2a displayed a satisfactory safety profile and after 6- to 12-month follow-up some of the patients showed improvement in a 6-minute walk test ($n = 4/9$), maximal oxygen uptake ($n = 4/9$), end systolic volume ($n = 5/9$) and ejection fraction ($n = 5/9$) (N.B. 2/9 patients with neutralising antibodies showed no benefit). These encouraging results led to a Phase II CUPID trial. Thirty-nine patients were administered either a placebo, or a low, medium or high dose of AAV1.SERCA2a via intracoronary infusion [68]. Subjects receiving a high dose of vector displayed a significant decrease in the frequency of cardiovascular events after 12 months. Furthermore, the duration of cardiovascular disease-related hospitalisation was substantially reduced. These promising results led to a subsequent larger Phase IIb CUPID trial. CUPID IIb was a randomised, multinational, double-blind, placebo-controlled trial involving 250 subjects with advanced HF who received a high dose (1×10^{13}) of AAV1.SERCA2a DNase-resistant particles [69]. Despite the previously encouraging results, CUPID IIb failed to demonstrate any difference between the subjects receiving AAV1.SERCA2a and subjects receiving a placebo. Post-hoc sub-analyses have provided some insight into differences that could explain the varied results between the CUPID I and CUPID IIb trials. Notably, the proportion of empty capsids to SERCA2a-containing capsids differed substantially between the two trials, with CUPID I delivering 90% empty capsids and

CUPID II delivering only 25% empty capsids. Empty capsids may serve as a decoy for neutralising antibodies and in turn, aid in transduction [92] (see Figure 2). Moreover, assessment of the number of viral genomes in cardiac tissue from deceased patients indicated that AAV-mediated expression of SERCA2a occurred in only a small proportion of cardiomyocytes [69].

Two other clinical trials using the SERCA2a vector were recently initiated. The Investigation of the Safety and Feasibility of AAV1/SERCA2a Gene Transfer in Patients With Chronic Heart Failure (SERCA-LVAD) Trial was intended to assess the therapeutic potential of AAV1.SERCA2a in 24 HF patients with left ventricular assist devices [93]. The AAV1-CMV-SERCA2a GENE Therapy Trial in Heart Failure (AGENT-HF) trial aimed to assess the potential of AAV1.SERCA2a to positively alter LV remodelling in 44 subjects with HF [94]. Due to the unsuccessful outcome of the CUPID IIb trial, both trials were prematurely terminated in 2016 [93,94].

Future Directions and Challenges

Over the last decade, substantial progress has been made in the development of AAV gene therapy as a potential therapeutic strategy for the treatment of HF. The contrasting success between the CUPID IIb clinical trial and numerous trials in large animal models suggests further preclinical development is necessary to make AAV gene therapy both a viable and realistic strategy. Recognising and compensating for the physiological differences between animals and humans, and using novel techniques, such as exosome-facilitated delivery to overcome host antibody neutralisation, are critical to ensure both the success and safety of AAV gene therapy. Additionally, developing, engineering and refining the cardiac specificity of vectors, further optimisation of the route and method of vector delivery, refining the necessary dose, overcoming vector packaging capacity limitations and controlling the duration of target gene expression will also be important for success. Furthermore, given the large financial price tag that comes with using AAV gene therapy as a treatment, new-found commercial interest by numerous developers [95] will be invaluable for upscaling AAV production to a level that will make it financially viable for human use in a clinical setting. Identifying and testing new molecular targets such as PI3K or MCAD in large animals may pave the way for treatments that offer greater clinical viability. Progression to the clinic is a slow and challenging task, but individual limitations are progressively being addressed. By integrating several approaches of optimisation, AAV gene therapy shows promise in becoming a realistic future clinical application for the treatment of HF.

Sources of Funding and Acknowledgements

S. Bass-Stringer is supported by a joint Baker Heart and Diabetes Institute-La Trobe University doctoral scholarship.

JR McMullen is a National Health and Medical Research Council Senior Research Fellow (1078985). BC Bernardo is supported by an Alice Baker and Eleanor Shaw Fellowship (Baker Foundation, Melbourne, Australia), and KL Weeks is supported by a National Heart Foundation of Australia Postdoctoral Fellowship (O12M6802) and an Emerging Leader Fellowship (Baker Institute). We wish to thank Yow Keat Tham for assistance with designing figures and formatting.

References

- [1] Savarese G, Lund LH. Global public health burden of heart failure. *Card Fail Rev* 2017;3:7–11.
- [2] Taylor CJ, Ryan R, Nichols L, Gale N, Hobbs FR, Marshall T. Survival following a diagnosis of heart failure in primary care. *Fam Pract* 2017;34:161–8.
- [3] Daya S, Berns KI. Gene therapy using adeno-associated virus vectors. *Clin Microbiol Rev* 2008;21:583–93.
- [4] Wold WS, Toth K. Adenovirus vectors for gene therapy, vaccination and cancer gene therapy. *Curr Gene Ther* 2013;13:421–33.
- [5] Connolly JB. Lentiviruses in gene therapy clinical research. *Gene Ther* 2002;9:1730–4.
- [6] Ramamoorth M, Narvekar A. Non viral vectors in gene therapy—an overview. *J Clin Diagn Res* 2015;9:GE01–6.
- [7] Savic N, Schwank G. Advances in therapeutic CRISPR/Cas9 genome editing. *Transl Res* 2016;168:15–21.
- [8] Zinn E, Vandenberghe LH. Adeno-associated virus: fit to serve. *Curr Opin Virol* 2014;8:90–7.
- [9] Ghosh A, Duan D. Expanding adeno-associated viral vector capacity: a tale of two vectors. *Biotechnol Genet Eng Rev* 2007;24:165–77.
- [10] Deyle DR, Russell DW. Adeno-associated virus vector integration. *Curr Opin Mol Ther* 2009;11:442–7.
- [11] Zaiss AK, Liu Q, Bowen GP, Wong NC, Bartlett JS, Muruve DA. Differential activation of innate immune responses by adenovirus and adeno-associated virus vectors. *J Virol* 2002;76:4580–90.
- [12] Vandendriessche T, Thorrez L, Acosta-Sanchez A, Petrus I, Wang L, Ma L, et al. Efficacy and safety of adeno-associated viral vectors based on serotype 8 and 9 vs. lentiviral vectors for hemophilia B gene therapy. *J Thromb Haemost* 2007;5:16–24.
- [13] Athanasopoulos T, Fabb S, Dickson G. Gene therapy vectors based on adeno-associated virus: characteristics and applications to acquired and inherited diseases (review). *Int J Mol Med* 2000;6:363–75.
- [14] Sun JY, Anand-Jawa V, Chatterjee S, Wong KK. Immune responses to adeno-associated virus and its recombinant vectors. *Gene Ther* 2003;10:964–76.
- [15] Hammoudi N, Ishikawa K, Hajjar RJ. Adeno-associated virus-mediated gene therapy in cardiovascular disease. *Curr Opin Cardiol* 2015;30:228–34.
- [16] Vassalli G, Bueler H, Dudler J, von Segesser LK, Kappenberger L. Adeno-associated virus (AAV) vectors achieve prolonged transgene expression in mouse myocardium and arteries in vivo: a comparative study with adenovirus vectors. *Int J Cardiol* 2003;90:229–38.
- [17] St George JA. Gene therapy progress and prospects: adenoviral vectors. *Gene Ther* 2003;10:1135–41.
- [18] Farraha M, Chong JJ, Kizana E. Therapeutic prospects of gene therapy for atrial fibrillation. *Heart Lung Circ* 2016;25:808–13.
- [19] Hauck B, Xiao W. Characterization of tissue tropism determinants of adeno-associated virus type 1. *J Virol* 2003;77:2768–74.
- [20] Zincarelli C, Soltys S, Rengo G, Koch WJ, Rabinowitz JE. Comparative cardiac gene delivery of adeno-associated virus serotypes 1–9 reveals that AAV6 mediates the most efficient transduction in mouse heart. *Clin Transl Sci* 2010;3:81–9.
- [21] Palomeque J, Chemaly ER, Colosi P, Wellman JA, Zhou S, Del Monte F, et al. Efficiency of eight different AAV serotypes in transducing rat myocardium in vivo. *Gene Ther* 2007;14:989–97.
- [22] Wang Z, Zhu T, Qiao C, Zhou L, Wang B, Zhang J, et al. Adeno-associated virus serotype 8 efficiently delivers genes to muscle and heart. *Nat Biotechnol* 2005;23:321–8.
- [23] Gao G, Bish LT, Sleeper MM, Mu X, Sun L, Lou Y, et al. Transendo-cardial delivery of AAV6 results in highly efficient and global cardiac gene transfer in rhesus macaques. *Hum Gene Ther* 2011;22:979–84.
- [24] Bish LT, Morine K, Sleeper MM, Sanmiguel J, Wu D, Gao G, et al. Adeno-associated virus (AAV) serotype 9 provides global cardiac gene transfer superior to AAV1, AAV6, AAV7, and AAV8 in the mouse and rat. *Hum Gene Ther* 2008;19:1359–68.
- [25] Muller OJ, Leuchs B, Pleger ST, Grimm D, Franz WM, Katus HA, et al. Improved cardiac gene transfer by transcriptional and transductional targeting of adeno-associated viral vectors. *Cardiovasc Res* 2006;70:70–8.
- [26] Pacak CA, Mah CS, Thattaliyath BD, Conlon TJ, Lewis MA, Cloutier DE, et al. Recombinant adeno-associated virus serotype 9 leads to preferential cardiac transduction in vivo. *Circ Res* 2006;99:e3–9.
- [27] Asokan A, Conway JC, Phillips JL, Li C, Hegge J, Sinnott R, et al. Reengineering a receptor footprint of adeno-associated virus enables selective and systemic gene transfer to muscle. *Nat Biotechnol* 2010;28:79–82.
- [28] Pulicherla N, Shen S, Yadav S, Debbink K, Govindasamy L, Agbandje-McKenna M, et al. Engineering liver-detargeted AAV9 vectors for cardiac and musculoskeletal gene transfer. *Mol Ther* 2011;19:1070–8.
- [29] Yang L, Jiang J, Drouin LM, Agbandje-McKenna M, Chen C, Qiao C, et al. A myocardium tropic adeno-associated virus (AAV) evolved by DNA shuffling and in vivo selection. *Proc Natl Acad Sci U S A* 2009;106:3946–51.
- [30] Damdindorj L, Karnan S, Ota A, Hossain E, Konishi Y, Hosokawa Y, et al. A comparative analysis of constitutive promoters located in adeno-associated viral vectors. *PLoS One* 2014;9:e106472.
- [31] Gregorevic P, Blankinship MJ, Allen JM, Crawford RW, Meuse L, Miller DG, et al. Systemic delivery of genes to striated muscles using adeno-associated viral vectors. *Nat Med* 2004;10:828–34.
- [32] Weeks KL, Gao X, Du XJ, Boey EJ, Matsumoto A, Bernardo BC, et al. Phosphoinositide 3-kinase p110alpha is a master regulator of exercise-induced cardioprotection and PI3K gene therapy rescues cardiac dysfunction. *Circ Heart Fail* 2012;5:523–34.
- [33] Pacak CA, Sakai Y, Thattaliyath BD, Mah CS, Byrne BJ. Tissue specific promoters improve specificity of AAV9 mediated transgene expression following intra-vascular gene delivery in neonatal mice. *Genet Vaccines Ther* 2008;6:13.
- [34] Pleger ST, Shan C, Ksienzyk J, Bekeredian R, Boekstegers P, Hinkel R, et al. Cardiac AAV9-S100A1 gene therapy rescues post-ischemic heart failure in a preclinical large animal model. *Sci Transl Med* 2011;3:92ra64.
- [35] Raake PW, Schlegel P, Ksienzyk J, Reinkober J, Barthelme J, Schinkel S, et al. AAV6.betaARKct cardiac gene therapy ameliorates cardiac function and normalizes the catecholaminergic axis in a clinically relevant large animal heart failure model. *Eur Heart J* 2013;34:1437–47.
- [36] Kolwicz Jr SC, Odom GL, Nowakowski SG, Moussavi-Harami F, Chen X, Reinecke H, et al. AAV6-mediated cardiac-specific overexpression of ribonucleotide reductase enhances myocardial contractility. *Mol Ther* 2016;24:240–50.
- [37] Teichman SL, Thomson KS, Regnier M. Cardiac myosin activation with gene therapy produces sustained inotropic effects and may treat heart failure with reduced ejection fraction. *Handb Exp Pharmacol* 2017;243:447–64.
- [38] Mearini G, Stimpel D, Geertz B, Weinberger F, Kramer E, Schlossarek S, et al. Mybpc3 gene therapy for neonatal cardiomyopathy enables long-term disease prevention in mice. *Nat Commun* 2014;5:5515.
- [39] Woitek F, Zentilin L, Hoffman NE, Powers JC, Ottiger I, Parikh S, et al. Intracoronary cytoprotective gene therapy: a study of VEGF-B167 in a pre-clinical animal model of dilated cardiomyopathy. *J Am Coll Cardiol* 2015;66:139–53.
- [40] Nishikimi T, Kuwahara K, Nakao K. Current biochemistry, molecular biology, and clinical relevance of natriuretic peptides. *J Cardiol* 2011;57:131–40.
- [41] Calcedo R, Wilson JM. Humoral immune response to AAV. *Front Immunol* 2013;4:341.
- [42] Madsen D, Cantwell ER, O'Brien T, Johnson PA, Mahon BP. Adeno-associated virus serotype 2 induces cell-mediated immune responses directed against multiple epitopes of the capsid protein VP1. *J Gen Virol* 2009;90:2622–33.
- [43] Mingozi F, High KA. Immune responses to AAV vectors: overcoming barriers to successful gene therapy. *Blood* 2013;122:23–36.

- [44] Masat E, Pavani G, Mingozzi F. Humoral immunity to AAV vectors in gene therapy: challenges and potential solutions. *Discov Med* 2013;15:379–89.
- [45] Blacklow NR, Hoggan MD, Rowe WP. Serologic evidence for human infection with adenovirus-associated viruses. *J Natl Cancer Inst* 1968;40:319–27.
- [46] Parks WP, Boucher DW, Melnick JL, Taber LH, Yow MD. Seroepidemiological and ecological studies of the adenovirus-associated satellite viruses. *Infect Immun* 1970;2:716–22.
- [47] Sprecher-Goldberger S, Thiry L, Lefebvre N, Dekegel D, de Halleux F. Complement-fixation antibodies to adenovirus-associated viruses, cytomegaloviruses and herpes simplex viruses in patients with tumors and in control individuals. *Am J Epidemiol* 1971;94:351–8.
- [48] Arruda VR, Xiao W. It's all about the clothing: capsid domination in the adeno-associated viral vector world. *J Thromb Haemost* 2007;5:12–5.
- [49] Liang Y, Mathiyalagan P, Kohlbrenner E, Chepurko E, Jeong D, Ceholiski D, et al. Abstract 15439: AAV-containing exosomes as a novel vector to improve AAV-mediated myocardial gene delivery in resistance to neutralizing antibody. *Circulation* 2017;136.
- [50] Hulot JS, Ishikawa K, Hajjar RJ. Gene therapy for the treatment of heart failure: promise postponed. *Eur Heart J* 2016;37:1651–8.
- [51] Chamberlain K, Riyad JM, Weber T. Cardiac gene therapy with adeno-associated virus-based vectors. *Curr Opin Cardiol* 2017;27:5–82.
- [52] Ishikawa K, Tilemann L, Ladage D, Agüero J, Leonardson L, Fish K, et al. Cardiac gene therapy in large animals: bridge from bench to bedside. *Gene Ther* 2012;19:670–7.
- [53] Hajjar RJ. Potential of gene therapy as a treatment for heart failure. *J Clin Invest* 2013;123:53–61.
- [54] Scimia MC, Cannavo A, Koch WJ. Gene therapy for heart disease: molecular targets, vectors and modes of delivery to myocardium. *Expert Rev Cardiovasc Ther* 2013;11:999–1013.
- [55] Kotin RM. Large-scale recombinant adeno-associated virus production. *Hum Mol Genet* 2011;20:R2–6.
- [56] Feng L, Guo M, Zhang S, Chu J, Zhuang Y, Zhang S. Optimization of transfection mediated by calcium phosphate for plasmid rAAV-LacZ (recombinant adeno-associated virus-beta-galactosidase reporter gene) production in suspension-cultured HEK-293 (human embryonic kidney 293) cells. *Biotechnol Appl Biochem* 2007;46:127–35.
- [57] Urabe M, Ding C, Kotin RM. Insect cells as a factory to produce adeno-associated virus type 2 vectors. *Hum Gene Ther* 2002;13:1935–43.
- [58] Bera A, Sen D. Promise of adeno-associated virus as a gene therapy vector for cardiovascular diseases. *Heart Fail Rev* 2017;22:795–823.
- [59] Rockman HA, Koch WJ, Lefkowitz RJ. Seven-transmembrane-spanning receptors and heart function. *Nature* 2002;415:206–12.
- [60] Reinkober J, Tscheschner H, Plegier ST, Most P, Katus HA, Koch WJ, et al. Targeting GRK2 by gene therapy for heart failure: benefits above beta-blockade. *Gene Ther* 2012;19:686–93.
- [61] Shiojima I, Sato K, Izumiya Y, Schiekofer S, Ito M, Liao R, et al. Disruption of coordinated cardiac hypertrophy and angiogenesis contributes to the transition to heart failure. *J Clin Invest* 2005;115:2108–18.
- [62] Ferrarini M, Arsic N, Recchia FA, Zentilin L, Zacchigna S, Xu X, et al. Adeno-associated virus-mediated transduction of VEGF165 improves cardiac tissue viability and functional recovery after permanent coronary occlusion in conscious dogs. *Circ Res* 2006;98:954–61.
- [63] Tao Z, Chen B, Tan X, Zhao Y, Wang L, Zhu T, et al. Coexpression of VEGF and angiopoietin-1 promotes angiogenesis and cardiomyocyte proliferation reduces apoptosis in porcine myocardial infarction (MI) heart. *Proc Natl Acad Sci U S A* 2011;108:2064–9.
- [64] Hasenfuss G, Reinecke H, Studer R, Meyer M, Pieske B, Holtz J, et al. Relation between myocardial function and expression of sarcoplasmic reticulum Ca(2+)-ATPase in failing and nonfailing human myocardium. *Circ Res* 1994;75:434–42.
- [65] Rincon MY, VandenDriessche T, Chuah MK. Gene therapy for cardiovascular disease: advances in vector development, targeting, and delivery for clinical translation. *Cardiovasc Res* 2015;108:4–20.
- [66] Beeri R, Chaput M, Guerrero JL, Kawase Y, Yosefy C, Abedat S, et al. Gene delivery of sarcoplasmic reticulum calcium ATPase inhibits ventricular remodeling in ischemic mitral regurgitation. *Circ Heart Fail* 2010;3:627–34.
- [67] Jaski BE, Jessup ML, Mancini DM, Cappola TP, Pauly DF, Greenberg B, et al. Calcium upregulation by percutaneous administration of gene therapy in cardiac disease (CUPID Trial), a first-in-human phase 1/2 clinical trial. *J Card Fail* 2009;15:171–81.
- [68] Jessup M, Greenberg B, Mancini D, Cappola T, Pauly DF, Jaski B, et al. Calcium upregulation by percutaneous administration of gene therapy in cardiac disease (CUPID): a phase 2 trial of intracoronary gene therapy of sarcoplasmic reticulum Ca²⁺-ATPase in patients with advanced heart failure. *Circulation* 2011;124:304–13.
- [69] Greenberg B, Butler J, Felker GM, Ponikowski P, Voors AA, Desai AS, et al. Calcium upregulation by percutaneous administration of gene therapy in patients with cardiac disease (CUPID 2): a randomised, multinational, double-blind, placebo-controlled, phase 2b trial. *Lancet* 2016;387:1178–86.
- [70] Kho C, Lee A, Jeong D, Oh JG, Chaanine AH, Kizana E, et al. SUMO1-dependent modulation of SERCA2a in heart failure. *Nature* 2011;477:601–5.
- [71] Tilemann L, Lee A, Ishikawa K, Agüero J, Rapti K, Santos-Gallego C, et al. SUMO-1 gene transfer improves cardiac function in a large-animal model of heart failure. *Sci Transl Med* 2013;5:211ra159.
- [72] Duarte-Costa S, Castro-Ferreira R, Neves JS, Leite-Moreira AF. S100A1: a major player in cardiovascular performance. *Physiol Res* 2014;63:669–81.
- [73] Yamasaki R, Berri M, Wu Y, Trombitas K, McNabb M, Keller Mayer MS, et al. Titin-actin interaction in mouse myocardium: passive tension modulation and its regulation by calcium/S100A1. *Biophys J* 2001;81:2297–313.
- [74] Most P, Boerries M, Eicher C, Schweda C, Volkens M, Wedel T, et al. Distinct subcellular location of the Ca²⁺-binding protein S100A1 differentially modulates Ca²⁺-cycling in ventricular rat cardiomyocytes. *J Cell Sci* 2005;118:421–31.
- [75] Ehlermann P, Remppis A, Guddat O, Weimann J, Schnabel PA, Mutsch J, et al. Right ventricular upregulation of the Ca(2+) binding protein S100A1 in chronic pulmonary hypertension. *Biochim Biophys Acta* 2000;1500:249–55.
- [76] Weber C, Neacsu I, Krautz B, Schlegel P, Sauer S, Raake P, et al. Therapeutic safety of high myocardial expression levels of the molecular inotrope S100A1 in a preclinical heart failure model. *Gene Ther* 2014;21:131–8.
- [77] Carr AN, Schmidt AG, Suzuki Y, del Monte F, Sato Y, Lanner C, et al. Type 1 phosphatase, a negative regulator of cardiac function. *Mol Cell Biol* 2002;22:4124–35.
- [78] Pathak A, del Monte F, Zhao W, Schultz JE, Lorenz JN, Bodi I, et al. Enhancement of cardiac function and suppression of heart failure progression by inhibition of protein phosphatase 1. *Circ Res* 2005;96:756–66.
- [79] Chen G, Zhou X, Nicolaou P, Rodriguez P, Song G, Mitton B, et al. A human polymorphism of protein phosphatase-1 inhibitor-1 is associated with attenuated contractile response of cardiomyocytes to beta-adrenergic stimulation. *FASEB J* 2008;22:1790–6.
- [80] Fish KM, Ladage D, Kawase Y, Karakikes J, Jeong D, Ly H, et al. AAV9: I-1c delivered via direct coronary infusion in a porcine model of heart failure improves contractility and mitigates adverse remodeling. *Circ Heart Fail* 2013;6:310–7.
- [81] Ishikawa K, Fish KM, Tilemann L, Rapti K, Agüero J, Santos-Gallego CG, et al. Cardiac I-1c overexpression with reengineered AAV improves cardiac function in swine ischemic heart failure. *Mol Ther* 2014;22:2038–45.
- [82] Sawicki KT, Shang M, Wu R, Chang HC, Khechaduri A, Sato T, et al. Increased heme levels in the heart lead to exacerbated ischemic injury. *J Am Heart Assoc* 2015;4:e002272.
- [83] Hao K, Hanawa H, Ding L, Ota Y, Yoshida K, Toba K, et al. Free heme is a danger signal inducing expression of proinflammatory proteins in cultured cells derived from normal rat hearts. *Mol Immunol* 2011;48:1191–202.
- [84] Hinkel R, Lange P, Petersen B, Gottlieb E, Ng JK, Finger S, et al. Heme oxygenase-1 gene therapy provides cardioprotection via control of post-ischemic inflammation: an experimental study in a pre-clinical pig model. *J Am Coll Cardiol* 2015;66:154–65.
- [85] Bernardo BC, Weeks KL, Pretorius L, McMullen JR. Molecular distinction between physiological and pathological cardiac hypertrophy: experimental findings and therapeutic strategies. *Pharmacol Ther* 2010;128:191–227.
- [86] Perrino C, Naga Prasad SV, Mao L, Noma T, Yan Z, Kim HS, et al. Intermittent pressure overload triggers hypertrophy-independent cardiac dysfunction and vascular rarefaction. *J Clin Invest* 2006;116:1547–60.
- [87] McMullen JR, Shioi T, Zhang L, Tarnavski O, Sherwood MC, Kang PM, et al. Phosphoinositide 3-kinase(p110alpha) plays a critical role for the induction of physiological, but not pathological, cardiac hypertrophy. *Proc Natl Acad Sci U S A* 2003;100:12355–60.
- [88] Prakoso D, De Blasio MJ, Qin C, Rosli S, Kiriazis H, Qian H, et al. Phosphoinositide 3-kinase (p110alpha) gene delivery limits diabetes-induced cardiac NADPH oxidase and cardiomyopathy in a mouse

- model with established diastolic dysfunction. *Clin Sci (Lond)* 2017;131:1345–60.
- [89] Houten SM, Wanders RJ. A general introduction to the biochemistry of mitochondrial fatty acid beta-oxidation. *J Inher Metab Dis* 2010;33:469–77.
- [90] Lin RC, Weeks KL, Gao XM, Williams RB, Bernardo BC, Kiriazis H, et al. PI3K(p110 alpha) protects against myocardial infarction-induced heart failure: identification of PI3K-regulated miRNA and mRNA. *Arterioscler Thromb Vasc Biol* 2010;30:724–32.
- [91] Bernardo BC, Weeks KL, Pongsukwechkul T, Gao X, Kiriazis H, Cemerlang N, et al. Gene delivery of medium chain acyl-coenzyme A dehydrogenase (MCAD) induces physiological cardiac hypertrophy and protects against pathological remodelling. *Clin Sci (Lond)* 2018;132:381–97.
- [92] Mingozzi F, Anguela XM, Pavani G, Chen Y, Davidson RJ, Hui DJ, et al. Overcoming preexisting humoral immunity to AAV using capsid decoys. *Sci Transl Med* 2013;5:194ra92.
- [93] Investigation of the Safety and Feasibility of AAV1/SERCA2a Gene Transfer in Patients With Chronic Heart Failure (SERCA-LVAD). *Clinical Trials U.S National Library of Medicine*; 2007.
- [94] AAV1-CMV-Serca2a GENE Therapy Trial in Heart Failure (AGENT-HF). *Clinical Trials U.S National Library of Medicine*; 2013.
- [95] Morrison C. Landmark gene therapy poised for US approval. *Nat Rev Drug Discov* 2017;16:739–41.
- [96] Kwon I, Schaffer DV. Designer gene delivery vectors: molecular engineering and evolution of adeno-associated viral vectors for enhanced gene transfer. *Pharm Res* 2008;25:489–99.
- [97] Mingozzi F, Chen Y, Murphy SL, Edmonson SC, Tai A, Price SD, et al. Pharmacological modulation of humoral immunity in a nonhuman primate model of AAV gene transfer for hemophilia B. *Mol Ther* 2012;20:1410–6.
- [98] Mingozzi F, Chen Y, Edmonson SC, Zhou S, Thurlings RM, Tak PP, et al. Prevalence and pharmacological modulation of humoral immunity to AAV vectors in gene transfer to synovial tissue. *Gene Ther* 2013;20:417–24.
- [99] Mimuro J, Mizukami H, Hishikawa S, Ikemoto T, Ishiwata A, Sakata A, et al. Minimizing the inhibitory effect of neutralizing antibody for efficient gene expression in the liver with adeno-associated virus 8 vectors. *Mol Ther* 2013;21:318–23.
- [100] Monteilhet V, Saheb S, Boutin S, Leborgne C, Veron P, Montus MF, et al. A 10 patient case report on the impact of plasmapheresis upon neutralizing factors against adeno-associated virus (AAV) types 1, 2, 6, and 8. *Mol Ther* 2011;19:2084–91.
- [101] Chicoine LG, Montgomery CL, Bremer WG, Shontz KM, Griffin DA, Heller KN, et al. Plasmapheresis eliminates the negative impact of AAV antibodies on microdystrophin gene expression following vascular delivery. *Mol Ther* 2014;22:338–47.
- [102] Huttner NA, Girod A, Perabo L, Edbauer D, Kleinschmidt JA, Buning H, et al. Genetic modifications of the adeno-associated virus type 2 capsid reduce the affinity and the neutralizing effects of human serum antibodies. *Gene Ther* 2003;10:2139–47.
- [103] Adachi K, Enoki T, Kawano Y, Veraz M, Nakai H. Drawing a high-resolution functional map of adeno-associated virus capsid by massively parallel sequencing. *Nat Commun* 2014;5:3075.
- [104] Maheshri N, Koerber JT, Kaspar BK, Schaffer DV. Directed evolution of adeno-associated virus yields enhanced gene delivery vectors. *Nat Biotechnol* 2006;24:198–204.
- [105] Kupatt C, Hinkel R, Pfosser A, El-Aouni C, Wuchrer A, Fritz A, et al. Cotransfection of vascular endothelial growth factor-A and platelet-derived growth factor-B via recombinant adeno-associated virus resolves chronic ischemic malperfusion role of vessel maturation. *J Am Coll Cardiol* 2010;56:414–22.
- [106] Hadri L, Bobe R, Kawase Y, Ladage D, Ishikawa K, Atassi F, et al. SERCA2a gene transfer enhances eNOS expression and activity in endothelial cells. *Mol Ther* 2010;18:1284–92.
- [107] Katz MG, Fargnoli AS, Williams RD, Steuerwald NM, Isidro A, Ivanina AV, et al. Safety and efficacy of high-dose adeno-associated virus 9 encoding sarcoplasmic reticulum Ca(2+) adenosine triphosphatase delivered by molecular cardiac surgery with recirculating delivery in ovine ischemic cardiomyopathy. *J Thorac Cardiovasc Surg* 2014;148:1065–72.
- [108] Katz MG, Brandon-Warner E, Fargnoli AS, Williams RD, Kendle AP, Hajjar RJ, et al. Mitigation of myocardial fibrosis by molecular cardiac surgery-mediated gene overexpression. *J Thorac Cardiovasc Surg* 2016;151:1191–200.
- [109] Fargnoli AS, Katz MG, Yarnall C, Isidro A, Petrov M, Steuerwald N, et al. Cardiac surgical delivery of the sarcoplasmic reticulum calcium ATPase rescues myocytes in ischemic heart failure. *Ann Thorac Surg* 2013;96:586–95.
- [110] Mariani JA, Smolic A, Prevolos A, Byrne MJ, Power JM, Kaye DM. Augmentation of left ventricular mechanics by recirculation-mediated AAV2/1-SERCA2a gene delivery in experimental heart failure. *Eur J Heart Fail* 2011;13:247–53.
- [111] Byrne MJ, Power JM, Prevolos A, Mariani JA, Hajjar RJ, Kaye DM. Recirculating cardiac delivery of AAV2/1SERCA2a improves myocardial function in an experimental model of heart failure in large animals. *Gene Ther* 2008;15:1550–7.
- [112] Kawase Y, Ly HQ, Prunier F, Lebeche D, Shi Y, Jin H, et al. Reversal of cardiac dysfunction after long-term expression of SERCA2a by gene transfer in a pre-clinical model of heart failure. *J Am Coll Cardiol* 2008;51:1112–9.
- [113] Milani-Nejad N, Janssen PM. Small and large animal models in cardiac contraction research: advantages and disadvantages. *Pharmacol Ther* 2014;141:235–49.
- [114] Yuan R, Tsaih SW, Petkova SB, Marin de Evsikova C, Xing S, Marion MA, et al. Aging in inbred strains of mice: study design and interim report on median lifespans and circulating IGF1 levels. *Aging Cell* 2009;8:277–87.
- [115] Hill AJ, Iazzo PA. Comparative cardiac anatomy. In: Iazzo PA, editor. *Handbook of cardiac anatomy, physiology, and devices*. Totowa, NJ: Humana Press; 2009. p. 87–108.
- [116] Camacho P, Fan H, Liu Z, He JQ. Large mammalian animal models of heart disease. *J Cardiovasc Dev Dis* 2016;3.
- [117] Byrne MJ, Raman JS, Alferness CA, Esler MD, Kaye DM, Power JM. An ovine model of tachycardia-induced degenerative dilated cardiomyopathy and heart failure with prolonged onset. *J Card Fail* 2002;8:108–15.
- [118] Starr C, Taggart R, Evers C, Starr L. *Biology: the unity and diversity of life*, 14th ed. Cengage Learning; 2016.
- [119] McCutcheon SN, Blair HT, Purchas RW. Body composition and organ weights in fleeceweight-selected and control Romney rams. *N Z J Agric Res* 1993;36:445–9.
- [120] Dutta S, Sengupta P. Men and mice: relating their ages. *Life Sci* 2016;152:244–8.
- [121] Ho D, Zhao X, Gao S, Hong C, Vatner DE, Vatner SF. Heart rate and electrocardiography monitoring in mice. *Curr Protoc Mouse Biol* 2011;1:123–39.
- [122] Holliday MA, Potter D, Jarrah A, Bearg S. The relation of metabolic rate to body weight and organ size. *Pediatr Res* 1967;1:185–95.
- [123] Cook S, Togni M, Schaub MC, Wenaweser P, Hess OM. High heart rate: a cardiovascular risk factor. *Eur Heart J* 2006;27:2387–93.
- [124] Doevendans PA, Daemen MJ, de Muinck ED, Smits JF. Cardiovascular phenotyping in mice. *Cardiovasc Res* 1998;39:34–49.

Chapter 2

Advancing knowledge of the PI3K signalling pathway, and its protective role in the heart.

Chapter 2. Preface

Chapter 2, Advancing knowledge of the PI3K signalling pathway, and its protective role in the heart investigates the safety of enhanced PI3K signalling, its relationship with physical activity, and the consequences of reduced PI3K signalling on cardiac function. The findings in this chapter provide important rationale for pursuing the subsequent studies presented in chapters three and four. *PI3K is critical for protection against atrial and ventricular pathology: Implications for the reverse J-shaped relationship between physical activity and cardiac risk* explores the cardiac physiology of transgenic mouse models with varying degrees (both increased and decreased) PI3K activity. In doing so, the window in which PI3K activity is beneficial is defined, and the safety of increased PI3K activity is further validated. Subsequently the role of PI3K in a setting of extreme exercise in both mice and humans is investigated, and potential novel markers of cardiac dysfunction in settings of extreme exercise are identified.

Chapter 2.

PI3K is critical for protection against atrial and ventricular pathology: Implications for the reverse J-shaped relationship between physical activity and cardiac risk

Submitted to and under review at 'Nature Communications', October 2021 by S Bass-Stringer, GS Yildiz, YK Tham, A Matsumoto, H Kiriazis, CA Harmawan, CM Tai, L Bottrell, M Ezeani, DG Donner, JYY Ooi, NA Mellett, J Luo, K Janssens, EJ Howden, CE Hagemeyer, PJ Meikle, RCY Lin, CJ Thomas, KL Weeks, A La Gerche, BC Bernardo, JR McMullen.

As first author, S Bass-Stringer contributed ~60% to this publication. This included contributions to the experiments, analyses, drafting, design and editing.

This manuscript is presented in the format of submission, except figures have been inserted within the text.

1 **PI3K is critical for protection against atrial and ventricular pathology:**
2 **Implications for the reverse J-shaped relationship between physical**
3 **activity and cardiac risk**

4

5 Sebastian Bass-Stringer^{1,2}, Gunes S Yildiz¹, Yow Keat Tham^{1,3,4}, Aya Matsumoto¹, Helen
6 Kiriazis^{1,4}, Claudia A Harmawan¹, Celeste MK Tai¹, Lauren Bottrell¹, Martin Ezeani¹,
7 Daniel G. Donner^{1,4}, Jenny Y. Y. Ooi¹, Natalie A. Mellett¹, Jieting Luo¹, Kristel
8 Janssens¹, Erin J Howden^{1,4}, Christoph E Hagemeyer⁵, Peter J Meikle^{1,4}, Ruby C Y Lin^{6,7},
9 Colleen J Thomas², Kate L Weeks^{1,3,4}, André La Gerche^{1,4}, Bianca C Bernardo^{1,3,8*}, Julie
10 R McMullen^{1,2, 3,4, 9*}.

11

12 1. Baker Heart and Diabetes Institute, Melbourne, VIC, 3004, Australia.

13 2. Department of Physiology, Anatomy and Microbiology, La Trobe University,
14 Bundoora, VIC, Australia.

15 3. Department of Diabetes, Central Clinical School, Monash University, Clayton, VIC,
16 3800, Australia.

17 4. Department of Cardiometabolic Health, University of Melbourne, Melbourne, VIC,
18 Australia.

19 5. Australian Centre for Blood Diseases, Monash University, VIC, Australia.

20 6. School of Medical Sciences, University of New South Wales, Sydney, NSW, Australia

21 7. Westmead Institute for Medical Research, Sydney, NSW, Australia

22 8. Department of Paediatrics, University of Melbourne, VIC, 3010, Australia.

23 9. Department of Physiology and Department of Medicine Alfred Hospital, Monash
24 University, VIC, Australia.

25

26

1 *** Correspondence:**

2 1. Prof Julie R. McMullen

3 Head, Cardiac Hypertrophy Laboratory, Baker Heart and Diabetes Institute.

4 75 Commercial Road, Melbourne VIC 3004 Australia

5 Phone: 61 3 8532 1194

6 Email: julie.mcmullen@baker.edu.au

7

8 2. Dr Bianca Bernardo

9 Cardiac Hypertrophy Laboratory, Baker Heart and Diabetes Institute.

10 75 Commercial Road, Melbourne VIC 3004 Australia

11 Email: Bianca.bernardo@baker.edu.au

12

13

14

15

16

17

18

19

20

21

22

23

24

25

26

1 **Abstract**

2 **Aims:** Physical inactivity, as well as extreme endurance exercise, can lead to increased
3 cardiac risk, but the molecular mechanisms underpinning the reverse J-shaped
4 relationship are poorly understood. Phosphoinositide 3-kinase (PI3K) is an essential
5 regulator of exercise-induced cardiac enlargement, and enhanced IGF1-PI3K-Akt
6 signalling is a potential therapeutic strategy for the failing heart. However, chronic
7 elevation of IGF1 can lead to pathology. In a serendipitous discovery, we identified atrial
8 enlargement and thrombi in mice with reduced PI3K. Here, we investigated whether too
9 little or too much PI3K can lead to cardiac abnormalities.

10 **Methods and results:** We generated cardiac-specific transgenic mice with varying
11 degrees of PI3K activity, undertook analyses in mice subjected to regular or extreme
12 exercise, and performed lipidomics in plasma from athletes with/without atrial fibrillation
13 (AF). Elevated PI3K was associated with a dose-dependent increase in heart size, and
14 preserved/enhanced function. This was not accompanied by dose response changes in
15 Akt, but rather calsequestrin 1. Reduced PI3K led to cardiac dysfunction, fibrosis,
16 arrhythmia, atrial enlargement and thrombi. GM3 ganglioside and TLR4 were elevated in
17 mice with reduced PI3K, and mice subjected to extreme exercise, but not mice with
18 increased PI3K. Dysregulation of GM3 and PI3K-related genes or lipids was identified in
19 the extreme exercised mice, and plasma from athletes with AF.

20 **Conclusion:** This study implicates reduced PI3K contributing to the association between
21 increased cardiac risk with physical inactivity, and extreme endurance exercise, but does
22 not support elevated PI3K contributing to cardiac pathology. Monitoring GM3 and PI3K-
23 related lipids may identify athletes at risk.

24

25 **Keywords:** Cardiac risk, exercise, athletes, atria, arrhythmia, hypertrophy

26

1 **Translational Perspective**

2 Physical inactivity or extreme endurance exercise can lead to increased cardiac risk, but
3 the mechanisms responsible are not well understood, and identifying those at risk is
4 challenging. We demonstrate that decreased activity of a key regulator of exercise-
5 induced hypertrophy and protection, phosphoinositide 3-kinase (PI3K), leads to cardiac
6 dysfunction, atrial enlargement and fibrosis, and increased susceptibility to atrial thrombi
7 in mice. We also identified evidence of dysregulation of the PI3K pathway in mice
8 subjected to extreme endurance exercise, and plasma from veteran athletes with atrial
9 fibrillation (AF). Assessment of plasma lipids related to the PI3K pathway may identify
10 athletes at risk of AF, and cardiac risk in inactive individuals or patients receiving drugs
11 that inhibit PI3K.

12

13

14

15

16

17

18

19

20

21

22

23

24

25

26

1 **Introduction**

2 The importance of physical activity or exercise for cardiovascular health is well-
3 established. Epidemiological studies have revealed strong inverse relationships between
4 the amount of exercise performed and either the likelihood of an adverse cardiovascular
5 event, or overall mortality^{1, 2}. Physical activity can also provide improved outcomes in
6 patients following a cardiac disease diagnosis or event^{3, 4}. On the other hand, there are
7 also reports that long-term extreme exercise can lead to increased risk of cardiac
8 pathology⁵⁻⁷. Thus, a U- or reverse J-shaped relationship between exercise and cardiac
9 health has been proposed, with evidence of both too little and too much exercise leading
10 to adverse cardiac events. While the health benefits of exercise are well accepted, the
11 “extreme exercise hypothesis” remains controversial. The exception to this is the growing
12 body of evidence demonstrating that high volumes of extreme endurance exercise is
13 associated with an increased risk of atrial pathology and atrial fibrillation (AF)⁶⁻¹³.

14
15 A key feature of regular exercise training is cardiac enlargement associated with
16 preserved/enhanced heart function, termed physiological cardiac hypertrophy¹⁴. This
17 enlargement occurs as an adaptive response to increases in volume and pressure load
18 during exercise training, and shown to be protective against cardiac fibrosis and cardiac
19 dysfunction in animal cardiac stress models^{15, 16}. Heart enlargement also occurs in a
20 setting of cardiac disease and is referred to as pathological hypertrophy. In contrast to
21 physiological hypertrophy, pathological hypertrophy is an independent risk factor for
22 heart failure, and is commonly distinguished by an increase in cardiac fibrosis, a
23 reduction in heart function, and an increase in markers of cardiac stress including atrial
24 and B-type natriuretic peptides (ANP, BNP)¹⁴. Numerous protective signalling pathways
25 are activated with exercise¹⁵, but evidence from multiple laboratories utilising genetic
26 mouse models, indicates the insulin-like growth factor 1 (IGF1)-phosphoinositide 3-

1 kinase p110 α (PI3K)-PDK1-Akt-FoxO1/CEBP β signalling axis is the most critical for
2 exercise-induced physiological cardiac hypertrophy and protection¹⁶⁻²⁵. As a
3 consequence, enhanced activation of this signalling cascade has been proposed as a
4 therapeutic approach for the failing heart. However, there is also evidence that chronic
5 activation of the IGF1 pathway might lead to adverse cardiac outcomes²⁶. Given the
6 IGF1-PI3K-Akt pathway is a critical molecular pathway increased in the heart in response
7 to exercise^{25, 27}, it is important to assess the “safety profile” and “therapeutic window” of
8 this pathway, and to determine whether it potentially contributes to the relationship
9 between high-intensity exercise volumes and increased cardiac risk.

10

11 In this study, we have focused on PI3K because 1) it is elevated in the heart with
12 exercise²⁷, 2) is a master regulator of exercise-induced hypertrophy and protection¹⁶, and
13 3) a preliminary observation from our laboratory suggested that depressed PI3K may lead
14 to atrial enlargement and thrombi formation. PI3K is a lipid kinase that catalyses the
15 conversion of phosphatidylinositol 4,5-bisphosphate (PIP₂) to phosphatidylinositol
16 (3,4,5)-trisphosphate (PIP₃), and this leads to downstream cardioprotective signalling. Our
17 previous work showed that cardiac-specific heterozygote transgenic mice (Tg) with
18 reduced PI3K activity, due to the expression of a dominant-negative PI3K (dnPI3K)
19 mutant on one allele (dnPI3K Tg(+/-)), had smaller hearts with normal heart function
20 under basal conditions²⁸. The dnPI3K Tg(+/-) mice displayed a blunted hypertrophic
21 response to swim training²⁰, highlighting the critical role of PI3K for exercise-induced
22 cardiac enlargement. Conversely, heterozygote Tg mice with increased cardiac PI3K
23 activity, due to a constitutively activated PI3K mutant (caPI3K Tg(+/-)), displayed a
24 physiological hypertrophic phenotype under basal conditions²⁸, and were protected
25 following myocardial infarction (MI), dilated cardiomyopathy (DCM) and pressure
26 overload^{16, 29, 30}. In a serendipitous discovery, when we unintentionally generated

1 homozygote dnPI3K Tg mice (dnPI3K Tg(+/+)) due to a breeding error, we found atrial
2 thrombi in a subset of dnPI3K Tg(+/) mice. The major goal of this study was to generate
3 and characterize both heterozygote and homozygote PI3K Tg mice to assess: i) if a dose-
4 dependent relationship exists between increased PI3K activity and adaptive physiological
5 hypertrophy, ii) whether a further increase in PI3K activity in homozygote caPI3K Tg
6 mice leads to cardiac pathology and arrhythmia, as seen in some athletes undertaking
7 extreme endurance exercise, and iii) if reduced PI3K in homozygote dnPI3K Tg mice is
8 associated with significant cardiac pathology, dysfunction, arrhythmia and atrial thrombi.

9

10 **Methods**

11 To study mice with different degrees of increased or decreased PI3K activity we
12 generated cardiac-specific heterozygote and homozygote caPI3K and dnPI3K transgenic
13 mice i.e. caPI3K Tg(+/-), caPI3K Tg(+/+), dnPI3K Tg(+/-), dnPI3K Tg(+/+). This study
14 represents the first generation and characterization of the homozygote mice. A detailed
15 description of all methods is provided in the Supplementary material.

16

17 **Results**

18 *caPI3K Tg mice display cardiac hypertrophy in a dose-dependent manner, and have*
19 *preserved or enhanced systolic function*

20 PI3K activity was elevated in the ventricles of caPI3K Tg(+/-) and caPI3K Tg(+/) mice
21 by 2.9 and 5.1-fold, respectively, compared to Ntg (Figure 1A; PI3K activity represented
22 by PIP). caPI3K Tg(+/) mice showed a 1.75-fold increase in PI3K activity vs caPI3K
23 Tg(+/-) mice (Figure 1A). Hearts of 20wk male and female mice were normalised to body
24 weight (BW) and tibia length (TL). Heart size, heart weight (HW)/BW and HW/TL of
25 caPI3K Tg(+/-) were increased vs Ntg in males and females (Figure 1B-D, Supp Table 1).
26 A further increase in heart size was identified in caPI3K Tg(+/) compared with caPI3K

1 Tg(+/-) (Figure 1B-D), indicating that the additional caPI3K allele and higher PI3K
2 activity was associated with a greater hypertrophic response. Atrial weight (AW)/TL was
3 modestly lower in male caPI3K Tg(+/-) vs Ntg, but not different in other groups (Figure
4 1E & Supp Table 1). Lung weight (LW)/TL was comparable in all groups (Figure 1F),
5 with no evidence of congestion or pathology at dissection.

6

7 By echocardiography, LV wall thicknesses (LVPW, IVS) and estimated LV mass were
8 significantly increased or tended to be increased in both caPI3K Tg models relative to Ntg
9 in males and females (Fig 1G, Supp Table 2). LV systolic function based on fractional
10 shortening was preserved or enhanced in both caPI3K Tg models (Figure 1G). In caPI3K
11 Tg groups with enhanced systolic function, this was largely due to a decrease in LVESD
12 (Figure 1G & Supp Table 2). Diastolic parameters were comparable between groups, with
13 no differences for E/A ratio, E'/A' ratio, E/E' ratio, IVRT or MV deceleration time (Fig
14 1H, Supp Table 3). There was no evidence of electrophysiological abnormalities based on
15 ECG in any group vs Ntg (Figure 1I, Supp Table 4), or arrhythmia (all groups presented
16 irregularities in cardiac rhythm for less than 4.5% of total time)(Figure 1I).

17

18

19

20

21

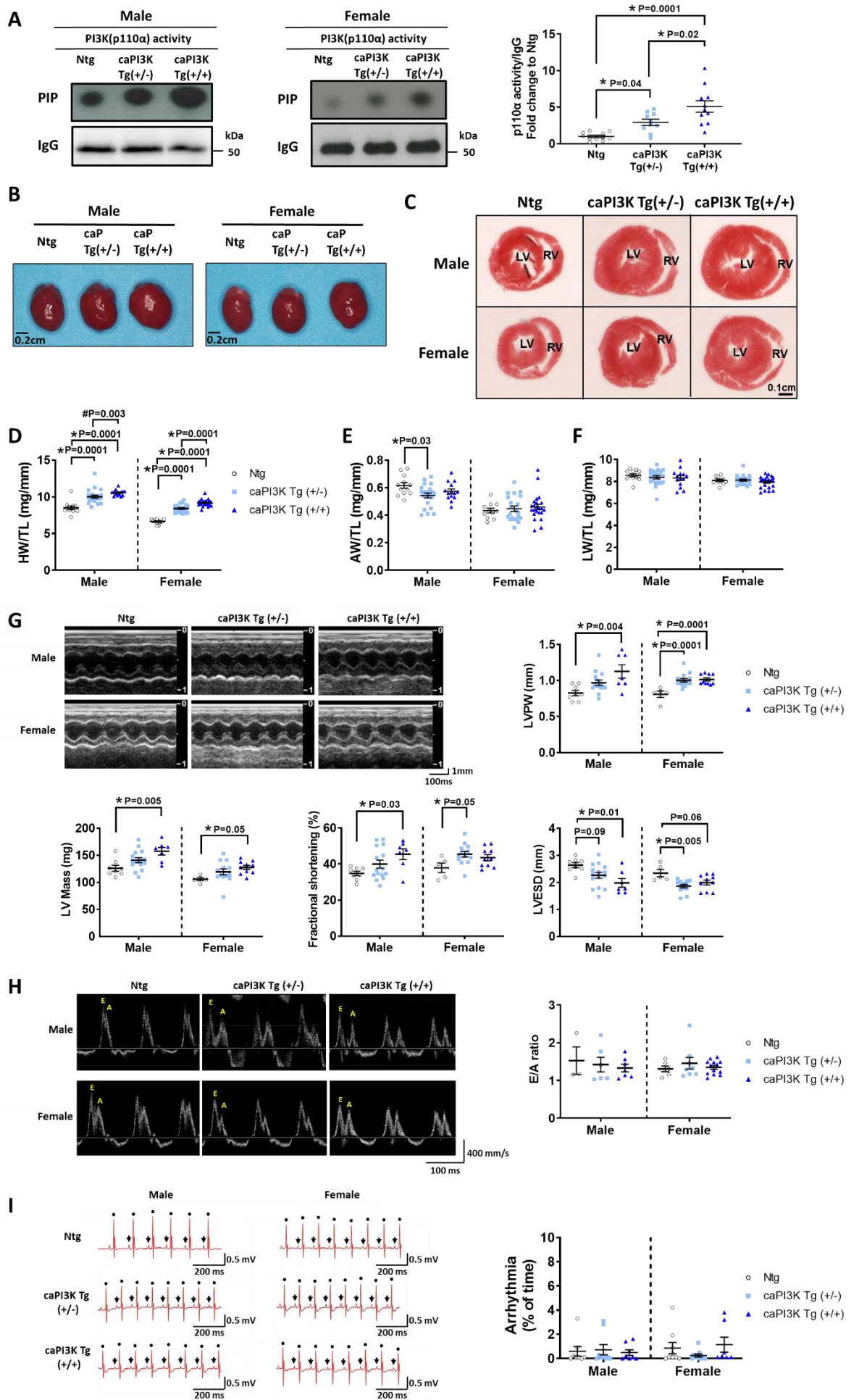
22

23

24

25

26



1 **Figure 1: Dose dependent increase in heart size of caPI3K transgenic mice and**
2 **normal or enhanced heart function A)** PI3K activity from immunoprecipitated p110 α
3 using a lipid kinase activity assay in ventricle tissue from 20 week old male and female
4 mice. PI3K activity (represented by PIP) is normalised to Western blotting of
5 immunoglobulin G (IgG). All data presented as mean \pm SEM. N=6 (Ntg male), 5 (Ntg
6 female), 5 (caPI3K Tg(+/-) male), 5 (caPI3K Tg(+/-) female), 5 (caPI3K Tg(+/+) male), 6
7 (caPI3K Tg(+/+) female). Male and female data combined; no statistical difference
8 between male and female of the same genotype. **B)** Representative hearts of male (top)
9 and female (bottom) Ntg, heterozygote caPI3K Tg (caP Tg(+/-)) and homozygote caPI3K
10 Tg (caP Tg(+/+)) mice at dissection. Scale bar=0.2 cm. **C)** Representative ventricular
11 sections of male and female Ntg, caPI3K Tg(+/-) and caPI3K Tg(+/+) mice. Scale
12 bar=0.1 cm. LV=left ventricle, RV=right ventricle. **D)** Heart weight (HW) normalised to
13 tibial length (TL). **E)** Atria weight (AW) and **F)** lung weight (LW) normalised to TL. All
14 data are presented as mean \pm SEM. N=12 (Ntg male), 11 (Ntg female), 22 (caPI3K (+/-)
15 male), 21 (caPI3K (+/-) female), 14 (caPI3K (+/+) male), 23 (caPI3K (+/+) female). *
16 One Way ANOVA followed by correction for multiple comparisons using Tukey's
17 method. # P-value by Mann-Whitney U-test vs. caPI3K Tg (+/-) of same sex.
18 **G)** Representative M-mode echocardiographic images from hearts of male (top) and
19 female (bottom) Ntg, caPI3K Tg(+/-) and caPI3K Tg(+/+) mice at 20 weeks of age. Left
20 ventricular (LV) posterior wall thickness (LVPW), echocardiography-derived LV mass,
21 fractional shortening %, and LV end systolic dimension (LVESD). All data presented as
22 mean \pm SEM. N=8 (Ntg male), 5 (Ntg female), 15 (caPI3K Tg(+/-) male), 13 (caPI3K
23 Tg(+/-) female), 7 (caPI3K Tg(+/+) male), 10 (caPI3K Tg(+/+) female). **H)**
24 Representative pulse wave Doppler (PW) echocardiographic images from hearts of male
25 and female Ntg, caPI3K Tg(+/-) and caPI3K Tg(+/+) Tg mice at 20 weeks of age. E
26 (early) and A (late) wave peak velocities indicated in representative images, with the E/A
27 ratio graphed. All data presented as mean \pm SEM. N=3 (Ntg male), 6 (Ntg female), 6
28 (caPI3K Tg(+/-) male), 8 (caPI3K Tg(+/-) female), 7 (caPI3K Tg(+/+) male), 13 (caPI3K
29 Tg(+/+) female). **I)** Left, representative ECG traces of Ntg, caPI3K Tg(+/-) and caPI3K
30 Tg(+/+) male and female mice at 20 weeks of age. Dots and arrows highlight R and P-
31 waves, respectively. Right, episodes of arrhythmia expressed as a percentage over an
32 interval of ~5-6 mins (further details are provided in the Data Supplement). All data
33 presented as mean \pm SEM. N=8 (Ntg male), 9 (Ntg female), 9 (caPI3K Tg(+/-) male), 10
34 (caPI3K Tg(+/-) female), 8 (caPI3K Tg(+/+) male), 7 (caPI3K Tg(+/+) female). *One
35 Way ANOVA followed by correction for multiple comparisons using Tukey's method.

1 *Homozygote dnPI3K Tg mice display cardiac dysfunction, arrhythmia and atrial*
2 *pathology*

3 Our previous studies which only characterized heterozygote dnPI3K Tg(+/-) mice,
4 showed that reduced cardiac PI3K resulted in mice with small hearts but relatively normal
5 heart function^{28, 31}. In the current study, PI3K activity was reduced in hearts of dnPI3K
6 Tg(+/-) and dnPI3K Tg(+/+) mice (Figure 2A), but the activity assay lacked sensitivity to
7 detect a further decrease in PI3K activity in dnPI3K Tg(+/+)vs dnPI3K Tg(+/-). However,
8 protein expression of total p85 (PI3K regulatory subunit) was lowest in dnPI3K Tg(+/+)
9 hearts, and tended to be lower in homozygote mice vs heterozygote mice (Figure 2B).
10 This decrease in p85 potentially reflects a reduction in binding stability between p85 and
11 the truncated p110 α subunit present in the dnPI3K Tg mice compared to endogenous
12 p110 α . As an additional marker to confirm a dose-response in signalling within the
13 dnPI3K Tg models, we assessed IGF1 receptor (IGF1R) gene expression which is
14 increased in dnPI3K Tg(+/-) mice as a feedback mechanism³². In the current study,
15 IGF1R gene expression was elevated in dnPI3K Tg(+/-), and increased further in dnPI3K
16 Tg(+/+) mice (Figure 2C). Both heterozygote and homozygote dnPI3K Tg mice had
17 smaller heart weights compared with Ntg, but there was no difference between the
18 heterozygote and homozygote mice (Figure 2D-F, Supp Table 5). Given the absence of a
19 dose response effect of the dnPI3K transgene on heart size, we isolated adult cardiac
20 myocytes from an additional cohort of dnPI3K Tg mice. The cell area and length of
21 cardiac myocytes from dnPI3K Tg(+/-) mice were smaller than Ntg, and further reduced
22 in dnPI3K Tg(+/+)(Figure 2G). Consistent with the smaller heart size, dnPI3K Tg(+/-)
23 also had smaller atria vs Ntg (Figure 2H, Supp Table 5). In contrast, dnPI3K Tg(+/+) had
24 greater atrial weights than dnPI3K Tg(+/-)(Figure 2H & I). Atrial thrombi were identified
25 in 7 of 34 homozygote dnPI3K Tg mice (Figure 2I). There was no evidence of thrombi in
26 any Ntg or dnPI3K Tg(+/-) mice.

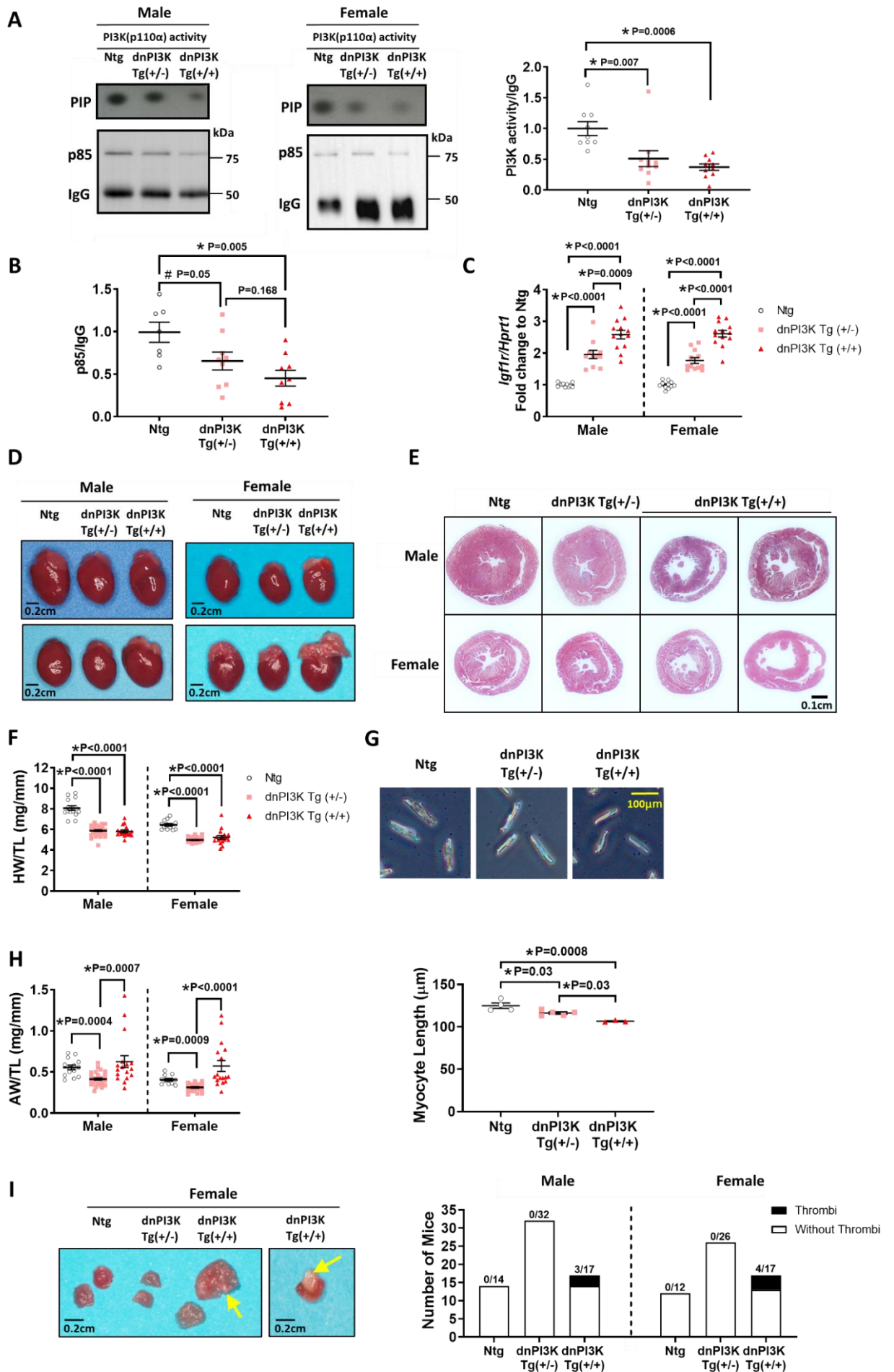


Figure 2: Distinct morphological phenotypes of heterozygote and homozygote dnPI3K transgenic mice

A) PI3K activity from immunoprecipitated p85 on a lipid kinase activity assay in ventricle tissue from 20 week old male and female mice. PI3K activity (PIP) is normalised to Western blotting of immunoglobulin G (IgG). All data presented as mean±SEM. N=9 Ntg (5 male, 4 female), 10 dnPI3K Tg(+/-) (6 male, 4 female), 10 dnPI3K Tg(+/+) (5 male, 5 female). **B)** Immunoprecipitation of PI3K regulatory subunit (p85) probed with a p85 antibody and normalised to Western blotting of IgG. N=7 Ntg (4 male, 3 female), 9 dnPI3K Tg(+/-) (5 male 4 female), 9 dnPI3K Tg(+/+) (4 male, 5 female). Male and female data combined; no statistical difference between male and female of the same genotype for A and B. **C)** Gene expression by qPCR of *Igf1r* relative to *Hprt1* from ventricle tissue of dnPI3K Tg mice and littermates: N=11 (Ntg male), 11(Ntg female), 11 (dnPI3K Tg(+/-) male), 12 (dnPI3K Tg(+/-) female), 13 (dnPI3K Tg(+/+) male), 13 (dnPI3K Tg(+/+) female). All data presented as mean±SEM. **D)** Hearts of male (left) and female (right) Ntg, heterozygote dnPI3K Tg (dnP Tg(+/-)) and homozygote dnPI3K Tg (dnP Tg(+/+)) mice at dissection. Scale bar=0.2 cm. Lower panel highlights the range of phenotypes in the homozygote mice i.e. dilated chambers and enlarged atria. **E)** Ventricular cross-sections of male and female Ntg, dnPI3K Tg(+/-) and dnPI3K Tg(+/+) mice. Scale bar=0.1 cm. For dnPI3K Tg(+/+) in D) and E), two examples of the varying phenotype are shown. A subset of dnPI3K Tg(+/+) mice appeared to have dilated hearts at dissection (right). **F)** Heart weight (HW) normalised to tibial length (TL). **G)** Images of isolated ventricular myocytes (upper, left), and quantitation of myocyte area, length and width from male Ntg (N=4), dnPI3K Tg(+/-) (N=5), dnPI3K Tg(+/+)(N=3). *One Way ANOVA followed by correction for multiple comparisons using Tukey's method. # P-value by unpaired t-test vs. dnPI3K Tg (+/-). **H)** Atria weight (AW) normalised to TL and photos at dissection **I)** (left, yellow arrows highlight thrombi). All data are presented as mean ± SEM. Panel F&H: N=14 (Ntg male), 12 (Ntg female), 32 (dnPI3K Tg(+/-) male), 26 (dnPI3K Tg(+/-) female), 17 (dnPI3K Tg(+/+) male), 17 (dnPI3K Tg(+/+) female). *One Way ANOVA followed by correction for multiple comparisons using Tukey's method. # P-value by unpaired t-test. **I)** Right, number of mice presenting with atrial thrombi at dissection.

1 LV wall thicknesses and estimated LV mass were generally lower in both dnPI3K Tg
2 groups (Figure 3A). LVESD was higher, and fractional shortening lower in dnPI3K
3 Tg(+/+) vs Ntg and dnPI3K Tg(+/-)(Figure 3A, Supp Table 6). As previously reported³¹,
4 ECG parameters were relatively normal in dnPI3K Tg(+/-) vs Ntg (Figure 3B). However,
5 there was evidence of some arrhythmia in dnPI3K Tg(+/-), particularly in females. In
6 dnPI3K Tg(+/+) mice, there was prominent ECG abnormalities including irregular R-R
7 intervals, and arrhythmia (Figure 3B-C, Supp Table 7).

8

9 *Distinct histological and molecular profiles in caPI3K Tg and dnPI3K Tg mice*

10 On histological analysis, there was no evidence of significant fibrosis in LV from any of
11 the heterozygote or homozygote caPI3K Tg (Figure 4A) or heterozygote dnPI3K Tg
12 (Figure 4B). By contrast, there was clear evidence of fibrosis in LV from both male and
13 female dnPI3K Tg(+/-)(Figure 4B, collagen fibres stain blue with Masson's Trichrome).
14 There was also evidence of fibrosis in left atrial samples from homozygote dnPI3K mice
15 (Figure 4C).

16 Next, we examined the expression of genes commonly altered in a setting of pathological
17 hypertrophy. Gene expression of *Nppa* (encoding ANP) and *Nppb* (encoding BNP) were
18 unchanged or decreased in the ventricles of caPI3K Tg groups (Figure 4D), but were
19 progressively increased in the dnPI3K Tg(+/-) and dnPI3K Tg(+/-)(Figure 4E). Collagen
20 genes (*Coll1a1* and *Col3a1*) were not significantly different in the caPI3K Tg models
21 (Figure 4D), but greater in the dnPI3K Tg models (Figure 4E). Collagen expression was
22 generally highest in the dnPI3K Tg(+/-)(Figure 4E), consistent with the histological
23 analysis (Figure 4B). Gene expression of *Atp2a2* which encodes Serca2a was largely
24 unchanged in the caPI3K Tg models (Figure 4D). A small but significant decrease in
25 caPI3K Tg(+/-) females (Figure 4D), was not associated with any systolic dysfunction
26 (Figure 1G). In contrast, there was a significant decrease in Serca2a in ventricles of male

- 1 and female dnPI3K Tg(+/+) mice (Figure 4E), and this corresponded with the systolic
- 2 dysfunction in homozygote dnPI3K Tg (Figure 3A).

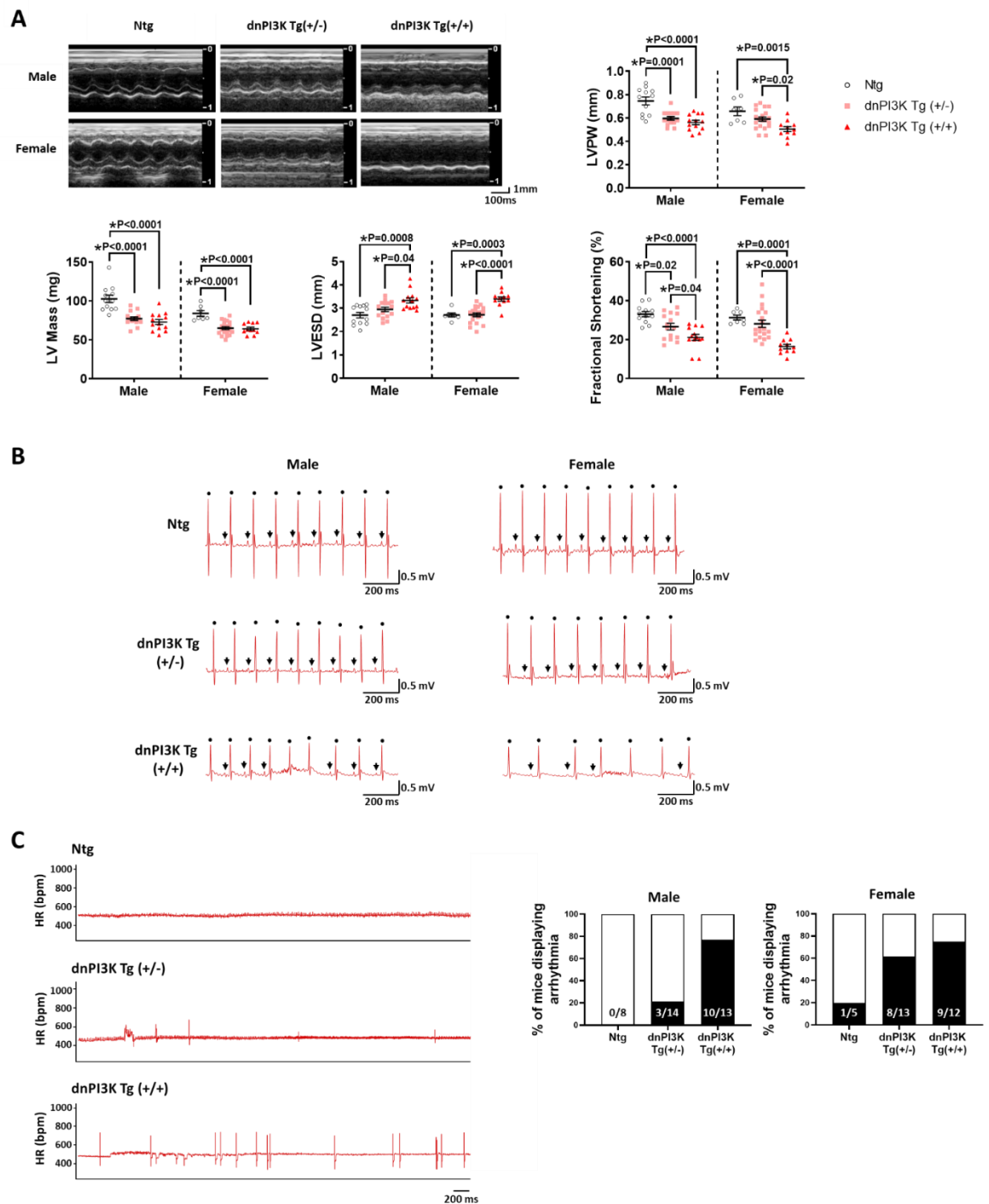


Figure 3: dnPI3K Tg(+/+) mice display cardiac dysfunction and arrhythmia

A) Representative M-mode echocardiographic measurements from hearts of male (top) and female (bottom) Ntg, dnPI3K Tg(+/-) and dnPI3K Tg(+/+) mice at 20 weeks of age. Left ventricular (+) LV posterior wall thickness (LVPW), estimated LV mass, LV end

systolic dimension (LVESD), and fractional shortening %. All data presented as mean±SEM. N=12 (Ntg male), 7 (Ntg female), 15 (dnPI3K Tg(+/-) male), 20 (dnPI3K Tg(+/-) female), 13 (dnPI3K Tg(+/+) male), 11 (dnPI3K Tg(+/+) female). *One Way ANOVA followed by correction for multiple comparisons using Tukey's method. **B**) Representative ECG traces of Ntg, dnPI3K Tg(+/-) and dnPI3K Tg(+/+) male and female mice at 20 weeks of age. Dots and arrows highlight R and clear P-waves, respectively. **C**) Left, examples of heart rate (HR) traces during ECG recordings showing irregularities/arrhythmia in the dnPI3K Tg mice vs Ntg. Right, percentage of mice displaying arrhythmia in each genotype during an interval of ~5-6 mins. The threshold for selecting mice displaying arrhythmia was set at >4.5% based on data obtained from Ntg mice in Figure 1I (further details provided in the Data Supplement). Numbers within the bar graphs refer to the number of mice displaying arrhythmia. N=8 (Ntg male), 5 (Ntg female), 14 (dnPI3K Tg(+/-) male), 13 (dnPI3K Tg(+/-) female), 13 (dnPI3K Tg(+/+) male), 12 (dnPI3K Tg(+/+) female).

1

2 *PI3K and exercise can induce hypertrophy and protection independent of Akt*

3 Phosphorylation of Akt, the most recognized downstream target of PI3K, was increased at
4 S473 in hearts of all caPI3K Tg groups, but unexpectedly no additional increase was
5 observed in caPI3K Tg(+/+) vs caPI3K Tg(+/-)(Figure 5A). Since Akt is phosphorylated
6 by PI3K at two phosphorylation sites (S473 and T308), phosphorylation at T308 was
7 subsequently assessed. Similar to pAkt S473, pAkt T308 was elevated to a similar degree
8 in hearts of caPI3K Tg(+/-) and caPI3K Tg(+/+) vs Ntg (Figure 5B). Further,
9 phosphorylation in individual mice at the S473 and T308 sites were strongly correlated (p
10 <0.0001). Within hearts of the dnPI3K Tg models, pAkt was generally lower compared to
11 Ntg, but no difference between the heterozygote and homozygote models was observed
12 (Figure 5C).

13

14

15

16

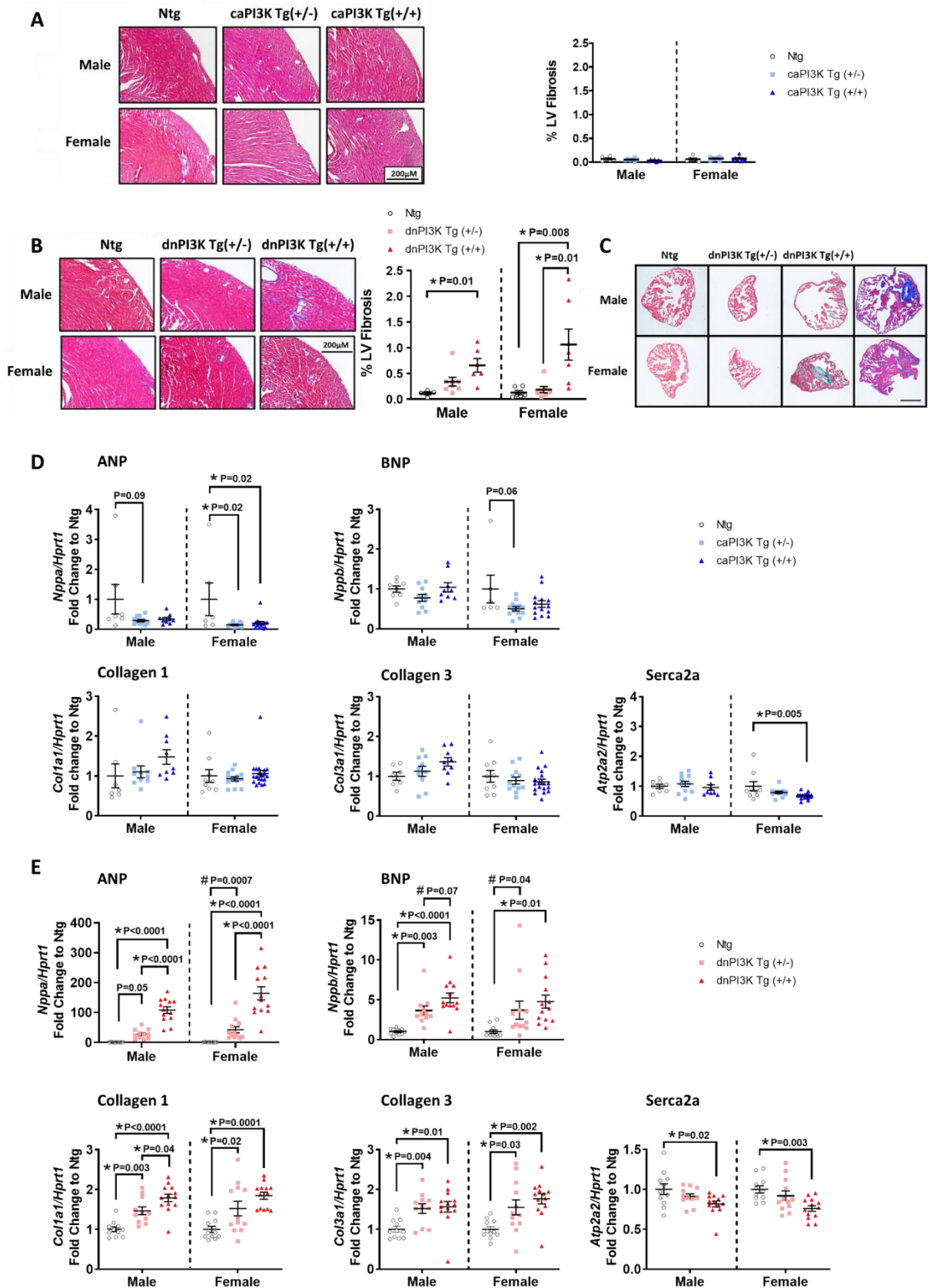


Figure 4: Fibrosis and cardiac stress markers in dnPI3K but not caPI3K Tg models

A) Left - Cross sections of left ventricle (LV) from hearts of Ntg, caPI3K Tg(+/-) and caPI3K Tg(+/+) mice at 20 weeks of age stained with Masson's Trichrome in males (top)

and females (bottom) and quantitation of % LV fibrosis (right). All data presented as mean±SEM. N=6 (Ntg male), 6 (Ntg female), 7 (caPI3K Tg(+/-) male), 8 (caPI3K Tg(+/-) female), 7 (caPI3K Tg(+/+) male), 8 (caPI3K Tg(+/+) female). Magnification x40, scale bar=200 µm. **B**) Left - Cross sections of LV from hearts of Ntg, dnPI3K Tg(+/-) and dnPI3K Tg(+/+) mice at 20 weeks of age stained with Masson's Trichrome in males (top) and females (bottom) and quantitation of % LV fibrosis (right). All data presented as mean±SEM. N=4 (Ntg male), 6 (Ntg female), 8 (dnPI3K Tg(+/-) male), 7 (dnPI3K Tg(+/-) female), 6 (dnPI3K Tg(+/+) male), 7 (dnPI3K Tg(+/+) female). Magnification x40, scale bar=200 µm. **C**) Left atrial samples from the Ntg and dnPI3K Tg models showing atrial fibrosis (blue) in the dnPI3K Tg(+/+) mice. **D and E**) Gene expression by qPCR of ANP, BNP, collagen 1 and 3, and *Serca2a* relative to *Hprt1* from ventricle tissue of 20 week old caPI3K Tg (panel D) and dnPI3K Tg mice (panel E). caPI3K Tgs and Ntg littermates: N=7-8 (Ntg male), 6-9 (Ntg female), 10-11 (caPI3K Tg(+/-) male), 12-13 (caPI3K Tg(+/-) female), 9 (caPI3K Tg(+/+) male), 14-20 (caPI3K Tg(+/+) female). dnPI3K Tg and Ntg littermates: N=11 (Ntg male), 11 (Ntg female), 11 (dnPI3K Tg(+/-) male), 12 (dnPI3K Tg(+/-) female), 13 (dnPI3K Tg(+/+) male), 13 (dnPI3K Tg(+/+) female). All data presented as mean±SEM. *One Way ANOVA followed by correction for multiple comparisons using Tukey's method. # Unpaired t-test.

1 Given the clear absence of a dose-dependent relationship in the caPI3K Tg models
2 between heart size and pAkt/total Akt, and in the dnPI3K Tg models between cardiac
3 pathology/dysfunction and pAkt/total Akt, we re-evaluated the contribution of Akt in
4 mediating caPI3K and exercise-induced hypertrophy by revisiting prior literature and
5 unpublished data from our prior studies. In a prior study, heterozygote dnPI3K mice and
6 kinase dead (kd) Akt mice were subjected to swim training for 4wks, but data from the
7 kdAkt mice had not been published. Heterozygote dnPI3K mice showed a blunted
8 response to exercise training²⁰, but this was not observed in kdAkt mice (Figure 5D),
9 suggesting a contribution of PI3K-dependent but Akt-independent mechanisms in
10 mediating exercise-induced physiological hypertrophy.

11

12

1 To examine other potential mediators regulated by PI3K which could contribute to the
2 different degrees of cardiac size and/or pathology in the PI3K Tg models, we revisited a
3 previous microarray data set from heterozygote caPI3K and dnPI3K mice²⁹. We had
4 recently ranked PI3K-regulated candidate genes based on P-value, and displaying an
5 inverse gene expression relationship in caPI3K and dnPI3K hearts³³. Calsequestrin 1
6 (*Casq1*) was one of the top ranked genes, and of interest because it was previously shown
7 to regulate skeletal muscle size and contractility³⁴. However, *Casq1* has been reported to
8 be expressed in skeletal muscle, and *Casq2* in cardiac muscle. We confirmed the *Casq1*
9 microarray and Taqman probes were specific for *Casq1*, and not *Casq 2* (Supplementary
10 Figure 3), and that *Casq1* is expressed in heart, together with skeletal muscle, but not
11 kidney or liver (Supplementary Figure 4). In the current study, qPCR revealed that *Casq1*
12 was elevated in caPI3K Tg(+/-) hearts vs Ntg, and increased further in caPI3K Tg(+/+)
13 hearts (Figure 5E). The opposite was observed in dnPI3K Tgs, with the lowest expression
14 in dnPI3K Tg(+/-) hearts (Figure 5E).

15

16

17

18

19

20

21

22

23

24

25

26

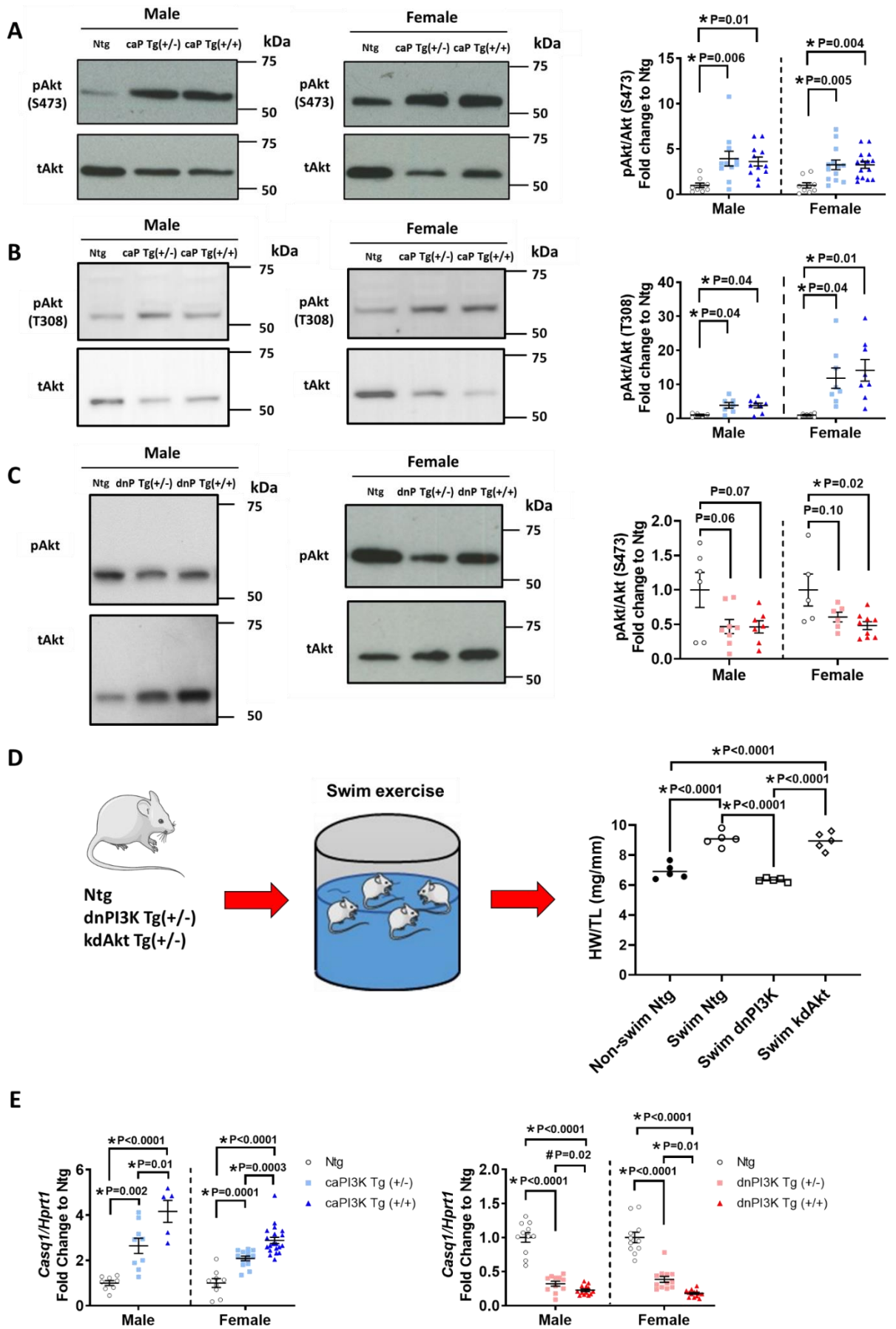


Figure 5: A component of PI3K and exercise-induced hypertrophy is Akt-independent **A & B)** Western blot images (left) and quantitation (right) of the phosphorylation of Akt (S473) panel A, and phosphorylation of Akt (T308) panel B in hearts of the caPI3K Tg models. N= 5-9 (Ntg male), 6-9 (Ntg female), 7-11 (caPI3K (+/-) male), 8-13 (caPI3K (+/-) female), 8-12 (caPI3K (+/+) male), 8-15 (caPI3K (+/+) female). **C)** Western blot images (left) and quantitation (right) of the phosphorylation of Akt (S473) in the dnPI3K Tg models. N= 6 (Ntg male), 5 (Ntg female), 8 (dnPI3K Tg(+/-) male), 6 (dnPI3K Tg(+/-) female), 7 (dnPI3K Tg (+/+) male), 9 (dnPI3K Tg(+/+) female). All data presented as mean±SEM. *One Way ANOVA followed by correction for multiple comparisons using Tukey's method. **D)** Ntg control mice, dnPI3K Tg(+/-) mice and kdAkt Tg(+/-) mice were subjected to 4 weeks of swim exercise for a previous study²⁰. Heart weight/tibia length (HW/TL). Data from the dnPI3K Tg(+/-) have previously been reported²⁰ but not in this format, and are included as a direct comparison for the kdAkt Tg(+/-) mice which have not been reported. All mice are male, N=5/group. *One Way ANOVA followed by correction for multiple comparisons using Tukey's method. **E)** Gene expression by qPCR of *Casq1* relative to *Hprt1* from ventricle tissue of 20 week old caPI3K Tg/dnPI3K Tg mice and Ntg littermates: Left, Ntg male & female (N=8,9), caPI3K Tg(+/-) male & female (N=9,13), caPI3K Tg(+/+) male & female (N=5, 20), and right: Ntg male & female (N=11,11), dnPI3K Tg(+/-) male & female (N=11,12), dnPI3K Tg(+/+) male & female (N=13, 13). All data presented as mean±SEM. *One Way ANOVA followed by correction for multiple comparisons using Tukey's method. # Unpaired t-test.

- 1 *Contribution of inflammatory signalling, GM3, and defective physiological signalling in*
- 2 *mediating pathology in a model of extreme endurance swim exercise and dnPI3K*
- 3 *Tg(+/+) mice*
- 4 Regular aerobic exercise activates the IGF1-PI3K-Akt pathway in the heart, but other
- 5 pathways are activated in a setting of extreme/intense endurance exercise. Prior work in
- 6 rodent models of extreme endurance exercise associated with atrial enlargement and
- 7 arrhythmia have shown evidence of activation of inflammatory pathways³⁵. There is also
- 8 cross-talk between the IGF1 and inflammatory pathways. We and others had previously

1 reported that increased levels of GM3 ganglioside, a glycosphingolipid within cellular
2 membranes, was associated with defective IGF1R signalling, insulin resistance,
3 dysregulation of inflammatory pathways via Toll-Like Receptor (TLR) signalling, and
4 AF³⁶⁻³⁸. Here, we investigated the potential contribution of these pathways in a setting of
5 extreme exercise by mining a freely available microarray data set from atria of mice
6 which had undergone intense swim training for 6wks, and shown to have atrial
7 enlargement, atrial fibrosis, and increased AF susceptibility³⁵. An enrichment of genes
8 involved with inflammatory pathways including, TLR4, NFκβ and tumour necrosis factor
9 α (TNFα) was previously presented in a heatmap format³⁵, and quantified by us in a
10 graphical format here (Figure 6A). In addition to this, we present previously unreported
11 new data from the profiling data set including an elevation of *St3gal5*, the gene encoding
12 GM3 synthase (GM3S; the enzyme responsible for the production of GM3, Figure 6A), as
13 well as dysregulation of genes critical for physiological PI3K-Akt1-CEBPβ-Cited4
14 signalling (Figure 6B).

15 To assess whether GM3 and TLR4 may have contributed to the more severe pathological
16 phenotype in the dnPI3K homozygote vs heterozygote Tg mice, we assessed GM3 lipids
17 by mass spectrometry, and TLR4 gene expression by qPCR. TLR4 gene expression was
18 elevated in hearts of dnPI3K Tg(+/-) vs Ntg, and elevated further in female dnPI3K
19 Tg(+/+) versus dnPI3K Tg(+/-)(Figure 6C). By contrast, TLR4 gene expression was not
20 significantly different from Ntg in the caPI3K Tg models (Figure 6C). Total GM3 lipids
21 were elevated in atria from both dnPI3K Tg models to a comparable degree, and there
22 was no change in the atria from the caPI3K Tg models vs Ntg (Figure 6D).

23

24 *Evidence of dysregulation of GM3 and PI3K signalling in veteran athletes with AF*

25 Given the clear evidence of cardiac dysfunction and pathology with reduced PI3K
26 (dnPI3K Tg(+/+)) but not increased PI3K (caPI3K Tg(+/+)), we assessed whether there

1 was any evidence of dysregulation in IGF1R-PI3K signalling in veteran athletes with AF
2 by assessing plasma lipid species. A description and comparison of athletes with and
3 without AF is presented in Supplementary Table 8. All athletes were male, and age,
4 gender and fitness were comparable between groups. We focused on GM3 which can
5 disrupt IGF1R-PI3K signalling, as well as phosphatidylinositol monophosphate (PIP1)
6 and lysophosphatidylinositol (LPI) which are regulators/constituents within the inositol-
7 PI3K signalling network³⁹(Figure 7A & B). In athletes with AF, total GM3 lipids and
8 specific GM3 species were elevated (Figure 7C), PIP1 levels were lower (Figure 7D), and
9 LPI levels were higher compared to athletes without AF (Figure 7E).

10

11

12

13

14

15

16

17

18

19

20

21

22

23

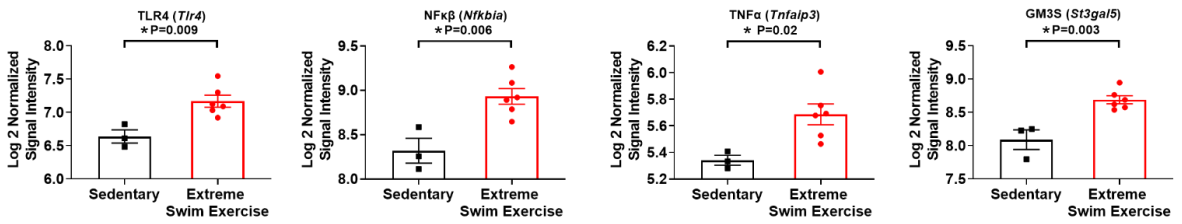
24

25

26

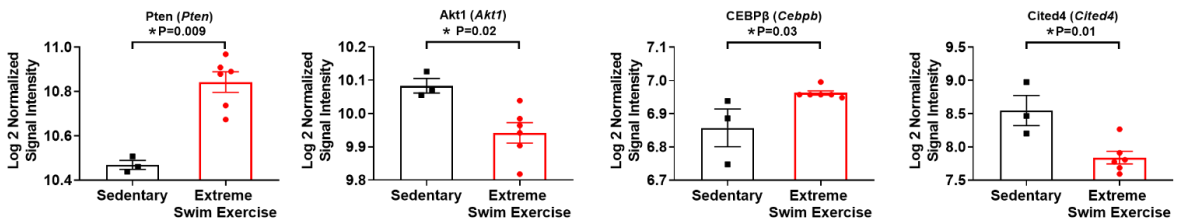
A Microarray

Upregulation of genes related to TLR4, NFκβ, TNFα & GM3 signalling with 8 weeks of extreme swim exercise

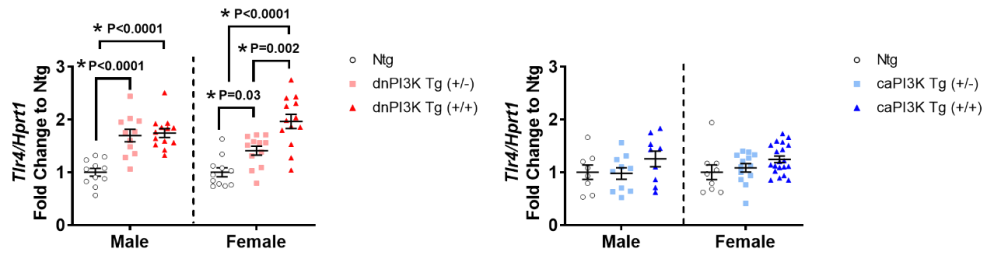


B Microarray

Dysregulation and inhibition of PI3K-Akt1-CEBPβ-Cited4 pathway with 8 weeks of extreme exercise



C qPCR



D Lipids

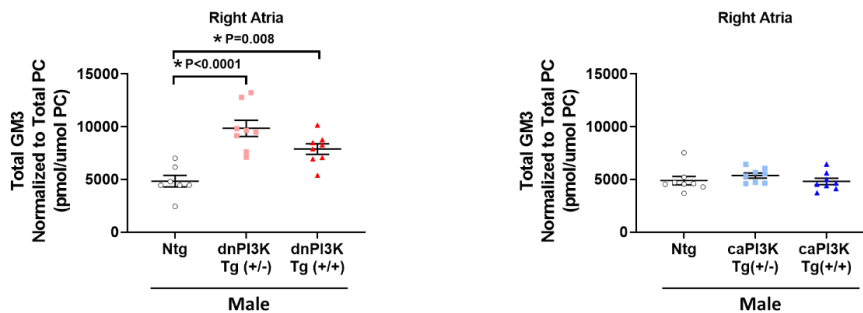


Figure 6: Inflammatory signalling, GM3, and defective physiological signalling in a model of extreme endurance swim exercise and dnPI3K Tg(+/-) mice

A) mRNAs related to TLR4 (*Tlr4*), NFκβ (*Nfkb1a*), TNFα (*Tnfaip3*) signalling & GM3 (GM3S gene expression, *St3gal5*), and **B**) mRNAs related to the PI3K-Akt1-CEBPβ-Cited4 pathway (*Pten*, *Akt1*, *Cebpb*, *Cited4*) by microarray in atria from sedentary mice (N=3), and mice subjected to 6 weeks of extreme swim exercise (N=6). Microarray deposited at <https://www.ebi.ac.uk/arrayexpress/experiments/E-MTAB-3106/>. **C**) Gene expression by qPCR of *Tlr4* relative to *Hprt1* from ventricle tissue of 20 week old

dnPI3K Tg/caPI3K Tg mice and Ntg littermates: Ntg male & female (N=11,11), dnPI3K Tg(+/-) male & female (N=11,12), dnPI3K Tg(+/+) male & female (N=13, 13), and caPI3K Tg mice : Ntg male & female (N=8,9), caPI3K Tg(+/-) male & female (N=10,13), caPI3K Tg(+/+) male & female (N=9, 20). **D**) Lipidomics was performed on right atria from 20 week old male dnPI3K Tg and Ntg littermates (Ntg: N=7, dnPI3K Tg(+/-): N=8, dnPI3K Tg(+/+): N=8), and caPI3K Tg and Ntg littermates (Ntg: N=8, caPI3K Tg(+/-): N=8, caPI3K Tg(+/+): N=8). All data presented as mean±SEM. Unpaired t-tests for panels **A** and **B**. * One Way ANOVA followed by correction for multiple comparisons using Tukey's method, for panel **C** and **D**.

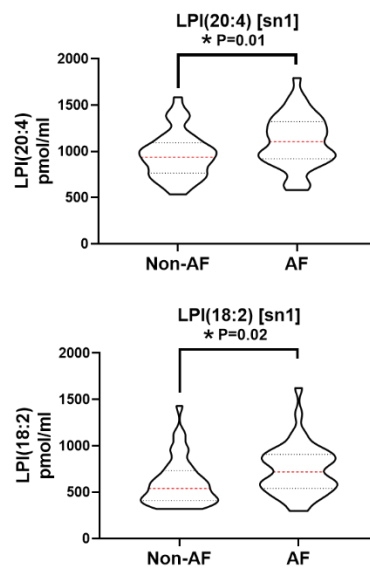
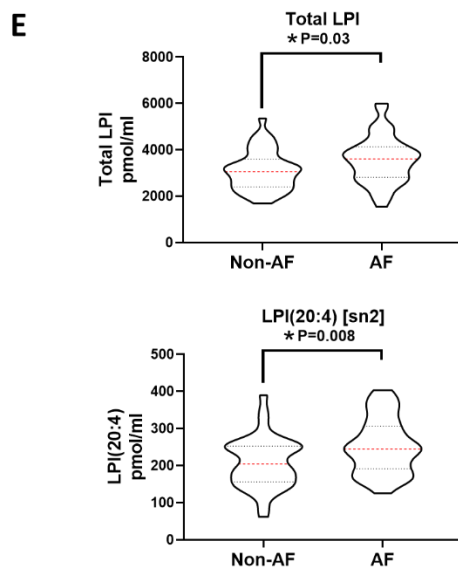
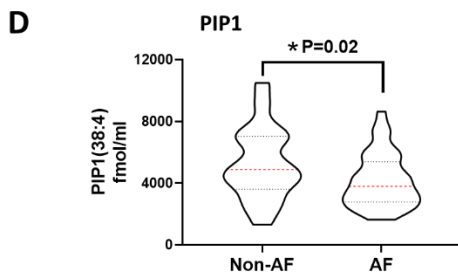
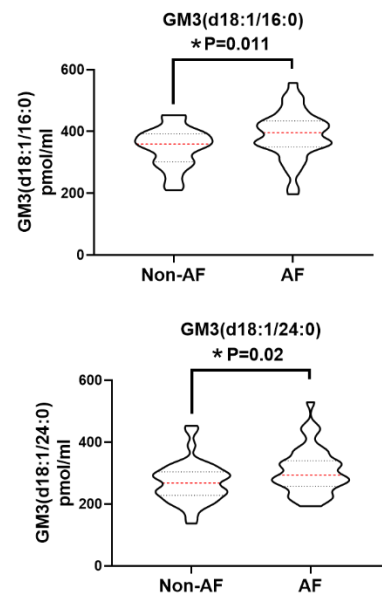
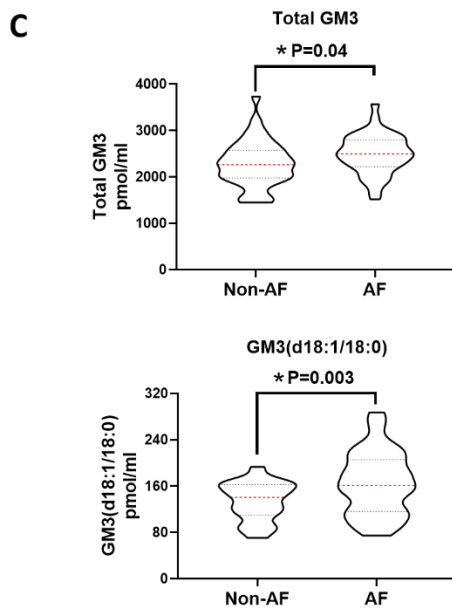
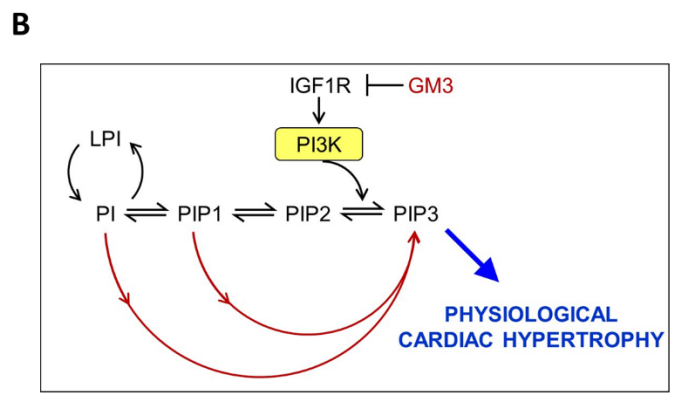
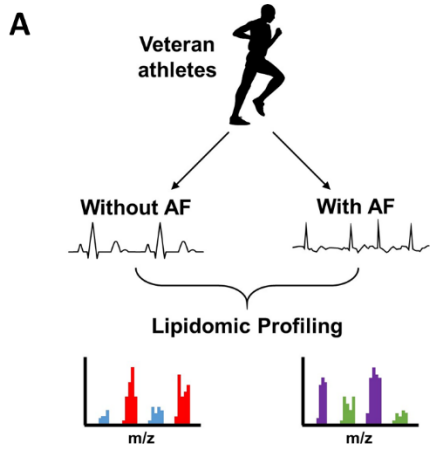


Figure 7: Dysregulation of GM3 and PI3K signalling in veteran athletes with AF

A) Lipidomics was performed on plasma from veteran athletes with and without AF. **B)** Relationship of phosphatidylinositol (PI) species, with PI3K and GM3 lipid species. Changes in regulators of the pathway can impact PI3K and the formation of PIP3. **C)** Total GM3 and individual GM3 lipid species. **D)** Phosphatidylinositol monophosphate (PIP1). **E)** Total lysophosphatidylinositol (LPI) and individual LPI lipid species. Data presented as violin plots, median with first and third quartiles. Athletes without AF, N=40; athletes with AF, N=40.

1 **Discussion**

2 The rationale for performing the current study arose from our interest in developing
3 PI3K-based therapies for the failing heart, a serendipitous observation of identifying atrial
4 enlargement and atrial thrombi in mice with reduced cardiac PI3K activity, and a
5 knowledge gap regarding the molecular mechanisms underlying the increased cardiac risk
6 with physical inactivity, extreme endurance exercise, and long-term activation of the
7 IGF1-PI3K-Akt pathway. An understanding of the mechanisms responsible has important
8 implications for understanding the “therapeutic window” of “exercise mimetics”, but also
9 identifying individuals at risk, and developing strategies to prevent cardiac pathology. In
10 this study, we examined the role of PI3K by studying mouse models with varying degrees
11 of PI3K activity in the heart. Here, we found no evidence of increased PI3K activity
12 causing cardiac dysfunction, arrhythmia, fibrosis or atrial pathology. By contrast, reduced
13 PI3K activity in the homozygote dnPI3K mice was associated with clear evidence of
14 cardiac dysfunction and fibrosis, as well as atrial enlargement and thrombi in a subset of
15 mice.

16

17

18

19

1 *No evidence that PI3K activity within physiological levels leads to cardiac dysfunction,*
2 *pathology or arrhythmia*

3 It was previously shown that heterozygote caPI3K Tg(+/-) mice have increased cardiac
4 PI3K activity, which was associated with an increase in heart weight characteristic of
5 physiological hypertrophy, i.e. normal heart function and no evidence of cell death or
6 fibrosis²⁸. In the current study, we generated homozygote mice (caPI3K Tg(+/+)) with the
7 goal of increasing cardiac PI3K activity further, but within physiological levels.
8 Swimming or voluntary wheel running in mice for 4wks was shown to increase
9 PI3K(p110 α) activity in the heart ~2-fold compared to untrained mice²⁷. PI3K activity
10 was elevated 2.9-fold in hearts of caPI3K Tg(+/-) and 5.1-fold in caPI3K Tg(+/+) vs Ntg,
11 and this was associated with a greater increase in heart weight in caPI3K Tg(+/+) mice.
12 Based on multiple measures, including atria and lung weights within a normal range,
13 preserved cardiac function, regular ECG parameters, and absence of fibrosis, the
14 hypertrophic response in caPI3K Tg(+/+) was characteristic of physiological hypertrophy.
15 At the molecular level, cardiac expression of ANP, BNP, and collagen genes was
16 comparable to Ntg or lower in caPI3K Tg(+/+) mice; consistent with previous studies in
17 caPI3K Tg(+/-) and/or exercise trained mice^{20 17 14, 30}. In comparing the homozygote
18 caPI3K Tg model with previous IGF1/PI3K/Akt models presenting with evidence of
19 cardiac dysfunction and pathology, there are some key differences. For example,
20 transgenic mice with cardiac myocyte over-expression of IGF1 initially developed
21 physiological hypertrophy, but this progressed to pathological hypertrophy over time. By
22 15wks there was evidence of fibrosis in IGF1 Tg mice, and cardiac function, which was
23 initially enhanced, progressively declined from 10wks of age. However, circulating IGF1
24 levels were also elevated and can lead to pathology due to secondary side effects in other
25 cardiac cell types (e.g. fibroblasts leading to fibrosis) and other organs²⁶. Cardiac
26 pathology was also identified in Akt models with very high transgene expression and Akt

1 activity (80-fold higher than control mice)⁴⁰, as well as models with inadequate
2 angiogenesis^{15, 41}. It remains unclear whether very high Akt activation leads to pathology
3 due to specific or non-specific mechanisms. However, an 80-fold increase in Akt activity
4 is well above physiological levels. Within the caPI3K models, the pAkt/total Akt ratio
5 was increased ~4-10 fold. The caPI3K Tg model does not display inadequate
6 angiogenesis, in fact, angiogenesis was elevated in mice receiving a caPI3K gene
7 therapy¹⁶. Within the current study, PI3K activity was chronically elevated in the hearts of
8 caPI3K Tgs for ~5 months. This is equivalent to ~15yrs in humans (based on lifespan)
9 and demonstrates that mid-long term activation of this pathway is safe in the adult mouse
10 heart^{42, 43}. However, we cannot exclude the possibility that higher PI3K activity (>10-
11 fold) or with longer term chronic expression, increased PI3K could also lead to cardiac
12 pathology. Aged caPI3K mice (20 months old) showed a very slight decline in fractional
13 shortening (Ntg: 44.7±0.9% vs caPI3K 42.6±0.6%)⁴².

14

15 *Reduced PI3K activity contributes to cardiac dysfunction, cardiac fibrosis, arrhythmia*
16 *and increased susceptibility to atrial thrombi*

17 Heterozygous dnPI3K Tg mice were previously shown to have smaller hearts with
18 relatively normal heart function, and without evidence of cell death or fibrosis²⁸. This
19 phenotype had been reproducible within multiple laboratories worldwide for over 15yrs²¹,
20 ^{28, 29, 44}. It therefore came as a surprise to identify atrial thrombi in dnPI3K Tg mice within
21 a more recent study. On further assessment, it became apparent there had been a breeding
22 error, which led to the generation of both heterozygote and homozygote dnPI3K mice,
23 and atrial enlargement and thrombi were only present in a subset of homozygote mice.
24 Given this unexpected observation, it was important to assess whether this result was
25 reproducible. In the current study, both heterozygote and homozygote dnPI3K Tg mice
26 displayed a small heart phenotype which was comparable based on heart weight.

1 However, dnPI3K Tg(+/+) mice displayed significant cardiac dysfunction and arrhythmia
2 in comparison to Ntg and dnPI3K Tg(+/-), and atrial enlargement and thrombi were only
3 present in dnPI3K Tg(+/+) mice. Some of our prior studies had implicated a decrease in
4 PI3K leading to an accelerated heart failure phenotype in settings of pressure overload,
5 DCM, diabetic cardiomyopathy and MI^{29-31, 45}. However, to our knowledge, our
6 observations in homozygote dnPI3K Tg mice represents the first study to implicate a
7 decrease in PI3K activity directly leading to severe cardiac dysfunction, serious ECG
8 abnormalities, atrial enlargement, atrial fibrosis, and atrial thrombi, i.e. in the absence of a
9 cardiac stress/disease model. The current work identifying atrial enlargement and
10 pathology in dnPI3K Tg(+/+) mice is significant because molecular mechanisms
11 associated with atrial pathology and thrombi are not well understood⁴⁶. From a clinical
12 perspective, it also has important implications for the use of any drugs that inhibit PI3K in
13 the heart. PI3K inhibitors are being actively developed within the cancer field, with
14 evidence of cardiotoxicity emerging^{47, 48}. We previously raised the concern of reduced
15 PI3K activity in the context of pre-existing cardiac stress or pathology^{30, 31, 49}. The current
16 study indicates that a decrease in PI3K alone, in the absence of significant cardiac
17 stress/pathology can also lead to adverse outcomes.

18

19 *Akt-independent mechanisms contribute to PI3K-induced hypertrophy and protection*

20 The phosphorylation of Akt is the best characterized downstream mediator of PI3K¹⁵, is
21 elevated in the heart with exercise, and Akt1 has been shown to be a critical mediator of
22 exercise-induced physiological cardiac hypertrophy^{21, 22}. In the current study, the
23 phosphorylation of Akt at both S473 and T308 phosphorylation sites relative to total Akt
24 was increased in the caPI3K Tg models, but unexpectedly no difference was observed
25 between caPI3K Tg(+/-) and caPI3K Tg(+/+) mice. Further, there was no apparent
26 association between the phosphorylation of Akt and the degree of cardiac pathology and

1 dysfunction in the dnPI3K homozygote and heterozygote Tg models. Collectively, this
2 prompted us to re-evaluate the Akt literature, as well as previous data from our own
3 studies. An increase in heart weight and PI3K activity in the caPI3K homozygote mice
4 compared to heterozygote mice, irrespective of Akt phosphorylation, suggests that a
5 component of PI3K-induced cardiac hypertrophy is occurring independent of Akt
6 phosphorylation. Consistent with this hypothesis, a kdAkt transgenic mutant was unable
7 to completely blunt caPI3K-induced hypertrophy in mice⁴⁰. Next, we re-examined the
8 hypertrophic response of Akt1 genetic models to exercise training in prior publications.
9 Data from previous studies showed that the blunted exercise-induced hypertrophic
10 response was more evident in global Akt1 knockout (KO) mice than cardiac-specific
11 kdAkt mice^{21, 50}. The findings in the global Akt1 KO mouse model are somewhat
12 confounded due to reduced Akt1 in other tissues, including skeletal muscle, which may
13 have had an impact on the ability of the mice to exercise to the same degree⁵⁰. On re-
14 visiting unpublished data from our own work, it was evident that the hypertrophic
15 response of dnPI3K heterozygote mice to exercise was substantially blunted, but this was
16 not apparent in the kdAkt mice. Together, this suggests that both caPI3K and exercise-
17 induced hypertrophy is mediated, at least in part, by a PI3K target which is independent
18 of Akt. Consistent with this hypothesis, myocardial metabolic and mitochondrial
19 adaptations in response to exercise have been shown to be mediated by PI3K activity
20 through Akt-independent signalling²¹.

21 To elucidate other potential mediators which might have contributed to the dose-response
22 phenotype in the caPI3K and dnPI3K Tg models, we revisited a list of PI3K-regulated
23 genes which we had ranked to identify genes which were inversely regulated in caPI3K
24 and dnPI3K Tg³³. Here, we show that calsequestrin 1 is increased and decreased in a dose
25 dependent manner in the caPI3K and dnPI3K Tg models, respectively. Studies in
26 calsequestrin 1 global KO mice indicated that calsequestrin 1 was essential for muscle

1 size/mass, normal sarcoplasmic reticulum development, and normal storage and release of
2 appropriate amounts of SR Ca²⁺³⁴. While the KO mice displayed muscle atrophy, the
3 heart was not specifically examined³⁴. Calsequestrin 1 was previously reported to largely
4 or exclusively be expressed in skeletal muscle, however, a very recent report published
5 after we commenced our own studies, has confirmed that calsequestrin 1 is expressed in
6 the adult heart, and reduced expression makes the heart susceptible to arrhythmias⁵¹.

7
8 *Potential role of defective IGF1R-PI3K signalling contributing to intense exercise-*
9 *induced cardiac complications, and increased risk with physical inactivity*

10 To date, there is limited knowledge regarding the molecular mechanisms responsible for
11 increased cardiac risk with “too much” or “too little” exercise/physical activity. Previous
12 work has implicated TNF α and p38 in mediating extreme exercise-induced atrial
13 enlargement and remodeling³⁵. Wildtype mice subjected to extreme swimming/treadmill
14 exercise (>70% of VO₂ max) for 6wks displayed atrial enlargement, fibrosis,
15 inflammation, and elevated TNF α -NF κ β -p38 signalling. These features were partially
16 prevented in TNF α KO mice or mice given a p38 inhibitor³⁵.

17 We previously reported that the phosphorylation of IGF1R, and PI3K activity were lower
18 in atrial appendages of patients with AF^{31, 36}. While it is well recognized that IGF1-PI3K-
19 Akt1- CEBP β -Cited4 signalling is elevated in the heart with regular aerobic exercise^{20, 25,}
20 ²⁷, we present evidence here that this pathway is defective in a setting of extreme
21 endurance exercise in mice (Figure 6B). This is further supported by a recent study which
22 showed that IGF1 gene expression was lower in the atria of mice subjected to intense
23 swim exercise for 2 weeks in mice⁵². Consistent with the idea that defective IGF1-PI3K
24 signalling could contribute to cardiac pathology in athletes undertaking endurance sports,
25 we show evidence of dysregulation of GM3, PIP1 and LPI lipids in plasma samples of
26 veteran athletes with AF.

1 On the lower end of the physical activity curve, findings from a low capacity running
2 (LCR) rat model are consistent with reduced cardiac PI3K contributing to cardiac
3 pathology due to physical inactivity. LCR rats were first identified by artificial selection
4 based on low intrinsic exercise capacity and shown to have an increased cardiovascular
5 risk profile⁵³. Left ventricles from LCR rats showed reduced cardiac mitochondrial
6 capacity, and cardiac myocyte abnormalities (myocyte dysfunction, and defective
7 contractile kinetics) which were not apparent in myocytes from LCR treated with a PI3K
8 activator (740YP)⁵⁴.

9

10 *Overview of IGF1-PI3K signalling with regular versus intense extreme exercise*

11 Circulating IGF1 levels increase in response to regular aerobic exercise, including
12 increased cardiac IGF1 formation⁵⁵⁻⁵⁷. In the heart, this activates PI3K signalling which
13 plays a role in the maintenance of cardiac structure, electrical function, improved cell
14 survival, increased antioxidant capacity, anti-inflammatory and anti-fibrotic properties³⁰,
15 ^{32, 45, 58} (Figure 8A, left panel, blue). In contrast, intense chronic exercise has been
16 associated with increased lipopolysaccharide (LPS), reduced IGF1, upregulation of TLR
17 signalling, activation and nuclear entry of NF κ B, and transcription of pro-inflammatory
18 cytokines including TNF α (Figure 8A, right panel, red)⁵⁹. There is also evidence that
19 TNF α induces an increase in gangliosides (including GM3) which contributes to defects
20 in insulin signalling⁶⁰, and that GM3 lipids can regulate TLR4 signalling³⁸. We previously
21 identified elevated GM3 lipids in atria from a mouse model with enlarged atria,
22 arrhythmia and increased susceptibility to AF³⁶. Of note, both regular aerobic exercise
23 and extreme intense exercise induce an immune response. However, intense long-term
24 exercise has been associated with higher levels of inflammatory mediators which can lead
25 to cardiac pathology when endogenous protective mechanisms are overwhelmed. Prior
26 work has suggested that PI3K inhibits cardiac inflammation and fibrosis by inhibiting

1 TLR4 signalling⁶¹, potentially via a mechanism involving PIP2. In a setting of elevated
2 PI3K activation (e.g. due to regular exercise or caPI3K Tg), PI3K converts PIP2 into
3 PIP3. Given TLR4 signalling also requires PIP2, elevated PI3K could negatively regulate
4 TLR4 signalling due to the limited availability of the PI3K substrate (PIP2)⁶²(Figure 8A,
5 left panel).

6

7

8

9

10

11

12

13

14

15

16

17

18

19

20

21

22

23

24

25

26

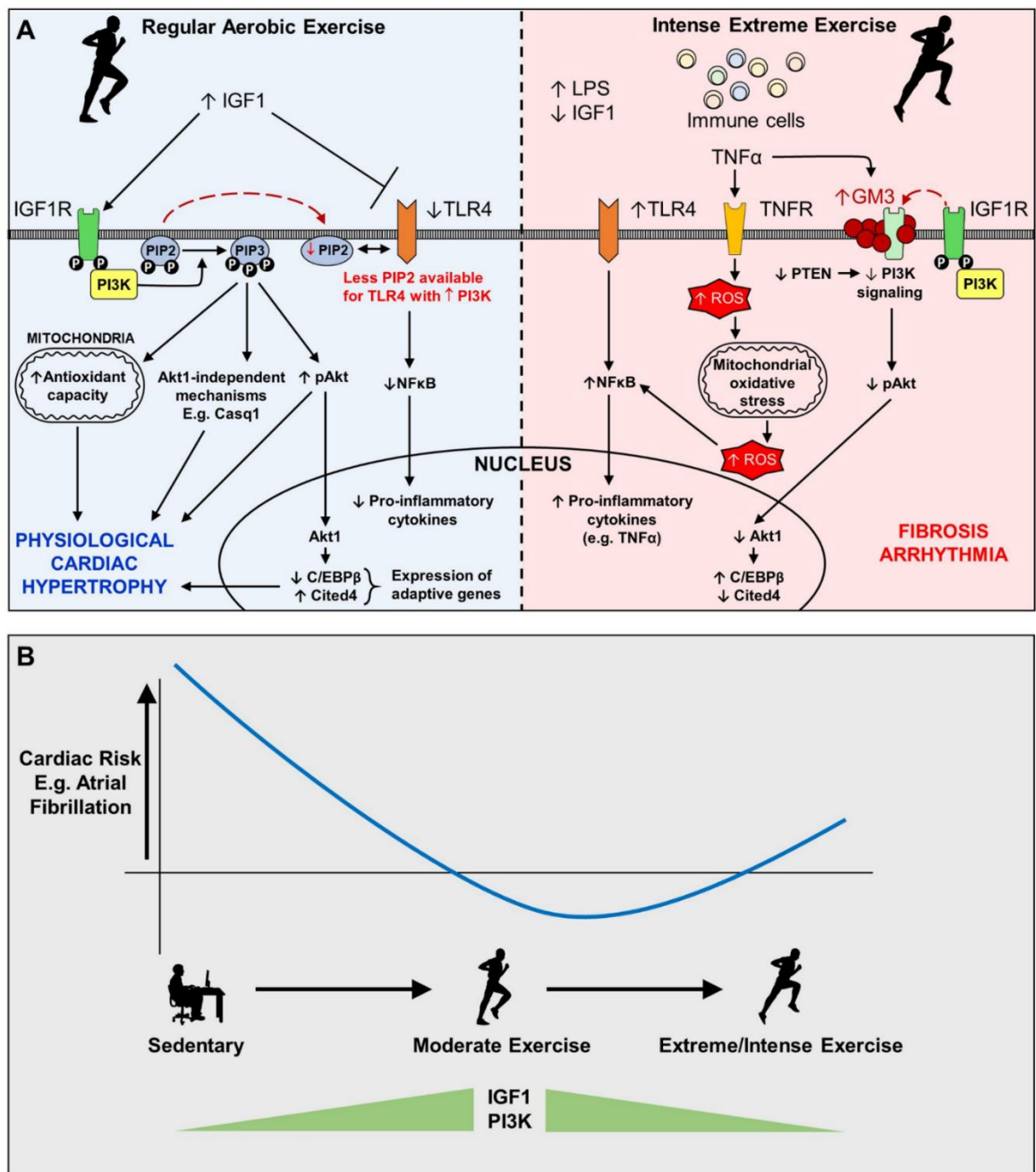


Figure 8: Overview schematics A) Overview of IGF1-PI3K signalling in the heart with regular and extreme exercise. Circulating IGF1 and cardiac formation of IGF1 is elevated with regular exercise (left side, blue). PI3K activity increases the phosphorylation of Akt but also acts via Akt independent mechanisms to induce physiological hypertrophy. In a setting of increased PI3K (exercise or caPI3K Tg) PIP2 is converted to PIP3, limiting the availability of PIP2 for TLR4 signalling, and subsequently reducing pro-inflammatory cytokines. Intense extreme exercise is associated with elevated LPS, lower IGF1, and increased TLR4 signalling (right side, red). There is also evidence of increased GM3 in response to increased TNF α , which would inhibit IGF1R-PI3K signalling. Increased GM3

reduces membrane fluidity, and disrupts the normal interaction of IGF1R with caveolins to induce downstream protective PI3K signalling. Collectively these signalling alterations will contribute to cell death, fibrosis and arrhythmia. **B)** Potential contribution of PI3K signalling to the reverse J-shaped relationship between physical activity and cardiac risk. An inverse relationship between PI3K activity and cardiac risk is hypothesized.

1 *Conclusion*

2 In summary, the current study demonstrates that in the absence of any cardiac insult,
3 reduced PI3K in the heart can lead to significant cardiac dysfunction, pathology, and an
4 increased susceptibility to atrial enlargement and thrombi. Given PI3K is elevated in the
5 heart with exercise, and increasing PI3K can restore abnormalities in a rat model with low
6 exercise capacity and an increased cardiac risk profile, we propose that reduced cardiac
7 PI3K contributes to the association between physical inactivity/sedentary behaviour and
8 increased cardiovascular risk (Figure 8B). In contrast, we found a dose-dependent
9 relationship between PI3K activity and physiological hypertrophy, with no evidence of
10 elevated PI3K directly contributing to cardiac dysfunction and pathology. Furthermore,
11 there is evidence of reduced IGF1/PI3K signalling with extreme exercise in a setting of
12 increased pro-inflammatory cytokines (Figure 6A&B and 8)^{52, 56, 63}. It therefore appears
13 unlikely that increasing PI3K to levels that would be attainable with exercise, would
14 contribute to the adverse outcomes seen in a small percentage of athletes undertaking high
15 volumes of extreme endurance exercise. However, in considering therapeutic approaches
16 targeting PI3K and other regulators of exercise-induced protection it is important to target
17 a physiological range, and monitor for any adverse consequences with chronic use.
18 Finally, multiple mechanisms and factors will contribute to elevated cardiac risk in
19 sedentary individuals and extreme endurance athletes⁹. Changes in PI3K alone will not
20 completely recapitulate what is observed in humans. However, because PI3K is increased
21 in the heart by physical activity/exercise, and a master regulator of exercise-induced
22 hypertrophy and protection, reduced PI3K will contribute to increased cardiac risk.

1 Screening of lipids for dysregulation of GM3 and PI3K signalling in athletes, may
2 identify athletes at increased risk of AF.

3

4 **Funding**

5 This work was supported by grants from the National Health and Medical Research
6 Council [grant number 1125514 to JRM, grant number 1120129 to JRM and CEH], and
7 in part by the Victorian Government's Operational Infrastructure Support Program. SB is
8 supported by a joint Baker Heart and Diabetes Institute-La Trobe University doctoral
9 scholarship. KLW and ALG are supported by Future Leader Fellowships from the
10 National Heart Foundation of Australia [grant number 102539 to KLW, grant number
11 102206 to ALG]. BCB is supported by an Alice Baker and Eleanor Shaw Fellowship (The
12 Baker Foundation, Australia). JRM is supported by a National Health and Medical
13 Research Council Senior Research Fellowship [grant number 1078985].

14

15 **Data availability**

16 The data underlying this article will be shared on reasonable request to the corresponding
17 author.

18

19 **Acknowledgements**

20 The authors wish to thank Esther Boey, Natalie Patterson and Amy Mitchell for technical
21 assistance. We acknowledge the use of facilities and technical assistance from the
22 Monash Histology Platform.

23

24 **Conflict of interest:** None declared

25

26

1 **References**

- 2 1. Kujala UM, Kaprio J, Sarna S, Koskenvuo M. Relationship of leisure-time
3 physical activity and mortality: the Finnish twin cohort. *JAMA* 1998;**279**(6):440-4.
- 4 2. Powell KE, Thompson PD, Caspersen CJ, Kendrick JS. Physical activity and the
5 incidence of coronary heart disease. *Annu Rev Public Health* 1987;**8**:253-87.
- 6 3. Fleg JL, Cooper LS, Borlaug BA, Haykowsky MJ, Kraus WE, Levine BD, Pfeffer
7 MA, Pina IL, Poole DC, Reeves GR, Whellan DJ, Kitzman DW, National Heart L, Blood
8 Institute Working G. Exercise training as therapy for heart failure: current status and
9 future directions. *Circ Heart Fail* 2015;**8**(1):209-20.
- 10 4. Boden WE, Franklin B, Berra K, Haskell WL, Calfas KJ, Zimmerman FH,
11 Wenger NK. Exercise as a therapeutic intervention in patients with stable ischemic heart
12 disease: an underfilled prescription. *Am J Med* 2014;**127**(10):905-11.
- 13 5. Galanti G, Stefani L, Mascherini G, Di Tante V, Toncelli L. Left ventricular
14 remodeling and the athlete's heart, irrespective of quality load training. *Cardiovasc*
15 *Ultrasound* 2016;**14**(1):46.
- 16 6. Buckley BJR, Lip GYH, Thijssen DHJ. The counterintuitive role of exercise in the
17 prevention and cause of atrial fibrillation. *Am J Physiol Heart Circ Physiol*
18 2020;**319**(5):H1051-h1058.
- 19 7. Eijsvogels TMH, Thompson PD, Franklin BA. The "Extreme Exercise
20 Hypothesis": Recent Findings and Cardiovascular Health Implications. *Curr Treat*
21 *Options Cardiovasc Med* 2018;**20**(10):84.
- 22 8. La Gerche A, Heidbuchel H. Can Intensive Exercise Harm the Heart?: You Can
23 Get Too Much of a Good Thing. *Circulation* 2014;**130**(12):992-1002.
- 24 9. Guasch E, Mont L. Diagnosis, pathophysiology, and management of exercise-
25 induced arrhythmias. *Nat Rev Cardiol* 2017;**14**(2):88-101.
- 26 10. Guasch E, Benito B, Qi X, Cifelli C, Naud P, Shi Y, Mighiu A, Tardif JC,
27 Tadevosyan A, Chen Y, Gillis MA, Iwasaki YK, Dobrev D, Mont L, Heximer S, Nattel S.
28 Atrial fibrillation promotion by endurance exercise: demonstration and mechanistic
29 exploration in an animal model. *J Am Coll Cardiol* 2013;**62**(1):68-77.
- 30 11. Merghani A, Malhotra A, Sharma S. The U-shaped relationship between exercise
31 and cardiac morbidity. *Trends Cardiovasc Med* 2016;**26**(3):232-40.
- 32 12. La Gerche A, Connelly KA, Mooney DJ, MacIsaac AI, Prior DL. Biochemical
33 and functional abnormalities of left and right ventricular function after ultra-endurance
34 exercise. *Heart* 2008;**94**(7):860-6.

- 1 13. La Gerche A, Claessen G, Dymarkowski S, Voigt JU, De Buck F, Vanhees L,
2 Droogne W, Van Cleemput J, Claus P, Heidebuchel H. Exercise-induced right ventricular
3 dysfunction is associated with ventricular arrhythmias in endurance athletes. *Eur Heart J*
4 2015;**36**(30):1998-2010.
- 5 14. Bernardo BC, Weeks KL, Pretorius L, McMullen JR. Molecular distinction
6 between physiological and pathological cardiac hypertrophy: experimental findings and
7 therapeutic strategies. *Pharmacol Ther* 2010;**128**(1):191-227.
- 8 15. Bernardo BC, Ooi JYY, Weeks KL, Patterson NL, McMullen JR. Understanding
9 Key Mechanisms of Exercise-Induced Cardiac Protection to Mitigate Disease: Current
10 Knowledge and Emerging Concepts. *Physiol Rev* 2018;**98**(1):419-475.
- 11 16. Weeks KL, Gao X, Du XJ, Boey EJ, Matsumoto A, Bernardo BC, Kiriazis H,
12 Cemerlang N, Tan JW, Tham YK, Franke TF, Qian H, Bogoyevitch MA, Woodcock EA,
13 Febbraio MA, Gregorevic P, McMullen JR. Phosphoinositide 3-Kinase p110alpha Is a
14 Master Regulator of Exercise-Induced Cardioprotection and PI3K Gene Therapy Rescues
15 Cardiac Dysfunction. *Circ Heart Fail* 2012;**5**(4):523-34.
- 16 17. McMullen JR, Shioi T, Huang WY, Zhang L, Tarnavski O, Bisping E, Schinke M,
17 Kong S, Sherwood MC, Brown J, Riggi L, Kang PM, Izumo S. The insulin-like growth
18 factor 1 receptor induces physiological heart growth via the phosphoinositide 3-
19 kinase(p110alpha) pathway. *J Biol Chem* 2004;**279**(6):4782-93.
- 20 18. Kim J, Wende AR, Sena S, Theobald HA, Soto J, Sloan C, Wayment BE, Litwin
21 SE, Holzenberger M, LeRoith D, Abel ED. Insulin-like growth factor I receptor signaling
22 is required for exercise-induced cardiac hypertrophy. *Mol Endocrinol* 2008;**22**(11):2531-
23 43.
- 24 19. Riehle C, Wende AR, Zhu Y, Oliveira KJ, Pereira RO, Jaishy BP, Bevins J,
25 Valdez S, Noh J, Kim BJ, Moreira AB, Weatherford ET, Manivel R, Rawlings TA, Rech
26 M, White MF, Abel ED. Insulin receptor substrates are essential for the bioenergetic and
27 hypertrophic response of the heart to exercise training. *Mol Cell Biol* 2014;**34**(18):3450-
28 60.
- 29 20. McMullen JR, Shioi T, Zhang L, Tarnavski O, Sherwood MC, Kang PM, Izumo
30 S. Phosphoinositide 3-kinase(p110alpha) plays a critical role for the induction of
31 physiological, but not pathological, cardiac hypertrophy. *Proc Natl Acad Sci U S A*
32 2003;**100**(21):12355-60.
- 33 21. O'Neill BT, Kim J, Wende AR, Theobald HA, Tuinei J, Buchanan J, Guo A, Zaha
34 VG, Davis DK, Schell JC, Boudina S, Wayment B, Litwin SE, Shioi T, Izumo S,
35 Birnbaum MJ, Abel ED. A conserved role for phosphatidylinositol 3-kinase but not Akt

- 1 signaling in mitochondrial adaptations that accompany physiological cardiac hypertrophy.
2 Cell Metab 2007;**6**(4):294-306.
- 3 22. DeBosch B, Treskov I, Lupu TS, Weinheimer C, Kovacs A, Courtois M, Muslin
4 AJ. Akt1 is required for physiological cardiac growth. Circulation 2006;**113**(17):2097-
5 104.
- 6 23. Noh J, Wende AR, Olsen CD, Kim B, Bevins J, Zhu Y, Zhang QJ, Riehle C, Abel
7 ED. Phosphoinositide dependent protein kinase 1 is required for exercise-induced cardiac
8 hypertrophy but not the associated mitochondrial adaptations. J Mol Cell Cardiol
9 2015;**89**(Pt B):297-305.
- 10 24. Bostrom P, Mann N, Wu J, Quintero PA, Plovie ER, Panakova D, Gupta RK,
11 Xiao C, MacRae CA, Rosenzweig A, Spiegelman BM. C/EBPbeta controls exercise-
12 induced cardiac growth and protects against pathological cardiac remodeling. Cell
13 2010;**143**(7):1072-83.
- 14 25. Weeks KL, Tham YK, Yildiz SG, Alexander Y, Donner DG, Kiriazis H,
15 Harmawan CA, Hsu AT, Bernardo BC, Matsumoto A, DePinho RA, Abel ED, Woodcock
16 EA, McMullen JR. FoxO1 is required for physiological cardiac hypertrophy induced by
17 exercise but not by constitutively active PI3K. Am J Physiol Heart Circ Physiol 2021.
- 18 26. Delaughter MC, Taffet GE, Fiorotto ML, Entman ML, Schwartz RJ. Local
19 insulin-like growth factor I expression induces physiologic, then pathologic, cardiac
20 hypertrophy in transgenic mice. FASEB J 1999;**13**(14):1923-9.
- 21 27. Perrino C, Naga Prasad SV, Mao L, Noma T, Yan Z, Kim H-S, Smithies O,
22 Rockman HA. Intermittent pressure overload triggers hypertrophy-independent cardiac
23 dysfunction and vascular rarefaction. J Clin Invest 2006;**116**(6):1547-60.
- 24 28. Shioi T, Kang PM, Douglas PS, Hampe J, Yballe CM, Lawitts J, Cantley LC,
25 Izumo S. The conserved phosphoinositide 3-kinase pathway determines heart size in
26 mice. EMBO J 2000;**19**(11):2537-48.
- 27 29. Lin RC, Weeks KL, Gao XM, Williams RB, Bernardo BC, Kiriazis H, Matthews
28 VB, Woodcock EA, Bouwman RD, Mollica JP, Speirs HJ, Dawes IW, Daly RJ, Shioi T,
29 Izumo S, Febbraio MA, Du XJ, McMullen JR. PI3K(p110 alpha) protects against
30 myocardial infarction-induced heart failure: identification of PI3K-regulated miRNA and
31 mRNA. Arterioscler Thromb Vasc Biol 2010;**30**(4):724-32.
- 32 30. McMullen JR, Amirahmadi F, Woodcock EA, Schinke-Braun M, Bouwman RD,
33 Hewitt KA, Mollica JP, Zhang L, Zhang Y, Shioi T, Buerger A, Izumo S, Jay PY,
34 Jennings GL. Protective effects of exercise and phosphoinositide 3-kinase(p110alpha)

- 1 signaling in dilated and hypertrophic cardiomyopathy. Proc Natl Acad Sci U S A
2 2007;**104**(2):612-7.
- 3 31. Pretorius L, Du XJ, Woodcock EA, Kiriazis H, Lin RC, Marasco S, Medcalf RL,
4 Ming Z, Head GA, Tan JW, Cemerlang N, Sadoshima J, Shioi T, Izumo S, Lukoshkova
5 EV, Dart AM, Jennings GL, McMullen JR. Reduced phosphoinositide 3-kinase
6 (p110alpha) activation increases the susceptibility to atrial fibrillation. Am J Pathol
7 2009;**175**(3):998-1009.
- 8 32. Waardenberg AJ, Bernardo BC, Ng DC, Shepherd PR, Cemerlang N, Sbroggio M,
9 Wells CA, Dalrymple BP, Brancaccio M, Lin RC, McMullen JR. Phosphoinositide 3-
10 kinase (PI3K(p110alpha)) directly regulates key components of the Z-disc and cardiac
11 structure. J Biol Chem 2011;**286**(35):30837-46.
- 12 33. Bass-Stringer S, Ooi JYY, McMullen JR. Clusterin is regulated by IGF1-PI3K
13 signaling in the heart: implications for biomarker and drug target discovery, and
14 cardiotoxicity. Arch Toxicol 2020;**94**(5):1763-1768.
- 15 34. Paolini C, Quarta M, Nori A, Boncompagni S, Canato M, Volpe P, Allen PD,
16 Reggiani C, Protasi F. Reorganized stores and impaired calcium handling in skeletal
17 muscle of mice lacking calsequestrin-1. J Physiol 2007;**583**(Pt 2):767-84.
- 18 35. Aschar-Sobbi R, Izaddoustdar F, Korogyi AS, Wang Q, Farman GP, Yang F,
19 Yang W, Dorian D, Simpson JA, Tuomi JM, Jones DL, Nanthakumar K, Cox B, Wehrens
20 XH, Dorian P, Backx PH. Increased atrial arrhythmia susceptibility induced by intense
21 endurance exercise in mice requires TNFalpha. Nat Commun 2015;**6**:6018.
- 22 36. Sapra G, Tham YK, Cemerlang N, Matsumoto A, Kiriazis H, Bernardo BC,
23 Henstridge DC, Ooi JY, Pretorius L, Boey EJ, Lim L, Sadoshima J, Meikle PJ, Mellet
24 NA, Woodcock EA, Marasco S, Ueyama T, Du XJ, Febbraio MA, McMullen JR. The
25 small-molecule BGP-15 protects against heart failure and atrial fibrillation in mice.
26 Nature Communications 2014;**5**:5705.
- 27 37. Prokazova NV, Samovilova NN, Gracheva EV, Golovanova NK. Ganglioside
28 GM3 and its biological functions. Biochemistry (Moscow) 2009;**74**(3):235-49.
- 29 38. Kanoh H, Nitta T, Go S, Inamori KI, Veillon L, Nihei W, Fujii M, Kabayama K,
30 Shimoyama A, Fukase K, Ohto U, Shimizu T, Watanabe T, Shindo H, Aoki S, Sato K,
31 Nagasaki M, Yatomi Y, Komura N, Ando H, Ishida H, Kiso M, Natori Y, Yoshimura Y,
32 Zonca A, Cattaneo A, Letizia M, Ciampa M, Mauri L, Prinetti A, Sonnino S, Suzuki A,
33 Inokuchi JI. Homeostatic and pathogenic roles of GM3 ganglioside molecular species in
34 TLR4 signaling in obesity. Embo j 2020;**39**(12):e101732.

- 1 39. Sasaki T, Takasuga S, Sasaki J, Kofuji S, Eguchi S, Yamazaki M, Suzuki A.
2 Mammalian phosphoinositide kinases and phosphatases. *Prog Lipid Res* 2009;**48**(6):307-
3 43.
- 4 40. Shioi T, McMullen JR, Kang PM, Douglas PS, Obata T, Franke TF, Cantley LC,
5 Izumo S. Akt/protein kinase B promotes organ growth in transgenic mice. *Mol Cell Biol*
6 2002;**22**(8):2799-809.
- 7 41. Shiojima I, Sato K, Izumiya Y, Schiekofer S, Ito M, Liao R, Colucci WS, Walsh
8 K. Disruption of coordinated cardiac hypertrophy and angiogenesis contributes to the
9 transition to heart failure. *J Clin Invest* 2005;**115**(8):2108-18.
- 10 42. Niizuma S, Inuzuka Y, Okuda J, Kato T, Kawashima T, Tamaki Y, Iwanaga Y,
11 Yoshida Y, Kosugi R, Watanabe-Maeda K, Machida Y, Tsuji S, Aburatani H, Izumi T,
12 Kita T, Kimura T, Shioi T. Effect of persistent activation of phosphoinositide 3-kinase on
13 heart. *Life Sci* 2012;**90**(15-16):619-28.
- 14 43. Dutta S, Sengupta P. Men and mice: Relating their ages. *Life Sci* 2016;**152**:244-8.
- 15 44. Crackower MA, Oudit GY, Kozieradzki I, Sarao R, Sun H, Sasaki T, Hirsch E,
16 Suzuki A, Shioi T, Irie-Sasaki J, Sah R, Cheng HY, Rybin VO, Lembo G, Fratta L,
17 Oliveira-dos-Santos AJ, Benovic JL, Kahn CR, Izumo S, Steinberg SF, Wymann MP,
18 Backx PH, Penninger JM. Regulation of myocardial contractility and cell size by distinct
19 PI3K-PTEN signaling pathways. *Cell* 2002;**110**(6):737-49.
- 20 45. Ritchie RH, Love JE, Huynh K, Bernardo BC, Henstridge DC, Kiriazis H, Tham
21 YK, Sapra G, Qin C, Cemerlang N, Boey EJ, Jandeleit-Dahm K, Du XJ, McMullen JR.
22 Enhanced phosphoinositide 3-kinase(p110alpha) activity prevents diabetes-induced
23 cardiomyopathy and superoxide generation in a mouse model of diabetes. *Diabetologia*
24 2012;**55**(12):3369-81.
- 25 46. Chen YC, Voskoboinik A, Gerche AL, Marwick TH, McMullen JR. Prevention of
26 Pathological Atrial Remodeling and Atrial Fibrillation: JACC State-of-the-Art Review.
27 *Journal of the American College of Cardiology* 2021;**77**(22):2846-2864.
- 28 47. Dreyling M, Morschhauser F, Bouabdallah K, Bron D, Cunningham D, Assouline
29 SE, Verhoef G, Linton K, Thieblemont C, Vitolo U, Hiemeyer F, Giurescu M, Garcia-
30 Vargas J, Gorbachevsky I, Liu L, Koechert K, Peña C, Neves M, Childs BH, Zinzani PL.
31 Phase II study of copanlisib, a PI3K inhibitor, in relapsed or refractory, indolent or
32 aggressive lymphoma. *Ann Oncol* 2017;**28**(9):2169-2178.
- 33 48. Kim RD, Alberts SR, Peña C, Genvresse I, Ajavon-Hartmann A, Xia C, Kelly A,
34 Grilley-Olson JE. Phase I dose-escalation study of copanlisib in combination with

- 1 gemcitabine or cisplatin plus gemcitabine in patients with advanced cancer. *Br J Cancer*
2 2018;**118**(4):462-470.
- 3 49. McMullen JR, Jay PY. PI3K(p110alpha) inhibitors as anti-cancer agents: minding
4 the heart. *Cell Cycle* 2007;**6**(8):910-3.
- 5 50. DeBosch B, Treskov I, Lupu TS, Weinheimer C, Kovacs A, Courtois M, Muslin
6 AJ. Akt1 Is Required for Physiological Cardiac Growth. *Circulation* 2006;**113**(17):2097-
7 2104.
- 8 51. Sun Z, Wang L, Han L, Wang Y, Zhou Y, Li Q, Wu Y, Talabieke S, Hou Y, Wu
9 L, Liu R, Fu Z, You H, Li BY, Zheng Y, Luo D. Functional Calsequestrin-1 Is Expressed
10 in the Heart and Its Deficiency Is Causally Related to Malignant Hyperthermia-Like
11 Arrhythmia. *Circulation* 2021.
- 12 52. Oh Y, Yang S, Liu X, Jana S, Izaddoustdar F, Gao X, Debi R, Kim DK, Kim KH,
13 Yang P, Kassiri Z, Lakin R, Backx PH. Transcriptomic Bioinformatic Analyses of Atria
14 Uncover Involvement of Pathways Related to Strain and Post-translational Modification
15 of Collagen in Increased Atrial Fibrillation Vulnerability in Intensely Exercised Mice.
16 *Front Physiol* 2020;**11**:605671.
- 17 53. Wisloff U, Najjar SM, Ellingsen O, Haram PM, Swoap S, Al-Share Q, Fernstrom
18 M, Rezaei K, Lee SJ, Koch LG, Britton SL. Cardiovascular risk factors emerge after
19 artificial selection for low aerobic capacity. *Science* 2005;**307**(5708):418-20.
- 20 54. Moreira JBN, Alves MNM, Britton SL, Koch LG, Wisloff U, Bye A. Pi3k
21 modulates cardiomyocyte phenotype in rats selected for low aerobic capacity. *Eur Heart J*
22 2013;**34 Suppl 1**:4202.
- 23 55. Neri Serneri GG, Boddi M, Modesti PA, Cecioni I, Coppo M, Padeletti L,
24 Michelucci A, Colella A, Galanti G. Increased cardiac sympathetic activity and insulin-
25 like growth factor-I formation are associated with physiological hypertrophy in athletes.
26 *Circ Res* 2001;**89**(11):977-82.
- 27 56. Cavalcante PAM, Gregnani MF, Henrique JS, Ornellas FH, Araújo RC. Aerobic
28 but not Resistance Exercise Can Induce Inflammatory Pathways via Toll-Like 2 and 4: a
29 Systematic Review. *Sports Med Open* 2017;**3**(1):42.
- 30 57. Berg U, Bang P. Exercise and circulating insulin-like growth factor I. *Horm Res*
31 2004;**62 Suppl 1**:50-8.
- 32 58. Yang KC, Foeger NC, Marionneau C, Jay PY, McMullen JR, Nerbonne JM.
33 Homeostatic regulation of electrical excitability in physiological cardiac hypertrophy. *J*
34 *Physiol* 2010;**588**(Pt 24):5015-32.

- 1 59. La Gerche A, Inder WJ, Roberts TJ, Brosnan MJ, Heidbuchel H, Prior DL.
2 Relationship between Inflammatory Cytokines and Indices of Cardiac Dysfunction
3 following Intense Endurance Exercise. *PLoS One* 2015;**10**(6):e0130031.
- 4 60. Sasaki N, Itakura Y, Toyoda M. Gangliosides Contribute to Vascular Insulin
5 Resistance. *Int J Mol Sci* 2019;**20**(8).
- 6 61. Liu F, Wen Y, Kang J, Wei C, Wang M, Zheng Z, Peng J. Regulation of TLR4
7 expression mediates the attenuating effect of erythropoietin on inflammation and
8 myocardial fibrosis in rat heart. *Int J Mol Med* 2018;**42**(3):1436-1444.
- 9 62. Laird MH, Rhee SH, Perkins DJ, Medvedev AE, Piao W, Fenton MJ, Vogel SN.
10 TLR4/MyD88/PI3K interactions regulate TLR4 signaling. *J Leukoc Biol* 2009;**85**(6):966-
11 77.
- 12 63. Eliakim A, Nemet D. Exercise training, physical fitness and the growth hormone-
13 insulin-like growth factor-1 axis and cytokine balance. *Med Sport Sci* 2010;**55**:128-140

Data Supplement

Methods

Animals

Studies were performed on male and female mice at approximately 4 months of age. Mice were housed in a temperature-controlled environment with a 12 h light cycle and had *ad libitum* access to standard rodent chow. Any exclusions of animals or experimental data are outlined in flow charts (Supplementary Figures 1 & 2).

Genotyping of mice

DNA was extracted from tail clippings and genotyping of caPI3K Tg(+/- or +/+) and dnPI3K Tg(+/- or +/+) mice were performed using Real-time PCR (RT-PCR) (Applied Biosystems 7500 Fast Real-Time PCR System). A SYBR[®] Green PCR Master Mix (Applied Biosystems[™]) was used in conjunction with standard SYBR[®] Green RT-PCR cycling conditions. Details of primers are presented below. Expression was normalized to Stat-1 using the $2^{-\Delta\Delta C_t}$ method of quantification and caPI3K/dnPI3K gene copy numbers were determined using known control samples. The genotype calculation was based on the knowledge that a heterozygote has one copy and a homozygote has two, therefore using primers specific to the transgene, we could confidently determine that one less PCR cycle would be required to amplify the (+/+) compared to the (+/-) mice. To confirm the initial genotype, mice were re-genotyped at the endpoint of the study with tail clippings taken at dissection.

Gene	Species	Forward Primer Name	Forward Primer Sequence 5'-3'	Reverse Primer Name	Reverse Primer Sequence 5'-3'	Amplicon Size (bp)	Tms & deg; C (F, R)	Intron Spanning	Single Peak in Melt Curve
Dominant negative PI3K; DD	Mouse	m-DD forward	ccctcctatctccccataa	m-DD reverse	cattggggagtaaaccattcca	151	60, 59	NO	Y
Constitutively active PI3K; QQ	Mouse	m-QQ forward	ggtgaatggggaatctgaat	m-QQ Reverse	tatattccccaggccaatg	137	60, 60	NO	Y
Signal transducer and activator of transcription 1; Stat1	Mouse	M-Stat1 forward	cagaaaagccacagcaatga	m-Stat1 reverse	ttagtcccggacacttggtc	103	59,60	NO	Y

Echocardiographic Assessment of Left Ventricular (LV) Structure and Function

M-mode echocardiography was performed using a 15 MHz linear array transducer (L15-7io, Philips iE33 Ultrasound Machine, North Ryde, NSW, Australia) for assessment of systolic function, and a 40 MHz linear array transducer (Vevo 2100 Ultrasound Machine, VisualSonics, Toronto, ON, Canada) for assessment of diastolic function.

Mice were anesthetized with isoflurane (3.5-4% induction, 1.7-1.8% maintenance). LV posterior wall and interventricular septum thickness at diastole, and LV systolic and diastolic chamber dimensions were measured. Fractional shortening and LV mass were calculated as:

Fractional shortening: $[(LVEDD - LVESD)/LVEDD] \times 100\%$, LV mass:

$[(AW+PW+LVEDD)^3 - LVEDD^3] \times 1.055$.

Pulse-wave and tissue Doppler were employed to measure parameters of LV diastolic function: E/A, E'/A', E/e' ratios, isovolumic relaxation time (IVRT) and E-wave deceleration time.

Electrocardiographic Assessment

Electrocardiograms (ECG) were recorded in mice anesthetized with isoflurane (3.5-4% induction, 1.6-2.0% maintenance) by subcutaneously placing 29-gauge electrode needles into the right upper leg, right lower leg and chest (lead II configuration). Cardiac rhythms were assessed for ~5-6 mins using the Powerlab system and BioAmp (ADInstruments). ECG parameters were analyzed using the LabChart 7 software (ADInstruments). Given p-waves can be difficult to detect in mice displaying arrhythmia, and QRS complexes can be inaccurately detected by the automated program, values were confirmed manually by measuring at least 20 different cardiac cycles.

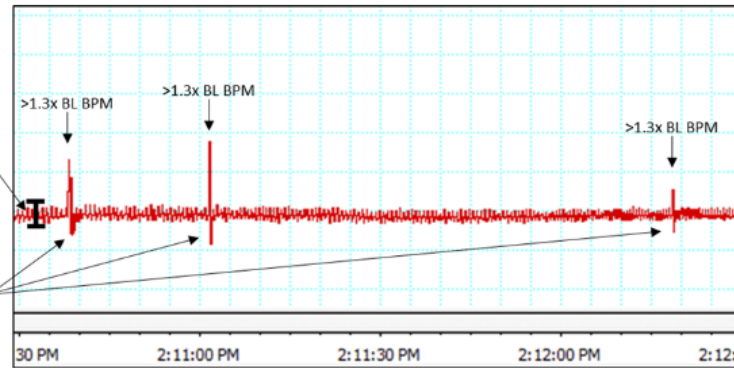
Arrhythmia criteria- Details of how arrhythmia was assessed is outlined in the figure below. This method was used to take into consideration differences between electrical noise on any given day or time between mice. Accuracy of this approach was confirmed by 2 independent investigators, and analysis was performed blinded to genotype.

A

Assessing arrhythmic episodes while accounting for differences in baseline electrical noise between days and mice.

The baseline range of BPM's is determined using LabChart 7 software

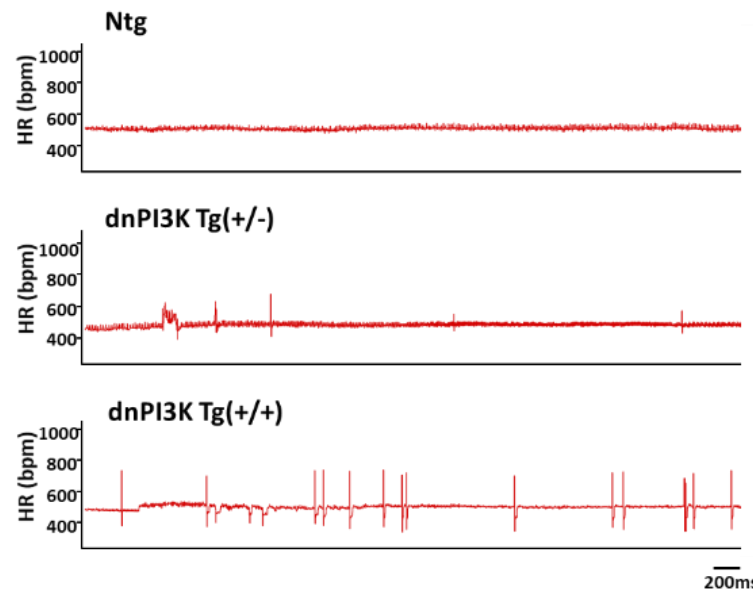
Arrhythmias are then calculated as a change in BPM >1.3x the baseline BPM range



B

% arrhythmic time

The % arrhythmic time is the proportion of time that the BPM is >1.3x the baseline BPM range compared to the total time of the ECG trace



% arrhythmia time	>Δ57bpm		
Total seconds	Total sinus time	% sinus time	% arrhythmia time
334.5	334.5	100.0	0.00

% arrhythmia time	>Δ37bpm		
Total seconds	Total sinus time	% sinus time	% arrhythmia time
290.8	277.2	95.3	4.7

% arrhythmia time	>Δ31bpm		
Total seconds	Total sinus time	% sinus time	% arrhythmia time
301.4	268.1	88.9	11.1

Tissue dissection and morphological analysis

Prior to dissection, mice were anaesthetized (pentobarbitone, 80 mg/kg) and killed via cervical dislocation. The heart, atria, and lungs were rinsed in PBS, patted dry with gauze and weighed. The apex of the heart was snap-frozen and kept for RNA and protein analyses, and the upper portion of the ventricle was kept for histology. The lower limbs were collected and later digested (1M NaOH for 6h, 37°C) for measurement of tibia length (TL) with a vernier calliper. Heart, lung and atrial weights were normalized to TL.

Isolation of adult cardiac myocytes

Ventricular myocytes were isolated from hearts of adult male mice (~16-17 weeks of age) using the Langendorff apparatus. Heparin (1 unit/g body weight) was injected (i.p.) 15 ~ 20min prior to removing the heart, and mouse euthanized with lethobarb (300mg/kg) followed by cervical dislocation. The hearts were immediately excised and washed in cold PBS. The aorta was cannulated using a 22G cannula needle, and retrogradely perfused with Wash Buffer 1 (5.4 mM KCl, 3.5 mM MgSO₄, 0.05 mM sodium pyruvate, 20 mM NaHCO₃, 11 mM glucose, 20 mM HEPES, 23.5 mM sodium glutamate, 4.87 mM sodium acetate, 56 µM phenol red, sodium chloride 1M, 10µM EDTA, 10 mM 2,3-butanedione monoxime, 5 mM creatine, 30 mM taurine, 0.1 IU/mL insulin, gassed with 95% O₂ and 5% CO₂, pH 7.25, 37°C) for 5 min at a flow rate 2-3ml/min. After the wash, medium was replaced with Digestion Buffer 1 (Wash Buffer 1, 3mg/mL collagenase II, 0.2% BSA) and the heart was placed in the warmed organ bath with continuous perfusion until digestion was complete (usually around 10~20min). The heart was then removed from the organ bath and placed into a 60mm culture dish. With 2ml of Digestion Buffer 1, ventricles were cut into small pieces using sterile fine scissors. Cell suspensions were filtered through 250µm mesh and collected in a 15ml round bottom tube. After adding Stop Buffer (Wash Buffer 1, 10% FCS), suspension was centrifuged at 20g for 3min at RT. The supernatant was removed and pellet washed with Wash Buffer 2 (Wash Buffer 1, 1% BSA). Meanwhile, the undigested tissue that did not pass through the filter was transferred into a sterile 50mL jar with Digestion Buffer 2 (Wash Buffer 1, 3mg/mL collagenase II, 2% BSA) and incubated for a further 10min in a 37°C water bath while gently rocking. After the second digestion, the suspension was washed with Stop Buffer and Wash Buffer 2, as described above. Cells from the first and second digestions were then combined and further incubated for 10min in a 37°C water bath with Benzoylase (75unit/mL, Wash Buffer 2). Cells were centrifuged and then underwent a series of calcium reintroductions (0.18mM, 0.45mM, 1.08mM of calcium by

serial diluting Stop Buffer with Plating Media; Minimum Essential Medium (MEM), 10% FCS, 10mM 2,3-butanedione monoxime, 10min incubation at RT for each wash). After the final calcium reintroduction, cell pellets were diluted in Plating Media and plated in laminin (19ug/ml) coated (at least 1hr before experimentation) imaging dish. Plates were placed in a 37°C incubator (95% O₂, 5% CO₂) for 1hr to allow myocyte attachment. Unattached cells were removed by replacing the Plating Media with Maintenance Media (MEM/0.5%BSA/1% 100xITS/1% CD lipid/1% pen strep). Photographs were taken using a microscope (Olympus IX71 with DP2-BSW software). Myocyte area and size (myocyte length and width) were measured using Fiji image processing software by converting images to binary and using the area and Feret's diameter measurement.

Histological Analysis

Ventricle and atrial samples were fixed in 4% paraformaldehyde. Tissue was paraffin-embedded, sectioned at a thickness of 4um and stained with Masson's Trichrome (Gribbles Pathology, Melbourne Australia or Monash Histology Platform) to assess for interstitial fibrosis. Images were acquired using a BX43 light microscope (Olympus, Center Valley, PA, USA) at 40x magnification. Fibrosis, as assessed by the number of blue pixels (collagen), was quantified using Image-Pro Plus 7. The percentage of fibrosis was calculated by dividing the blue-stained collagen tissue (fibrotic) by the total area of the LV (combined fibrotic area and pink/red stained healthy myocardium tissue).

Gene Expression Analyses- qPCR

Ventricles were snap-frozen in liquid nitrogen and total RNA extraction was performed by homogenizing ~1/4 of a ventricle with 500ul of TRI reagent (Sigma-Aldrich, St Louis, MI, USA) using the homogeniser PRO 200[®] (Harvard Apparatus, 72-1297) and following manufacturer's instructions.

The quality and concentration of the RNA was determined using the Nanodrop spectrometer (Thermo Scientific, Waltham, MA, USA). cDNA was synthesized using 2ug of RNA with the High-Capacity cDNA Reverse Transcription Kit (Life Technologies, Carlsbad, CA, United States) according to the manufacturer's instructions. RT-PCR was performed using the TaqMan[®] Fast Advanced Master Mix and TaqMan[®] probes (Life Technologies) and ran on the Applied Biosystems 7500 real-time PCR machine following the manufacturer's instructions. The RT-PCR was performed in triplicate by multiplexing the specific gene of

interest (details provided in table format below) and the housekeeping gene Hypoxanthine phosphoribosyltransferase 1 (*Hprt1*) in each well. *Hprt1* was used to standardize for cDNA concentration and the $2^{-\Delta\Delta C_t}$ method of quantification was used for analysis. Mean CT values greater than 40 were considered undetermined. An SD <0.5 between technical replicates was used.

Gene	TaqMan® Gene Expression Assay	Amplicon Length (bp)	Exon Spanning	Dye	RefSeq
natriuretic peptide type A; ANP (<i>Nppa</i>)	Mm01255747_g1	85	Yes	FAM	NM_008725.2
natriuretic peptide type B; BNP (<i>Nppb</i>)	Mm01255770_g1	68	Yes	FAM	NM_001287348.1 NM_008726.5
ATPase, Ca ⁺⁺ transporting, cardiac muscle, slow twitch 2; SERCA2a (<i>Atp2a2</i>)	Mm01201431_m1	90	Yes	FAM	NM_001110140.3 NM_009722.3 NR_027838.1
collagen, type I, alpha 1; Collagen 1 (<i>Col1a1</i>)	Mm00801666_g1	89	Yes	FAM	NM_007742.3
collagen, type III, alpha 1; Collagen 3 (<i>Col3a1</i>)	Mm00802300_m1	88	Yes	FAM	NM_009930.2
insulin-like growth factor 1 receptor (<i>Igf1r</i>)	Mm00802831_m1	106	Yes	FAM	NM_010513.2
toll-like receptor 4 (<i>Tlr4</i>)	Mm00445273_m1	87	Yes	FAM	NM_021297.2
calsequestrin 1 (<i>Casq1</i>)	Mm00486725_m1	77	Yes	FAM	NM_009813.2
Hypoxanthine guanine phosphoriboxyl transferase (<i>Hprt1</i>)	Mm01545399_m1	81	Yes	VIC	NM_013556.2

Gene expression- microarray

Data was mined from a previous microarray study assessing gene expression in atrial samples from adult male mice which had been subjected to extreme swim exercise for 6 weeks²⁷.

Microarray deposited at <https://www.ebi.ac.uk/arrayexpress/experiments/E-MTAB-3106/> (accession code: E-MTAB-3106).

Western Blotting

Protein extraction and quantitation was performed as previously described²⁸. Cardiac tissue lysates containing 75ug of protein were separated by SDS-PAGE. Protein was immobilized to a polyvinylidene difluoride (PVDF) membrane (MERCCK, Frankfurt, Germany) using the wet tank transfer method at 4°C for 16 hours at 9 volts. Membranes were blocked with 5% skim milk in Tris-buffered saline and 0.1% Tween 20 (TBST). Membranes were probed with the following antibodies: p-AKT (Ser473) (Cell Signalling #9271, 1:500), p-AKT (T308) (Cell Signalling #9275, 1:500), and AKT (Cell Signalling #9272, 1:1000). Membranes were incubated with anti-rabbit antibodies conjugated to HRP. Proteins were visualized using SuperSignal® West Pico PLUS Chemiluminescent Substrate (Thermo Scientific).

PI3K Lipid Kinase Activity Assay

A lipid kinase activity assay was used to measure PI3K activity in ventricular tissue, as described^{23,29}. Briefly, 500ug of protein was immunoprecipitated using an anti-p110 α antibody (#4249, Cell Signalling) and combined with Protein A Sepharose CL-4B beads (GE Healthcare, 17-0780-01) according to the manufacturer's instructions. 10 μ l of a 1:1 ratio of phosphatidylinositol and phosphatidylserine were sonicated in 30 μ l of HEPES buffer (1M HEPES, 40mM EDTA, 1M DTT and 0.015% NP-40) and added to immunoprecipitated protein attached to the Sepharose beads. This was followed by the addition of ATP and 10 μ Ci of [γ -³²P]ATP (PerkinElmer, BLU502A250UC). The reaction was created by shaking (1400 RPM) for 10 mins at RT and stopped using 2M HCl. The addition of 160ul of 1:1 chloroform-methanol mixture was used to extract the lipids. The organic phase was collected and the phospholipid product resolved on a thin liquid chromatography (TLC) plate (Merck, 1.05553.0001) overnight in an acidic solvent system containing 65:35 isoproponal:2M acetic acid. After drying, the TLC plates were subjected to autoradiography film (GE Healthcare, 28906845) at -80°C. The radiolabeled signal was standardized against immunoglobulin G signals from Western blots of remaining immunoprecipitates.

Supplementary Table 1: Morphology of male and female Ntg, caPI3K Tg (+/-) and caPI3K Tg (+/+) mice.

Genotype	Male			Female		
	Ntg	caPI3K Tg (+/-)	caPI3K Tg (+/+)	Ntg	caPI3K Tg (+/-)	caPI3K Tg (+/+)
No. of animals	12	22	14	11	21	23
Age (weeks)	20.5 ± 0.2	20.5 ± 0.1	20.8 ± 0.2	20.8 ± 0.1	20.7 ± 0.1	20.9 ± 0.1
Body Weight (g)	33.4 ± 0.8	32.4 ± 0.4	32.1 ± 0.7	26.3 ± 0.7	26.6 ± 0.4	25.9 ± 0.4
Tibia Length (mm)	16.8 ± 0.1	16.6 ± 0.1	16.6 ± 0.1	16.6 ± 0.0	16.6 ± 0.0	16.6 ± 0.0
Heart Weight (HW, mg)	142.7 ± 4.5	166.8 ± 3.7*	175.1 ± 1.8* (#P=0.008)	110.0 ± 1.9	139.7 ± 2.0*	152.2 ± 1.7*†
Atria Weight (AW, mg)	10.3 ± 0.3	9.1 ± 0.3*	9.5 ± 0.3	7.2 ± 0.3	7.4 ± 0.3	7.6 ± 0.3
Lung Weight (LW, mg)	143.5 ± 2.2	139.3 ± 2.5	137.8 ± 3.5	134.3 ± 1.9	134.9 ± 1.6	131.5 ± 1.9
HW/BW (mg/g)	4.29 ± 0.11	5.17 ± 0.12*	5.40 ± 0.15*	4.22 ± 0.16	5.28 ± 0.10*	5.91 ± 0.01*†
HW/TL (mg/mm)	8.51 ± 0.24	10.02 ± 0.20*	10.55 ± 0.11* (#P=0.003)	6.63 ± 0.10	8.41 ± 0.12*	9.20 ± 0.95*†
AW/TL (mg/mm)	0.62 ± 0.02	0.54 ± 0.02*	0.57 ± 0.02	0.43 ± 0.02	0.45 ± 0.02	0.46 ± 0.02
LW/TL (mg/mm)	8.56 ± 0.14	8.38 ± 0.14	8.31 ± 0.22	8.10 ± 0.10	8.12 ± 0.09	7.94 ± 0.11

Table shows age, body weight (BW), heart weight (HW), atria weight (AW), lung weight (LW), and tibia length (TL). All data presented as mean ± SEM. One-way ANOVA followed by correction for multiple comparisons using Tukey's method. *P<0.01 vs. Ntg of same sex; † P<0.05 vs caPI3K Tg (+/-) of the same sex. # P-value by Mann-Whitney U-test vs. caPI3K Tg (+/-) of same sex (data not normally distributed using the Shapiro-Wilk normality test).

Supplementary Table 2: Systolic echocardiographic measurements from hearts of male and female Ntg, caPI3K Tg (+/-) and caPI3K Tg (+/+) mice at 20 weeks of age.

	Male			Female		
Genotype	Ntg	caPI3K Tg (+/-)	caPI3K Tg (+/+)	Ntg	caPI3K Tg (+/-)	caPI3K Tg (+/+)
No. of animals	8	15	7	5	13	10
Age (weeks)	20.1 ± 0.1	20.2 ± 0.1	20.5 ± 0.2	20.5 ± 0.1	20.4 ± 0.1	20.6 ± 0.1
HR (bpm)	569 ± 15	537 ± 18	544 ± 19	579 ± 19	540 ± 17	518 ± 14
LVPW (mm)	0.83 ± 0.04	0.97 ± 0.04 (#P=0.02)	1.13 ± 0.09*	0.81 ± 0.04	1.00 ± 0.03*	1.01 ± 0.02*
IVS (mm)	0.84 ± 0.03	1.00 ± 0.04*	1.08 ± 0.06*	0.79 ± 0.06	0.92 ± 0.04 (#P=0.054)	0.95 ± 0.04 (#P=0.04)
LVEDD (mm)	4.03 ± 0.09	3.74 ± 0.09	3.60 ± 0.12*	3.76 ± 0.09	3.42 ± 0.07*	3.52 ± 0.08
LVESD (mm)	2.63 ± 0.09	2.26 ± 0.11 (#P=0.03)	1.98 ± 0.16*	2.34 ± 0.14	1.86 ± 0.06*	1.99 ± 0.09 (#P=0.05)
FS (%)	34.7 ± 1.3	39.9 ± 2.3	45.4 ± 3.0*	37.9 ± 2.6	45.4 ± 1.6*	43.5 ± 1.7
Estimated LV Mass (mg)	126.1 ± 5.5	141.1 ± 4.7 (#P=0.06)	157.4 ± 7.0*	105.9 ± 2.9	119.4 ± 5.5	127.6 ± 3.8*

Heart rate (HR), left ventricular (LV) posterior wall thickness (LVPW) and interventricular septum thickness (IVS) at diastole, LV end diastolic dimension (LVEDD), LV end systolic dimension (LVESD), fractional shortening % (FS %), echocardiography-derived LV mass. All data presented as mean ± SEM. One-way ANOVA followed by correction for multiple comparisons using Tukey's method. * P<0.05 vs. Ntg of same sex. # P-value by unpaired t-test vs. Ntg of same sex.

Supplementary Table 3: Diastolic echocardiographic measurements from hearts of male and female Ntg, caPI3K Tg (+/-) and caPI3K Tg (+/+) mice at 20 weeks of age.

	Genotype	Male			Female		
		Ntg	caPI3K Tg (+/-)	caPI3K Tg (+/+)	Ntg	caPI3K Tg (+/-)	caPI3K Tg (+/+)
Pulse-wave Doppler	No. of animals	3	6	7	6	8	13
	HR (bpm)	536 ± 20	513 ± 16	522 ± 12	505 ± 12	510 ± 18	492 ± 7
	E/A	1.53 ± 0.37	1.42 ± 0.20	1.33 ± 0.10	1.31 ± 0.08	1.46 ± 0.16	1.35 ± 0.05
	IVRT (ms)	11 ± 1	13 ± 1	13 ± 0	13 ± 1	14 ± 0	14 ± 0
	MV DT (ms)	21 ± 2	22 ± 2	19 ± 1	19 ± 2	20 ± 2	22 ± 1
Tissue Doppler	No. of animals	4	6	7	5	7	12
	HR (bpm)	549 ± 18	501 ± 16	520 ± 13	480 ± 12	504 ± 14	483 ± 9
	E'/A'	1.24 ± 0.33	0.91 ± 0.06	1.19 ± 0.07	1.28 ± 0.09	1.08 ± 0.14	1.11 ± 0.15
	E/E'	-35.46 ± 6.67	-31.37 ± 2.96	-26.87 ± 1.88	-27.39 ± 2.97	-30.38 ± 4.47	-32.62 ± 2.11

Heart rate (HR) independently determined during both pulse wave Doppler and tissue Doppler analysis, E(mm/s)/A (mm/s) ratio (E/A), isovolumic relaxation time (IVRT), mitral valve deceleration time (MV DT), E' (mm/s)/A' (mm/s) ratio (E'/A), E (mm/s)/E' (mm/s) ratio (E/E'). All data presented as mean ± SEM. One-way ANOVA followed by correction for multiple comparisons using Tukey's method. * P<0.05 vs. Ntg of same sex. Due to an inability to clearly separate E and A waves, some animals were excluded from analyses.

Supplementary Table 4: Electrocardiographic measurements from male and female Ntg, caPI3K Tg (+/-) and caPI3K Tg (+/+) mice at 20 weeks of age.

Genotype	Male			Female		
	Ntg	caPI3K Tg (+/-)	caPI3K Tg (+/+)	Ntg	caPI3K Tg (+/-)	caPI3K Tg (+/+)
No. of animals	9	10	8	9	10	7
HR (bpm)	507 ± 11	526 ± 10	520 ± 16	528 ± 18	499 ± 9	482 ± 10
RR interval (ms)	119.0 ± 2.7	114.7 ± 2.1	116.4 ± 3.9	114.8 ± 4.0	120.7 ± 2.7	124.9 ± 2.6
QRS interval (ms)	9.6 ± 0.4	9.6 ± 0.2	8.9 ± 0.4	9.4 ± 0.2	9.5 ± 0.2	9.4 ± 0.3
P Amplitude (mV)	0.15 ± 0.01	0.16 ± 0.01	0.15 ± 0.01	0.17 ± 0.01	0.16 ± 0.01	0.16 ± 0.01
PR interval (ms)	38.1 ± 1.1	38.5 ± 0.6	37.3 ± 1.2	36.4 ± 0.6	39.4 ± 0.9	38.0 ± 1.5
R Amplitude (mV)	1.29 ± 0.07	1.11 ± 0.05	1.16 ± 0.13	1.36 ± 0.09	1.02 ± 0.05*	1.24 ± 0.09
Arrhythmia (% of beats)	0.63 ± 0.28	0.47 ± 0.24	0.16 ± 0.06	0.36 ± 0.19	0.11 ± 0.04	0.63 ± 0.26

All data presented as mean ± SEM. One-way ANOVA followed by correction for multiple comparisons using Tukey's method. * P<0.05 vs. Ntg of same sex. Some animals were excluded due to excessive background electrical noise, preventing accurate assessment.

Supplementary Table 5: Morphology of male and female Ntg, dnPI3K Tg (+/-) and dnPI3K Tg (+/+) mice.

Genotype	Male			Female		
	Ntg	dnPI3K Tg (+/-)	dnPI3K Tg (+/+)	Ntg	dnPI3K Tg (+/-)	dnPI3K Tg (+/+)
No. of animals	14	32	17	12	26	17
Age (weeks)	20.8 ± 0.2	20.8 ± 0.1	20.8 ± 0.2	20.8 ± 0.3	20.8 ± 0.2	20.9 ± 0.2
Body Weight (g)	33.9 ± 1.0	32.8 ± 0.6	33.5 ± 0.8	26.1 ± 0.7	26.6 ± 0.7	27.8 ± 0.8
Tibia Length (mm)	16.7 ± 0.1	16.8 ± 0.1	16.7 ± 0.1	16.7 ± 0.1	16.7 ± 0.1	16.9 ± 0.1
Heart Weight (HW, mg)	134.8 ± 4.2	98.4 ± 1.6*	97.1 ± 2.6*	107.5 ± 2.2	82.8 ± 1.0*	88.2 ± 3.1*
Atria Weight (AW, mg)	9.3 ± 0.5	7.0 ± 0.3*	10.5 ± 1.3†	6.8 ± 0.3	5.2 ± 0.2*	9.7 ± 1.1†
Lung Weight (LW, mg)	142.7 ± 3.8	140.8 ± 1.9	138.7 ± 2.7	131.3 ± 2.9	133.1 ± 1.5	141.7 ± 5.0
HW/BW (mg/g)	3.99 ± 0.11	3.01 ± 0.05*	2.91 ± 0.06*	4.13 ± 0.07	3.14 ± 0.06*	3.19 ± 0.11*
HW/TL (mg/mm)	8.07 ± 0.23	5.87 ± 0.09*	5.81 ± 0.13*	6.44 ± 0.13	4.97 ± 0.05*	5.23 ± 0.18*
AW/TL (mg/mm)	0.56 ± 0.03	0.41 ± 0.01*	0.63 ± 0.07†	0.41 ± 0.02	0.31 ± 0.01*	0.57 ± 0.07†
LW/TL (mg/mm)	8.54 ± 0.21	8.40 ± 0.10	8.29 ± 0.13	7.86 ± 0.14	7.99 ± 0.08	8.39 ± 0.27

Table shows age, body weight (BW), heart weight (HW), atria weight (AW), lung weight (LW), and tibia length (TL). All data presented as mean ± SEM. One-way ANOVA followed by correction for multiple comparisons using Tukey's method. * P<0.01 vs. Ntg of same sex; † P<0.05 vs dnPI3K (+/-) of the same sex. Kruskal Wallis was used for AW and AW/TL because the data were not normally distributed due to the presence of atrial thrombi in some mice.

Supplementary Table 6: Systolic echocardiographic measurements from hearts of male and female Ntg, dnPI3K Tg (+/-) and dnPI3K Tg (+/+) mice at 20 weeks of age.

	Male			Female		
Genotype	Ntg	dnPI3K Tg (+/-)	dnPI3K Tg (+/+)	Ntg	dnPI3K Tg (+/-)	dnPI3K Tg (+/+)
No. of animals	12	15	13	7	20	11
Age (weeks)	20.1 ± 0.2	20.0 ± 0.2	20.1 ± 0.3	20.6 ± 0.5	20.4 ± 0.3	20.1 ± 0.4
HR (bpm)	553 ± 17	531 ± 13	510 ± 15	528 ± 18	524 ± 9	508 ± 12
LVPW (mm)	0.75 ± 0.03	0.60 ± 0.02*	0.56 ± 0.02*	0.66 ± 0.04	0.59 ± 0.02	0.51 ± 0.02*†
IVS (mm)	0.69 ± 0.03	0.56 ± 0.02*	0.46 ± 0.02*†	0.61 ± 0.04	0.51 ± 0.02*	0.48 ± 0.02*
LVEDD (mm)	4.02 ± 0.12	4.01 ± 0.06	4.22 ± 0.08	3.94 ± 0.08	3.78 ± 0.04	4.05 ± 0.07†
LVESD (mm)	2.71 ± 0.12	2.95 ± 0.09	3.34 ± 0.11*†	2.71 ± 0.08	2.72 ± 0.08	3.40 ± 0.09*†
FS (%)	33.1 ± 1.3	26.6 ± 1.7*	21.1 ± 1.6*†	31.3 ± 1.3	28.1 ± 1.9	16.4 ± 1.1*†
Estimated LV Mass (mg)	102.7 ± 4.8	77.2 ± 2.2*	73.0 ± 3.2*	84.1 ± 3.6	65.0 ± 1.9*	64.3 ± 2.1*

Heart rate (HR), left ventricular (LV) posterior wall thickness (LVPW) and interventricular septum thickness (IVS) at diastole, LV end diastolic dimension (LVEDD), LV end systolic dimension (LVESD), fractional shortening % (FS %), estimated LV mass. All data presented as mean ± SEM. One-way ANOVA followed by correction for multiple comparisons using Tukey's method. * P<0.05 vs. Ntg of same sex; † P<0.05 vs dnPI3K (+/-) of the same sex.

Supplementary Table 7: Electrocardiographic measurements from male and female Ntg, dnPI3K Tg (+/-) and dnPI3K Tg (+/+) mice at 20

Genotype	Male			Female		
	Ntg	dnPI3K Tg (+/-)	dnPI3K Tg (+/+)	Ntg	dnPI3K Tg (+/-)	dnPI3K Tg (+/+)
No. of animals	8	14	13	5	13	12
HR (bpm)	529 ± 13	520 ± 7	512 ± 11	498 ± 14	499 ± 7	514 ± 12
RR interval (ms)	114.2 ± 2.7	115.9 ± 1.6	118.1 ± 2.6	121.1 ± 3.5	120.7 ± 1.7	117.7 ± 2.9
QRS interval (ms)	10.0 ± 0.4	10.2 ± 0.3	10.9 ± 0.2	9.8 ± 0.2	10.6 ± 0.2	11.5 ± 0.3*
P Amplitude (mV)	0.17 ± 0.01	0.14 ± 0.01*	0.11 ± 0.01*†	0.17 ± 0.01	0.15 ± 0.01	0.09 ± 0.01*†
PR interval (ms)	36.2 ± 0.9	37.1 ± 1.0	36.8 ± 0.9	38.4 ± 1.1	39.5 ± 0.6	39.3 ± 0.6
R Amplitude (mV)	1.45 ± 0.11	1.30 ± 0.08	1.03 ± 0.07*†	1.58 ± 0.12	1.39 ± 0.06	1.04 ± 0.07*†
Arrhythmia (% of beats)	0.44 ± 0.12	2.85 ± 1.52	9.41 ± 3.55	1.10 ± 1.05	6.55 ± 3.78	6.88 ± 2.98

weeks of age.

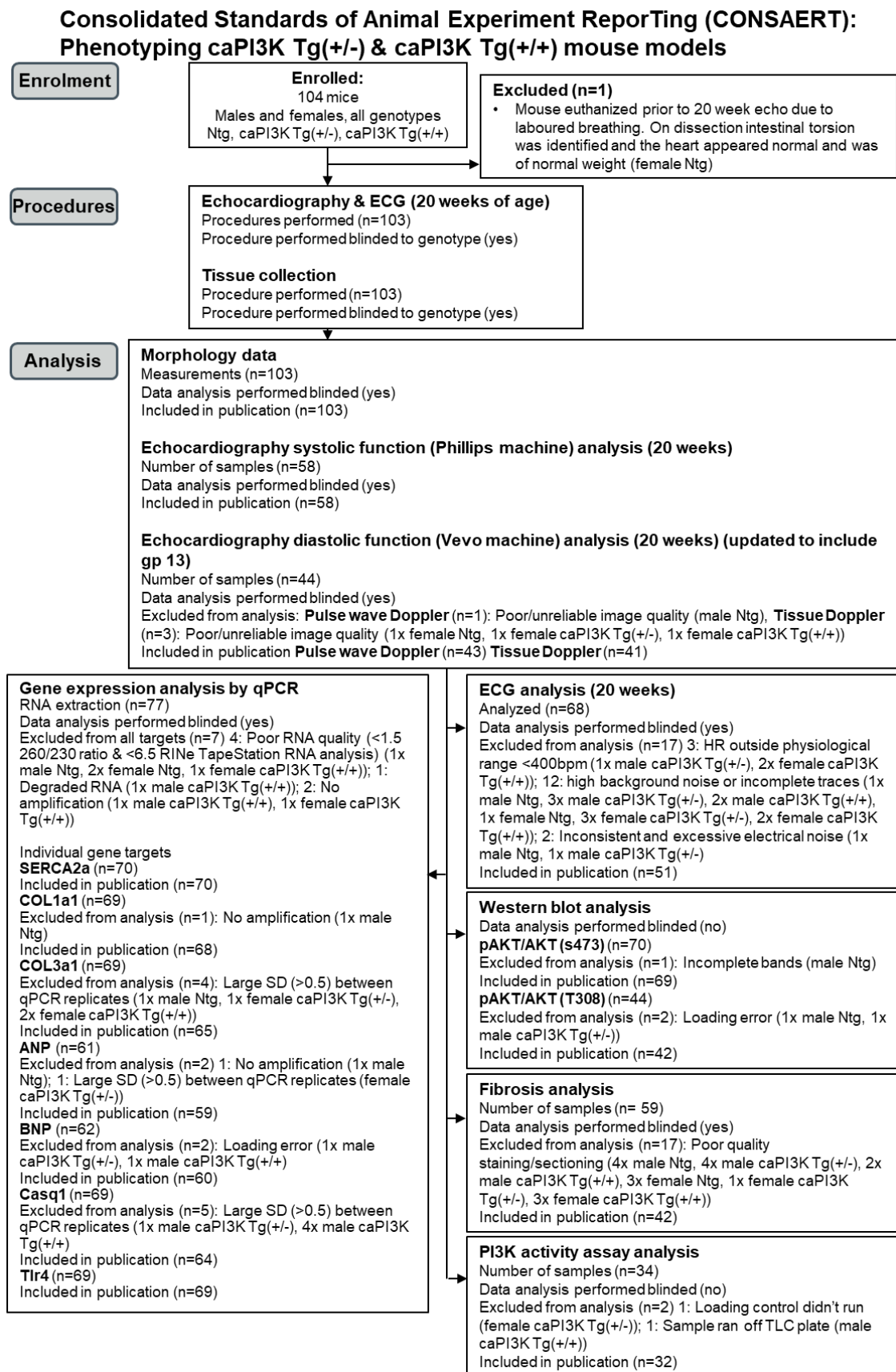
All data presented as mean ± SEM. One-way ANOVA followed by correction for multiple comparisons using Tukey's method. * P<0.05 vs. Ntg of same sex. Some animals were excluded due to excessive background electrical noise.

Supplementary Table 8: Demographics of athletes with and without AF.

Variables	With AF (n=40)	Without AF(n=40)	p value
Age (years)	63 (8)	63 (8)	0.98
BMI (kg/m ²)	25.5 (2.6)	26.0 (3.1)	0.26
Resting Heart Rate (bpm)	54 (10)	53 (9)	0.76
Resting Systolic Blood pressure (mmHg)	135 (22)	134 (14)	0.89
Resting Diastolic Blood Pressure (mmHg)	75 (12)	76 (9)	0.85
Peak VO ₂ (ml/kg/min)	37.5 (10.3)	36.5 (9.6)	0.64
Peak exercise heart rate (bpm)	168 (18)	164 (14)	0.17
Total cholesterol (mmol/L)	5.1 (1.0)	4.9 (1.0)	0.52
HDL cholesterol (mmol/L)	1.8 (0.8)	2.2 (1.2)	0.14
LDL cholesterol (mmol/L)	3.1 (0.9)	3.1 (0.7)	0.96
Triglycerides (mmol/L)	1.0 (0.7)	1.2 (0.8)	0.30
HMG-CoA reductase inhibitors 'statins', n (%)	9 (22.5)	11 (27.5)	0.80

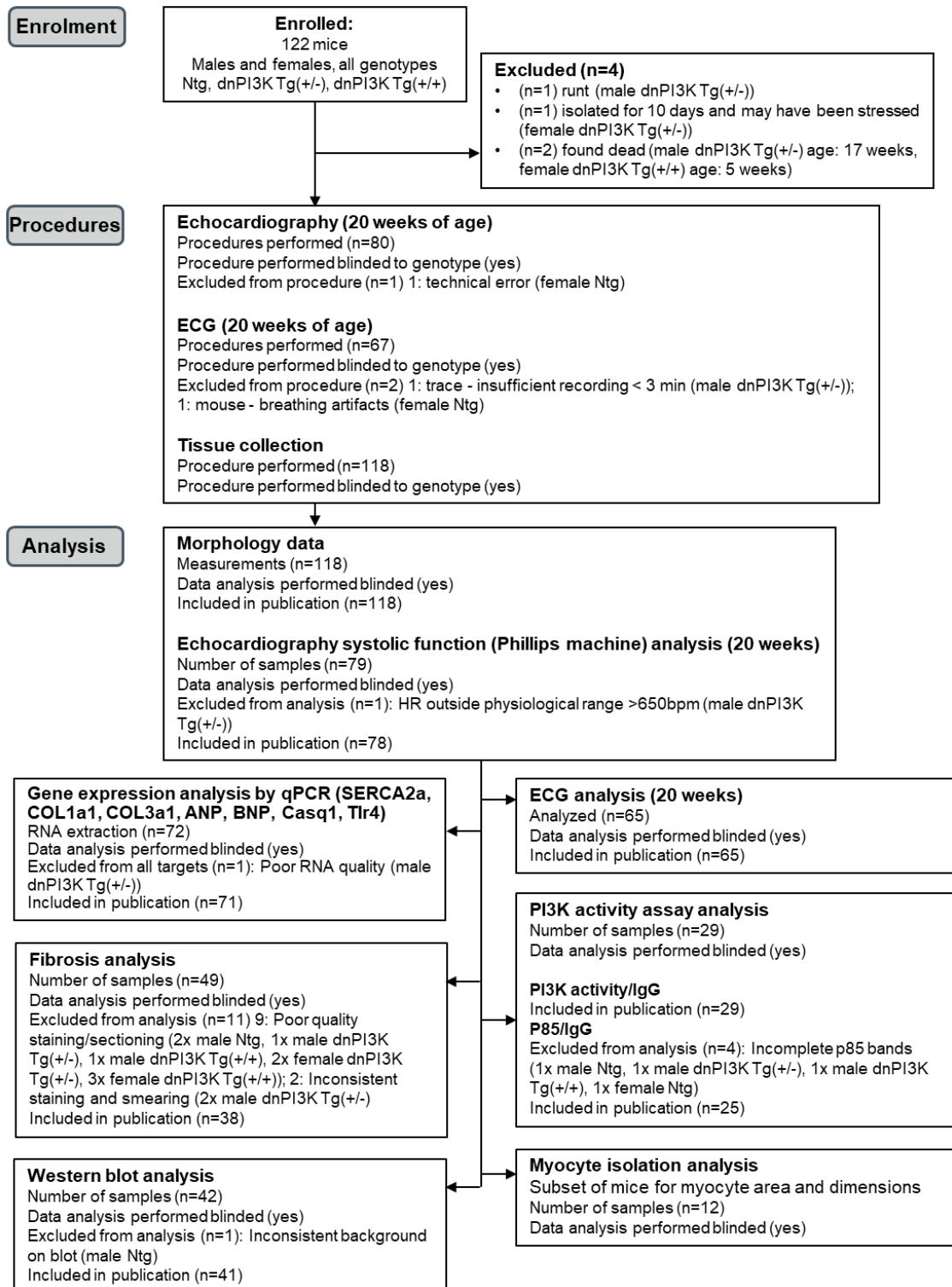
All data presented as mean (SD). Groups were compared using unpaired t-tests.

Supplementary Figure 1: Exclusion flowchart for the caPI3K Tg models.



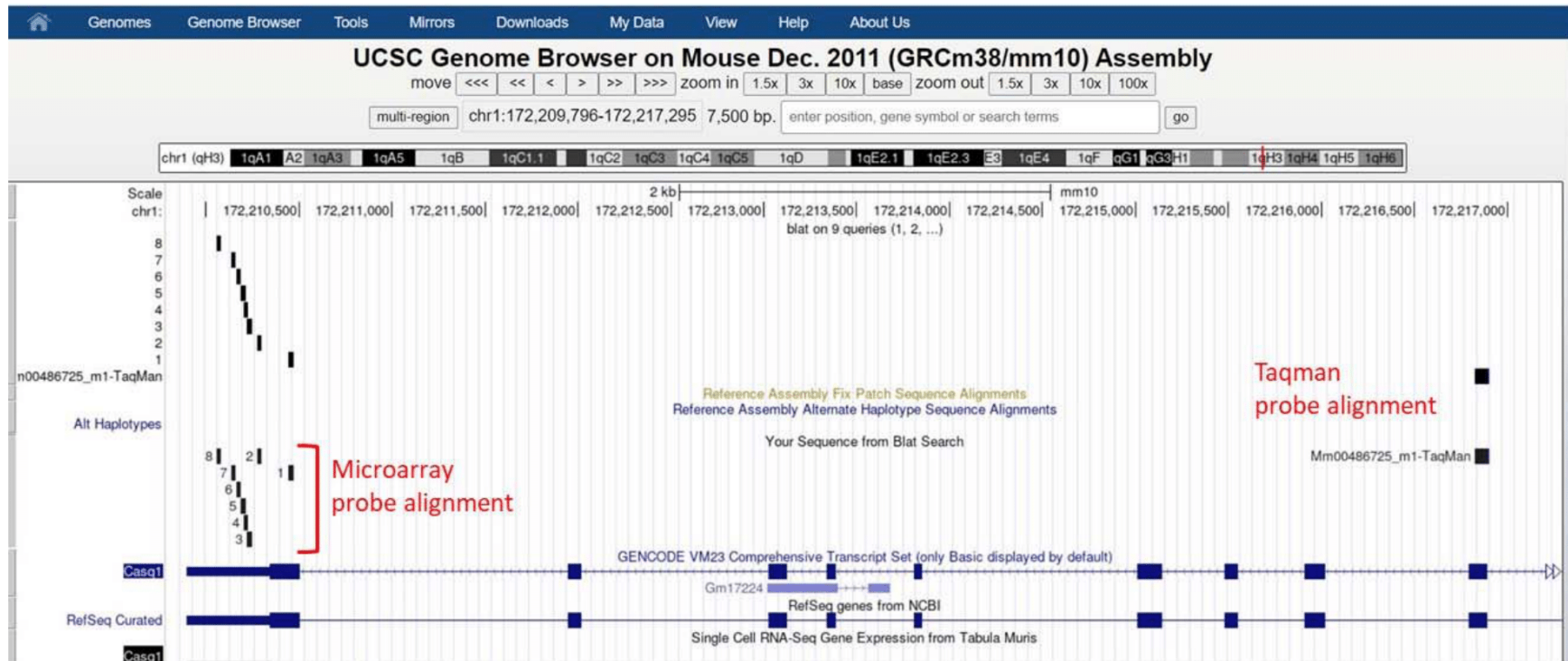
Supplementary Figure 2: Exclusion flowchart for the dnPI3K Tg models.

**Consolidated Standards of Animal Experiment Reporting (CONSAERT):
Phenotyping dnPI3K Tg(+/-) & dnPI3K Tg(+/+) mouse models**



Supplementary Figure 3

Using the alignment tool, BLAT, the Casq1 microarray probes and Taqman probe only align with Casq1, not Casq2.



Alignment of unique Affymetrix microarray probe Casq1 (MOUSE430_2:1422598_AT, n=8) and Taqman probe (Casq1 Mm00486725_m1) alignment using BLAT in UCSC (UCSC Genome Browser, <https://genome.ucsc.edu>) showed specific alignment to one single sequence ID - Mus musculus calsequestrin 1 (Casq1), mRNA. (from RefSeq NM_009813); Gencode Transcript: ENSMUST00000003554.10; Gencode Gene: ENSMUSG00000007122.11; Transcript (Including UTRs); Position: mm10 chr1:172,209,894-172,219,868 Size: 9,975 Total Exon Count: 11 Strand: -

Sequence alignment of mouse *Casq1* (upper line) and *Casq2* (lower line) using BLAST, and location of the *Casq1* Taqman probe highlighted in blue.

```

EMBOSS_001 -----TT--CCTCCTCTGACCCTT---TTTCTCTGGCTCTGT-CG-
EMBOSS_001 TGTAAGGTATCTAGGGCTTGGCCTC--CCAG-CCCCTGCTGGCTCTT-GCTCTGTGCGC

EMBOSS_001 -----GCAGTTT----CTCCAGGACCCAGCAGTGTCTCTG-----TCCACTGC
EMBOSS_001 ATGTGTGCA-TTTGAGCCTCCA-----CAGTTTGTCTGAGCCCACGACTACACAGC

EMBOSS_001 T-CTGGCCCA-----CTCT--CTACCCACCCCACTGGAGCCCTA
EMBOSS_001 TGCAGGACCAAGGAGGTGAAAGCAGCCTTTGTTCCTCACCAACATCT-----CTA

EMBOSS_001 A---CT--CAGGATTCTGTATCCGAGGGCACCTCTCCCTATTTCAGCTAACCTCCTCT
EMBOSS_001 AGAACCTTCC--ATCCTGTCTTCCATG-----ATCTCTAT-----TCT

EMBOSS_001 GGACCAGGAG-AGCAGG-----CCCA-----GATTGTACTACCTCCATGAGAGCT
EMBOSS_001 GGAGACTGAGAAGCAAGACTTTTCCAAATGAAGAGGATT----TACCT-----GCT

EMBOSS_001 ACCGACAGGATGGGGCCAGAGCAGTGTCCGAGCTGCGGCTGGCA-CTGCTGTTGTACT
EMBOSS_001 -----CATGGTGGG-----GTTT-----ATCTGCTGT-----

EMBOSS_001 GGTGCTAGGACGCCAGGTTAGGGTCCAGGGGGAAGATGGGTGGACTTCCCTGAGTA
EMBOSS_001 -----CCC---TGAGCGG---GGCAGAAGAGGGCTGAAGTTCCCCACGTA

EMBOSS_001 CGACGGTGTGGACCGTGTGATCAATGTGAACGCC-----AAGAACTACAAGAACGTG
EMBOSS_001 CGATGGGAAAGACCGAGTGGTCA-----GCCTTCTGAGAAGAACCTCAAGCAGATG

EMBOSS_001 TTTAAGAAGTATGAGGTGCTGGCCCT-CCTC---TACCATGAGCC-----CCCCGAG
EMBOSS_001 TTGAAGAGATATGATTTGCT---CTGTCTTATTACCACGAACCTGTGTCTTC-----

EMBOSS_001 GACGACAAGGCCTCGCAGAGACAATTTGAGATGGAGGAGCTAATCCTGGAGTTAGCAGCC
EMBOSS_001 --AGACAAGGTCTCACA AAAACAGTTCAGCTGAAGGAGATTGTACTGGAGCTTGTGGCC

EMBOSS_001 CAAGTCTTAGAAGACAAGGGTGTGGCTTTGGCCTGGTGGACTCAGA-GAAGGATGC--A
EMBOSS_001 CAGGTCTGGAACATAAAAAACATAGGCTTTGTGATGGTGGATTG-GAGGAAAGAGGCCAA

EMBOSS_001 GCTGTGGCCAAGA AACTAGGACTAACTGAAGAAGCAGCGTTTATGTGTTCAAAGGAGAT
EMBOSS_001 GC--TTGCTAAGAGGCTGGGATTTCAGTGAAGAAGGAAGCCTGTATGTCTGAAGGGTGA-

EMBOSS_001 GAAGTC-----ATTGAATATGACGGCGAGTTTCTGCAGACACTCTG-----GTGGAGT
EMBOSS_001 -----CCGCACGATGAGTTTGACGGGGAGTTTCGCAGCAGA-----TGCTTAGTGGAAT

EMBOSS_001 TTCTTGCTT-GATGTCCTAGAAGACCCTGTAGAGTTGAT--TGAAGGTGAACGA---GAG
EMBOSS_001 TTCT-CITGGATCTCATTGAAGACCCAGTGA--GATCGTGAA---TAACAAGCTGGAG

EMBOSS_001 CTGCAGGCATTTGAGAATATTGAAGATGAAATCAAACCTATTGGCTACTTCAAGAGCAA
EMBOSS_001 GTCCAGGCCTTTGAGCGCATCGAGGACCAGACCAAGCTCCTGGCTTCTTCAAGAATGAG

EMBOSS_001 GACTCAGAGCATTACAAAGCCTACGAGGACGCAGCTGAAGAGTTCATCCCTACATCCCT
EMBOSS_001 GACTCAGAATATTACAAAGCATTCCAAGAGGACAGTGAACACTTCCAGCCTTACATCAAG

EMBOSS_001 TTCTTGCTTACCTTCGACA--GCAAGGTGGCAAAGAAGCTGACTCTGAAGTTGAATGAGA
EMBOSS_001 TTCTTTGCCACCTTTGACAAGGC--GGTGGCAAAGAAGTTATCCTTGAAGATGAACGAAG

EMBOSS_001 TTGATTTCTACGAGGCTTTCATGGAAGAGCCTATGAC--CATCCCAGACAAGCCCAACAG
EMBOSS_001 TTGGCTTCTATGAGCCATTTATGGATGAGCCCA--ACGTCATCCCTAACAAACCGTACAC

EMBOSS_001 TGAAGAGGAGATTGT-CAGCTTCTGGAGGAGCA-CAGGAGATCAACCCTGAGGAAACTG
EMBOSS_001 AGAAGAGGAGCTTGTGGAG-TTTGTGAAGGAACATCA-AAGACCCACCT-----AC-G

```

EMBOSS_001 AAGCCTG-----AGAG--TATGTACGAGACTTGG-----GAGGATGACCTGGATGG
EMBOSS_001 TCGCTTGC GCCCAGAGGACATGTTTGAAACATGGACTACAGGAGAAGACGACTTGAATGG

EMBOSS_001 AATCCACATTGTCGCCTTTGCAGAGGAAGCA--GATCCCGATGGCTATGAGTTCTTAGAG
EMBOSS_001 GATCCACATCGTGGCCTTTGCGGA-GAAG-AGTGACCCAGATGGCTATGAGTTCCTAGAG

EMBOSS_001 ACTCTCAAGGCTGTGGCCCAAGACAACACTGAGAACCCCGACCTCAGTATCATCTGGATT
EMBOSS_001 ATCTGAAACAGGTTGCCCGGACAACACTGACAACTCTGACTTGAGCATCTTGTGGATT

EMBOSS_001 GATCCTGATGACTTCCCGCTGCTGGTCCCGTACTGGGAGAAGACCTTTGACATTGACCTG
EMBOSS_001 GACCCAGATGACTTCCACTGCTTGTGCTTACTGGGAGAAGACTTCAAGATTGACCTG

EMBOSS_001 T--CAGCTCCACAAATAGGAGTTGTCAATGTTACAGACGCCGACAGCATATGGATGGAGA
EMBOSS_001 TTCAAG--CCACAGATTGGGGTGGTGAATGTAACCGATGCTGACAGTATCTGGATGGAGA

EMBOSS_001 T---GGATAACGAGGAGGACCTGCCTTCTGCTGATGAGCTGGAGGACTGGCTGGAGGACG
EMBOSS_001 TCCAGAT---GATGACGACCTGCCACAGCTGAGGAGCTGGAAGACTGGATTGAAGATG

EMBOSS_001 TG----CTGGAGGGGAGATCAACAC---AGAGGATGACGACGACGATGACGACGATG--
EMBOSS_001 TGCTTTCTGGA----AAGATCAACACTGAAGATGATGACAATGAAGATGAAGATGATGAT

EMBOSS_001 -----ACGATGACGATGATGATGACGACGACTA-----
EMBOSS_001 GGTGATGACAACGATGACGATGATGATGACGACGATGATAATGATAATTCTGATGAGGAT

EMBOSS_001 -----GATGACGAGTG-----GCCGTGG-----
EMBOSS_001 AATGAAGACAGTGTGATGACGA-TGATGACGATGAATAGCTCCAGCCCTGGGTGATTCT

EMBOSS_001 -----CAGCCGAGTAC-----CAGCCCCA-----
EMBOSS_001

EMBOSS_001 GATGAGTGACATTACAACCA-CCATGTACCATACAGACAGCCCAAGGGGCGCAAGCAG
EMBOSS_001

EMBOSS_001 -----CTTGCTCC-----TACT----TGTT---
EMBOSS_001 TGGTGCCACACCTAGTACGCTCTTTCTCTTCCAGCATCTTTTCTAGTCTGTTCTT

EMBOSS_001 -----GTACCTTTCTGCCATCTG--TGCCCTT-----CCCTG--GGCTC---CT-
EMBOSS_001 GGCAGGAGTGGTACATTTAG-----TGAATGCCTTCCAAACCCAGCAGGCTCACACTG

EMBOSS_001 -TGGGACACTAG---GTCATTCTC----TACTAC-----AGGGCCAA----
EMBOSS_001 CAGGGACAGAAGGGGAGTGATTCCCATGCTGACTACTTCTAACCATTGAGGAACAATCAG

EMBOSS_001 --CTGTGGTC--TGC-ATACA----GGGTGCTTGAGGTC-----CTGG-----T
EMBOSS_001 CCCT-TGTTCTTTGCTAGACAATCAGGGGTCATGGAATTCTGGGAGTCTGGGGACTGTAT

EMBOSS_001 CTC-----CCTCTCC-----GA-----GGAGAAAAGGAGCT
EMBOSS_001 CTCCTGACACCTTACTCAAGTTTACTTACTGTCTTTGATCCAGATGGTGACA--GAAC

EMBOSS_001 ----GCTTTTCTTAG-----ATCCAGCCAG-----
EMBOSS_001 GACAGCTTGTATTAGTTTACAAGCAGGGAGTGGCCTTCTAATCAGAGTCCAGGAAGGGC

EMBOSS_001 -----TTCTCTCATCT-----GACTTGCTTCT-----TC--CCCCATACC
EMBOSS_001 ACATGATTATCCAATCTCCCGCAAACCCAGA--GCATCTGTGAACCTCAGACCCAAAGCC

EMBOSS_001 TT-----ATCTG-----TTTCT-----
EMBOSS_001 TTTGGATGCAATTAGAAATGCCTTGAAATGTGTGGGCATTGCCATCATTCTGGAATAT

EMBOSS_001 -----CTTCCC-----GCCACTCCCAT
EMBOSS_001 TAGGATGATGAGTGGGGTCTATGACTCTATGAACATCCCATTAATTGCCAAGCCTCAT

```

EMBOSS_001      A-----CTT-----
EMBOSS_001      ATATTACCAGTGGTAAGAGAGGCTGAAGGATAAAAGGCTTTTCATTTTTCTGATGGAGA

EMBOSS_001      -----AACGGTTTGCAA
EMBOSS_001      CCGTTTAGGTCTCTGAATGGGCTGCTGGCTGCCAGAGTGAGCTGGGAAGTGAATGCAC

EMBOSS_001      ACTCTTCT-----CTATCCCATTC-----TCAAATC-----
EMBOSS_001      CCTC-TCTGTCCCCGCTAGTGAGCTGTCCCA-TTCTGAGTTAAAATCGCTTTATCCACTG

EMBOSS_001      -----TTAA-----ACCTCTCTCACTGTCCTGACCCTGGCCAG-----
EMBOSS_001      GTCAAATTAACCTCTCCCATTATCAGCACTCCCACAGT--TGA-CCAGGGCAGCGACCAT

EMBOSS_001      -----GAGG----AAGGGA-----
EMBOSS_001      TAAGAGTTCACGATGCCCTGAGGCACCAAGGAAAAAAAAAGAAAAGAAAAGAATCCCAA

EMBOSS_001      -----GGTACTGTGTTAGGGGCTA-----
EMBOSS_001      GTGCCTTTTGAATTGCTGAAAGTAACAGTGTGCTTGGTA--GTGTTAGTTGCTAAGTGT

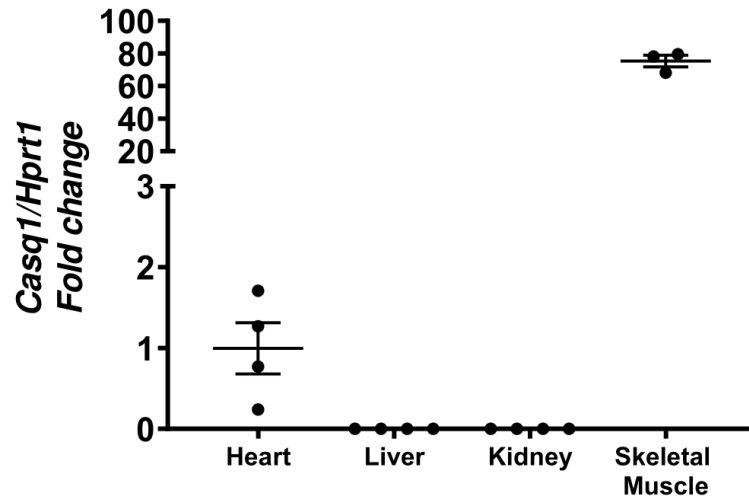
EMBOSS_001      --TAATCTTA----GCCATCTCCTGTAA-----TGTATT
EMBOSS_001      CCTAA-CCTATTTTTGAAAT---CTGTAAACATGGAGAAGACTCTGTGTGGTGTGTTTT

EMBOSS_001      TGGGTCAA---TGCAAGGCCT-----TAATAAAGAAATCTGGGC---AGA
EMBOSS_001      TG---AAACTGGGC-AGTCCTTTTATGGAATAGTAATAAACTAAT---GGACATTAGA

EMBOSS_001      ATGA-----
EMBOSS_001      CTCATGTTTTGAAAAAAAAAAAAAAAAAAAAAAAAAAAAAAAAA

```

Supplementary Figure 4

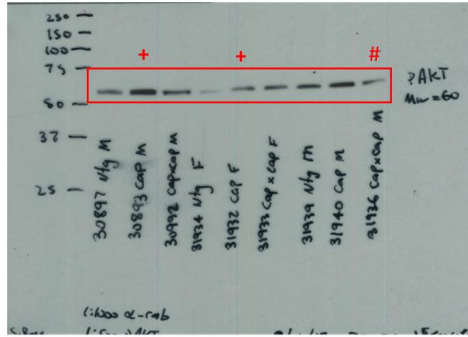


Gene expression by qPCR of *Casq1* relative to *Hprt1* in heart, liver, kidney and skeletal muscle from control adult mice (~ 12 months of age). Expressed as a fold change relative to heart. N=3-4/group.

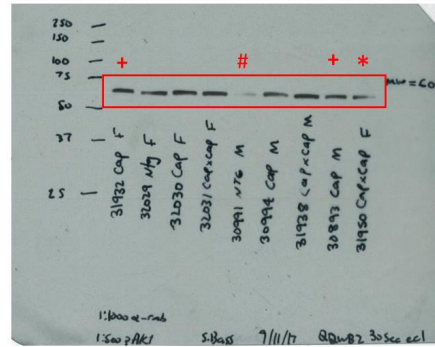
Ntg, caPI3K Tg(+/-), caPI3K Tg(+/+)

A. Western blots pAKT(S473)/AKT 1-6 probed for pAKT (S473) (Cell Signalling Technology 9271)

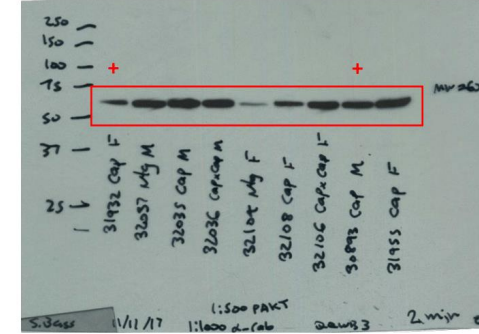
WB1A (pAKT(S473))



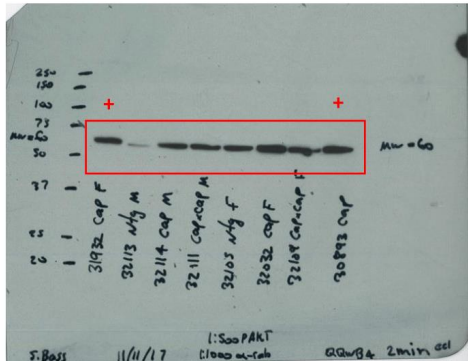
WB2A (pAKT(S473))



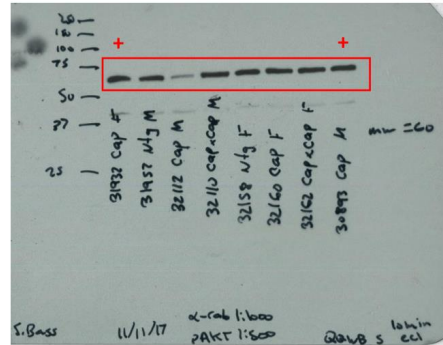
WB3A (pAKT(S473))



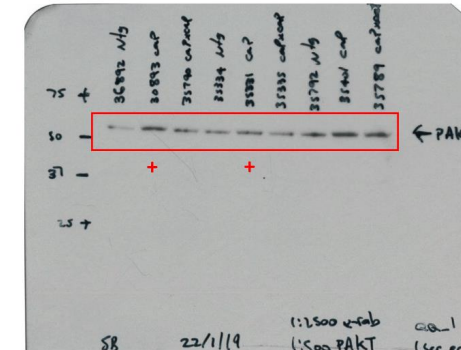
WB4A (pAKT(S473))



WB5A (pAKT(S473))

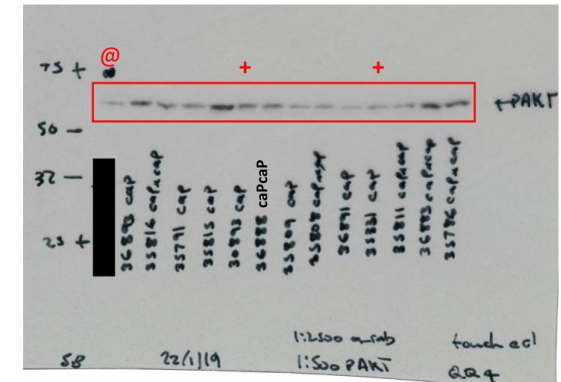
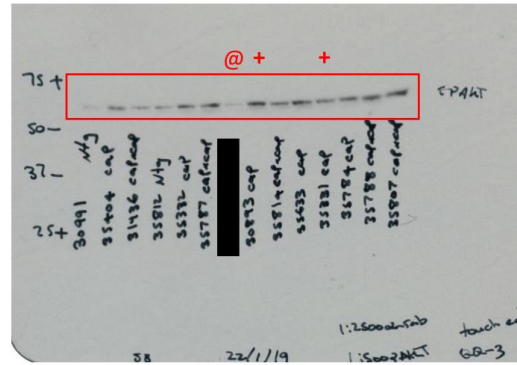
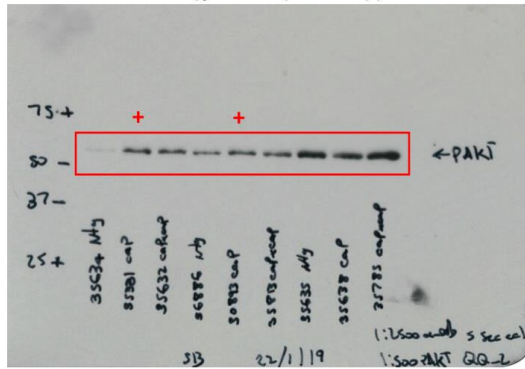


WB6A (pAKT(S473))

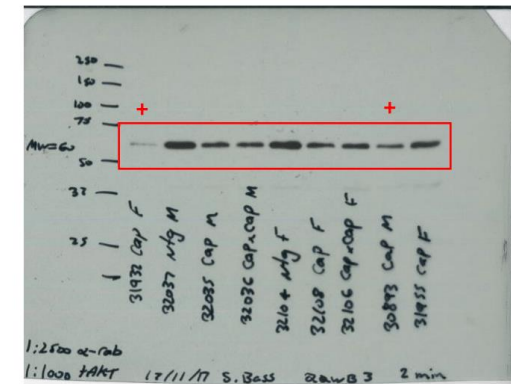
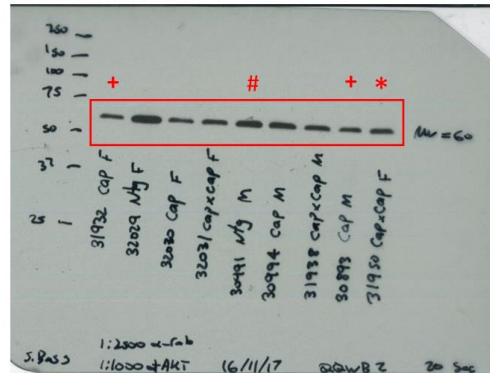
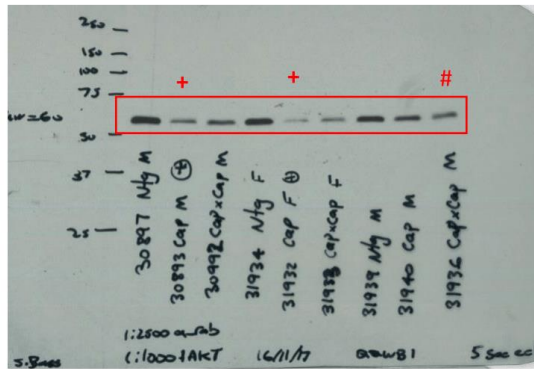


- * Sample excluded entirely – incomplete band
- # Sample excluded from blot due to incomplete band but repeated in a later blot
- + Common sample across blots

A. (cont) Western blots pAKT(S473)/AKT 7-9 probed for pAKT (S473) (Cell Signalling Technology 9271)
 WB7A (pAKT(S473)) WB8A (pAKT(S473)) WB9A (pAKT(S473))



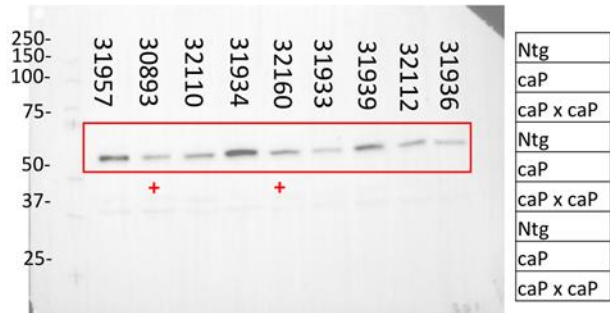
B. Western blots pAKT/AKT 1-3 probed for AKT (Cell Signalling Technology 9272)
 WB1A (AKT) WB2A (AKT) WB3A (AKT)



- * Sample excluded entirely
- # Sample excluded from blot but repeated in a later blot
- @ Sample not relevant to study
- + Common sample across blots

B. Western blots pAKT(T308)/AKT 1-6 probed for AKT (Cell Signalling Technology 9272)

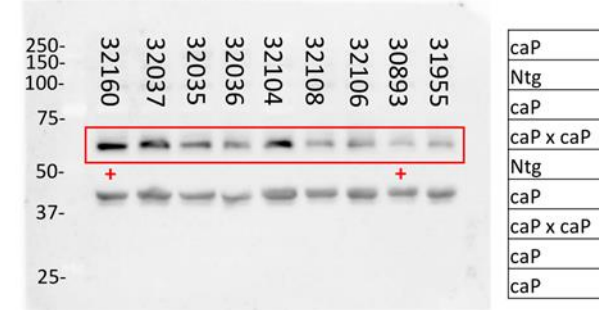
WB1B (AKT)



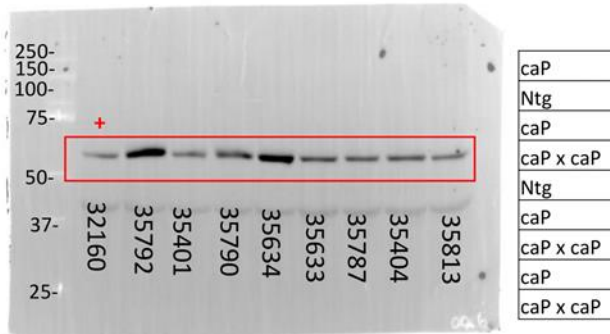
WB2B (AKT)



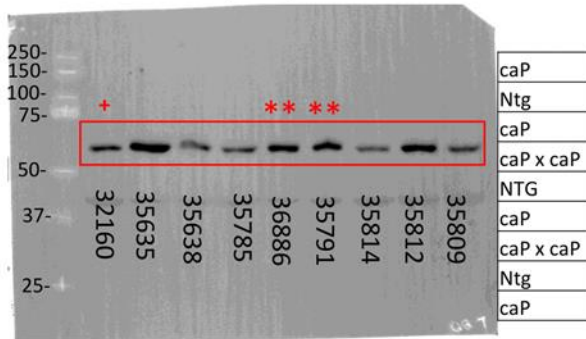
WB3B (AKT)



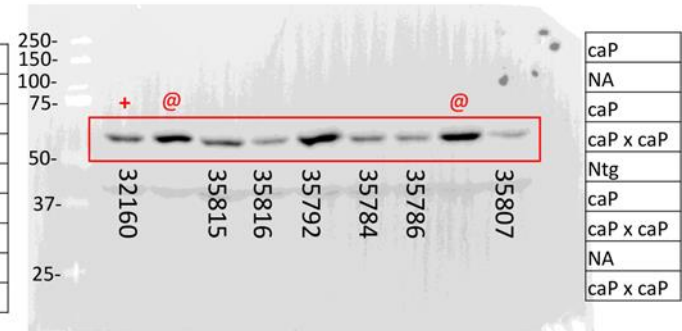
WB4B (AKT)



WB5B (AKT)



WB6B (AKT)

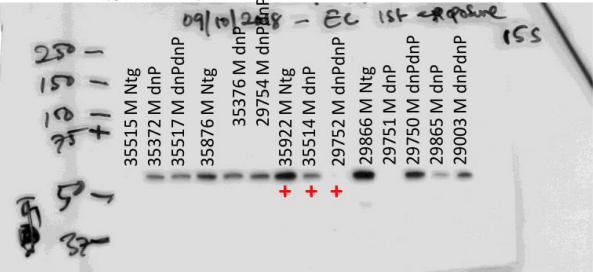


- ** Loading error – lysates from two samples mixed
- @ Sample not relevant to study
- + Common sample across blots

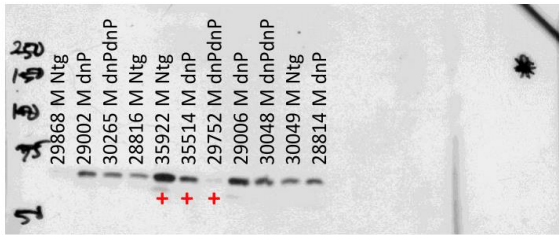
Ntg, dnPI3K Tg(+/-), dnPI3K Tg(+/+)

A. Male Western blots pAKT/AKT probed for pAKT

WB1C (pAKT)

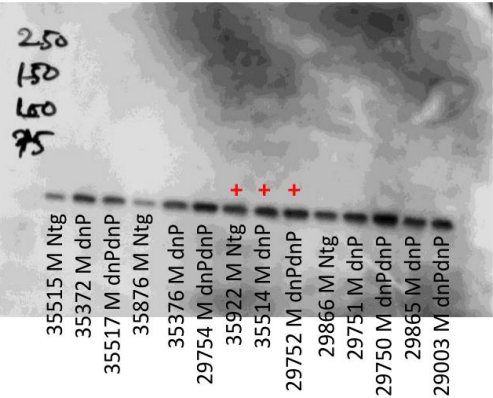


WB2C (pAKT)

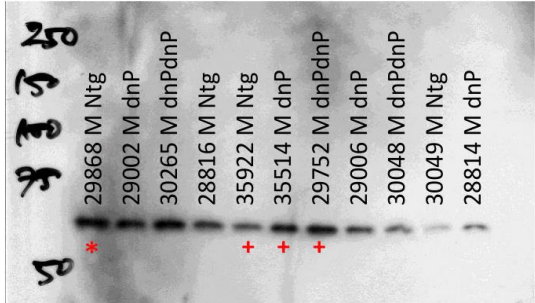


B. Male Western blots pAKT/AKT probed for tAKT

WB1C (AKT)



WB2C (AKT)



- * Sample excluded entirely, uneven background
- + Common sample across blots

Chapter 3

A step-by-step method to detect neutralizing antibodies against AAV using a colorimetric cell-based assay

Chapter 3. Preface

The third chapter, *A step-by-step method to detect neutralizing antibodies against AAV using a colorimetric cell-based assay* forms part of the translational component of this thesis. It focuses on the development of a tool to facilitate AAV-mediated gene therapy research. This chapter contains a manuscript, which describes in detail a method and protocol for the detection of neutralising antibodies against recombinant AAV. The value of this protocol stems from the method being rapid, simple and cost effective. This tool was an important component used in the fourth chapter of this thesis.

Chapter 3.

A step-by-step method to detect neutralizing antibodies against AAV using a colorimetric cell-based assay

Submitted to and under review at '*Journal of Visualized Experiments*', September 2021 by S Bass-Stringer, CJ Thomas, CN May, KL Weeks and JR McMullen.

As first author, S Bass-Stringer contributed ~80% to this publication. This included contributions to the experiments, analyses, drafting, design and editing.

This manuscript is presented in the format of submission, except figures have been inserted within the text.

1 **A step-by-step method to detect neutralizing antibodies against AAV using a colorimetric cell-**
2 **based assay**

3 Sebastian Bass-Stringer ^{a,b}, Colleen J. Thomas ^{b,c}, Clive N. May ^c, Paul Gregorevic ^d, Kate L. Weeks
4 ^{a,e,g}, Julie R. McMullen ^{a,b,e,f,g}

5 ^a Baker Heart and Diabetes Institute, Melbourne, Vic, Australia

6 ^b Department of Physiology, Anatomy and Microbiology, La Trobe University, Melbourne, Vic,
7 Australia

8 ^c Florey Institute of Neuroscience and Mental Health, University of Melbourne, Melbourne, Vic,
9 Australia

10 ^d Department of Physiology, Centre for Muscle Research (CMR), The University of Melbourne,
11 Melbourne, Vic, Australia

12 ^e Department of Diabetes, Central Clinical School, Monash University, Melbourne, Vic, Australia

13 ^f Department of Physiology and Department of Medicine Alfred Hospital, Monash University,
14 Melbourne, Vic, Australia

15 ^g Baker Department of Cardiometabolic Health, The University of Melbourne, Melbourne, Vic,
16 Australia

17

18 **Correspondence**

19 1. Prof Julie R McMullen

20 Baker Heart and Diabetes Institute

21 Melbourne VIC, Australia

22 Email: julie.mcmullen@baker.edu.au

23 2. Dr Kate L. Weeks

24 Baker Heart and Diabetes Institute

25 Melbourne VIC, Australia

26 Email: kate.weeks@baker.edu.au

27 3. A/Prof Paul Gregorevic

28 The University of Melbourne

29 Melbourne, Vic, Australia

30 Email: pgre@unimelb.edu.au

31

32

33

34

35

1 **Summary**

2 A comprehensive laboratory protocol and analysis workflow is described for a rapid, cost
3 effective and straight forward colorimetric cell-based assay for the detection of neutralizing
4 elements against AAV6.

5

6 **Abstract**

7 Recombinant adeno-associated viruses (rAAV) have proven to be a safe and successful vector for
8 the transfer of genetic material to treat a variety of health conditions in both the laboratory and
9 the clinic. However, the presence of pre-existing neutralizing antibodies (NAbs) against AAV
10 capsids poses an ongoing challenge for the successful administration of gene therapies in both
11 large animal experimental models and human populations. Preliminary screening for host
12 immunity against AAV is necessary to ensure the efficacy of AAV-based gene therapies as both a
13 research tool and as a clinically viable therapeutic agent. This protocol describes a colorimetric *in*
14 *vitro* assay to detect neutralizing factors against AAV serotype 6 (AAV6). The assay utilizes the
15 reaction between an AAV encoding an alkaline phosphatase (AP) reporter gene and its substrate
16 NBT/BCIP, which upon combination generates an insoluble quantifiable purple stain.

17 In this protocol serum samples are combined with an AAV expressing AP and incubated to
18 permit potential neutralizing activity to occur. Virus serum mixture is subsequently added to
19 cells to allow for viral transduction of any AAVs that have not been neutralized. The NBT/BCIP
20 substrate is added and undergoes a chromogenic reaction, which corresponds to viral
21 transduction and in turn the neutralizing activity. The proportion of area coloured is quantitated
22 using a free software tool to allow for the generation of neutralizing titers. This assay provides a
23 simple, rapid and cost-effective method to detect NAbs against AAVs.

24

25

26

27

28

29

30

31

1 Introduction

2 Adeno-associated viruses (AAV) are increasingly used as vectors for the delivery of gene
3 therapies to trial treatments for a variety of health conditions that impact the cardiovascular,
4 pulmonary, circulatory, ocular and central nervous systems¹⁻⁵. The popularity of AAV vectors as a
5 leading gene therapy platform stems from their positive safety profile, long-term transgene
6 expression and wide-ranging tissue specific tropisms^{1,6}. Successful outcomes in animal studies
7 have paved the way for over fifty AAV gene therapy clinical trials that have successfully reached
8 their efficacy endpoints⁷, as well as release of the first commercially available AAV gene therapy
9 drug approved by the US Food and Drug Administration⁸. Following initial successes, AAV have
10 continued to gain traction in both the basic and clinical research sectors as a vector of choice
11 and are currently the only *in vivo* gene therapy approved for clinical use in the US and Europe⁹.
12 Nonetheless, the presence of pre-existing neutralizing antibodies (NAbs) against AAV vector
13 capsids remains a hindrance to both preclinical research, and the efficacy of clinical trials. NAbs
14 are present in both naïve human and animal populations and inhibit gene transduction following
15 *in vivo* administration of an AAV vector¹. AAV seropositivity is an exclusion criterion for most
16 gene therapy trials and therefore preliminary screening for host immunity is crucial in both the
17 laboratory and the clinic. Establishing an assay that can detect the presence of NAbs against AAV
18 is an essential step in the pipeline of any AAV gene therapy-based research project.

19 Neutralizing activity is usually determined using either a cell-based *in vitro* or *in vivo*
20 transduction inhibition assay. *In vivo* NAb assays usually involve administering serum from a test
21 subject (e.g., human or large animal) into mice, followed by an AAV with a reporter gene,
22 followed by testing for the expression of the reporter gene or corresponding antigen. *In vitro*
23 assays determine NAb titers by incubating serum or plasma from a human or large animal in
24 serial dilutions with a recombinant AAV (rAAV) that expresses a reporter gene. Cells are infected
25 with the serum/virus mixture and the extent to which the expression of the reporter gene is
26 inhibited is assessed compared with controls. *In vitro* assays are widely used for NAb screening
27 due to their comparatively lower cost, rapidity in testing and greater capacity for standardization
28 and validation^{10,11} compared with *in vivo* assays. *In vivo* assays are often reported to have
29 greater sensitivity^{12,13}, but the same claim has been made with respect to *in vitro* assays^{11,14}.

30 To date, *in vitro* NAb assays have mostly used fluorescence (Green fluorescent protein) or
31 luminescence (Luciferase) as the reporter gene to detect neutralization, and although light-based
32 methods have merit in many contexts, a colorimetric/chromogenic NAb assay may be more
33 advantageous in some circumstances. Colorimetric assays to assess neutralization have been
34 successfully employed for other viruses such as influenza and adenovirus^{15,16}. Their
35 attractiveness stems from their simplicity, lower cost and the requirement for only everyday

1 laboratory apparatus and tools¹⁷. Here we provide a detailed protocol for an *in vitro* NAb assay
2 against AAV that utilizes the chromogenic reaction between an AAV encoding an alkaline
3 phosphatase (AP) reporter gene and a nitro blue tetrazolium /5-bromo-4-chloro-3-indolyl
4 phosphate (NBT/BCIP) substrate. This step-by-step protocol was developed based on a previous
5 report that utilized a hPLAP (human placental alkaline phosphatase) reporter gene (AAV6-hPLAP)
6 for the detection of neutralizing activity against AAV¹⁸. This assay is cost effective, time efficient,
7 easy to set up and requires only minimal technical skills, laboratory equipment and reagents.
8 Moreover, the simplicity of this assay gives it the potential to be optimized for broad application
9 across different types of cells, tissues or viral serotypes.

10

11 **Protocol**

12 All aspects of animal care and experimentation were conducted in accordance with Florey
13 Institute of Neuroscience and Mental Health guidelines and the Australian Code for the Care and
14 Use of Animals for Scientific Purposes (National Health and Medical Research Council of
15 Australia, 8th edition, 2013).

16

17 A schematic overview of the assay protocol is provided in Figure 1

18

19

20

21

22

23

24

25

26

27

28

29

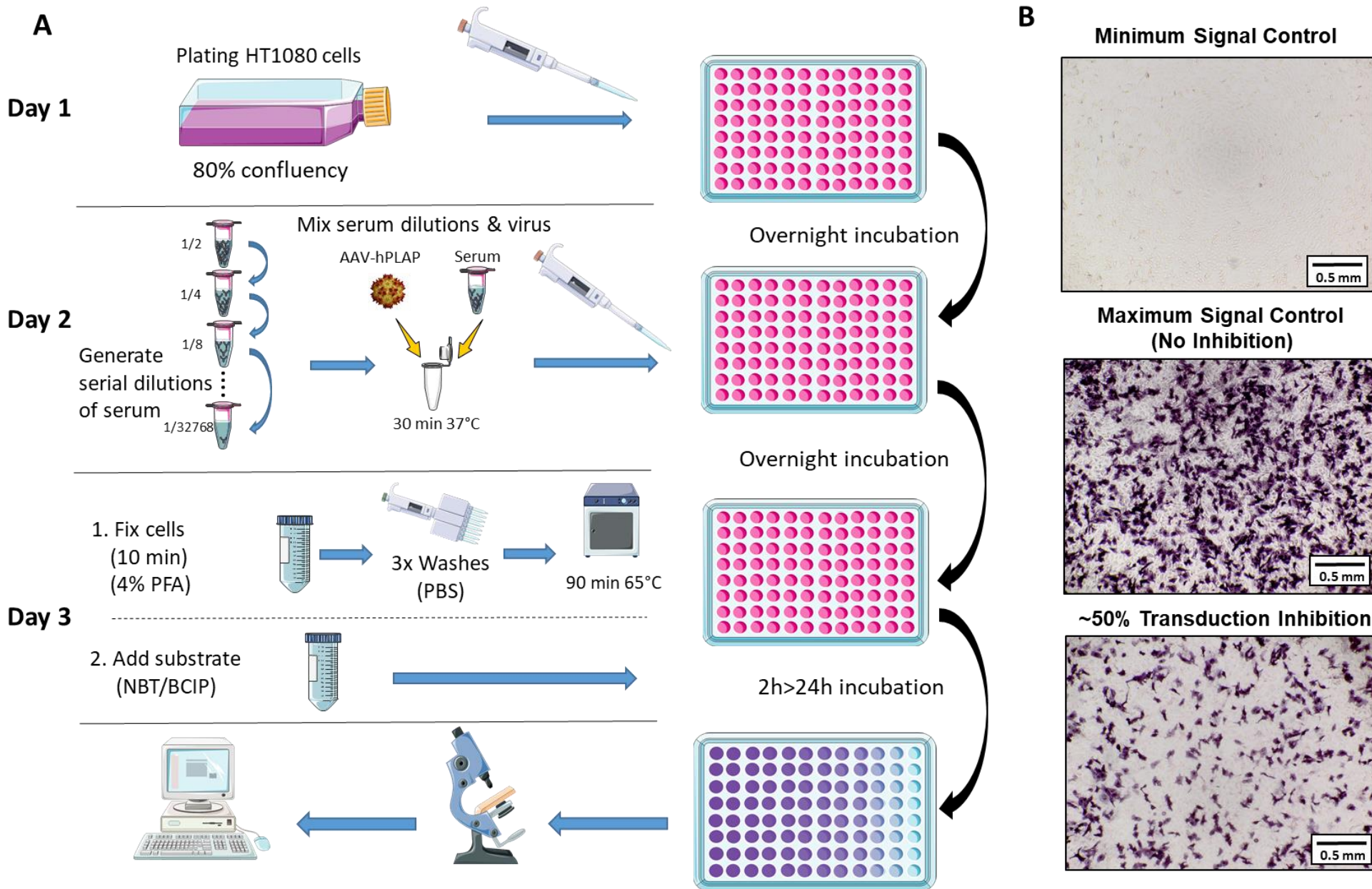


Figure 1: Schematic diagram of NAb assay protocol. **A)** Visual representation of the NAb assay illustrating the primary steps involved in the three-day protocol. Briefly, cells are grown and plated overnight. The following day, serial dilutions of serum are prepared, incubated with AAV and then incubated with the cells overnight. The next day, cells are fixed, washed, incubated, combined with substrate and incubated again followed by imaging and quantitation. **B)** Representative images of a minimum signal control (complete AAV inhibition), a maximum signal control (no inhibition) and an ovine serum sample with ~50% signal inhibition. Scale bar = 0.5 mm.

1 **Initial preparation**

2 **1.1.** Serum from sheep can be collected in 8ml Vacuette serum separator tubes, left at RT
3 for 20-30 minutes and spun down at 3000 RPM for 15 minutes. The clear supernatant is
4 serum and is aliquoted and stored at -80°C.

5 **1.2.** Heat inactivate fetal bovine serum (FBS) by placing it in a water bath at 56°C for 30
6 minutes and swirling intermittently. For precision, place a thermometer in a second
7 bottle containing an equivalent volume of water and add it to the heat bath at the same
8 time as the FBS bottle. Begin timing when the thermometer reaches 56°C.

9 **1.3.** Employ proper aseptic technique and cell culture practice for all subsequent steps that
10 are performed in the cell culture hood^{19, 20}. All objects and the hood itself should be
11 sprayed with 70% ethanol prior to use and cleaned with 1% sodium hypochlorite upon
12 completion.

13 **1.4.** Make complete Dulbecco's Modified Eagle Medium (DMEM) by combining high glucose
14 DMEM with 10% heat inactivated FBS and 1% Penicillin Streptomycin. Filter using the
15 Millipore Express Filtering System.

16 **1.5.** Establish HT1080 cells and passage in a 75cm² square flask as described in Agilent
17 Technologies AAV-HT1080 cell culture guidelines (Catalog #240109). Create multiple
18 frozen stocks of cells. It is advised that cells not be used after twenty passages as
19 further passaging may influence the assay results.

20

21 **2. Day 1 – Plating cells**

22 **2.1.** Passage HT1080 cells until they reach ~80% confluency.

- 1 **2.2.** Wash the cells in 10 mL of pre-warmed (37°C) 1x phosphate buffered saline (PBS) and
2 trypsinize cells for 3-4 minutes in 4 mL of pre-warmed 0.05% trypsin-EDTA. Inactivate
3 the trypsin with 6 mL of pre-warmed complete DMEM. Calculate the number and
4 concentration of viable cells using a haemocytometer and the trypan blue exclusion
5 method²¹.
- 6 **2.3.** Dilute the cells to a concentration of 1×10^5 cells/mL with complete DMEM and seed 100
7 μ l of cells/well into 96-well flat-bottomed plates (1×10^4 cells per well). Incubate the
8 plate at 37°C, 5% CO₂ overnight for 16-22 hours.
- 9
- 10 **3. Day 2 – Infecting cells**
- 11 **3.1.** Remove plate/s from the incubator and use a light microscope to confirm cells are
12 evenly dispersed within the wells and the confluency is roughly 50%. If cells are not
13 within a range of 45-55% confluency, repeat the ‘Day 1’ protocol and adjust initial cell
14 concentration accordingly.
- 15 **3.2.** Generate serial dilutions of the serum of interest in 1.5 mL microcentrifuge tubes using
16 pre-warmed complete DMEM as the diluent. Table 1 provides an example of how to
17 generate a dilution cascade for triplicate samples.
- 18 **3.3.** To perform the assay in triplicate, prepare a 7.5×10^6 vg/ μ l working solution of AAV-
19 hPLAP (this can be provided upon request) and add 66 μ l of the virus working solution
20 to each tube containing a serum dilution (330 μ l total volume/dilution, see Table 1).
21 NOTE: A no serum control, no serum and virus control and a NAb positive control
22 sample should also be included for each run performed and under identical treatment.
- 23 **3.3.1.** A viral working solution of 7.5×10^6 vg/ μ l is used to generate a concentration of
24 15k viruses/cell Multiplicity of infection (MOI).
- 25 **3.3.2.** The volume described (330 μ l) accounts for triplicate samples +10% of the serum
26 & virus mixture. Performing replicates of the assay is highly recommended for
27 accurate determination of neutralizing activity.
- 28 **3.4.** Mix the virus and serum by pipetting and place the tubes in an incubator at 37°C, 5%
29 CO₂ for 30 minutes to allow potential neutralization to occur.
- 30 **3.5.** For each dilution, add 100 μ l of the virus/serum mixture to each well on the 96-well
31 plate containing 1×10^4 cells/well. Table 2 provides an example 96-well plate sample
32 layout.

- 1 **3.6.** Wrap the 96-well plate containing cells, serum and AAV-hPLAP in foil and place in an
 2 incubator at 37°C, 5% CO₂ overnight for 16-24 hours to allow AAV entry into the cells.
 3

Dilution cascade label	Dilution	3 x sample (240 µL) + 10% buffer volume (24 µL)	Ratio of serum:media
Dilution 1 (D1)	1/2	264 µL serum 264 µL media	50:50
Dilution 2 (D2)	1/4	264 µL D1 + 264 µL media	25:75
Dilution 3 (D3)	1/8	264 µL D2 +264µL media	12.5:87.5
Dilution 4 (D4)	1/16	264 µL D3 +264 µL media	6.25:93.75
Dilution 5 (D5)	1/32	264 µL D4 +264 µL media	3.13:96.87
Dilution 6 (D6)	1/64	264 µL D5 +264 µL media	1.56:98.44
Dilution 7 (D7)	1/128	264 µL D5 +264 µL media	0.78:99.22
Dilution 8 (D8)	1/256	264 µL D5 +264 µL media	0.39:99.61
Dilution 9 (D9)	1/512	264 µL D7 + 264 µL media	0.2:99.8
Dilution 10 (D10)	1/2048	132 µL D8 + 396 µL media	0.05:99.95
Dilution 11 (D11)	1/8192	132 µL D9 + 396 µL media	0.01:99.99
Dilution 12 (D12)	1/32768	132 µL D10 + 396 µL media	0.003:99.997

Table 1: Volumes of serum and diluent required to generate serial dilutions of serum in triplicate.

	Serum sample #1			Serum sample #2			Serum sample #3			Mono AB (mAb), controls and extra samples		
	1	2	3	4	5	6	7	8	9	10	11	12
A	1/2	1/2	1/2	1/2	1/2	1/2	1/2	1/2	1/2	50 ng MAb	50 ng MAb	50 ng MAb
B	1/4	1/4	1/4	1/4	1/4	1/4	1/4	1/4	1/4	5 ng MAb	5 ng MAb	5 ng MAb
C	1/8	1/8	1/8	1/8	1/8	1/8	1/8	1/8	1/8	0.5 ng MAb	0.5 ng MAb	0.5 ng MAb
D	1/16	1/16	1/16	1/16	1/16	1/16	1/16	1/16	1/16	MO (-C)	MO (-C)	MO (-C)
E	1/32	1/32	1/32	1/32	1/32	1/32	1/32	1/32	1/32	VO (+C)	VO (+C)	VO (+C)
F	1/64	1/64	1/64	1/64	1/64	1/64	1/64	1/64	1/64	Sample #1 1/512	Sample #1 1/512	Sample #1 1/512
G	1/256	1/256	1/256	1/256	1/256	1/256	1/256	1/256	1/256	Sample #2 1/512	Sample #2 1/512	Sample #2 1/512
H	1/512	1/512	1/512	1/512	1/512	1/512	1/512	1/512	1/512	Sample #3 1/512	Sample #3 1/512	Sample #3 1/512

Table 2: Example 96-well plate layout for assessing naïve serum samples in dilutions ranging from 1/2 to 1/512. Higher dilutions are incorporated into the assay if assessing a sample known to be positive for AAV NAb (post administration samples) or if a higher titer is required. MO (-C): Media only control. VO (+C): Virus and media only control. mAb: Monoclonal antibody against AAV (NAb positive control).

1 **4. Day 3 - Fixing and adding substrate to cells**

2 **4.1.** CAUTION: Paraformaldehyde (PFA) is a probable carcinogen and is toxic from skin or
3 eye contact or inhalation. Handle in a fume hood with proper personal protective
4 equipment as well as a facemask. Make fresh 4% PFA diluted in PBS (~7 mL required per
5 96-well plate) and allow to cool to room temperature (RT).

6 **4.2.** Aspirate the media from the 96-well plate and add 50 μ l of 4% PFA to each well. Wrap
7 the plate in foil and leave at RT for 10 minutes to fix the cells.

8 **4.3.** Wash and aspirate the cells with 200 μ l of RT PBS. Repeat washing step twice. A
9 multichannel pipette is an efficient option for the washing steps.

10 **4.4.** Pipette 200 μ l of pre-warmed PBS to each well, wrap the plate in foil and incubate at
11 65°C for 90 minutes to denature endogenous alkaline phosphatase activity.

12 **4.5.** Aspirate wells and wash cells in cold (4°C) PBS. Aspirate, wash in cold double-distilled
13 H₂O (DDW) and aspirate again.

14 **4.6.** Dissolve a pellet of BCIP/NBT in 10 mL of DDW by vortexing and pipette 50 μ l to each
15 well.

16 **4.7.** Wrap the plate in foil and incubate at RT for 2-24 hours. NOTE: Be consistent with
17 incubation time between runs.

18 **4.8.** Using a light microscope camera, take photos of each well using a 4x objective lens and
19 ensure that the same exposure, white balancing and light settings are used throughout.
20 The wells should be positioned identically and the edges of the well should not be
21 visible in the photos. Save photos as TIF format or similar.

22

23

24 **5. Quantitation to determine neutralizing activity using ImageJ**

25 **5.1.** Download and install the freely available software "ImageJ":

26 <https://imagej.nih.gov/ij/download.html>

27 **5.2.** Open the image to be analyzed in ImageJ (Figure 2).

28 **5.3.** If using colored images, convert to grayscale by selecting 'Image' > 'Type' > '8-bit'.

- 1 **5.4.** Click 'Image' > 'Adjust' > 'Threshold'. Adjust the threshold until all colored areas are
2 covered, but the background is not. NOTE: It is recommended to use the same
3 threshold setting for all images captured from the same plate.
- 4 **5.5.** Click 'Analyze' > 'Set Measurements' and tick the 'Area', 'Limit to Threshold', 'Area
5 Fraction' and 'Display label' checkboxes and click ok.
- 6 **5.6.** The signal reading (percentage of coloration) of a given well can then be determined by
7 clicking 'Analyze' > 'Measure'.
- 8 **5.7.** Perform quantitation for all sample replicates. Exclude any wells that are contaminated,
9 show uneven cell distribution, or vary in cell density or lighting (See Supplementary
10 Figure 1 for examples of wells that should be considered for exclusion. Typically, 3-4
11 wells may require exclusion from a 96-well plate).
- 12 **5.8.** Figure 2 provides a visual representation of the quantitation process using ImageJ.
- 13
- 14
- 15
- 16
- 17
- 18
- 19
- 20
- 21
- 22
- 23
- 24
- 25
- 26
- 27

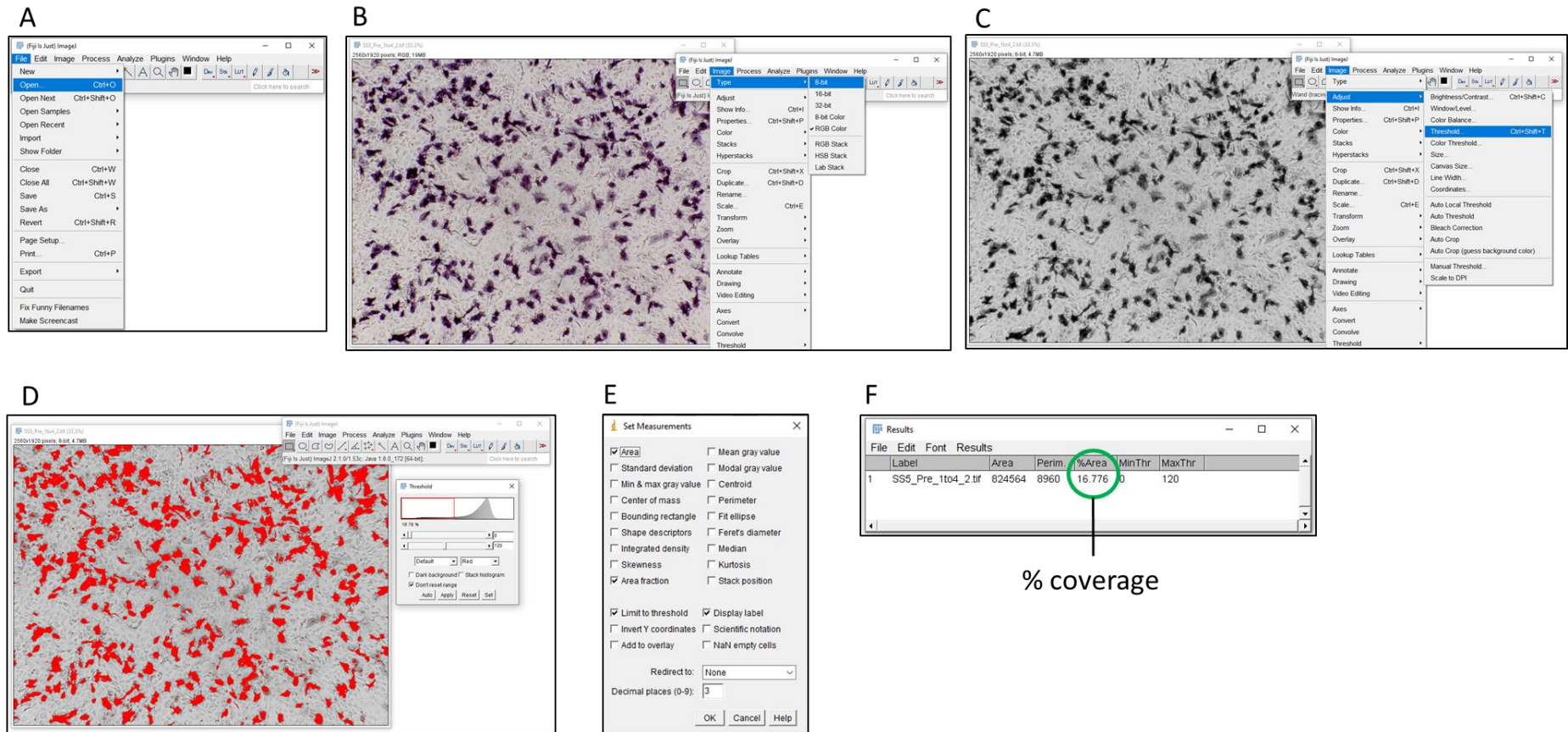


Figure 2: Steps for determining percentage colouration using ImageJ software. **A)** Open the image to be analyzed with ImageJ software. **B)** Convert the image to 8-bit grayscale. **C)** Open the threshold window **D)** Adjust the maximum threshold so all coloured areas are covered but background area is not (this threshold should be consistent across an entire plate). **E)** Select the ‘Analyze’ drop box, click ‘Set measurements’ and tick ‘Area’, ‘Area fraction’, ‘Limit threshold’ and ‘Display label’ and click ‘OK’. **F)** Click ‘Measure’ to measure the covered area. The % area indicates the proportion of the image that was coloured. This can then be used with the control samples to determine the TI_{50} titer.

1 **6. Determination of Transduction Inhibition (TI₅₀) titer**

2 **6.1.** Determine the average readout from replicates for the:

- 3 • Media only control (baseline signal reading).
- 4 • Virus + media only control (maximum signal reading).

5

6 **6.2.** Calculate the percentage of inhibition using the following formula:

7 $100\% - [(Test\ sample\ signal\ readout\ (virus + serum\ of\ interest\ sample) - baseline\ signal$
8 $readout\ (media\ only)) / (maximum\ signal\ readout\ (media\ and\ virus\ only) - baseline$
9 $signal\ readout)] \times 100\% = \% Transduction\ inhibition.$

10 **6.3.** Calculate the average percentage inhibition from all replicates and dilutions for each
11 sample.

12 **6.4.** The TI₅₀ titer of the sample can be set as the lowest dilution that yields 50% or greater
13 inhibition of hPLAP activity, e.g., if a 1/8 dilution has greater than 50% inhibition (but
14 1/4 does not) we report the TI₅₀ titer as 1/8.

15

16 **7. Determination of neutralized AAV particles**

17 **7.1.** The number of neutralized AAV particles per μ l of serum for a given sample can be
18 calculated by employing the following formula:

19 • $((MOI \times cell\ count/well) / (volume\ of\ serum / dilution\ factor\ of\ TI_{50}\ titer)) / 2$
20 $(dividing\ by\ 2\ accounts\ for\ the\ TI_{50}\ measuring\ 50\% \ of\ neutralized\ particles) =$
21 $neutralized\ AAV\ particles / \mu l\ of\ serum.$

22 • So, for a sample that gives a TI₅₀ titer of 1/4 (25% serum, 75% diluent) in which
23 the assay used 80 μ l of undiluted serum and an MOI of 15k was plated onto
24 1×10^4 cells, we would calculate: $((15000 \times 10000) / (80/4)) / 2 = 3.75 \times 10^6$
25 $neutralized\ particles / \mu l\ of\ serum.$

26

27

28

29

1 **Representative results**

2 *Transduction assay to establish the optimal viral dosage for plate coverage*

3 We selected HT1080 cells, a well-established fibrosarcoma cell line, for this assay. A
4 concentration of 1×10^4 HT1080 cells/well provided ~50% cell confluency in each well of a 96-well
5 plate. To determine the optimal viral concentration for the assay, we added a rAAV encoding a
6 hPLAP (human placental alkaline phosphatase) reporter gene (AAV6-hPLAP) in triplicate at a
7 range of concentrations of vector genome (vg) containing particles per cell (MOI: 0, 150, 500,
8 1500, 5000, 15000, 50000 & 150000 (Figure 3A)). An MOI of 15000 (1.5×10^8 vg/well) conferred
9 36% plate coloration and was selected as the optimal viral dosage. A positive correlation was
10 observed between coloration and viral concentrations for all MOI between 0 and 15000 ($n=6$,
11 $r=0.995$, $P<0.001$). This concentration adequately displayed the reporter gene signal above
12 background in the presence of high concentrations of NAb (low plate coloration), whilst not
13 losing sensitivity due to color saturation in the absence of NAb (high coloration, Figure 3B).

14 The efficacy of the assay when exposed to neutralizing elements was trialed using serial
15 dilutions of an anti-AAV6 mouse monoclonal antibody (mAb) in triplicate. The standard approach
16 of using the first dilution to display 50% or more transduction inhibition (TI_{50}) was applied to
17 determine the neutralizing titer of a given sample (see Methods). Assessing \log_{10} dilutions, the
18 anti-AAV6 mAb displayed a TI_{50} titer of ~10 ng/mL (1 ng total mAb), whilst a concentration of 500
19 ng/mL (50 ng total Ab) and above completely inhibited reporter gene expression (Figure 3C).

20

21 *Assessment of NAb against AAV6 in sheep samples*

22 Serum was collected from the carotid vein using a 16 G needle cut-off and syringe from
23 conscious naïve healthy adult sheep ($n=11$) and screened to determine the TI_{50} titer using our
24 colorimetric NAb assay. Two-fold serial dilutions ranging from a 1/2 to a 1/512 dilution were
25 assessed for each serum sample in duplicate or triplicate. The 1/2 dilution contained a total of 40
26 μ l of serum, which corresponded to a concentration of 1.88×10^6 AAV particles per μ l of serum.
27 The degree of AAV neutralization varied within the naïve sample population, with TI_{50} titer values
28 ranging from as low as 1/2 (blue line) to as high as 1/80 (green line, 1.88×10^6 to 7.5×10^7
29 neutralized AAV particles/ μ l serum) (Figure 4A).

30

31

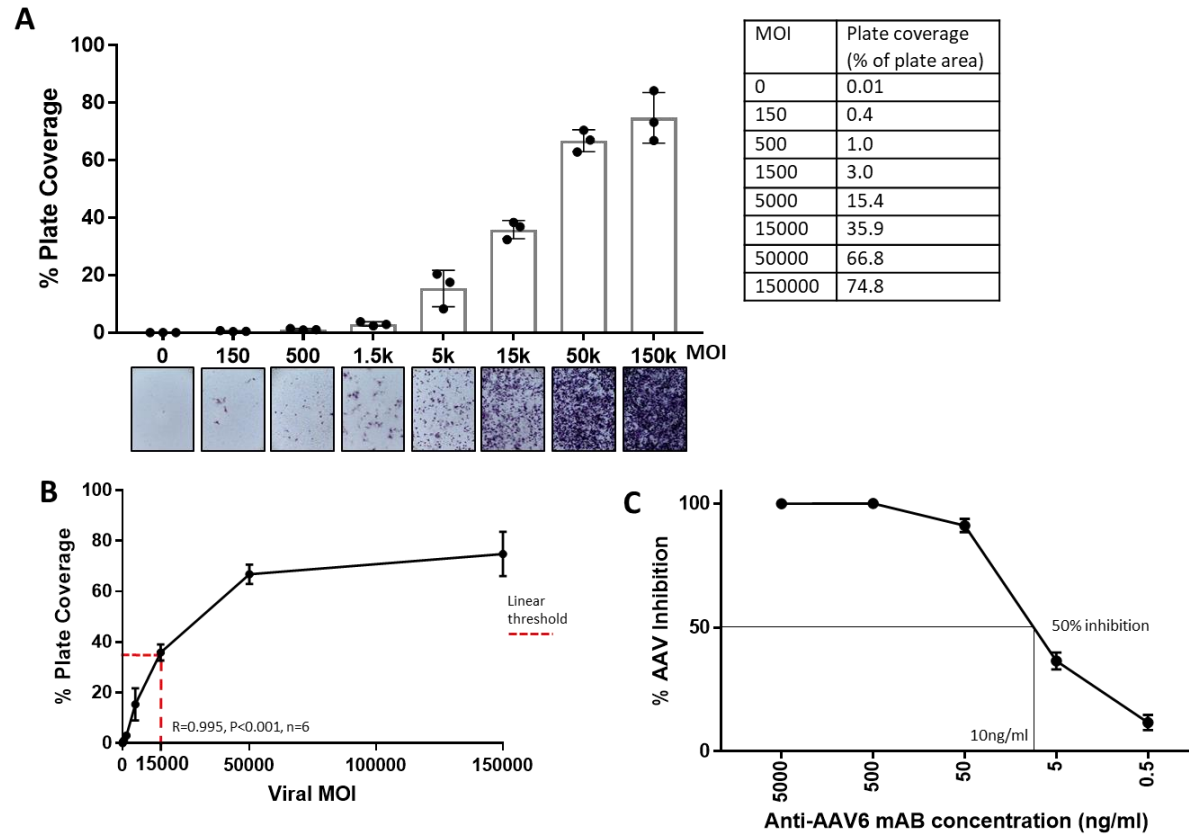


Figure 3: Optimization of viral dose & assessment of assay efficacy against an anti-AAV6 monoclonal antibody (mAB). **A)** Proportion of coloration (% of total area) for individual wells at different multiplicities of infection (MOI) and representative images (below) displaying the corresponding chromogenic reaction between the alkaline phosphatase (hPLAP) and NBT/BCIP for each viral dose (left). Percentage plate coverage is also displayed in tabulated form (right). Each data point represents a technical replicate ($n=3$ replicates per MOI). **B)** A representation of the correlation between coloration and MOI shown in figure 3A. The red dotted line represents the highest concentration tested that did not affect the linear correlation between coloration and viral concentration. **C)** Neutralizing activity against AAV6 from an anti-AAV6 monoclonal antibody at \log_{10} dilutions. 50% inhibition of AAV6 transduction (TI_{50}) is observed at a concentration of ~ 10 ng/mL. $n=3$ replicates per dilution. Data represent mean \pm SEM.

1 Subsequently, we performed direct cardiac injection ($n=5$) of AAV6 at doses ranging between
2 5×10^{12} and 3×10^{13} vg to naïve sheep. Briefly, sheep were anaesthetized as previously described²².
3 The heart was exposed from the left lateral position, the pericardium opened and AAV
4 administered via 10-40 $\sim 20 \mu\text{l}$ injections into the LV myocardium (anterior) in region around the
5 2nd branch of the left anterior descending coronary artery (LAD). The pericardium, intercostal
6 muscle, subcutaneous tissue and skin were closed and anaesthetic removed. Serum was
7 collected from all animals prior to and six to eight weeks after AAV administration from the pre-
8 cannulated right jugular vein using a 16G needle cut-off and syringe ($\sim 5 \text{ml}$ serum/animal). The
9 colorimetric NAb assay was employed to determine the change in NAb titer following AAV6
10 administration. Post-AAV serum samples were screened in triplicate as 2- to 4-fold serial
11 dilutions ranging from a 1/2 to a 1/32768 dilution. Assay results indicated that AAV inhibition TI_{50}
12 titer values prior to AAV administration ranged from 1/4 to 1/80 (3.75×10^6 to 7.5×10^7 neutralized
13 AAV particles/ μl serum; Figure 4B). Following AAV cardiac injection a clear and consistent
14 contrast in the NAb titer was observed compared with pre-AAV serum titers (Figure 4B, Table 3).
15 The lowest AAV dose (5×10^{12} vg) displayed a 1/2048 TI_{50} titer (dashed blue line, 1.92×10^9
16 neutralized AAV particles/ μl serum) and the remainder of the doses ($1-3 \times 10^{13}$ vg) displayed TI_{50}
17 titers ranging from 1/12000 to $>1/32768$ (1.13×10^{10} to $>3 \times 10^{10}$ neutralized AAV particles/ μl
18 serum).
19

Sheep ID	Administration status	Dose received (vg)	NAb Titer (TI_{50})	AAV neutralized / μl serum	Fold change Pre vs Post
Sheep 1	Pre-AAV	1×10^{13}	1/5	5.6×10^6	6400
	Post -AAV		1/32000	3×10^{10}	
Sheep 2	Pre-AAV	1×10^{13}	1/80	7.5×10^7	200
	Post -AAV		1/16000	1.5×10^{10}	
Sheep 3	Pre-AAV	5×10^{12}	1/16	1.5×10^7	125
	Post -AAV		1/2000	1.9×10^9	
Sheep 4	Pre-AAV	2×10^{13}	1/4	3.8×10^6	>10000
	Post -AAV		$>1/32000$	$>3 \times 10^{10}$	
Sheep 5	Pre-AAV	3×10^{13}	1/8	7.5×10^6	1700
	Post -AAV		1/12000	2.3×10^{10}	

Table 3: Impact of AAV exposure on neutralizing activity. Neutralizing activity for sheep assessed both before and after receiving direct cardiac injection of a rAAV6 at varying doses. The dose received pre and post TI_{50} titers and fold change following administration are displayed.

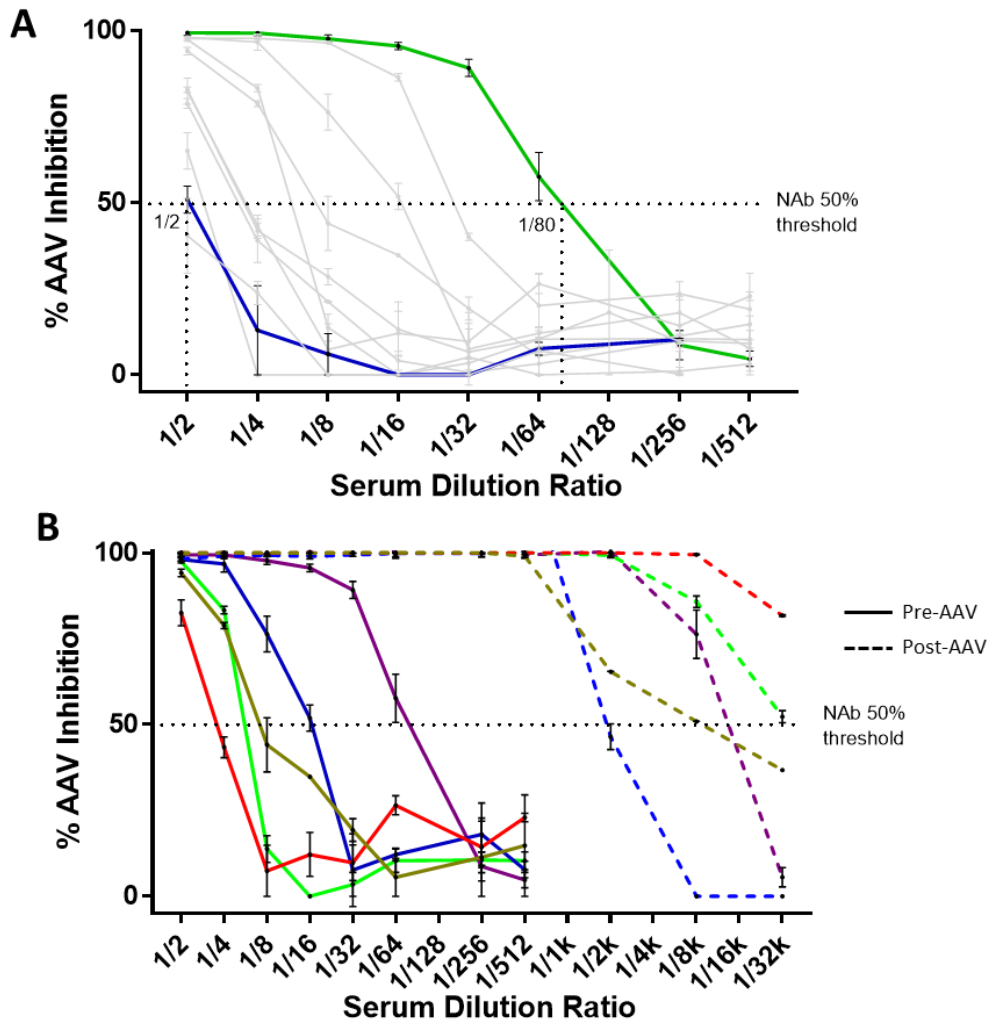


Figure 4: Example of neutralising antibody (Nab) assay results using ovine serum samples. **A)** Adeno-Associated Virus (AAV) neutralizing activity of serum samples collected from 11 naïve sheep, measured in 2-fold serial dilutions ranging from 1/2 to 1/512. Colored lines are representative samples with low and high neutralizing activity, grey lines represent the other nine samples. The dotted line represents 50% transduction inhibition (TI_{50}) and the corresponding TI_{50} titers for the low (blue) and high (green) representative samples. **B)** AAV neutralizing activity of serum samples collected from five sheep before and after receiving a dose of AAV via direct cardiac injection. Neutralizing activity assessed in 2-fold serial dilutions ranging from 1/2 to 1/32768. Each color represents serum from a different animal, filled lines represent pre-AAV administration and dotted lines represent post-AAV administration. $n=2-3$ replicates per dilution for each sample. Data represent mean \pm SEM.

1 Discussion

2 In this report we describe in detail a colorimetric assay which assesses the extent of AAV
3 neutralization in a given serum sample by evaluating a chromogenic reaction that corresponds to
4 the degree of *in vitro* viral transduction. The development of the protocol was based on the
5 known chromogenic reaction between the enzyme alkaline phosphatase and NBT/BCIP which
6 has been widely utilized as a staining tool for the detection of protein targets in applications
7 such as immunohistochemistry, and as a reporter tool for evaluating viral transduction^{18, 23-25}. Its
8 merit stems from its time and cost effectiveness, accessibility, ease of setting up and performing,
9 whilst still demonstrating a high degree of efficacy. The rAAV6 employed in this assay (AAV-
10 hPLAP) carries the reporter gene human placental alkaline phosphatase (hPLAP) and is driven by
11 a cytomegalovirus (CMV) promoter²⁴ (Supplementary Figure 2). NBT/BCIP is a hPLAP substrate
12 that is initially dephosphorylated by alkaline phosphatase and sequentially undergoes
13 oxidization to form a dimer which results in an insoluble product that is a vibrant purple color²⁶.

14 In selecting the optimal MOI for this assay, we aimed to establish a viral concentration that
15 would provide sufficient expression of the AAV reporter gene through virus-cell binding, and in
16 conjunction with the NBT/BCIP substrate, provide coloration within a range that could be
17 accurately measured. An MOI of 15000 was selected, as it was the highest concentration tested
18 that did not affect the linear correlation between coloration and viral concentration. Higher
19 concentrations (50 000 and 150 000 MOI) caused the concentration-color response curve to
20 plateau, indicating color saturation (Figure 3B). Assessment of viral MOIs between 0 and 15000
21 (n=6) and their corresponding level of coloration resulted in $r=0.995$ ($P<0.001$), validating the
22 sensitivity of the assay by establishing a very strong positive correlation between viral
23 concentration and reporter-gene driven coloration. Given potential variability in factors such as
24 cell culture conditions, laboratory technicians, techniques and equipment as well as variations in
25 viral batches, it is recommended that any new user perform a preliminary trial assessment of the
26 optimal MOI when establishing a NAb assay.

27 The MOI chosen for a given NAb assay is major contributing factor in the overall titer observed
28 for a given serum sample. If we had chosen an MOI of 5000 instead of 15000, we would
29 anticipate a 3-fold difference in titer value. This has historically been problematic in the field of
30 AAV gene therapy, as different pre-clinical and clinical trials have implemented AAV NAb assays
31 with MOI values ranging from less than 1000 to as high 25000¹¹, meaning any kind of cross-study
32 comparison of NAb titers for a given AAV serotype is of little to no value. It has recently been
33 suggested that reporting titers as neutralized AAV particles per μl of serum can provide values
34 that are more comparable across different studies^{9, 27}. There are numerous other factors that
35 may contribute to variation in titers between studies, such as the choice of cell line, reporter

1 gene, incubation times and culture conditions. To facilitate the standardization of AAV NAb
2 assays, we have reported both the titer values and neutralized AAV particles/ μ l of serum.

3 It is important to include a serial dilution of a known NAb sample on every plate to act as both a
4 positive control and a common sample between plates. This is important to identify any possible
5 variability between separate runs. A neutralizing monoclonal antibody against the AAV of
6 interest is an ideal positive control and standard, but a serum sample known to be positive for
7 NAb is also acceptable. We validated the assay's efficacy by demonstrating that a monoclonal
8 Ab specific to intact AAV6 particles (ADK6) can quantitatively inhibit transduction in
9 concentration-dependent manner.

10 Preclinical trials using large animal models provide a crucial stepping-stone between the
11 laboratory and the clinic due to the physiological resemblance that animals such as sheep and
12 pigs share with humans^{1, 28, 29}. Historically, the vast majority of candidate AAV gene therapies
13 that have made it to clinical trials have undergone preliminary trials in large animals¹. Multiple
14 studies have demonstrated that both humans and a range of large animals including sheep, pigs,
15 dogs, rabbits and non-human primates can harbour neutralizing antibodies against AAV6 as well
16 as many other AAV serotypes^{30, 31}. This highlights the importance of preliminary screening for
17 NAb prior to trials in both large animal models and humans. We tested serum samples from
18 sheep that had no previously known exposure to AAV, of which 10 of 11 displayed TI_{50} titers
19 $<1/30$ ($<3 \times 10^7$ neutralized AAV particles/ μ l serum), whilst one displayed a TI_{50} titer of $1/80$
20 (7.5×10^7 neutralized AAV particles/ μ l serum). Five of the sheep went on to receive direct cardiac
21 muscle injection of rAAV. Amongst all samples, administration of AAV dramatically changed the
22 neutralizing activity, with fold change increases ranging from a 125 to a >10000 fold in TI_{50} titer
23 values between pre and post AAV exposure (Table 3). Of note, the lowest AAV6 dose
24 administered (5×10^{12} vg) corresponded to the lowest post-AAV TI_{50} titer value (TI_{50} titer $1/2000$)
25 and fold change increase (125 fold). While we observed no clear evidence of pre-existing NAb
26 within the 11 naïve sheep at levels which would prevent AAV transduction (all TI_{50} titer values
27 $<1/100$), data from the 5 sheep which received a direct injection of AAV would suggest a cut off
28 for NAb positivity would be $>1/1000$ (based on pre- and post-AAV values). The stark difference
29 between the pre- and post-NAb titer and the capacity to detect titers $>1/32000$ provides further
30 validation of the efficacy and sensitivity of the assay. Of note, establishment of a cut-point at
31 which a sample is deemed positive for neutralizing activity is an important subsequent step
32 when determining a threshold for NAb positive animals. This can be determined by assessing the
33 variability in a group ($\sim n \geq 30$) naïve samples from a specific population of interest. This allows for
34 the establishment of criteria to determine a statistically derived cut-point in which a sample is
35 deemed positive for neutralizing activity. Alternatively, including positive control samples from

1 animals both pre- and post-AAV administration, as we show here (Figure 4B) can provide a clear
2 indication of the positive titer range for neutralizing activity. Recommendations regarding the
3 establishment of cut-point thresholds as well as validation and optimization of *in vitro*
4 neutralizing assays have been described extensively in the literature³²⁻³⁵. The use of the
5 microscope camera to image wells is useful in that it provides very high-quality images that can
6 accurately differentiate the degree of neutralization. However, the use of a high-resolution
7 flatbed or plate scanner may provide a more rapid approach to imaging the wells if the quality
8 and lighting of images can be maintained.

9 In summary, this *in vitro* assay provides a rapid, cost effective, easily accessible, and simple
10 method to detect the presence of neutralizing antibodies against rAAV6. This assay has the
11 capacity to be adjusted and optimized to perform with different AAV serotypes with relative
12 ease. The AAV6-hPLAP vector can be provided for the purpose of this assay upon request.

13

14 **Acknowledgments**

15 This study was funded by a National Health and Medical Research Council Project Grant to JRM
16 and CJT (ID 1163732), and in part by the Victorian Government's Operational Infrastructure
17 Support Program. SB is supported by a joint Baker Heart and Diabetes Institute-La Trobe
18 University Doctoral Scholarship. KLW is supported by The Shine On Foundation and a Future
19 Leader Fellowship from the National Heart Foundation of Australia (ID 102539). JRM is
20 supported by a National Health and Medical Research Council Senior Research Fellowship (ID
21 1078985).

22

23 **Disclosures**

24 The authors have nothing to disclose.

25

26

27

28

29

30

31

32

1 **References**

- 2 1. Bass-Stringer S, Bernardo BC, May CN, Thomas CJ, Weeks KL, McMullen JR. Adeno-
3 Associated Virus Gene Therapy: Translational Progress and Future Prospects in the Treatment of
4 Heart Failure. *Heart Lung Circ.* Nov 2018;27(11):1285-1300. doi:10.1016/j.hlc.2018.03.005
- 5 2. Casey GA, Papp KM, MacDonald IM. Ocular Gene Therapy with Adeno-associated Virus
6 Vectors: Current Outlook for Patients and Researchers. *J Ophthalmic Vis Res.* Jul-Sep
7 2020;15(3):396-399. doi:10.18502/jovr.v15i3.7457
- 8 3. Lykken EA, Shyng C, Edwards RJ, Rozenberg A, Gray SJ. Recent progress and
9 considerations for AAV gene therapies targeting the central nervous system. *J Neurodev Disord.*
10 May 18 2018;10(1):16. doi:10.1186/s11689-018-9234-0
- 11 4. Guggino WB, Cebotaru L. Adeno-Associated Virus (AAV) gene therapy for cystic fibrosis:
12 current barriers and recent developments. *Expert Opin Biol Ther.* Oct 2017;17(10):1265-1273.
13 doi:10.1080/14712598.2017.1347630
- 14 5. Perrin GQ, Herzog RW, Markusic DM. Update on clinical gene therapy for hemophilia.
15 *Blood.* Jan 31 2019;133(5):407-414. doi:10.1182/blood-2018-07-820720
- 16 6. Wang D, Tai PWL, Gao G. Adeno-associated virus vector as a platform for gene therapy
17 delivery. *Nat Rev Drug Discov.* May 2019;18(5):358-378. doi:10.1038/s41573-019-0012-9
- 18 7. Kuzmin DA, Shutova MV, Johnston NR, et al. The clinical landscape for AAV gene
19 therapies. *Nat Rev Drug Discov.* Mar 2021;20(3):173-174. doi:10.1038/d41573-021-00017-7
- 20 8. Russell S, Bennett J, Wellman JA, et al. Efficacy and safety of voretigene neparvovec
21 (AAV2-hRPE65v2) in patients with RPE65-mediated inherited retinal dystrophy: a randomised,
22 controlled, open-label, phase 3 trial. *Lancet.* Aug 26 2017;390(10097):849-860.
23 doi:10.1016/S0140-6736(17)31868-8
- 24 9. Weber T. Anti-AAV Antibodies in AAV Gene Therapy: Current Challenges and Possible
25 Solutions. *Front Immunol.* 2021;12:658399. doi:10.3389/fimmu.2021.658399
- 26 10. Meliani A, Leborgne C, Triffault S, Jeanson-Leh L, Veron P, Mingozi F. Determination of
27 anti-adeno-associated virus vector neutralizing antibody titer with an in vitro reporter system.
28 *Hum Gene Ther Methods.* Apr 2015;26(2):45-53. doi:10.1089/hgtb.2015.037
- 29 11. Falese L, Sandza K, Yates B, et al. Strategy to detect pre-existing immunity to AAV gene
30 therapy. *Gene Ther.* Dec 2017;24(12):768-778. doi:10.1038/gt.2017.95
- 31 12. Wang D, Zhong L, Li M, et al. Adeno-Associated Virus Neutralizing Antibodies in Large
32 Animals and Their Impact on Brain Intraparenchymal Gene Transfer. *Mol Ther Methods Clin Dev.*
33 Dec 14 2018;11:65-72. doi:10.1016/j.omtm.2018.09.003
- 34 13. Wang M, Crosby A, Hastie E, et al. Prediction of adeno-associated virus neutralizing
35 antibody activity for clinical application. *Gene Ther.* Dec 2015;22(12):984-92.
36 doi:10.1038/gt.2015.69
- 37 14. Kruzik A, Koppensteiner H, Fetahagic D, et al. Detection of Biologically Relevant Low-
38 Titer Neutralizing Antibodies Against Adeno-Associated Virus Require Sensitive In Vitro Assays.
39 *Hum Gene Ther Methods.* Apr 2019;30(2):35-43. doi:10.1089/hgtb.2018.263

- 1 15. Lehtoranta L, Villberg A, Santanen R, Ziegler T. A novel, colorimetric neutralization assay
2 for measuring antibodies to influenza viruses. *J Virol Methods*. Aug 2009;159(2):271-6.
3 doi:10.1016/j.jviromet.2009.04.015
- 4 16. Johnston PB, Grayston JT, Loosli CG. Adenovirus neutralizing antibody determination by
5 colorimetric assay. *Proc Soc Exp Biol Med*. Feb 1957;94(2):338-43. doi:10.3181/00379727-94-
6 22937
- 7 17. Xiaoli Zhu TG. *Nano-Inspired Biosensors for Protein Assay with Clinical Applications*.
8 Elsevier; 2019.
- 9 18. Arnett AL, Garikipati D, Wang Z, Tapscott S, Chamberlain JS. Immune Responses to
10 rAAV6: The Influence of Canine Parvovirus Vaccination and Neonatal Administration of Viral
11 Vector. *Front Microbiol*. 2011;2:220. doi:10.3389/fmicb.2011.00220
- 12 19. Coecke S, Balls M, Bowe G, et al. Guidance on good cell culture practice. a report of the
13 second ECVAM task force on good cell culture practice. *Altern Lab Anim*. Jun 2005;33(3):261-87.
14 doi:10.1177/026119290503300313
- 15 20. An Introduction to Working in the Hood.
- 16 21. Strober W. Trypan Blue Exclusion Test of Cell Viability. *Curr Protoc Immunol*. Nov 2
17 2015;111:A3 B 1-A3 B 3. doi:10.1002/0471142735.ima03bs111
- 18 22. Thomas CJ, Lim NR, Kedikaetswe A, et al. Evidence that the MEK/ERK but not the
19 PI3K/Akt pathway is required for protection from myocardial ischemia-reperfusion injury by
20 3',4'-dihydroxyflavonol. *Eur J Pharmacol*. Jul 5 2015;758:53-9. doi:10.1016/j.ejphar.2015.03.054
- 21 23. Barger A, Graca R, Bailey K, et al. Use of alkaline phosphatase staining to differentiate
22 canine osteosarcoma from other vimentin-positive tumors. *Vet Pathol*. Mar 2005;42(2):161-5.
23 doi:10.1354/vp.42-2-161
- 24 24. Gregorevic P, Schultz BR, Allen JM, et al. Evaluation of vascular delivery methodologies
25 to enhance rAAV6-mediated gene transfer to canine striated musculature. *Mol Ther*. Aug
26 2009;17(8):1427-33. doi:10.1038/mt.2009.116
- 27 25. Sharma A, Ghosh A, Hansen ET, Newman JM, Mohan RR. Transduction efficiency of AAV
28 2/6, 2/8 and 2/9 vectors for delivering genes in human corneal fibroblasts. *Brain Res Bull*. Feb 15
29 2010;81(2-3):273-8. doi:10.1016/j.brainresbull.2009.07.005
- 30 26. Smejkal GB, Kaul CA. Stability of nitroblue tetrazolium-based alkaline phosphatase
31 substrates. *J Histochem Cytochem*. Sep 2001;49(9):1189-90. doi:10.1177/002215540104900914
- 32 27. Orłowski A, Katz MG, Gubara SM, Fagnoli AS, Fish KM, Weber T. Successful Transduction
33 with AAV Vectors after Selective Depletion of Anti-AAV Antibodies by Immunoabsorption. *Mol*
34 *Ther Methods Clin Dev*. Mar 13 2020;16:192-203. doi:10.1016/j.omtm.2020.01.004
- 35 28. Entrican G, Wattedgedera SR, Griffiths DJ. Exploiting ovine immunology to improve the
36 relevance of biomedical models. *Mol Immunol*. Jul 2015;66(1):68-77.
37 doi:10.1016/j.molimm.2014.09.002
- 38 29. Walters EM, Prather RS. Advancing swine models for human health and diseases. *Mo*
39 *Med*. May-Jun 2013;110(3):212-5.

- 1 30. Rapti K, Louis-Jeune V, Kohlbrenner E, et al. Neutralizing antibodies against AAV
2 serotypes 1, 2, 6, and 9 in sera of commonly used animal models. *Mol Ther.* Jan 2012;20(1):73-
3 83. doi:10.1038/mt.2011.177
- 4 31. Tellez J, Van Vliet K, Tseng YS, et al. Characterization of naturally-occurring humoral
5 immunity to AAV in sheep. *PLoS One.* 2013;8(9):e75142. doi:10.1371/journal.pone.0075142
- 6 32. Gupta S, Devanarayan V, Finco D, et al. Recommendations for the validation of cell-
7 based assays used for the detection of neutralizing antibody immune responses elicited against
8 biological therapeutics. *J Pharm Biomed Anal.* Jul 15 2011;55(5):878-88.
9 doi:10.1016/j.jpba.2011.03.038
- 10 33. Gupta S, Indelicato SR, Jethwa V, et al. Recommendations for the design, optimization,
11 and qualification of cell-based assays used for the detection of neutralizing antibody responses
12 elicited to biological therapeutics. *J Immunol Methods.* Apr 10 2007;321(1-2):1-18.
13 doi:10.1016/j.jim.2006.12.004
- 14 34. Shankar G, Devanarayan V, Amaravadi L, et al. Recommendations for the validation of
15 immunoassays used for detection of host antibodies against biotechnology products. *J Pharm*
16 *Biomed Anal.* Dec 15 2008;48(5):1267-81. doi:10.1016/j.jpba.2008.09.020
- 17 35. Immunogenicity Testing of Therapeutic Protein Products — Developing and Validating
18 Assays for Anti-Drug Antibody Detection (U.S. Department of Health and Human Services Food
19 and Drug Administration) (2019).

20

21

22

23

24

25

26

27

28

29

30

31

32

33

34

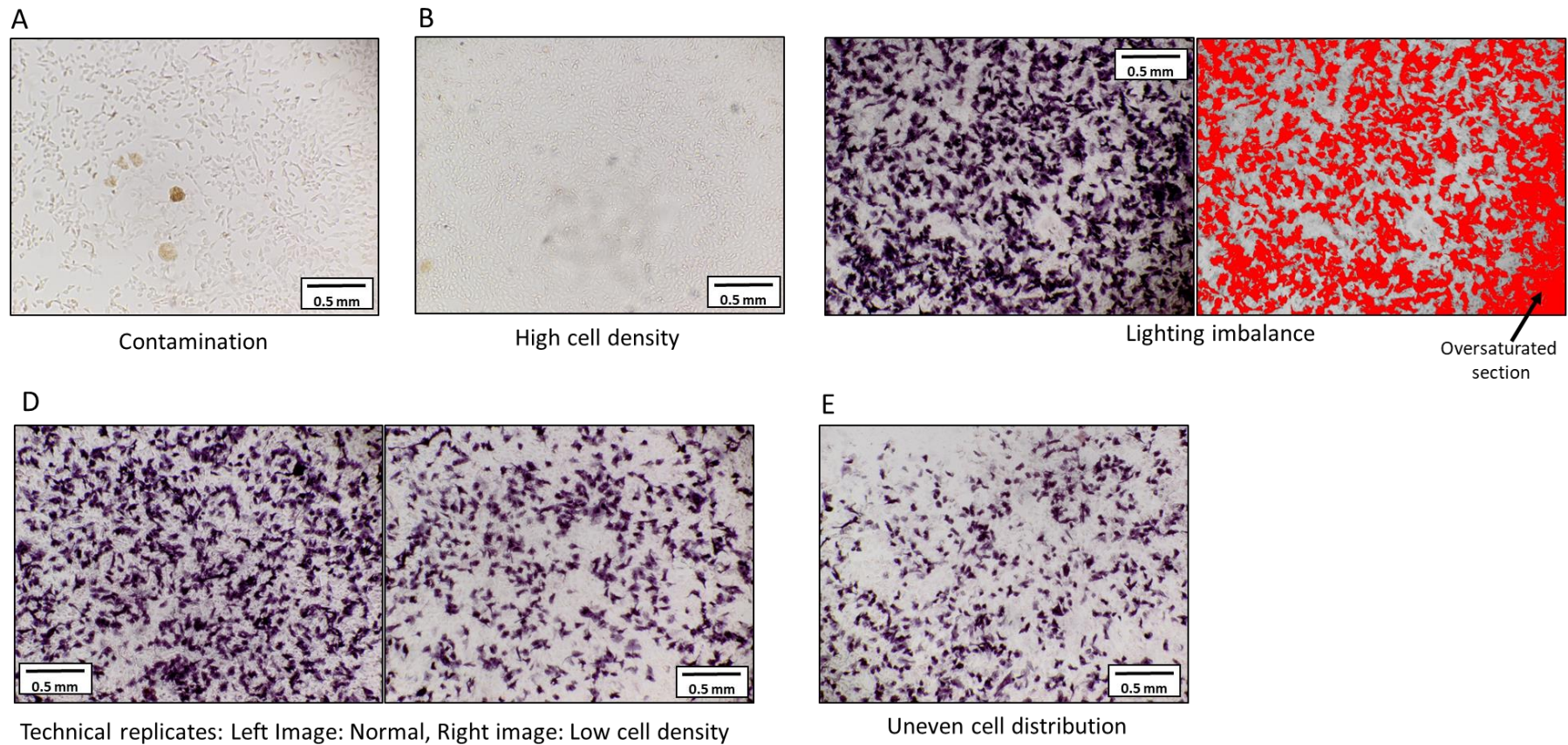
35

36

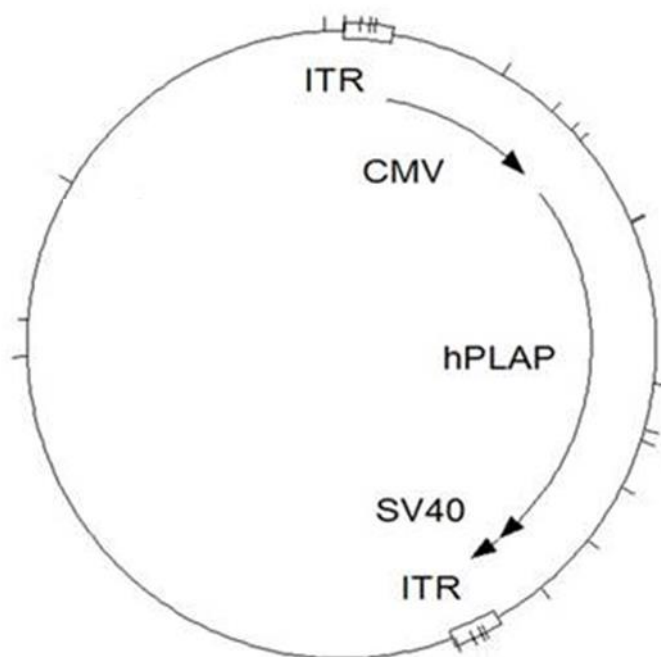
37

38

Supplementary Data



Supplementary Figure 1: Visual examples of different reasons for excluding sample wells. **A)** The presence of contamination as can be seen by clumps of in the centre. **B)** High cell density. **C)** Uneven lighting of well (left image), corresponding thresholding of the same well displaying excess coverage in bottom right corner (right image). **D)** Technical replicate images, image on left representing results with normal cell density, image on right reflecting results with low cell density. **E)** Cells unevenly distributed across a well.



Supplementary Figure 2: Simplified plasmid map displaying hPLAP insert. CMV: Cytomegalovirus promoter. hPLAP: human placental alkaline phosphatase. SV40: Simian virus 40 polyadenylation signal. ITR: Inverted terminal repeat sequences.

Supplementary Table 1: Comprehensive list of materials, equipment and software required to set up and perform this assay

Name of Material/ Equipment	Company	Catalog Number	Comments/Description
0.05% Trypsin/EDTA	Gibco	25300-054	
50 mL conical centrifuge tube	Falcon	14-432-22	Or equivalent
75cm ² square flasks	Falcon	353136	Or equivalent
96 well flat bottomed plate	Falcon	353072	
Aluminium foil			
Anti-AAV6 (intact particle) mouse monoclonal antibody, (ADK6)	PROGEN	610159	Positive control monoclonal antibody
AAV6-CMV-hPLAP Vector			Muscle Research & Therapeutics Lab (University of Melbourne, Australia) AAV6-CMV-hPLAP can be provided upon request.

BCIP/NBT	SIGMAFAST	B5655	
Cell and tissue culture safety cabinet			
Fetal Bovine Serum	Gibco	10099-141	
Haemocytometer			
High glucose Dulbecco's Modified Eagle Medium (DMEM)	Gibco	11965118	
HT1080 cells	ATCC		
ImageJ Software			Freely available: https://imagej.nih.gov/ij/index.html
Incubator			37°C, 5% CO ₂
Light microscope with camera			Capable of taking photos with a 4x objective lens
Oven			For a 65°C incubation
Paraformaldehyde	MERCK	30525-89-4	
Penicillin Streptomycin	Gibco	15140-122	
Phosphate buffered saline			
Electronic Pipette			5 & 10ml stripette inserts
Pipettes and tips			20 µL, 200 µL & 1 mL single pipettes and tips & 200 µL multichannel pipette
Stericup quick release filter	Millipore	S2GPU10RE	Used for combining media reagents
Trypan blue solution	Sigma-Aldrich	T8154	
VACUETTE TUBE 8 ml CAT Serum Separator Clot Activator	Greiner BIO-ONE	455071	Used for serum collection & processing from sheep
Water bath			

Chapter 4

Generation of an AAV encoding a truncated-PI3K with enhanced cardiac expression capabilities for use in the mouse and sheep heart

Chapter 4. Preface

The fourth chapter of this thesis, *Generation of an AAV encoding a truncated-PI3K with enhanced cardiac expression capabilities for use in the mouse and sheep heart* forms the primary translational component of this thesis. In this chapter, some of the limitations of AAV gene therapy are addressed and optimisations are developed to improve some of the short fallings. A cardiac specific promoter and an enhancer element aimed at improving cardiac specificity and expression of AAV transgenes respectively are trialled. Having demonstrated the safety and cardioprotective capabilities of PI3K in chapter two, we trial AAV-mediated PI3K-based gene therapies using a truncated PI3K transgene in healthy mice and sheep as well as in a mouse model of cardiac injury.

Chapter 4.

Generation of an AAV encoding a truncated-PI3K with enhanced cardiac expression capabilities for use in the mouse and sheep heart

This chapter has been written up as a complete manuscript by S Bass-Stringer, CJ Thomas, CN May, H Qian, P Gregorevic, A Brown, H Kiriazis, BC Bernardo, DG Donner, KL Weeks and JR McMullen. This work was delayed due to the COVID pandemic and will be submitted after some minor additional experiments.

As first author, S Bass-Stringer contributed ~70% to this manuscript. This included contributions to the experiments, analyses, drafting, design and editing.

Generation of an AAV encoding a truncated-PI3K with enhanced cardiac expression capabilities for use in the mouse and sheep heart

Sebastian Bass-Stringer^{a,b}, Colleen J. Thomas^{b,c}, Clive N. May^c, Hongwei Qian^d, Paul Gregorevic^d, Aascha Brown^a, Helen Kiriazis^{a,g}, Bianca C. Bernardo^{a,e,h}, Daniel G. Donner^{a,g}, Kate L. Weeks^{a,e,g} and Julie R. McMullen^{a,e,b,f,g}.

^a Baker Heart and Diabetes Institute, Melbourne, Vic, Australia

^b Department of Physiology, Anatomy and Microbiology, La Trobe University, Melbourne, Vic, Australia

^c Florey Institute of Neuroscience and Mental Health, University of Melbourne, Melbourne, Vic, Australia

^d Department of Physiology, Centre for Muscle Research (CMR), The University of Melbourne, Melbourne, Vic, Australia

^e Department of Diabetes, Central Clinical School, Monash University, Melbourne, Vic, Australia

^f Department of Physiology and Department of Medicine Alfred Hospital, Monash University, Melbourne, Vic, Australia

^g Baker Department of Cardiometabolic Health, The University of Melbourne, Melbourne, Vic, Australia

^h Department of Paediatrics, University of Melbourne, VIC, 3010, Australia.

Correspondence

1. Prof Julie R McMullen

Baker Heart and Diabetes Institute

Melbourne VIC, Australia

Email: julie.mcmullen@baker.edu.au

2. Dr Kate L. Weeks

Baker Heart and Diabetes Institute

Melbourne VIC, Australia

Email: kate.weeks@baker.edu.au

Abstract

Introduction: Phosphoinositide 3-kinase (PI3K, p110 α) is a master regulator of exercise-induced heart growth and protection. Transgenic mice with increased cardiac PI3K activity due to a constitutively active PI3K (caPI3K) transgene develop physiological hypertrophy and are protected following cardiac insults. The aim of this study was to develop and characterise novel PI3K-based gene therapies for the failing heart.

Methods: We generated PI3K-based adeno-associated virus (AAV6) gene therapies, with differing enhancers, promoters and transgene components. Healthy adult male C57Bl/6 mice were administered PI3K-based gene therapy candidates or saline. Therapeutic efficacy, transduction efficiency and cardiac-specificity were assessed through molecular analyses. The most promising AAV construct was administered to a mouse model with established cardiac dysfunction due to myocardial ischemia/reperfusion injury (I/R: 1hr ischemia with reperfusion, n=15-18/group); AAV delivered 24h post-I/R. Morphological, molecular and histological analyses were performed on mouse hearts 12 weeks post-AAV. Direct cardiac injections of PI3K-based AAV gene therapies were performed in healthy sheep to assess cardiac transduction in a large animal model (n=3).

Results: A cardiac troponin T (cTnT) promoter together with a small segment of PI3K (iSH2) provided efficient cardiac-selective transduction in the mouse heart, with no off-target effects. The inclusion of an enhancer component (IVS2) increased transduction of the AAV in the mouse and sheep heart. The truncated PI3K transgene (iSH2) was significantly easier to manufacture than an AAV with caPI3K, and could activate PI3K signalling. In healthy mice, the AAV6-cTnT-IVS-iSH2 construct generated cardiac PI3K activity in the heart. I/R hearts treated with AAV6-cTnT-IVS-iSH2 displayed increased phosphorylation of Akt compared to saline treated mice at 3 months (n=8-14/group, P=0.03), but no significant change in cardiac function or cardiac structure was observed between groups. iSH2 effectively transduced healthy sheep hearts and generated PI3K activity.

Conclusion: This study describes the development of a novel PI3K-based AAV that successfully transduced the healthy and failing mouse heart and healthy sheep heart, and enhanced protective Akt signalling.

Introduction

Heart failure (HF) is a debilitating condition, which directly contributes to lower quality of life and increased mortality and morbidity on a global scale. As life expectancy increases, so too does the burden on the heart and in turn the prevalence of HF and other life-threatening cardiac conditions. Five-year survival rates following a diagnosis of HF have been reported at less than 50%¹, demonstrating the urgent need for the development of novel therapeutics.

The importance of exercise as both a preventative measure and a treatment for HF has been well established and physical inactivity has been shown to be a primary risk factor in the development of HF²⁻⁴. A large body of evidence also demonstrates that following a diagnosis of HF, the use of physical activity as a therapeutic intervention can improve outcomes such as reversing cardiac remodelling, reducing mortality, and hospitalisation, and improving quality of life⁵⁻⁹. Unfortunately, due to the debilitating nature of HF, exercise therapy is not always an option. This is especially so in the later stages of the disease when the physiological impact of decreased cardiac function is greatest. Exercise compliance can also be low in patients with HF. While no therapeutic intervention is likely to mimic all the beneficial systemic effects of exercise, the development of therapies that can mimic the benefits of exercise on the heart may provide significant benefit, particularly if this approach also allows HF patients to increase their physical activity.

Phosphoinositide 3-kinase (PI3K, p110 α) is a heterodimeric lipid kinase consisting of a regulatory subunit (p85) and a catalytic subunit (p110 α). Activation of PI3K and subsequent downstream signalling requires interaction between the two subunits and the conversion of phosphatidylinositol 4,5-bisphosphate (PIP₂) to phosphatidylinositol (3,4,5)-trisphosphate (PIP₃). *In vitro* studies have demonstrated that a small fragment of the regulatory subunit called inter-SH2 (iSH2) alone is required for binding to the catalytic subunit p110 α and the conversion of PIP₂ to PIP₃¹⁰. Our laboratory has extensively demonstrated that PI3K is a critical mediator of exercise-induced physiological cardiac hypertrophy and cardioprotection¹¹⁻¹⁶. Exercise training induces an increase in PI3K activity in the mouse heart¹⁷, and chronic exercise training is associated with physiological/adaptive cardiac hypertrophy in animal models¹⁸. Furthermore, transgenic mice with increased PI3K activity due to expression of a constitutively active

form of PI3K (caPI3K) display physiological heart growth irrespective of exercise status, and display cardioprotection following a variety of cardiac insults^{14-16, 19}.

We previously reported improved cardiac function in a mouse model of pressure overload following administration of an AAV containing the same caPI3K construct used to generate the caPI3K transgenic mice, and attenuation of cardiac dysfunction in models of diabetes^{16, 20 21}. These findings demonstrated the potential to replicate some of the benefits of exercise through a therapeutic modality targeting a key regulator of exercise-induced hypertrophy and protection¹⁶. The development of a clinically viable AAV therapeutic product requires optimisation to address factors such as cardiac specificity, vector transduction capacity and the cost of drug development. A disadvantage of the original caPI3K-AAV was that expression was driven by a promoter (cytomegalovirus, CMV) that was not cardiac-specific, and AAV yields were low due to the large construct size (~5.15 kb; maximum AAV capacity ~5.2 kb)^{22, 23}. The aims of the current study were to: 1) generate a smaller truncated PI3K construct to circumvent the limited packaging capacity of AAV and the significant consequential costs of development, 2) improve the cardiac specificity and transduction capacity of the AAV through the use of a cardiac-specific cardiac troponin T promoter (cTnT) and enhancer elements, 3) develop an AAV construct which could provide robust transgene expression to the heart of a large animal model, and 4) assess the efficacy of the new truncated PI3K AAV in a clinically relevant mouse model of HF.

Methods

Generation of AAVs

Expression cassettes consisting of a promoter (CMV or cTnT), an enhancer element Intervening Sequence 2 (IVS2)²⁴, caPI3K (iSH2p110) or iSH2 and a synthetic polyadenylation sequence (SpA) were cloned into a plasmid containing inverted terminal repeat (ITR) regions from AAV2²⁵ (see Figure 1). The CMV promoter, IVS2, caPI3K, iSH2 and SpA have been described elsewhere (^{10, 16, 24}). The truncated cTnT promoter consisted of 477 nucleotides from the promoter region of human *TNNT2* (gcggccgcctcgagtctgctcccagctggcctcccaggcctgggttctggcctctgctttatcaggattctcaagagggacagctggtttatgttgcatgactgttcctgcatatctgctctggttttaaatagcttatctgctagcctgctcccagctggcctcccaggcctgggttctggcctctgctttatcaggattctcaagaggacagctggtttatgttgcatgactgttcctgcatatctgctctggtt

ttaaatagcttatctgagcagctggaggaccacatgggcttatatggggcacctgccaataatagcagccaacacccccccctgtcgcacattcctcctggctcaccaggccccagccccacatgcctgcttaagccctctccatcctctgcctcaccagctccccgctgagactgagcagacgcctccaggatctgtcggcagctaattaat). Recombinant AAV6 vectors were produced by co-transfecting HEK293T cells with the corresponding plasmids and pDGM6²⁵, a plasmid encoding AAV capsid proteins and adenoviral genes required for the packaging and production of functional AAV6 vectors. Purified AAV vectors were titered by qPCR using primers to detect either the cTnT⁴⁷⁷ (Forward: CATGACTGTTCCCTGCATATC, reverse: TAAACCAGCTGTCCCTCTT) or CMV (Forward: GCGGTAGGCGTGTACGGTGG, reverse: CGTGGATGGCGTCTCCAGGC) promoters. AAVs were generated by Associate Professor Paul Gregorevic at the Muscle Research and Therapeutics Laboratory at the University of Melbourne.

An AAV6 containing a caPI3K construct with a CMV promoter was produced (AAV6-CMV-caPI3K), as previously described¹⁶. Here, we generated five new PI3K-based AAV constructs with the goal of attaining cardiac specificity and increasing transgene expression.

Construct 1) AAV6-cTnT-caPI3K: The ubiquitous CMV promoter within AAV6-CMV-caPI3K was replaced with the cTnT⁴⁷⁷ promoter. Replacing the CMV promoter with the cTnT⁴⁷⁷ promoter would reduce the construct size from ~5.15 kb to ~4.97 kb and improve cardiac specificity (Figure 1A).

Constructs 2 & 3) AAV6-CMV-iSH2 & AAV6-cTnT-iSH2: iSH2, a fragment of the PI3K regulatory subunit p85 that interacts with the p110 α catalytic subunit and is sufficient for its activation¹⁰ was derived from the *Mus musculus* sequence for *Pik3r1* (encoding p85alpha), synthesised by Genscript and subcloned into the AAV plasmids containing either the CMV or cTnT⁴⁷⁷ promoters. iSH2 is significantly smaller at only ~0.75 kb compared to the original ~3.9 kb caPI3K transgene (Figure 1B).

Constructs 4 & 5) AAV6-CMV-IVS2-iSH2 & AAV-cTnT-IVS2-iSH2: Identical to constructs 2 & 3, respectively, but with the addition of an enhancer element IVS2. IVS2 is rabbit β -globin intron 2 and has been demonstrated to improve transgene expression²⁶. The size of IVS2 + iSH2 combined is only ~1.32 kb compared to the ~3.9 kb caPI3K transgene (Figure 1C).

Further details and sequences of all constructs are provided within the data supplement.

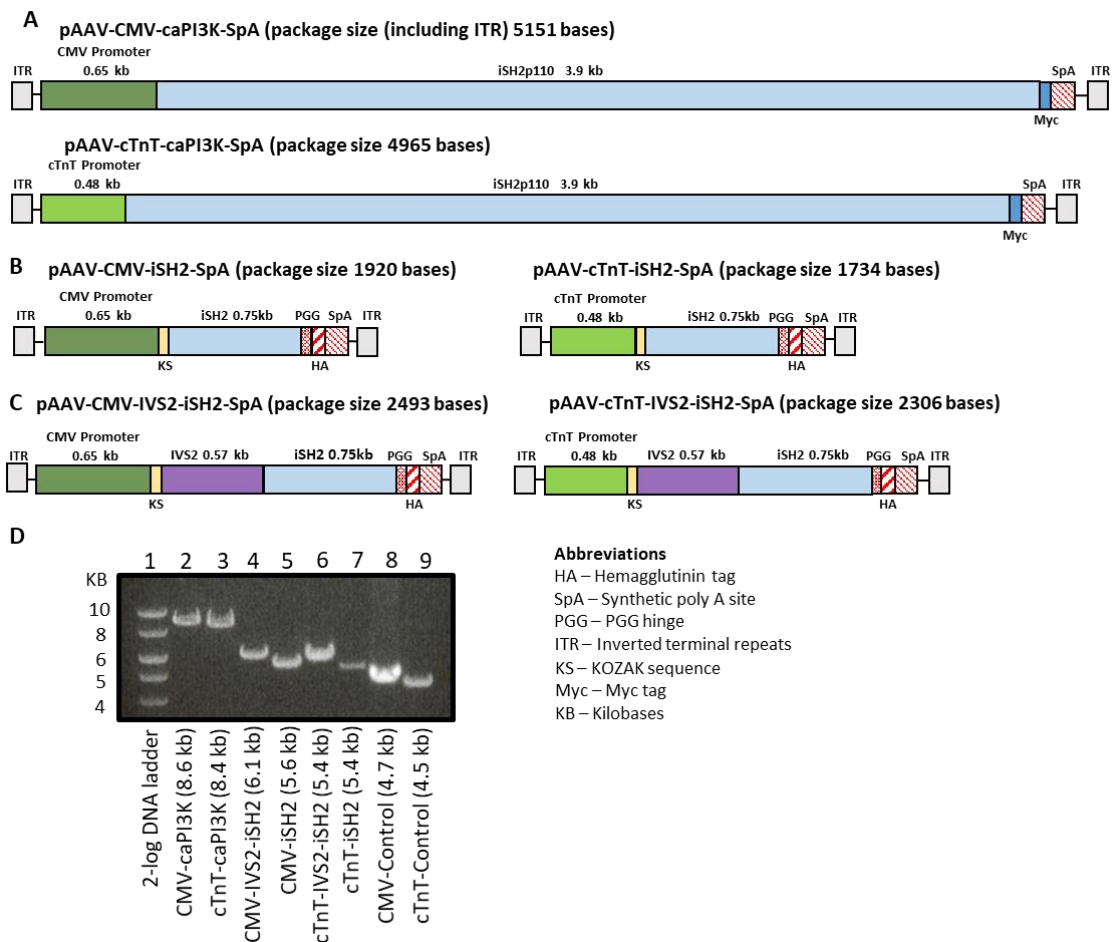


Figure 1. New PI3K-based constructs. A) AAV constructs encoding full length constitutively activated PI3K (iSH2p110), driven by the CMV promoter (upper) or cTnT promoter (lower). B) Truncated PI3K constructs encoding the iSH2 fragment of p85, driven by either the CMV promoter (left) or cTnT promoter (right). C) Truncated PI3K constructs encoding the iSH2 fragment of p85 together with the intron IVS2, driven by either the CMV promoter (left) or cTnT promoter (right). D) Gel electrophoresis image of linearised plasmids containing the PI3K-based constructs or empty control constructs that were inserted into AAV6 vectors.

Colony screening to confirm generation of new PI3K constructs

The new constructs described above were generated by Genscript. iSH2 and IVS2-iSH2 sequences were synthesised by Genscript and subcloned into pAAV6-CMV-MCS-SpA¹⁶ or pAAV6-cTnT⁴⁷⁷-MCS-SpA. Plasmid DNA for each construct was combined with DH5- α cells and incubated on ice for 30 minutes, followed by heat shock at 42°C for 50 seconds and incubation on ice for an additional 2 minutes. Cell/plasmid mixture was made up to 1 mL with pre-warmed Luria-Bertani (LB) broth shaken for 1 hour (37°C, 225 RPM). Cells were spun down (4500 RPM, 2 min), the supernatant was removed (800 μ L) and following resuspension, the cells were incubated overnight on a LB agar plate. The following day, four individual colonies were scraped on to four corners of a new LB agar plate and incubated an additional six hours (37°C). A colony was scraped from each

corner of the new LB agar plate, added to 4 ml of LB broth with 1% ampicillin, and shaken overnight (37°C, 225 RPM). The following day 1 mL from the tubes were spun down and plasmid DNA was purified using the QIAGEN miniprep kit (standard protocol 3.B, 3.C & centrifugation protocol). Clone Manager software (version 5, Sci Ed Software) was used to determine and select *HindIII* as the single cut restriction enzyme and *MscI* as the double cut restriction enzyme for each construct. Master mixes of each enzyme (15 µL each) were made for all four colonies (as well as +/- controls) and mixed with 5 µL of DNA that was previously purified using the miniprep kit (2 uL of original plasmid for a positive control) and incubated for 2 hours at 37°C. Samples were subsequently run on a 0.7% agarose gel at 100 V for 45 minutes using a 2-log ladder. All constructs were the correct size and were unchanged following transformation relative to the original plasmid DNA ordered from Genscript.

Animal care and experimentation

Mice care and experimental protocols were approved by the Alfred Research Alliance Animal Ethics Committee (application number E/1964/2019/B & E/1797/2018/B) and performed in accordance with the Australian Code for the Care and Use of Animals for Scientific Purposes (National Health and Medical Research Council of Australia, 8th edition, 2013). rAAV6 vectors were systemically administered via tail vein injection (29G needle, 150 uL) to conscious male wild type C57BL/6 mice generated at the People And Cures (PAC) facility through the Alfred Research Alliance (Melbourne, Victoria, Australia).

All aspects of sheep animal care and experimentation were conducted in accordance with Florey Institute of Neuroscience and Mental Health guidelines and the Australian Code for the Care and Use of Animals for Scientific Purposes (National Health and Medical Research Council of Australia, 8th edition, 2013). Application number 15-086-FINMH.

Experimental protocols

1. Assessment of cardiac transduction and PI3K signalling with iSH2 +/- IVS2:

Following randomisation and blinding, 8-week-old male C57Bl/6 mice were administered 2×10^{11} , 1×10^{12} or 2×10^{12} vector genomes (vg) of AAV6-CMV-iSH2 or AAV6-CMV-IVS2-iSH2. Additionally, 2×10^{11} vg of an empty control vector (AAV6-CMV-Con) or

saline were administered as controls. Mice were euthanased 8 weeks post-AAV administration.

2. Assessment of cardiac specificity and expression driven by the cTnT⁴⁷⁷ promoter versus CMV promoter: Following randomisation and blinding, 8-week-old male C57Bl/6 mice were administered 2×10^{11} , 1×10^{12} or 2×10^{12} vg AAV6-cTnT-caPI3K or 2×10^{11} vg of AAV6-CMV-caPI3K. 2×10^{11} vg of a control vector (AAV6-CMV-Con) or saline were administered as controls. Mice were euthanased 8 weeks post-AAV administration.

3. Assessment of AAV6-cTnT-IVS2-iSH2 in healthy adult mice: Following randomisation and blinding, 8-week-old male C57Bl/6 mice were administered 2×10^{12} vg AAV6-cTnT-IVS2-iSH2 or saline. Mice were euthanased 8 weeks post-AAV administration.

4. Assessment of AAV6-cTnT-IVS2-iSH2 in a mouse model of ischemia/reperfusion injury: Ten-week old male C57Bl/6 mice underwent baseline echocardiography prior to cardiac-ischemic reperfusion (I/R) surgery (ligation of the left coronary artery for one hour followed by reperfusion) as previously described²⁷. Immediately after myocardial I/R surgery was performed, a three-lead ECG recording of each mouse was used to confirm ST-segment elevation (and successful ligation). At 24 h post-surgery, mice were anaesthetised with isoflurane (induction: 3-4.5% in room air, maintenance: 1-2% in room air) and placed on a heated and articulated ECG platform. Gated (ECG) and ungated parasternal long-axis cine loops were obtained by an ultra-high frequency ultrasound probe (MS-550D) using the Vevo® 2100 System (Visualsonics, Fujifilm, Canada). Analysis was performed using the manufacturer's VevoLAB software to discern inactive from active relative radial tissue displacement in the long axis. Inactive/zero relative tissue displacement provides a rigorous surrogate for ischemic area/infarct size and is used to exclude mice with small/irregular infarctions (resulting from e.g. missed ligation or collateral branching of the coronary arteries). Only mice with tissue displacement 45 ± 10 % of the left ventricle were included in the study (N=5 excluded)²⁸. Following randomisation and blinding, mice were subsequently administered 2×10^{12} vg AAV6-cTnT-IVS2-iSH2, AAV6-cTnT-Control or saline. Mice underwent echocardiography followed by pressure-volume (PV) loop analysis and euthanasia 12-weeks post-surgery.

Echocardiographic assessment of left ventricular structure and function

M-mode echocardiography was performed using a 40 MHz linear array transducer (Vevo 2100® Ultrasound Machine, VisualSonics, Fujifilm, Canada) and analysis was performed using the manufacturer's VevoLAB software for assessment of systolic cardiac function. Mice were anaesthetised with isoflurane (3.8% induction, 1.7% maintenance). Fractional shortening and left ventricle (LV) volumes were calculated as follows: Fractional shortening: $[(LVEDD - LVESD)/LVEDD] \times 100\%$, LV volume diastole (μL): $[(7/(2.4+LVID;d)) \times LVID;d^3]$, LV volume systole (μL): $[(7/(2.4+LVID;s)) \times LVID;s^3]$. Image acquisition and data analyses were performed blinded.

Pressure-volume loop analysis

Mice were anaesthetised with isoflurane (4 % induction, 1.6-1.8 % maintenance) and placed in a supine position. An incision was made in the neck, and a Millar pressure-volume catheter (model SPR-839) was inserted into the right common carotid artery and advanced until the tip was just above the aortic valve. Steady-state blood pressure measurements were made, then the transducer was guided through to the LV to measure LV pressure and volume parameters. To determine end-systolic and end-diastolic PV relationships, the abdominal vena cava was occluded by gently pressing a cotton tip through the abdomen for 7-10 heart beats. Parallel conductance was corrected for by bolus I.V. infusion of 20 % w/v hypertonic saline (via the jugular vein). Alpha-calibration of the volume trace was performed by software adjustments for endpoint echocardiographic measures (cardiac output) for each animal.

Tissue dissection and morphological analysis

Healthy adult mice: Animals were anaesthetised (pentobarbitone, 80 mg/kg i.p.) and euthanased by cervical dislocation. The atria were removed from the heart; the ventricles dissected (for protein extraction) and snap frozen in liquid nitrogen.

Mice subjected to I/R injury: Prior to dissection, mice were anaesthetised with isoflurane as described above, and PV loop measurements were performed followed by euthanasia through cardiac puncture followed by cervical dislocation. Hearts were removed, weighed and the apex and base were snap frozen in liquid nitrogen. The middle-ventricle was used for histology.

For all cohorts of mice, heart, atria, lungs, gastrocnemius muscle, kidney, brain, liver and spleen were weighed and snap frozen for tissue analyses. Lower limbs were collected,

digested (1 M NaOH for 6 h, 37°C) and tibia measured with a Vernier calliper to determine tibia length (TL).

Histological analysis

From the I/R cohort, thinly sliced transverse/short axis rings (1-2 mm) were dissected from the LV of each mouse heart inferior to the ligation, and placed into cassettes for fixation in 10% Neutral Buffered Formalin (NBF) for 24 hours. All subsequent tissue processing and acquisition of images were performed by the Monash Histology Platform (Clayton, VIC Australia). Tissue was processed, paraffin embedded and sectioned at a thickness of 4 µm and stained with Masson's Trichrome to measure interstitial fibrosis. Images were acquired by bright field scanning using a 20x objective. The ImageJ package Fiji incorporating a simple macro was used to perform colour deconvolution and objective measurement of area positivity for collagen staining (fibrosis, blue) as a percentage of total tissue (blue and red) area. Separate 4 µm sections underwent immunohistochemistry staining with antibodies (and fluorophores) for: Troponin-T 1:200 (BD Biosciences 564766), CD68 1:1000 (Abcam ab125212) & DAPI (Thermofisher). Immunofluorescent images were then acquired by darkfield scanning using 20x objective. The ImageJ package Fiji with a separate macro that performed cellular watershedding (i.e., cellular boundary determination between adjacent DAPI-stained nuclei) and objective measurement of CD68+ and CD68- cells was used to determine the percentage of CD68+ cells, a marker of macrophages. All analyses were performed blinded.

Western blotting analysis

Protein extraction and quantitation was performed as previously described²⁹. Protein lysates from cardiac tissue containing 75-100 µg of protein were separated by SDS-PAGE. Protein was immobilised on a polyvinylidene difluoride (PVDF) membrane (MERCK, Frankfurt, Germany) using a wet tank transfer for 16 hours, 9 volts, 4°C. Membranes were subsequently blocked in 5% skim milk powder in Tris-buffered saline and 0.1% Tween 20 (TBST). Membranes were probed with the following antibodies: HA-tag (C29F4) (Cell Signalling #3724, 1:2000), α-tubulin (Cell Signaling #2144, 1:5000) p-Akt (Ser473) (Cell Signaling #9271, 1:500) and Akt (Cell Signaling #9272, 1:1000). Membranes were incubated with anti-rabbit antibodies conjugated to HRP. Proteins were visualised using SuperSignal® West Pico PLUS Chemiluminescent Substrate (Thermo

Scientific). Western blots were imaged using the G:BOX gel doc system (SYNGENE) and quantitation was performed using the GeneTools software (SYNGENE). All raw Western blot images are provided within the data supplement.

Immunoprecipitation & lipid kinase activity assay analysis

A lipid kinase activity assay was employed to assess PI3K activity in heart tissue as previously described³⁰. 250 µg (I/R cohort) or 500 µg (healthy mice cohorts) of protein was immunoprecipitated using a HA-tag antibody (C29F4) (Cell Signalling #3724) and Protein A Sepharose CL-4B beads (GE Healthcare, 17-0780-01) according to the manufacturer's instructions. Beads were washed twice in HEPES buffer (1 M HEPES, 40 mM EDTA, 1 M DTT and 0.015% IGEPAL) and split evenly into two separate tubes. A 1:1 ratio of phosphatidylinositol and phosphatidylserine stored in chloroform (10 µl) was evaporated into gel pellets using a SpeedVac vacuum concentrator (ThermoFisher), sonicated in 130 µl of HEPES buffer and mixed with one half of the immunoprecipitated protein attached to Sepharose beads. ATP and 10 µCi of [γ -³²P]-ATP (PerkinElmer, BLU502A250UC) were subsequently added to the Sepharose beads. A reaction was generated by shaking (1400 RPM) for 10 minutes and stopped with 2 M HCl. 160 µL of 1:1 chloroform-methanol mixture was added to extract the lipids. The organic phase was collected (phospholipids) and resolved using a thin liquid chromatography (TLC) plate (Merck, 1.05553.0001) overnight in an acid solvent consisting of 65:35 isopropanol: 2 M acetic acid. The TLC plate was dried and added to a cassette underneath autoradiography film (GE Healthcare, 28906845) at -80°C. The radiolabel signal was standardised against immunoglobulin G signals by running Western blots from the second half of the immunoprecipitate from each sample. All raw activity images are provided within the data supplement.

Direct cardiac AAV injection and dissection of healthy sheep

Sheep experimental protocols were approved by the Florey Institute for Neuroscience and Mental Health; application number 15-086-FINMH). AAV was administered to three adult ewes (~50kg) via direct cardiac injection. Briefly, sheep were anaesthetised with isoflurane, intubated and placed on artificial respiration³¹. The heart was exposed from the left lateral position, the pericardium was opened and 1-2 cm radius circles were sutured into isolated positions on the surface of the LV myocardium, above and below the second branch of the left anterior descending artery, to mark sites for direct cardiac

injection. 5×10^{12} to 1×10^{13} vg of AAV was administered via 10-15 ~20 μ l injections evenly distributed within each sutured circle directly into the myocardium on a 45° angle. The pericardium, intercostal muscle, subcutaneous tissue and skin were closed, and anaesthetic removed. Approximately 6 weeks following AAV administration sheep were euthanased, the heart was removed and myocardium tissue from the sutured sites and remote regions were snap frozen for analysis.

- Sheep #1 received 5×10^{12} vg of both AAV6-CMV-caPI3K and AAV6-cTnT-caPI3K at separate sites on the LV.
- Sheep #2 received 1×10^{13} vg of both AAV6-CMV-iSH2 and AAV6-CMV-IVS2-iSH2 at separate sites on the LV.
- Sheep #3 received 1×10^{13} vg of AAV6-CMV-iSH2, AAV6-cTnT-iSH2 & AAV6-cTnT-IVS2-iSH2 at separate sites on the LV.

Statistical analysis & exclusions

Statistical analyses were performed using Graphpad Prism version 7 (La Jolla, CA, USA). Results are presented as mean \pm SEM. Differences between groups were determined using unpaired t-tests or one-way analysis of variance (ANOVA) followed by the Tukey's posthoc test. A value of $P < 0.05$ was considered significant. Any animal or sample exclusions are described in the data supplement.

Results

Successful generation of new PI3K-AAV constructs

Restriction digests were undertaken to confirm the generation of the new PI3K-AAV constructs (Figure 1A). Figure 1D highlights the smaller sizes of the iSH2 constructs (lanes 4-7) in comparison to the original construct (AAV6-CMV-caPI3K, lane 2) and construct 1 (AAV6-cTnT-caPI3K, lane 3). The constructs (insert sequences and flanking sequences within the pAAV plasmid) were sequence verified by Genscript.

Validation and characterisation of iSH2 AAVs in the healthy mouse heart

It was previously reported that iSH2 binds to the p110 α catalytic subunit of PI3K and promotes activation of PI3K in cultured cells¹⁰. First, we wanted to 1) evaluate the transduction efficacy of the iSH2-based AAV vector with the ubiquitous CMV promoter (AAV6-CMV-iSH2, Figure 1B) in providing robust cardiac expression and activating PI3K *in vivo*, and 2) examine whether the same AAV incorporating an enhancer element (IVS2; AAV6-CMV-IVS2-iSH2, Figure 1C) could increase cardiac expression of iSH2 further. Both vectors were administered to a small group of healthy 8-week old male mice at three doses: i) 2×10^{11} vg (low dose), n=3/treatment; ii) 1×10^{12} vg (mid dose), n=3/treatment; iii) 2×10^{12} vg (high dose), n=2-3/treatment. Tissue was collected 8 weeks post-AAV administration. Cardiac expression of iSH2 (assessed by detection of the HA tag by Western blotting) was observed in all mice in a dose-dependent manner for both AAV6-CMV-iSH2 and AAV6-CMV-IVS2-iSH2 (Figure 2A). At a dose of 1×10^{12} vg the addition of IVS2 in the AAV6 construct (AAV6-CMV-IVS2-iSH2) led to a significant increase in cardiac transgene expression of greater than 3-fold in comparison to the same construct without IVS2 (AAV6-CMV-iSH2) (Figure 2A, P=0.005). Animal numbers were insufficient to perform statistical analysis at the higher dose (2×10^{12} vg) but the difference between +/- IVS2 was less apparent (Figure 2A).

Next, to determine if the iSH2 fragment was capable of binding and activating PI3K *in vivo*, we used a HA-tag antibody to immunoprecipitate iSH2 from ventricular lysates of mice that received AAV6-CMV-IVS2-iSH2. The catalytic subunit p110 α was present in immunoprecipitates from mice that received the medium (1×10^{12} vg) and high dose (2×10^{12} vg) of AAV6-CMV-IVS2-iSH2 (Figure 2B). PI3K activity assays revealed that iSH2-bound p110 α was functional, phosphorylating the lipid substrate. Subsequently, we evaluated the difference in production yield of our vectors relative to the size of the packaged inserts. The value of creating smaller functional PI3K constructs is driven by the capability of circumventing the limited packaging capacity of AAV, and because the generation of smaller constructs is economically advantageous in the development of AAV gene therapies. A 150mm plate preparation generated an average yield of 1.9×10^{11} vg of the larger 5.15kb AAV6-CMV-caPI3K vector, whereas the smaller AAV6-CMV-IVS2-iSH2 vector (2.3kb) generated an 18-fold increase in production yield (3.55×10^{12} vg per 150mm plate).

The recombinant AAV serotype 6 (AAV6) has been demonstrated to be advantageous for cardiac gene therapies due to it preferentially transducing striated muscle such as heart, skeletal muscle and diaphragm²⁵. We previously showed that cardiac muscle can be efficiently transduced using a AAV6 vector carrying a CMV promoter with a caPI3K construct¹⁶, however the CMV promoter also drove expression in skeletal muscle when a dose of 2×10^{11} vectors was administered. Since PI3K has tumorigenic properties in non-cardiac cells, we investigated whether replacement of the CMV promoter in our original AAV6 vector encoding caPI3K with a cTnT promoter (Figure 1A) would improve cardiac specificity. Here, we administered three doses of AAV6-cTnT-caPI3K to mice and observed comparable expression to the original AAV6-CMV-caPI3K vector in the heart at 2×10^{11} vg (Figure 2C). caPI3K expression was enhanced further at 1×10^{12} vg of AAV6-cTnT-caPI3K (Figure 2C). Intravenous tail vein administration of the highest dose (2×10^{12} vg) of the AAV6-cTnT-caPI3K vector led to strong expression in the heart with no evidence of expression in skeletal muscle, brain, lung, kidney, liver or spleen (Figure 2D).

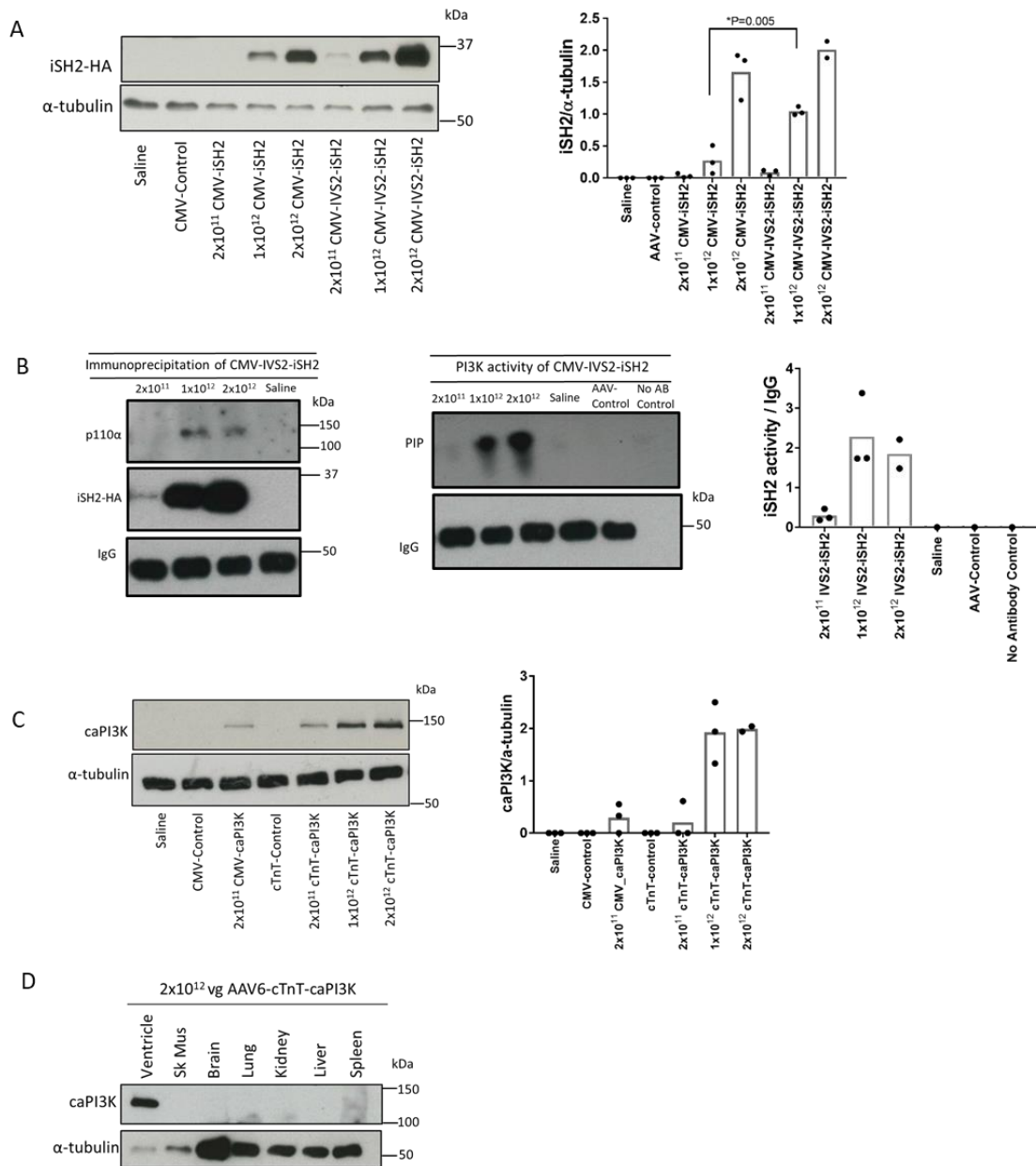


Figure 2. Validating the efficacy of iSH2, IVS2 and the cTnT⁴⁷⁷ promoter at multiple doses. A) Detection of iSH2 in cardiac tissue using an HA-tag antibody following intravenous administration of 2x10¹¹ vg, 1x10¹² vg or 2x10¹² vg of AAV6-CMV-iSH2 or AAV6-CMV-IVS2-iSH2 in healthy mice. Saline and 2x10¹¹ vg of empty AAV6-CMV-Control vector were administered as negative controls. B) Cardiac lysates from mice administered 2x10¹¹ vg, 1x10¹² vg or 2x10¹² vg of AAV6-CMV-IVS2-iSH2 or saline were immunoprecipitated using an HA-tag antibody to purify iSH2-containing complexes and the resulting Western blots probed with an anti-p110 α antibody (left panel). A lipid kinase activity assay using the iSH2-HA immunoprecipitates revealed iSH2-HA-associated PI3K activity, as reflected by the higher PIP signal (middle and right panel). C) Expression of caPI3K driven by a cTnT promoter in cardiac tissue following intravenous administration of 2x10¹¹ vg, 1x10¹² vg or 2x10¹² vg. Saline, 2x10¹¹ vg of AAV6-CMV-Control and AAV6-cTnT-Control vectors were administered as negative controls and 2x10¹¹ vg of AAV6-CMV-caPI3K was administered to compare expression of cTnT to the CMV promoter. D) Expression of caPI3K in cardiac tissue compared to non-cardiac tissues following intravenous administration of 2x10¹² vg of AAV6-cTnT-caPI3K in a healthy mouse. N=2-3 per group. Statistical analysis performed using an unpaired t-test.

AAV6-cTnT-IVS2-iSH2 did not increase heart size in healthy adult mice

Having established efficacy of the iSH2 construct, the IVS2 enhancer and the cTnT promoter, we administered AAV6-cTnT-IVS2-iSH2 at a dose of 2×10^{12} vg or saline to a small cohort of 10-week old healthy adult male C57Bl/6 mice. Heart size and weights were comparable between the AAV6-cTnT-IVS2-iSH2 and saline groups (Figure 3A and Table 1). There were also no significant differences in atria, lung, kidney, liver or spleen weights between groups (Table 1). Cardiac transduction of iSH2 was confirmed in hearts of all mice administered AAV6-cTnT-IVS2-iSH2 by Western blotting, which detected the HA tag within the AAV construct (Figure 3B). The phosphorylation of Akt relative to total Akt tended to be higher in hearts from mice receiving AAV6-cTnT-IVS2-iSH2 ($P=0.08$, Figure 3C).

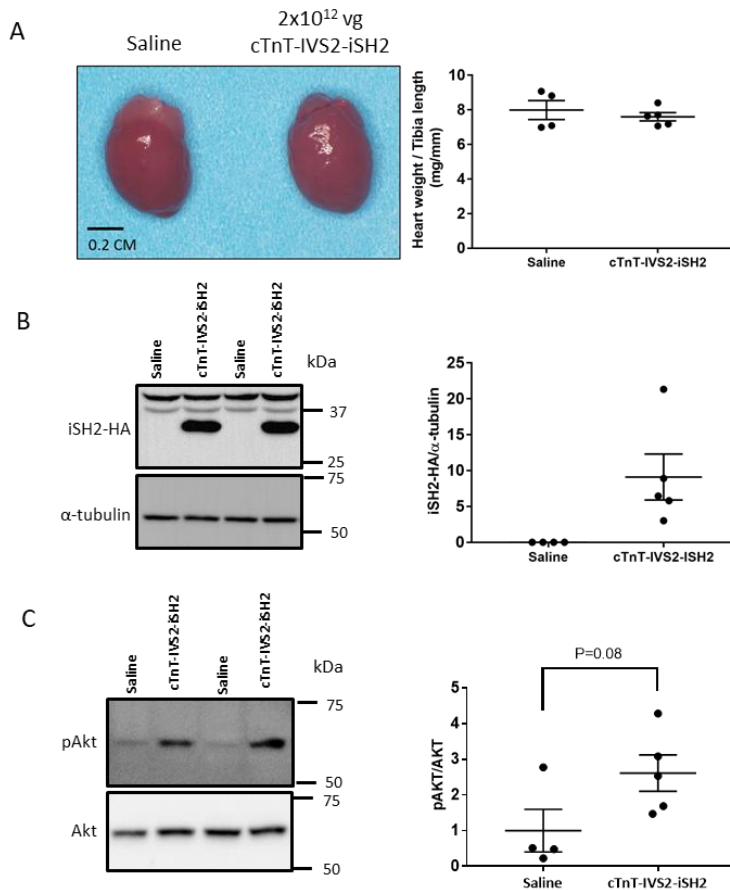


Figure 3. AAV6-cTnT-IVS2-iSH2 administration to a cohort of healthy adult mice. A) Representative hearts from control and treated groups (Left panel). Heart weight normalised to tibia length 8-weeks after administration of 2×10^{12} vg cTnT-IVS2-iSH2. B) Western blot representative images showing HA-tagged iSH2 normalised to α -tubulin. C) Phosphorylation of Akt as a ratio of total Akt from cardiac tissue. $N=4-5$ per group. Statistical analysis performed using an unpaired t-test. All data presented as mean \pm SEM.

AAV6-cTnT-IVS2-iSH2 increased the phosphorylation of Akt but did not improve systolic function following ischemia/reperfusion injury

To examine whether iSH2 could enhance PI3K signalling and improve heart function in a setting of cardiac injury, 10-week old male C57Bl/6 mice were subjected to one-hour of cardiac ischemia followed by reperfusion (I/R), and 24 h later administered AAV-cTnT-IVS2-iSH2 (2×10^{12} vg), an AAV-Control (identical AAV lacking the IVS2-iSH2 insert, 2×10^{12} vg) or saline (Figure 4A). One day post-I/R, and just prior to AAV administration, the area at risk of the heart assessed by echocardiography was comparable between groups ($45\% \pm 10\%$, Figure 4B).

Robust expression of iSH2 was observed in the myocardium of 14 of 15 I/R injury mice that received the vector, and this corresponded with iSH2-specific PI3K activity (Figure 4C & D). The one mouse with very low iSH2-HA expression was excluded from all subsequent analyses (Supp Figure 11).

Prior to assessing any effect of AAV6-cTnT-IVS2-iSH2 in the I/R model, organ weights from the saline and empty vector control group (AAV6-cTnT-control) were compared. Unexpectedly, morphological changes were identified in the AAV control group compared to the saline group, including a significant increase in spleen and kidney weights, as well as heart weight normalized to tibia length (Table 2). This finding was surprising given there were no differences in organ weights from healthy adult mice administered saline or AAV6-cTnT-IVS2-iSH2 at the same dose (Table 1). Findings in the I/R mice administered empty control vector suggest the vector led to a non-specific effect in the cardiac stress setting. Despite the increase in HW/TL in I/R mice administered AAV6-cTnT-Control, there were no significant differences in cardiac function or performance based on echocardiography and PV-loop analyses performed 12 weeks after AAV administration (Tables 3 & 4). However, given the increase in HW/TL and other organ weights in the I/R mice administered AAV-cTnT-control, the most relevant control for the AAV6-cTnT-IVS2-iSH2 I/R group is the AAV control group rather than the saline group.

There were no significant differences in heart weight or other tissue weights between the I/R mice administered AAV6-cTnT-IVS2-iSH2 or AAV6-cTnT-control (Figure 4E, Table 5). There were also no significant differences in cardiac function based on echocardiography parameters such as ejection fraction between groups (Figure 4F, Table 6). Performance measures from PV-loop analyses, including stroke work, were largely

unchanged (Figure 4G, Table 7) but there was a significant decrease in end-systolic pressure volume relationship (ESPVR) between the AAV-iSH2 and AAV-Control groups (Table 7).

Macrophage infiltration and fibrotic deposition play a key role in tissue repair following cardiac ischemia. Masson's trichrome staining performed on mid-ventricle rings revealed no differences in the amount of fibrotic tissue between groups (Figure 5A). The percentage of CD68-positive cells, which detects monocytes and macrophages, was also not significantly different between groups (Figure 5B).

Given there was no functional or histological improvement identified in I/R mice receiving AAV6-cTnT-IVS2-iSH2, we undertook Western blot analysis to assess whether pAkt which is known to mediate cardiac protection was elevated. Western blotting from non-infarcted ventricular tissue revealed an increase in the phosphorylation of Akt relative to total Akt in I/R mice administered AAV6-cTnT-IVS2-iSH2 versus saline, and a similar trend was identified in comparison to AAV-cTnT-control (Figure 5C).

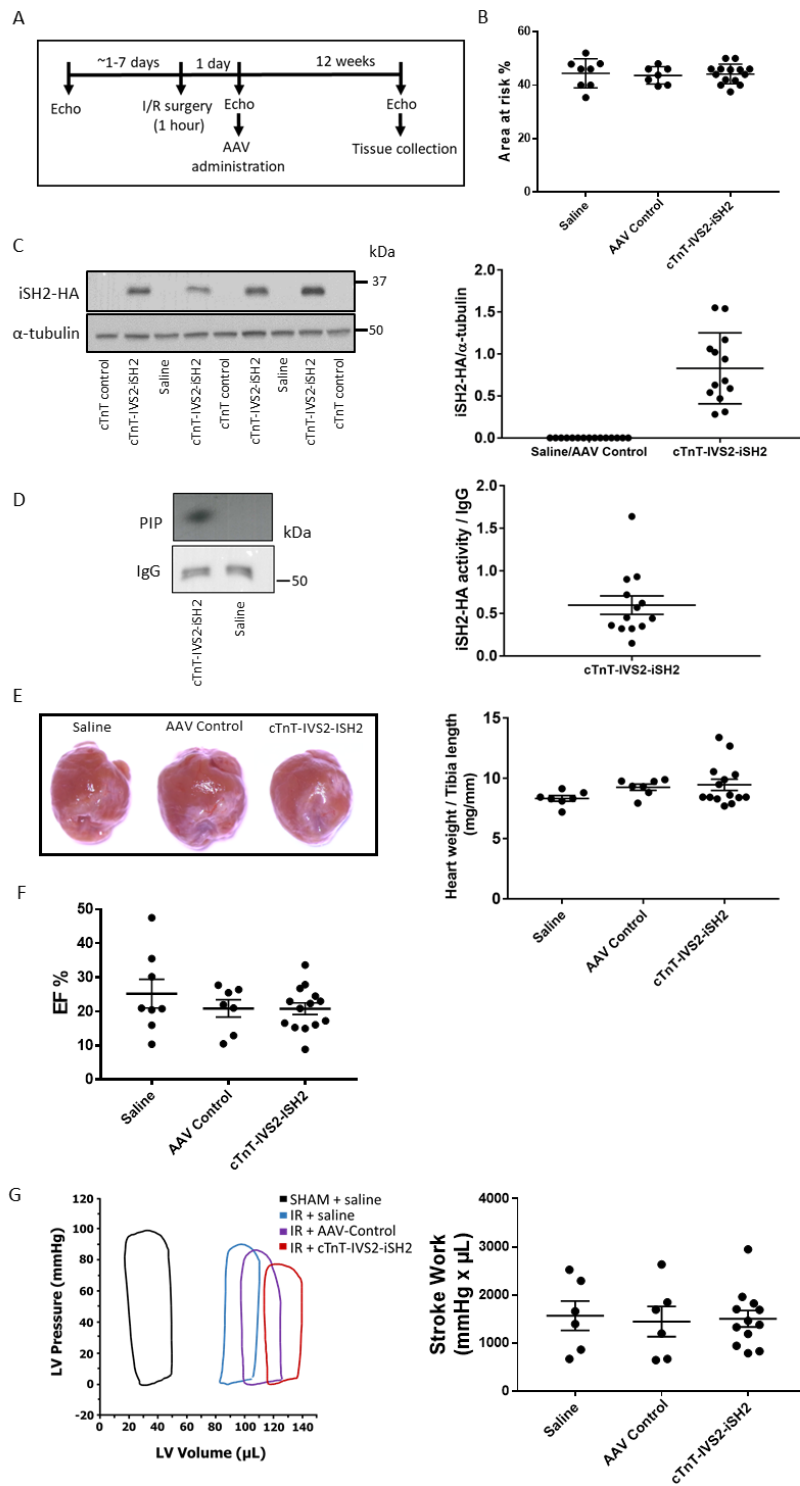


Figure 4. Administration of AAV6-cTNT-IVS2-iSH2, saline or AAV6-cTnT-Control (AAV-Control) in a setting of cardiac dysfunction due to ischemia/reperfusion (I/R) injury. A) Schematic showing timing of the I/R surgery, echocardiography assessments and AAV intervention. B) The estimated area at risk for each group after I/R surgery and AAV administration based on 24 hour post-surgery echocardiography analysis. C) Cardiac expression of iSH2-HA normalised to α -tubulin following administration of 2×10^{12} vg of AAV-cTnT-IVS2-iSH2, saline or AAV6-cTnT-Control (AAV-Control). D) iSH2-HA-associated PI3K activity of all mice that received the AAV-cTnT-IVS2-iSH2 vector. E) Representative hearts from each group and the corresponding heart weight normalised to tibia length. F) Cardiac function indicated by % ejection fraction (EF). G) Representative pressure-volume loops at 12-weeks following I/R surgery: Loops recorded during haemodynamic studies performed at endpoint for mice of each study group, alongside a sham-operated comparator (no infarction, negative control). Stroke work assessed from pressure-volume loops. All data presented as mean \pm SEM. N=6-8 (Saline), N=6-7 (AAV-Control), N=12-14 (AAV6-cTnT-IVS2-iSH2).

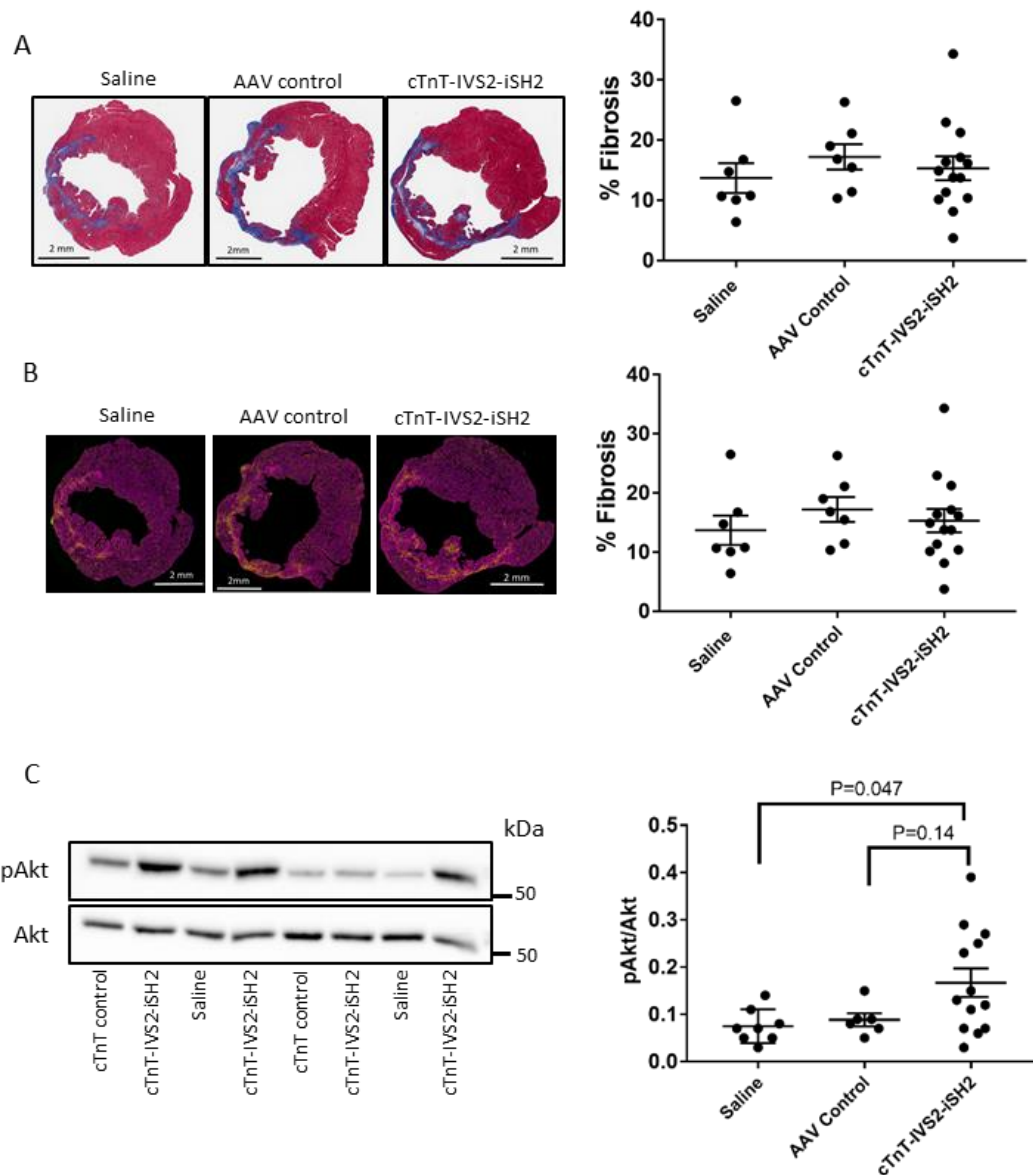


Figure 5. AAV-cTnT-IVS2-iSH2 histological analyses and Akt phosphorylation in a setting of cardiac dysfunction due to I/R. Mid ventricle rings stained with A) Masson's trichrome to assess the % of interstitial fibrosis in the heart or B) stained with the fluorophores troponin-T, CD68 and DAPI to determine % CD68 positive cells. C) Phosphorylation of Akt normalised to total Akt in cardiac tissue for all groups. All data presented as mean \pm SEM. N=6-8 (Saline), N=5-7 (AAV Control), N=10-14 (AAV-cTnT-IVS2-iSH2).

AAV6-iSH2 transduces the healthy sheep heart and activates PI3K by phosphorylating PIP

Assessment of cardiac transduction of AAV6 in the ovine heart was first evaluated by performing direct cardiac injections of the original caPI3K construct driven by either the CMV or the cTnT promoter, i.e., AAV6-CMV-caPI3K and AAV6-cTnT-caPI3K (Figure 6A). Limitations due to large construct size and cost in producing these AAVs meant the highest dose assessed was 5×10^{12} vg. No evidence of transduction was identified in the sheep heart with either AAV-caPI3K construct, whereas a clear signal was identified in the hearts of mice that had received an i.v. injection of 2×10^{11} vg of AAV6-CMV-caPI3K (Figure 6A).

Next, we examined the ability of the smaller AAV constructs to transduce the sheep heart, i.e., iSH2 constructs with the CMV or cTnT promoter +/- IVS2 (Figure 6B & C). Successful transduction of the sheep heart was observed at all sites of administration with the smaller AAV vectors. Sheep #2 was administered 1×10^{13} vg of AAV6-CMV-iSH2 or AAV6-CMV-IVS2-iSH2 via direct cardiac injection into separate regions of the LV (Figure 6B, left panel). Similar expression of iSH2-HA was observed for both constructs and no iSH2-HA was expressed in remote cardiac regions. The degree of expression was comparable to the expression from the heart of a mouse that had received 1×10^{12} vg of the same constructs (Figure 6B, right panel). Sheep #3 received 1×10^{13} vg of AAV6-CMV-iSH2, AAV6-cTnT-iSH2 and AAV6-cTnT-IVS2-iSH2 into three separate regions of the heart (Figure 6C, left panel). The CMV promoter out-performed the cTnT promoter in regards to the amount of iSH2-HA expression, but the addition of IVS2 in conjunction with the cTnT promoter ameliorated this loss of expression relative to the CMV promoter in sheep #3 (Figure 6C). iSH2 was immunoprecipitated from heart lysates from Sheep 2 & 3 using the HA tag antibody. iSH2-associated PI3K activity was observed in tissue from all injection sites whilst no iSH2-associated PI3K activity was observed in a sample from a remote cardiac region (Figure 6D). In summary, efficient transduction of the sheep heart was observed at all sites of administration with the smaller AAV vectors, and iSH2 expression and PI3K activation in the sheep heart was comparable to the mouse heart.

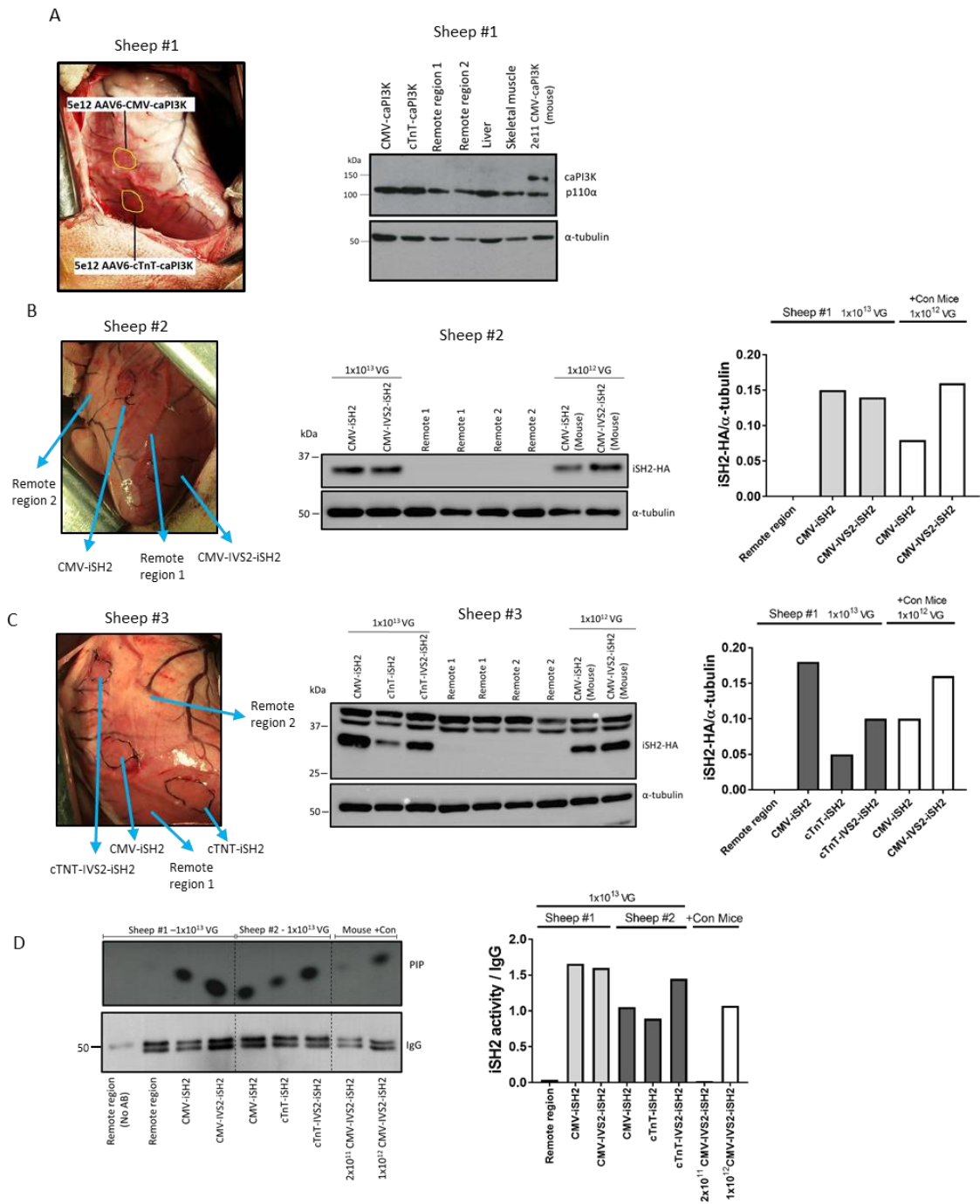


Figure 6. Administration of AAVs containing caPI3K and iSH2 to three healthy sheep. A) AAV cardiac injection sites collected for tissue analysis from Sheep #1 that received 5×10^{12} vg AAV6-CMV-caPI3K and AAV6-cTnT-caPI3K (left). Expression of caPI3K, endogenous p110 α and α -tubulin from the corresponding injection sites and from the heart of a mouse that was administered AAV6-CMV-caPI3K (right). B) Cardiac injection sites and remote region collected for tissue analysis from Sheep #2 that received 1×10^{13} vg AAV6-CMV-iSH2 and AAV6-CMV-IVS2-iSH2 (left). iSH2-HA expression from administration sites, remote regions and positive control mice using an HA-tag antibody (middle and right). C) Cardiac injection sites and remote region collected for tissue analysis from Sheep #3 that received 1×10^{13} vg AAV6-CMV-iSH2, AAV6-cTnT-iSH2 and AAV6-cTnT-IVS2-iSH2 (left). iSH2 expression of administration sites, remote regions and positive control mice using an HA tag antibody (middle and right). D) iSH2-HA-associated PI3K activity in sheep that received iSH2 vectors (Sheep #2 and #3) and positive control mice.

Discussion

There is growing interest in developing and optimising therapeutics that can recapitulate the benefits of exercise on the heart by enhancing critical molecular signalling pathways such as the IGF1-PI3K-Akt cascade. The role of PI3K in regulating heart growth is well established, and numerous studies have demonstrated its capacity to provide cardioprotection following a variety of cardiac insults using transgenic mouse models with increased or decreased PI3K¹²⁻¹⁶. Transgenic mice with a constitutively activated PI3K allele (caPI3K) have increased cardiac PI3K activity, larger hearts and are protected to a similar degree to exercise trained mice in response to pressure overload or dilated cardiomyopathy^{12, 16}, suggesting cardiac PI3K can mimic, at least in part, the beneficial effects of exercise. In contrast, transgenic mice with a dominant negative PI3K allele have reduced PI3K activity, smaller hearts and display worse outcomes following a cardiac insult^{19, 30}. The key aims of this study were to 1) generate an easy-to-manufacture, cardiac specific gene therapy, which could activate and mimic the protective effects of PI3K, and 2) assess whether the new gene therapy provides protection in a mouse model of I/R injury. In this study we report that AAV6 mediated expression of a PI3K(p85) fragment, iSH2, is sufficient to activate PI3K signalling in hearts of healthy mice and sheep, and in mice following a cardiac injury. This demonstrated that fragments of large proteins can mediate downstream signalling *in vivo* and may provide a viable approach to circumventing the limited packaging capacity and high costs of AAV therapies. We also report preliminary findings that IVS2, a rabbit β -globin intron can enhance expression of AAV6-delivered constructs in the heart. The new iSH2 gene therapy did not improve cardiac function in a setting of I/R injury, but increased cardioprotective phosphorylation of Akt. Further studies will be required to assess the therapeutic potential of the AAV6-cTnT-IVS-iSH2 construct in cardiac disease settings.

AAV is one of the most successful vectors for gene delivery due to its positive safety profile, capacity to mediate long-term transgene expression (> 1 year) following a once off delivery and very mild host immune response³². However, the limited packaging capacity of AAV and high costs associated with production of rAAVs still pose barriers to the delivery of large transgenes and economic viability, respectively. It has previously been demonstrated that rAAVs have a maximum package size of ~5 kb and attempts to insert transgenes exceeding the packaging capacity become truncated after ~5.2 kb at the 5' end of the vector genome²². We previously reported that an AAV-caPI3K vector that is 5.15 kb in size transduced the mouse heart and improved heart function in a setting of

pressure overload¹⁶, and prevented cardiac dysfunction in settings of diabetic cardiomyopathy¹⁵. Although the 5.15 kb transgene still provided efficacy at the upper limit of the AAV packaging capacity, production of an AAV containing such a large transgene was inefficient, and labour intensive. To overcome this limitation and assess if a small fragment of PI3K could still be functional in the hearts of mice and sheep, we generated an AAV containing an inter-SH2 domain (iSH2): a small fragment that sits between the two SH2 domains of the p85 regulatory subunit of PI3K. The role and sequence of this subunit was first described by Klippel *et.al.*¹⁰ who demonstrated that in cultured cells the iSH2 domain alone was capable of binding to the p110 α catalytic subunit of PI3K and generating PI3K activity. Moreover, p85 lacking iSH2 is unable to bind to p110 α and form a functional heterodimer. Our studies replicated these findings in animal models by demonstrating that iSH2 could bind to p110 α and generate downstream PI3K activity. The phosphorylation of Akt, a key downstream event of PI3K signalling, tended to be higher (P=0.08) in hearts of healthy adult mice administered AAV-cTnT-IVS2-iSH2 and significantly higher in the hearts of mice that had undergone I/R (P=0.03). In regards to economic viability, using the much smaller iSH2 construct (~2.3 kb size) instead of the caPI3K construct (~5.15 kb) drastically improved the efficiency of AAV vector production (~18-fold increase in production yield) and significantly reduced the production cost.

To improve cardiac transgene expression we trialed inserting β -globin intron 2 (IVS2) between the promoter and transgene to determine if it was capable of improving AAV6-mediated cardiac transgene expression. IVS1 & 2 were initially reported to improve transcriptional efficiency in plasmid vector systems more than thirty years ago²⁴. In the current study, the impact of IVS2 was most prominent at the 1×10^{12} vg dose in which we observed a 3-fold increase in cardiac transgene expression. The efficacy of IVS2 in improving transgene expression has also been observed through microinjection of plasmid DNA³³, and more recently it was shown to provide greater than a 5-fold increase in AAV-mediated transgene expression in the liver of mice²⁶. In line with these findings, we now show that that incorporation of IVS2 into a cardiac promoter driven by AAV6 can improve transgene expression in the heart. This is significant, because the human and large animal heart has been challenging to transduce^{32, 34, 35}. In the CUPID2 clinical trial which administered AAV1 encoding a SERCA2a transgene or placebo to 243 HF patients, no improvement in cardiac function or LV remodelling was identified. One explanation provided for the lack of efficacy was inadequate transduction efficiency with

AAV-mediated expression of SERCA2a occurring in only a small proportion of cardiomyocytes³⁶. Thus, any tool which can enhance AAV-mediated transduction such as IVS2 may prove valuable in improving transduction of the human heart. The value of the truncated PI3K AAV constructs was further highlighted when evaluating transduction of the sheep heart. We were unable to detect any transduction of our AAVs containing caPI3K, but identified a strong signal with constructs containing iSH2. Furthermore, the addition of IVS2 improved the transduction of AAV6-cTnT-iSH2 in the sheep heart.

Having developed a new AAV gene therapy tool with the capacity to generate PI3K activity, and efficiently transduce the mouse and sheep heart, we next examined the therapeutic potential of this AAV in a mouse model of I/R injury. The phosphorylation of Akt was significantly higher in hearts of I/R mice treated with AAV-cTnT-IVS2-iSH2 compared with saline controls. Despite the increased phosphorylation of Akt in the I/R model, this was not associated with positive outcomes based on morphology, cardiac function, cardiac fibrosis or % CD68 positive cells. A number of factors may have contributed to the lack of functional improvement. First, the dose of the AAV in the I/R model may have been too high, leading to some systemic toxicity, and limiting the ability to identify any cardiac protection. The same dose (2×10^{12} vg) did not appear to be associated with any phenotype in healthy adult mice in which organ weights and appearance were indistinguishable from control saline mice. However, in the I/R model, spleen, kidney and HW/TL ratio were all higher in mice receiving AAV in comparison to saline. This does not represent a significant immune response since spleen weights were only marginally elevated (~ 90-95 mg in the AAV groups vs 82 mg in the saline group), and in the healthy basal cohort, spleen weights were ~90 mg in the saline cohort. Further, there was no evidence of exacerbated depressed cardiac function or performance in I/R mice administered AAV6-cTnT-control versus saline. However, given normalised heart and kidney weights were elevated in the I/R cohorts receiving AAV, we cannot exclude this may have impacted the results. Second, the delivery of AAV may have occurred too late to provide benefit. Transduction of AAV6 in the mouse heart has been reported to peak 21 days following administration³⁷. Given we administered AAV one day after I/R surgery, irreversible cardiac damage may already have occurred by the time the heart was sufficiently expressing iSH2 (3 weeks following the cardiac insult). Third, the elevation in Akt phosphorylation in the I/R heart (average of ~2-fold) may have been inadequate in this severe cardiac disease model. However, of note, we previously identified an improvement in heart function in a pressure overload model, and the phosphorylation of

Akt was elevated ~1.6-1.7- fold. Moreover, Akt has previously been observed to protect against an I/R injury in the mouse heart³⁸. Though the degree of Akt activation was not quantitatively assessed. Cardiac protection following administration of AAV6/9 vectors with complement component 1q (C1q) and tumour necrosis factor related protein 5 (CTRP5) or a novel muscle-specific micropeptide dwarf open reading frame (DWORF) to mice following I/R or myocardial infarction injuries have been previously observed^{39, 40}. The time point of AAV administration was a key difference between these studies and ours, as the AAV vectors were administered three and eight weeks prior to the cardiac insult, respectively. Further, in the study assessing AAV-DWORF that enhances SERCA2a activity, the AAV was administered prior to adult hood at postnatal day 5 and CTRP5 study also differed in that a slightly different model of I/R injury was used, 24 hours after reperfusion the LAD was re-tied permanently, providing only a temporary reperfusion. Moreover, given that cardiac function is governed by a multitude of signalling pathways, approaches such as dual-AAV mediated therapies that can target multiple protective pathways simultaneously are likely to confer greater functional improvements. This has already shown promise in improving outcomes as well as facilitating the administration of transgenes too large for a single AAV vector in numerous non-cardiac AAV-based therapeutic trials⁴¹.

In conclusion, in this report we have described the development and optimisation of a truncated PI3K AAV gene therapy (AAV6-cTnT-IVS2-iSH2) which can efficiently transduce the mouse and sheep heart. Future studies in cardiac stress settings should administer AAV6-cTnT-IVS2-iSH2 at a lower dose and an earlier time point to assess the therapeutic potential of this new gene therapy tool.

References

1. Taylor CJ, Ordóñez-Mena JM, Roalfe AK, et al. Trends in survival after a diagnosis of heart failure in the United Kingdom 2000-2017: population based cohort study. *BMJ*. Feb 13 2019;364:l223. doi:10.1136/bmj.l223
2. He J, Ogden LG, Bazzano LA, Vupputuri S, Loria C, Whelton PK. Risk factors for congestive heart failure in US men and women: NHANES I epidemiologic follow-up study. *Arch Intern Med*. Apr 9 2001;161(7):996-1002. doi:10.1001/archinte.161.7.996
3. Djousse L, Driver JA, Gaziano JM. Relation between modifiable lifestyle factors and lifetime risk of heart failure. *JAMA*. Jul 22 2009;302(4):394-400. doi:10.1001/jama.2009.1062
4. Naylor M, Vasan RS. Preventing heart failure: the role of physical activity. *Curr Opin Cardiol*. Sep 2015;30(5):543-50. doi:10.1097/HCO.0000000000000206
5. Flynn KE, Pina IL, Whellan DJ, et al. Effects of exercise training on health status in patients with chronic heart failure: HF-ACTION randomized controlled trial. *JAMA*. Apr 8 2009;301(14):1451-9. doi:10.1001/jama.2009.457
6. Hambrecht R, Gielen S, Linke A, et al. Effects of exercise training on left ventricular function and peripheral resistance in patients with chronic heart failure: A randomized trial. *JAMA*. Jun 21 2000;283(23):3095-101. doi:10.1001/jama.283.23.3095
7. O'Connor CM, Whellan DJ, Lee KL, et al. Efficacy and safety of exercise training in patients with chronic heart failure: HF-ACTION randomized controlled trial. *JAMA*. Apr 8 2009;301(14):1439-50. doi:10.1001/jama.2009.454
8. Pandey A, Parashar A, Kumbhani D, et al. Exercise training in patients with heart failure and preserved ejection fraction: meta-analysis of randomized control trials. *Circ Heart Fail*. Jan 2015;8(1):33-40. doi:10.1161/CIRCHEARTFAILURE.114.001615
9. Wisloff U, Stoylen A, Loennechen JP, et al. Superior cardiovascular effect of aerobic interval training versus moderate continuous training in heart failure patients: a randomized study. *Circulation*. Jun 19 2007;115(24):3086-94. doi:10.1161/CIRCULATIONAHA.106.675041
10. Klippel A, Escobedo JA, Hu Q, Williams LT. A region of the 85-kilodalton (kDa) subunit of phosphatidylinositol 3-kinase binds the 110-kDa catalytic subunit in vivo. *Mol Cell Biol*. Sep 1993;13(9):5560-6. doi:10.1128/mcb.13.9.5560-5566.1993
11. Bass-Stringer S, Tai CMK, McMullen JR. IGF1-PI3K-induced physiological cardiac hypertrophy: Implications for new heart failure therapies, biomarkers, and predicting cardiotoxicity. *J Sport Health Sci*. Nov 24 2020;doi:10.1016/j.jshs.2020.11.009
12. McMullen JR, Amirahmadi F, Woodcock EA, et al. Protective effects of exercise and phosphoinositide 3-kinase(p110alpha) signaling in dilated and hypertrophic cardiomyopathy. *Proc Natl Acad Sci U S A*. Jan 9 2007;104(2):612-7. doi:10.1073/pnas.0606663104
13. Pretorius L, Du XJ, Woodcock EA, et al. Reduced phosphoinositide 3-kinase (p110alpha) activation increases the susceptibility to atrial fibrillation. *Am J Pathol*. Sep 2009;175(3):998-1009. doi:10.2353/ajpath.2009.090126
14. Lin RC, Weeks KL, Gao XM, et al. PI3K(p110 alpha) protects against myocardial infarction-induced heart failure: identification of PI3K-regulated miRNA and mRNA. *Arterioscler Thromb Vasc Biol*. Apr 2010;30(4):724-32. doi:10.1161/ATVBAHA.109.201988
15. Ritchie RH, Love JE, Huynh K, et al. Enhanced phosphoinositide 3-kinase(p110alpha) activity prevents diabetes-induced cardiomyopathy and superoxide generation in a mouse model of diabetes. *Diabetologia*. Dec 2012;55(12):3369-81. doi:10.1007/s00125-012-2720-0
16. Weeks KL, Gao X, Du XJ, et al. Phosphoinositide 3-kinase p110alpha is a master regulator of exercise-induced cardioprotection and PI3K gene therapy rescues cardiac dysfunction. *Circ Heart Fail*. Jul 1 2012;5(4):523-34. doi:10.1161/CIRCHEARTFAILURE.112.966622
17. Perrino C, Naga Prasad SV, Mao L, et al. Intermittent pressure overload triggers hypertrophy-independent cardiac dysfunction and vascular rarefaction. *J Clin Invest*. Jun 2006;116(6):1547-60. doi:10.1172/JCI25397

18. Bernardo BC, Ooi JYY, Weeks KL, Patterson NL, McMullen JR. Understanding Key Mechanisms of Exercise-Induced Cardiac Protection to Mitigate Disease: Current Knowledge and Emerging Concepts. *Physiol Rev.* Jan 1 2018;98(1):419-475. doi:10.1152/physrev.00043.2016
19. McMullen JR, Shioi T, Zhang L, et al. Phosphoinositide 3-kinase(p110alpha) plays a critical role for the induction of physiological, but not pathological, cardiac hypertrophy. *Proc Natl Acad Sci U S A.* Oct 14 2003;100(21):12355-60. doi:10.1073/pnas.1934654100
20. Prakoso D, De Blasio MJ, Qin C, et al. Phosphoinositide 3-kinase (p110alpha) gene delivery limits diabetes-induced cardiac NADPH oxidase and cardiomyopathy in a mouse model with established diastolic dysfunction. *Clin Sci (Lond).* Jun 1 2017;131(12):1345-1360. doi:10.1042/CS20170063
21. Prakoso D, De Blasio MJ, Tate M, et al. Gene therapy targeting cardiac phosphoinositide 3-kinase (p110alpha) attenuates cardiac remodeling in type 2 diabetes. *Am J Physiol Heart Circ Physiol.* Apr 1 2020;318(4):H840-H852. doi:10.1152/ajpheart.00632.2019
22. Wu Z, Yang H, Colosi P. Effect of genome size on AAV vector packaging. *Mol Ther.* Jan 2010;18(1):80-6. doi:10.1038/mt.2009.255
23. Grieger JC, Samulski RJ. Packaging capacity of adeno-associated virus serotypes: impact of larger genomes on infectivity and postentry steps. *J Virol.* Aug 2005;79(15):9933-44. doi:10.1128/JVI.79.15.9933-9944.2005
24. Buchman AR, Berg P. Comparison of intron-dependent and intron-independent gene expression. *Mol Cell Biol.* Oct 1988;8(10):4395-405. doi:10.1128/mcb.8.10.4395-4405.1988
25. Gregorevic P, Blankinship MJ, Allen JM, et al. Systemic delivery of genes to striated muscles using adeno-associated viral vectors. *Nat Med.* Aug 2004;10(8):828-34. doi:10.1038/nm1085
26. Wang L, Muthuramu I, Somanathan S, et al. Developing a second-generation clinical candidate AAV vector for gene therapy of familial hypercholesterolemia. *Mol Ther Methods Clin Dev.* Sep 10 2021;22:1-10. doi:10.1016/j.omtm.2021.04.017
27. Gao XM, Wu QZ, Kiriazis H, et al. Microvascular leakage in acute myocardial infarction: characterization by histology, biochemistry, and magnetic resonance imaging. *Am J Physiol Heart Circ Physiol.* May 1 2017;312(5):H1068-H1075. doi:10.1152/ajpheart.00073.2017
28. Donner D, Kiriazis H, Gao X, & Du X. A novel non-invasive measurement of myocardial infarct size in the mouse using cardiac ultrasound tissue displacement mapping. *Journal of Molecular and Cellular Cardiology.* 2020;(140):6-7.
29. Sapra G, Tham YK, Cemerlang N, et al. The small-molecule BGP-15 protects against heart failure and atrial fibrillation in mice. *Nat Commun.* Dec 9 2014;5:5705. doi:10.1038/ncomms6705
30. Shioi T, Kang PM, Douglas PS, et al. The conserved phosphoinositide 3-kinase pathway determines heart size in mice. *EMBO J.* Jun 1 2000;19(11):2537-48. doi:10.1093/emboj/19.11.2537
31. Thomas CJ, Lim NR, Kedikaetswe A, et al. Evidence that the MEK/ERK but not the PI3K/Akt pathway is required for protection from myocardial ischemia-reperfusion injury by 3',4'-dihydroxyflavonol. *Eur J Pharmacol.* Jul 5 2015;758:53-9. doi:10.1016/j.ejphar.2015.03.054
32. Bass-Stringer S, Bernardo BC, May CN, Thomas CJ, Weeks KL, McMullen JR. Adeno-Associated Virus Gene Therapy: Translational Progress and Future Prospects in the Treatment of Heart Failure. *Heart Lung Circ.* Nov 2018;27(11):1285-1300. doi:10.1016/j.hlc.2018.03.005
33. Chatterjee S, Min L, Karuturi RK, Lufkin T. The role of post-transcriptional RNA processing and plasmid vector sequences on transient transgene expression in zebrafish. *Transgenic Res.* Apr 2010;19(2):299-304. doi:10.1007/s11248-009-9312-x
34. Lyon AR, Babalis D, Morley-Smith AC, et al. Investigation of the safety and feasibility of AAV1/SERCA2a gene transfer in patients with chronic heart failure supported with a left ventricular assist device - the SERCA-LVAD TRIAL. *Gene Ther.* Dec 2020;27(12):579-590. doi:10.1038/s41434-020-0171-7
35. Hajjar RJ, Ishikawa K. Introducing Genes to the Heart: All About Delivery. *Circ Res.* Jan 6 2017;120(1):33-35. doi:10.1161/CIRCRESAHA.116.310039

36. Greenberg B, Butler J, Felker GM, et al. Calcium upregulation by percutaneous administration of gene therapy in patients with cardiac disease (CUPID 2): a randomised, multinational, double-blind, placebo-controlled, phase 2b trial. *Lancet*. Mar 19 2016;387(10024):1178-86. doi:10.1016/S0140-6736(16)00082-9
37. Zincarelli C, Soltys S, Rengo G, Koch WJ, Rabinowitz JE. Comparative cardiac gene delivery of adeno-associated virus serotypes 1-9 reveals that AAV6 mediates the most efficient transduction in mouse heart. *Clin Transl Sci*. Jun 2010;3(3):81-9. doi:10.1111/j.1752-8062.2010.00190.x
38. Fujio Y, Nguyen T, Wencker D, Kitsis RN, Walsh K. Akt promotes survival of cardiomyocytes in vitro and protects against ischemia-reperfusion injury in mouse heart. *Circulation*. Feb 15 2000;101(6):660-7. doi:10.1161/01.cir.101.6.660
39. Peng M, Liu Y, Zhang XQ, Xu YW, Zhao YT, Yang HB. CTRP5-Overexpression Attenuated Ischemia-Reperfusion Associated Heart Injuries and Improved Infarction Induced Heart Failure. *Front Pharmacol*. 2020;11:603322. doi:10.3389/fphar.2020.603322
40. Makarewich CA, Bezprozvannaya S, Gibson AM, Bassel-Duby R, Olson EN. Gene Therapy With the DWORF Micropeptide Attenuates Cardiomyopathy in Mice. *Circ Res*. Oct 23 2020;127(10):1340-1342. doi:10.1161/CIRCRESAHA.120.317156
41. Tornabene P, Trapani I. Can Adeno-Associated Viral Vectors Deliver Effectively Large Genes? *Hum Gene Ther*. Jan 2020;31(1-2):47-56. doi:10.1089/hum.2019.220

Table 1. Morphological data from healthy adult mouse cohort.

	Saline	AAV6-cTnT-IVS2-iSH2 (2x10 ¹² vg)	P-value†
No. of animals	4	5	
Age (weeks)	19.4 ± 0.3	19.5 ± 0.1	0.79
Body Weight (BW, g)	30.1 ± 1.8	29.8 ± 1.8	0.91
Tibia Length (TL, mm)	16.8 ± 0.2	16.8 ± 0.2	0.93
Heart Weight (HW, mg)	134.3 ± 10.5	127.8 ± 5.0	0.57
Atria Weight (AW, mg)	8.4 ± 1.4	7.1 ± 0.6	0.21
Lung Weight (LW, mg)	161.8 ± 12.4	153.6 ± 4.5	0.52
Liver Weight (LivW, mg)	1435.0 ± 130	1309.0 ± 63.6	0.38
Kidney Weight (KW, mg; right and left)	470.4 ± 40.0	430.9 ± 12.8	0.34
Spleen Weight (SW, mg)	90.7 ± 7.0	86.6 ± 4.0	0.60
HW/BW (mg/g)	4.5 ± 0.1	4.3 ± 0.2	0.55
HW/TL (mg/mm)	8.0 ± 0.6	7.6 ± 0.2	0.50
AW/TL (mg/mm)	0.5 ± 0.0	0.4 ± 0.0	0.14
LW/TL (mg/mm)	9.6 ± 0.6	9.1 ± 0.2	0.45
LivW/TL (mg/mm)	85.3 ± 6.9	77.8 ± 3.2	0.32
KW/TL (mg/mm)	28.0 ± 2.1	25.6 ± 0.6	0.27
SW/TL (mg/mm)	90.7 ± 7.0	86.6 ± 4.0	0.54

Results presented as mean ± SEM. †Unpaired t-tests.

Table 2. Myocardial Ischemia-Reperfusion mice cohort morphology administered saline or AAV6-cTnT-Control.

	Saline	AAV6-cTnT-Control	P-value†
No. of animals	8	7	
Age (weeks)	23.2 ± 0.2	23.8 ± 0.2	0.13
Body Weight (BW, g)	35.0 ± 0.9	36.5 ± 1.0	0.17
Tibia Length (TL, mm)	16.9 ± 0.1 (n=7)	17.1 ± 0.1	0.22
Heart Weight (HW, g)	144.9 ± 5.0	157.9 ± 4.0	0.07
Atria Weight (AW, mg)	8.5 ± 0.9	9.1 ± 1.0	0.68
Lung Weight (LW, mg)	162.4 ± 16.1	157.9 ± 3.9	0.81
Liver Weight (LivW, mg)	1206.0 ± 84.5	1209.0 ± 67.9	0.65
Kidney Weight (KW, mg; left)	194.0 ± 5.7	221.9 ± 7.7	0.01*
Spleen Weight (SW, mg)	81.4 ± 2.2	95.5 ± 4.1	0.01*
HW/BW (mg/g)	4.1 ± 0.1	4.3 ± 0.1	0.26
HW/TL (mg/mm)	8.3 ± 0.2 (n=7)	9.3 ± 0.3	0.02*
AW/TL (mg/mm)	0.5 ± 0.0 (n=7)	0.5 ± 0.1	0.48
LW/TL (mg/mm)	8.7 ± 0.2 (n=7)	9.3 ± 0.2	0.08
LivW/TL (mg/mm)	73.7 ± 4.8 (n=7)	70.1 ± 4.0	0.65
KW/TL (mg/mm)	11.4 ± 0.4 (n=7)	13.0 ± 0.5	0.02*
SW/TL (mg/mm)	4.9 ± 0.1 (n=7)	5.6 ± 0.2	0.02*

Results presented as mean ± SEM. †Unpaired t-tests. * P<0.05 AAV6-cTnT-Control vs Saline.

One saline mouse had a tibia broken for both legs (n=7 for saline for tibia measurements)

Table 3. Echocardiography: Myocardial Ischemia-Reperfusion mice IR cohort administered saline or AAV6-cTnT-Control.

	Saline	AAV6-cTnT-Control	P-value†
No. of animals	8	7	
Heart Rate (BPM)	521 ± 24	490 ± 10	0.28
End-systolic area (mm)	26.0 ± 2.4	28.1 ± 1.3	0.46
End-diastolic area (mm)	31.1 ± 2.0	33.1 ± 1.5	0.43
End-systolic volume (μL)	84.3 ± 13.6	98.9 ± 7.1	0.38
End-diastolic volume (μL)	109.2 ± 12.8	125.3 ± 8.9	0.33
Stroke Volume (μL)	24.9 ± 2.6	26.4 ± 4.1	0.77
Ejection Fraction (%)	25 ± 4	21 ± 3	0.41
Fractional Shortening (%)	7 ± 0	7 ± 1	0.88
Cardiac Output (ml/min)	12.5 ± 1.5	12.8 ± 2.0	0.91
Area Change (%)	17.5 ± 2.7	15.3 ± 1.5	0.50

Results presented as mean ± SEM. †Unpaired t-tests.

BPM: Beats per minute.

Table 4. PV-loop analysis: Myocardial Ischemia-Reperfusion mice cohort administered saline or AAV6-cTnT-Control.

	Saline	AAV6-cTnT-Control	P-value†
No. of animals	6	6	
Heart Rate (BPM)	555 ± 22	583 ± 14	0.31
SW (mmHg x μL)	1569 ± 304	1449 ± 313	0.79
Developed pressure (mmHg)	87.8 ± 3.2	85.4 ± 2.8	0.58
End-systolic pressure (mmHg)	85.2 ± 2.4	83.5 ± 2.5	0.65
End-diastolic pressure (mmHg)	4.8 ± 0.7	7.8 ± 3.3	0.39
Ea (mmHg/μL)	4.0 ± 0.5	4.7 ± 0.8	0.45
Power Maximum (mmHg x μL/s)	14567 ± 731	16198 ± 7366	0.83
dP/dt Maximum (mmHg/s)	8710 ± 917	7896 ± 636	0.48
dP/dt Minimum (mmHg/s)	-7438 ± 534	-6129 ± 588	0.13
dV/dt Maximum (μL/s)	1005 ± 172	801.5 ± 176	0.42
dV/dt Minimum (μL/s)	-846 ± 107	-802 ± 198	0.85
Tau (ms)	5.7 ± 0.3	6.5 ± 0.4	0.17
ESPVR	2.0 ± 0.3 (n=5)	2.9 ± 0.4 (n=4)	0.12
EDPVR	0.3 ± 0.0 (n=5)	0.4 ± 0.1 (n=4)	0.61
Systolic Pressure (Arterial)	83.3 ± 3.7	80.2 ± 3.0	0.52
Diastolic pressure (Arterial)	52.0 ± 3.9	52.7 ± 2.9	0.89
Pulse pressure (Arterial)	31.3 ± 1.5	27.5 ± 1.0	0.06

Results presented as mean ± SEM. †Unpaired t-tests.

BPM: Beats per minute, SW: Stroke work, ESPVR: End systolic pressure volume relationship, EDPVR: End diastolic pressure volume relationship. Numbers are lower for ESPVR and EDPVR as not all animals were suitable for this analysis.

Table 5. Myocardial Ischemia-Reperfusion mice cohort morphology.

	Saline	AAV6-cTnT-Control	AAV6-cTnT-IVS2-iSH2	P value†
No. of animals	8	7	14	
Age (weeks)	23.2 ± 0.2	23.8 ± 0.2	23.4 ± 0.1	0.18
Body Weight (BW, g)	35.0 ± 0.9	36.5 ± 1.0	35.3 ± 1.0	0.61
Tibia Length (TL, mm)	16.9 ± 0.1 (n=7)	17.1 ± 0.1	16.9 ± 0.1	0.33
Heart Weight (HW, mg)	144.9 ± 5.0	157.9 ± 4.0	160.3 ± 8.1	0.33
Atria Weight (AW, mg)	8.5 ± 0.9	9.1 ± 1.0	11.1 ± 1.3	0.30
Lung Weight (LW, mg)	162.4 ± 16.1	157.9 ± 3.9	167.3 ± 8.2	0.81
Liver Weight (LivW, mg)	1206.0 ± 84.5	1209.0 ± 67.9	1198.0 ± 50.6	0.99
Kidney Weight (KW, mg; left)	194.0 ± 5.7	221.9 ± 7.7	224.4 ± 9.0	0.05
Spleen Weight (SW, mg)	81.4 ± 2.2	95.5 ± 4.1	90.1 ± 4.3	0.12
HW/BW (mg/g)	4.1 ± 0.1	4.3 ± 0.1	4.5 ± 0.2	0.24
HW/TL (mg/mm)	8.3 ± 0.2 (n=7)	9.3 ± 0.3	9.5 ± 0.5	0.20
AW/TL (mg/mm)	0.5 ± 0.0 (n=7)	0.5 ± 0.1	0.7 ± 0.1	0.16
LW/TL (mg/mm)	8.7 ± 0.2 (n=7)	9.3 ± 0.2	9.9 ± 0.5	0.16
LivW/TL (mg/mm)	73.7 ± 4.8 (n=7)	70.1 ± 4.0	70.9 ± 3.1	0.16
KW/TL (mg/mm)	11.4 ± 0.4 (n=7)	13.0 ± 0.5	13.3 ± 0.5	0.06
SW/TL (mg/mm)	4.9 ± 0.1 (n=7)	5.6 ± 0.2	5.3 ± 0.2	0.20

Results presented as mean ± SEM. †One -way ANOVA with Tukey's posthoc test. One saline mouse had a tibia broken for both legs (n=7 for saline for tibia measurements).

Table 6. Echocardiography myocardial Ischemia-Reperfusion mice cohort.

	Saline	AAV6- cTnT- Control	AAV6- cTnT-IVS2- iSH2	P-value†
No. of animals	8	7	14	
Heart Rate (BPM)	521 ± 24	490 ± 10	523 ± 11	0.30
End-systolic area (mm)	26.0 ± 2.4	28.1 ± 1.3	30.2 ± 2.4	0.43
End-diastolic area (mm)	31.1 ± 2.0	33.1 ± 1.5	34.9 ± 2.3	0.48
End-systolic volume (μL)	84.3 ± 13.6	98.9 ± 7.1	113.2 ± 14.6	0.35
End-diastolic volume (μL)	109.2 ± 12.8	125.3 ± 8.9	139.9 ± 15.5	0.34
Stroke Volume (μL)	24.9 ± 2.6	26.4 ± 4.1	26.7 ± 2.2	0.90
Ejection Fraction (%)	25 ± 4	21 ± 3	21 ± 2	0.45
Fractional Shortening (%)	7 ± 0	7 ± 1	6 ± 1	0.71
Cardiac Output (ml/min)	12.5 ± 1.5	12.8 ± 2.0	13.9 ± 1.2	0.77
Area Change (%)	17.5 ± 2.7	15.3 ± 1.5	14.4 ± 1.2	0.43

Results presented as mean ± SEM. †One -way ANOVA with Tukey's posthoc test.
BPM: Beats per minute

Table 7. Pressure-Volume loop analysis Myocardial Ischemia-Reperfusion mice cohort.

Haemodynamic Parameters	Saline	AAV6-cTnT-Control	AAV6-cTnT-IVS2-iSH2	P-value†
No. of animals	6	6	12	
Heart Rate (BPM)	555 ± 22	583 ± 14	538 ± 13	0.15
SW (mmHg x μL)	1569 ± 304	1449 ± 313	1506 ± 172	0.95
Developed pressure (mmHg)	87.8 ± 3.2	85.4 ± 2.8	77.7 ± 2.9	0.06
End-systolic pressure (mmHg)	85.2 ± 2.4	83.5 ± 2.5	76.1 ± 2.9	0.07
End-diastolic pressure (mmHg)	4.8 ± 0.7	7.8 ± 3.3	6.2 ± 0.7	0.50
Ea (mmHg/μL)	4.0 ± 0.5	4.7 ± 0.8	3.2 ± 0.3	0.09
Power Maximum (mmHg x μL/s)	14567 ± 7312	16198 ± 7366	17130 ± 2702	0.90
dP/dt Maximum (mmHg/s)	8710 ± 917	7896 ± 636	7196 ± 568	0.31
dP/dt Minimum (mmHg/s)	-7438 ± 534	-6129 ± 588	-5529 ± 440	0.05
dV/dt Maximum (μL/s)	1005 ± 172	801.5 ± 176	1088 ± 208	0.64
dV/dt Minimum (μL/s)	-846 ± 107	-802 ± 198	-914 ± 98	0.82
Tau (ms)	5.7 ± 0.3	6.5 ± 0.4	6.5 ± 0.2	0.16
ESPVR	2.0 ± 0.3 (n=5)	2.9 ± 0.4 (n=4)	1.5 ± 0.2 (n=9)	0.008*
EDPVR	0.3 ± 0.0 (n=5)	0.4 ± 0.1 (n=4)	0.4 ± 0.0 (n=9)	0.67
Systolic Pressure (Arterial)	83.3 ± 3.7	80.2 ± 3.0	75.9 ± 2.4	0.21
Diastolic pressure (Arterial)	52.0 ± 3.9	52.7 ± 2.9	47.7 ± 3.0	0.45
Pulse pressure (Arterial)	31.3 ± 1.5	27.5 ± 1.0	28.2 ± 1.6	0.30

Results presented as mean ± SEM. †One -way ANOVA with Tukey's posthoc test.

*AAV- Control vs AAV-iSH2. BPM: Beats per minute, SW: Stroke work, ESPVR: End systolic pressure volume relationship, EDPVR: End diastolic pressure volume relationship. Numbers are lower for ESPVR and EDPVR as not all animals were suitable for this analysis.

Supplementary data- Generation of AAV6 vectors

Generation of AAV6 vectors

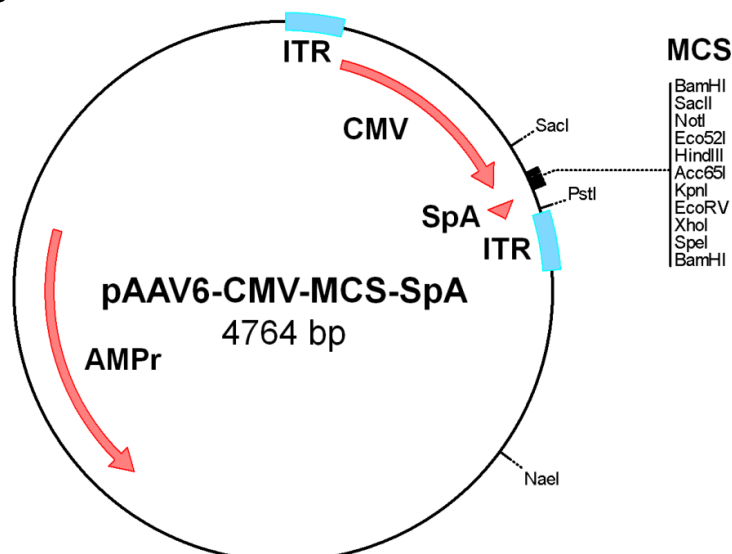
This section describes the generation of AAV6 constructs containing the cTnT promoter, constitutively active phosphoinositide 3-kinase (caPI3K-made with iSH2p110), iSH2 and IVS2 inserts. The generation of these constructs stems from and follows on from the generation AAV6-CMV-MCS-SpA (Figure S1 A and B) AAV6-CMV-caPI3K-SpA (S1 C and D) which have previously been described in detail ¹.

A

```

GAGCTG GTTTAGTGAACCGTCAGATCGCCTGGAGACGCCATCCACGCTGTTTTGACCTCCATAGAAGACAC
CGGGACCGATCCAGC GGATCCCGCGGGCGGCCGCAAGCTTGGTACCGATATCCTCGAGACTAGTGGATC
CGAATAAAAGATCTTTATTTTCATTAGATCTGTGTGTGTTTGTGTG CTGCAG TACGTAGATAAG
TAGCATGGCGGGTTAATCATTAACTACAAGGAACCCCTAGTGATGGAGTTGGCCACTCCCTCTCTGCGCGC
TCGCTCGCTCACTGAGGCCGGGCGACCAAAGGTCGCCCGACGCCCGGGCTTTGCCCGGGCGGCCTCAGTGA
GCGAGCGAGCGCCAGCTGGCGTAATAGCGAAGAGGCCCGCACCCGATCGCCCTCCCAACAGTTGCGCAG
CCTGAATGGCGAATGGAATTCAGACGATTGAGCGTCAAATGTAGGTATTTCCATGAGCGTTTTTCTGT
TGCAATGGCTGGCGTAATATTGTTCTGGATATTACCAGCAAGGCCGATAGTTTGAGTCTTCTACTCAGG
CAAGTGATGTTATTACTAATCAAAGAAGTATTGCGACAACGGTTAATTTGCGTGATGGACAGACTCTTTTA
CTCGGTGGCCTCACTGATTATAAAAAACTTCTCAGGATTCTGGCGTACC GTTCTGTCTAAAATCCCTTT
AATCGCCTCCTGTTTAGCTCCCGCTCTGATTCTAACGAGGAAAGCACGTTATACGTGCTCGTCAAAGCAA
CCATAGTACGCGCCCTGTAGCGGCGCATTAAAGCGCGGGTGTGGTGGTTACGCGCAGCGTGACCGCTAC
ACTTGCCAGCGCCCTAGCGCCGCTCCTTTCGCTTCTTCCCTTCTTCTCGCCACGTTG GCCGGC
    
```

B



Supplementary figure 1. DNA sequences and maps of plasmid AAV6 (pAAV6)-CMV-MCS-SpA and pAAV6-CMV-caPI3K-SpA. A) Purple highlighting: SacI and NaeI restriction sites, grey highlighting: 3' end of CMV promoter, yellow highlighting: MCS (BamHI restriction sites in red text), green highlighting: SpA, blue highlighting: PstI restriction site, red highlighting: buffer nucleotides. C) DNA sequence of iSH2p110. D) Plasmid map of pAAV6-CMV-iSH2p110-SpA. AMP^r: ampicillin resistance gene, CMV: cytomegalovirus promoter, ITR: inverted terminal repeat, SpA: synthetic polyadenylation signal.

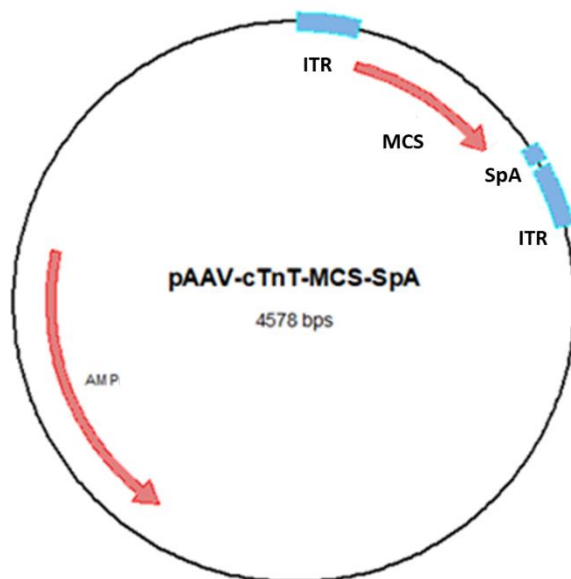
Generation of pAAV6-cTnT-MCS-SpA from pAAV6-CMV-MCS-SpA

A

```

TACGTAAGCGCTgcggcgcctcgagctctgctcccagctggccctcccaggcctggggtgctggc
ctctgctttatcaggattctcaagagggacagctggtttatgttgcatgactgttccctgcata
ctgctctgggttttaaatagcttatctgctagcctgctcccagctggccctcccaggcctggggtg
ctggcctctgctttatcaggattctcaagagggacagctggtttatgttgcatgactgttccctg
catactgctctgggttttaaatagcttatctg
attcctccctggctcaccaggccccagccacatgcctgcttaaagccctctccatcctctgcct
caccagtcctcgctgagactgagcagacgctccaggatctgtcggcagctaattaatGGATC
CCGCGGGCGGCCGCAAGCTTGGTACCGATATCCTCGAGACTAGTGGATCC AATAAAAGATCTT
TATTTTCATTAGATCTGTGTGTTGGTTTTTGTGTGCTGCAGTACGTA
    
```

B



Supplementary figure 2. Generation of pAAV6-cTnT-MCS-SpA from pAAV6-CMV-caPI3K-SpA. A) The DNA sequence containing a new promoter (cTnT⁴⁷⁷) inserted between a AfeI (green) restriction site and the first BamHI restriction site (GGATCC) of pAAV6-MCS-SpA (B) to form pAAV6-cTnT-MCS-SpA. A) Purple highlighting: SnaBI restriction sites, grey highlighting: 3' end of cTnT promoter, red highlighting: MCS site designed previously for pAAV6-CMV-MCS-SpA, yellow highlighting: Two BamHI restriction sites (GGATCC) flanking the MCS site and a PstI restriction site (CTGCAG), green highlighting: AfeI unique restriction site, blue highlighting: Synthetic poly A tail (SpA) sequence, dark green highlighting: buffer nucleotides, B) The restriction sites flanking the promoter and MCS site are shown. A PstI site was inserted between the SpA and the 3' ITR of pAAV6-CMV-MCS-SpA for easy removal of the SpA if required. ITR: inverted terminal repeat, AMP^r: ampicillin resistance gene, SpA: synthetic polyadenylation sequence, MCS: Multiple cloning site.

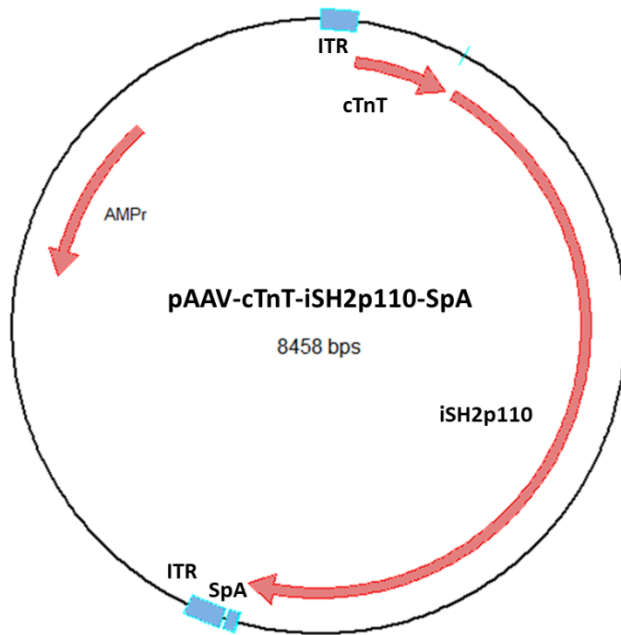
Generation of AAV6-cTnT-iSH2p110-SpA

iSH2p110 (caPI3K) was cloned into pAAV6-cTnT-MCS-SpA by GenScript. The construct was received from GenScript in a pUC57 vector. pUC57 was transformed into *E. coli* competent cells to amplify the plasmid. The iSH2p110 fragment was excised out of pUC57 vector by restriction enzyme digests, HindIII then separated and purified. The DNA was ligated into the pAAV6-cTnT-MCS-SpA vector (Figure S2).

A

```
ATGGCTCAGTATAATCCCAAATTGGATGTGAAATTACTTTATCCAGTATCCAAATACCAACAGGATCAAGTTGTCAAAGAAGATAATATT
GAAGCTGTAGGGAAAAAATTACATGAATATAAACAACACTCAGTTTCAAGAAAAAAGTCGAGAAATATGATAGATTATATGAAGAATATACCCGC
ACATCCCAGGAAATCCAAATGAAAAGGACAGCTATTGAAGCATTTAATGAAACCATAAAAAATTTGAAGAACAGTGCAGACCCCAAGAG
CGGTACAGCAAAGAAATACATAGAAAAGTTTAAACGTGAAGGCAATGAGAAAAGAAATACAAAGGATTATGCATAAATATGATAAGTTGAAG
TCTCGAATCAGTGAATTTATTGACAGTAGAAGAAGATTGGAAGAAGACTTGAAGAAGCAGGCAGCTGAGTATCGAGAAAATTGACAAAACGT
ATGAACAGCATTAACCAGACCTTATCCAGCTGAGAAAAGACGAGAGACCAATACTTGATGTGGTTGACTCAAAAAGGTGTTCCGCAAAAAG
AAGTTGAACGAGTGGTTGGGCAATGAAAACACTGAAGACCAATATTCAGTGGTGAAGATGATGAAGATTGCCCATCATGATGAGAAG
ACATGGAATGTTGGAAGCAGCAACCGAAACAAAGCTGAAAACCTGTTGCGAGGGAAAGCGAGATGGCACTTTTCTGTCCGGGAGAGCAGT
AAACAGGGCTGCTATGCCTGCTGTAGTGGTGCCTGGGATTTCCGGTGGTGGTGGTGGTGGTGGTGGTGGTGGTGGTGGTGGTGGTGGTGGTGGT
GAACTGTGGGGCATCCACTTGATGCCCCAAGAATCCTAGTAGAATGTTTACTACCAAATGGGATGATAGTACTTTAGAATGCCTCCGT
GAGGCTACGTTAATAACGATAAAGCATGAACATTTTAAAGAAGCAAGAAAATACCCTCTCCATCAACTTCTTCAAGATGAATCTTCTTAC
ATTTTCGTAAGTGTACCAGAAAGCAGAAAGGGAAGAATTTTTTGATGAAACAAGACGACTTTGTGACCTTCGGCTTTTTCAACCCCTTT
TTAAAAGTAATTGAACAGTAGGCAACCGTGAAGAAAAGATCCTCAATCGAGAAAATGGTTTTGCTATCGGCATGCCAGTGTGTGAATTC
GATATGGTTAAAGATCCAGAAGTACAGGACTTCCGAAGAAATATTTCTCAATGTTGTAAAGAAGCTGTGGATCTTAGGGATCTTAATTCA
CCTCATAGTAGAAGCAATGTATGTTTATCCTCCAAATGTAGAATCTTACCAGAACTGCCAAAGCACATATATAAATAAATTGGATAAAGGG
CAAATAATAGTGGTGATTTGGGTAATAGTTTCTCCAAATAATGACAAAACAGAAGTATACTCTGAAAATCAACCATGACTGTGTGCCAGAA
CAAGTAATTTGCTGAAGCAATCAGGAAAAAACTCGAAGTATGTTGCTATCATCTGAACAATAAACTCTGTGTTTTAGAATATCAGGGC
AAGTATATTTTAAAGTGTGTGGATGTGATGAATACTTCTAGAAAAATATCCTCTGAGTCAGTATAAGTATATAAGAAGCTGTATAATG
CTTGGGAGGATGCCCAATTTGATGCTGATGGCTAAAGAAAGCCTCTATTTCTCAACTGCCAATGGACTGTTTTACAATGCCATCATATTC
AGACGCATCTCCACAGCTACGCCATATATGAATGGAGAAACATCTACAAAATCCCTTTGGGTATAAATAAGTGCACCTCAGAATAAAAAAT
CTTTGTGCAACCTATGTGAATGTAATAATTCGAGACATTGACAAGATTTATGTTGCAACAGGTATCTACCATGGAGGAGAACCCTTATGT
GATAATGTGAACACTCAAAGAGTACCTTGTTCCAATCCCAGGTGGAATGAATGGCTGAATTACGATATATACATTCCTGATCTTCTCTCGT
GCTGCTCGACTTTGCCTTTCCATTTGTTCTGTTAAAGGCCGAAAGGGTGTAAAGAGGAAACACTGTCCATTTGGCCTGGGGAAATATAAAC
TTGTTTGATTACACAGATACTCTAGTATCTGAAAAATGGCTTTGAATCTTTGGCCAGTACCTCATGGACTAGAAGATTTGCTGAACCCCT
ATTGGTGTACTGGATCAAATCCAAATAAAGAAACTCCATGTTTAGAGTTGGAGTTTACTGAGTGGTTCAGCAGTGTGGTAAAGTTTCCAGAT
ATGTCAGTGATTGAAGAGCATGCCAATTTGGTCTGTATCCCGTGAAGCAGGATTTAGTTATTTCCCATGCAGGACTGAGTAACAGACTAGCT
AGAGACAATGAATTAAGAGAAAATGATAAAGAACAGCTCCGAGCAATTTGTACACGAGATCCTCTATCTGAAATCACTGAGCAAGAGAAA
GATTTTCTGTGGAGCCACAGACACTATTGTGTAACATATCCCCGAAATTTACCCAAATGCTTCTGTCTGTTAAATGGAACCTTAGAGAT
GAAGTAGCTCAGATGTACTGCTTGGTAAAAGATTTGGCCTCCAATCAAGCCTGAACAGGCTATGGAGCTTCTGGACTGCAATTTACCAGAT
CCTATGGTTCCGAGTTTTGCTGTTCCGGTCTTAGAAAAATATTTAACAGATGACAACTTTCTCAGTACCTAATTCAGCTAGTACAGGTA
CTAAAATATGAACAGTATTTGGATAACCTGCTTGTGAGATTTTTACTCAAAAAGCGTTAACTAATCAAAGGATCCGGTCACTTTTTCTTT
TGGCATTAAAATCTGAGATGCACAATAAAACAGTTAGTCAGAGGTTTGGCCTGCTTTTGGAGTCTTATGCGCTGCATGTGGGATGTAT
CTGAAGCACCTTAATAGGCAAGTTGAGGCTATGGAAAAGCTCATTAACTTGACTGACATTTCTCAAACAAGAGAAGAAGGATGAAACACAA
AAGGTACAGATGAAGTTTTTAGTTGAGCAAATGCGGCGACAGATTTTCATGGATGCTCTCCAGGGCTTTCTGTCTCTCTAAACCCCTGCT
CATCAGCTGGGAAATCTCAGGCTGAAGAGTGTGCAATATGTCTTCTGCAAAAAGGCCACTGTGGTGAATTTGGGAGAACCAGACATC
ATGTCAGAATTACTCTTTTCAAGAACAATGAGATCATCTTTAAAAATGGGGATGATTTATGGCAAGATATGCTAACCCCTCAGATTATTCGC
ATTATGGAATAATCTGGCAAAAATCAAGGCTTGTGATCTCGAATGTTACCTTATGGATGTCTGTCAATCGGTGACTGTGTGGACTTATC
GAGGTGGTGAAGAAATCTCACACTATAATGCAGATTCAGTGTAAAGGAGGCTGAAAGGTGCACTGCAGTTTAAACAGCCACACACTCCAT
CAGTGGCTCAAAGACAAGAAACAGGGGGAAATATATGATGCGGCCATCGATTTGTTTACAGATCATGTGCTGGATATTGTGTTGCCACC
TTCATTTTGGGAATTTGGAGATCGTCACAATAGTAATATCATGGTTAAAGATGATGGACAACCTGTTTCATATAGATTTTGGACACTTTTTG
GATCACAAGAAGAAAAAATTTGGTTATAAACGAGAGCGCGCTTGTGTTTGGACACAAGATTTCTTAATAGTGATTAGTAAAGGAGCC
CAAGAATGCACAAGACAAGAGAATTTGAGAGGTTTCAAGAGATGTGTTACAAGGCTTATCTAGCTATTCCGAGCATGCCAATCTCTTC
ATAAATCTTTTCTCAATGATGCTTGGCCCTGGAATGCCAGAACTGCAATCTTTTGATGATATTGCATACATTCGAAAGACCCCTAGCTTTA
GATAAACTGAGCAAGAGGCTTTGGAGTATTTTCATGAAACAAATGAATGATGCACACCATGGTGGCTGGACAACAAAATGGATTGGATC
TTCACACAATTAACAGCATGCATTGAACCCCGGGGAGAGCAGAAGCTGATTTCCGAGGAGGACCTGAACTGA
```

B



Supplementary figure 3: DNA sequence and plasmid map of pAAV6-cTnT-iSH2p110-SpA. A) DNA sequence of iSH2p110. B) Plasmid map of pAAV6-cTnT-iSH2p110-SpA. AMPr: ampicillin resistance gene, cTnT-477: cardiac troponin T promoter, ITR: inverted terminal repeat, SpA: synthetic polyadenylation sequence.

Generation of AAV6-cTnT-iSH2-HA-SpA & AAV6-CMV-iSH2-HA-SpA from AAV-cTnT-MCS-SpA & AAV-CMV-MCS-SpA

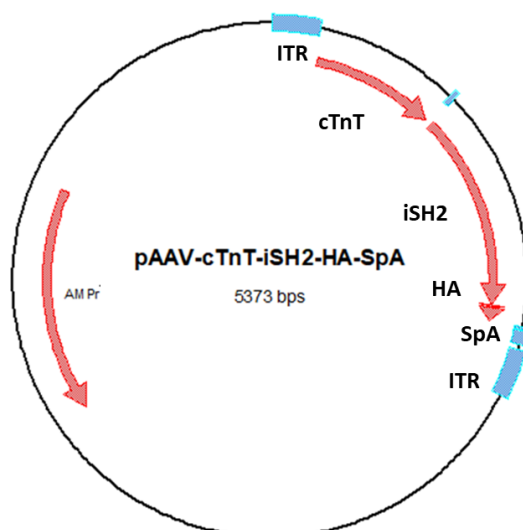
iSH2I-HA (iSH2) construct described in (Klippel *et al.* (1993) *Mol Cell Biol* 13(9): 5560-5566) was cloned into both pAAV6-CMV-MCS-SpA and pAAV6-cTnT-MCS-SpA. Klippel *et al.* generated their constructs from mouse p85 α cDNA. They made two iSH2 constructs: iSH2I and iSH2II. iSH2II was slightly longer than iSH2I. Association of iSH2I or iSH2II with p110 α induced a comparable increase in PI3K activity (same as full length p85). Klippel *et al.* used the iSH2I construct for their subsequent experiments and included a PGG hinge and a HA-tag (iSH2 domain spans amino acids 434-599 of mouse p85 α). Mouse iSH2 with a PGG hinge and a HA-tag sequence at the C-terminus was cloned into pAAV6-CMV-MCS-SpA & pAAV6-cTnT-MCS-SpA using HindIII and SpeI restriction sites. Chemocompetent cells were transformed with DNA from the ligation reactions and colonies screened for plasmids containing the inserted DNA construct by digesting with enzymes.

A

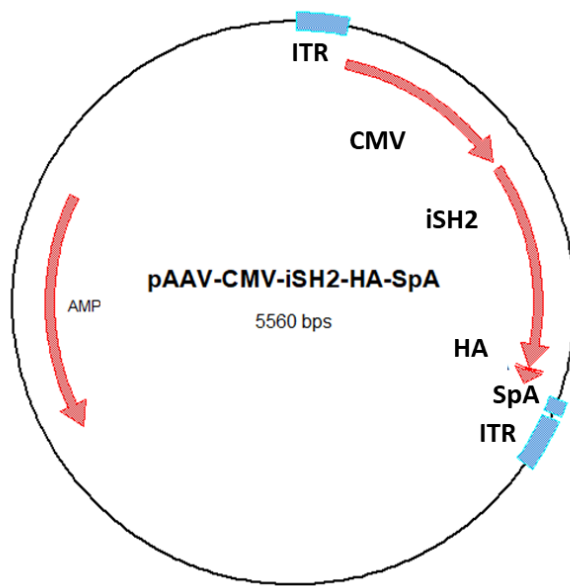
```

AAGCTTGCCACCATGGCTCAGTACAACCCCAAGCTGGATGTGAAGTTGCTCTACCCAGTGTCCAAATACCAG
CAGGATCAAGTTGTCAAAGAAGATAATATTGAAGCTGTAGGGAAAAAATTACATGAATATAAATACTCAATTT
CAAGAAAAAAGTCGGGAATATGATAGATTATATGAGGAGTACACCCGTACTTCCCAGGAAATCCAAATGAAA
AGAACGGCTATCGAAGCATTTAATGAAACCATAAAAAATATTTGAAGAACAATGCCAAACCCAGGAGCGGTAC
AGCAAAGAATACATAGAGAAGTTTAAACGCGAAGGCAACGAGAAAAGAAATTCAAAGGATTATGCATAACCAT
GATAAGCTGAAGTCGCGTATCAGTGAGATCATTGACAGTAGGAGGAGGTTGGAAGAAGACTTGAAGAAGCAG
GCAGCTGAGTACCGAGAGATCGACAAACGCATGAACAGTATTAAGCCGGACCTCATCCAGTTGAGAAAAGACA
AGAGACCAATACTTGATGTGGCTGACGCAGAAAGGTGTGCGGCAGAAGAAGCTGAACGAGTGGCTGGGGAAT
GAAAATACCGAAGATCAATACTCCCTGGTAGAAGATGATGAGGATTTGCCCCACCATGACGAGAAGACGTGG
AATGTCGGGAGCAGCAACCGAAACAAAGCGGAGAACCTATTGCGAGGGAAGCGAGACGGCACTTTCCTTGTC
CGGGAGAGCAGTAAGCAGGGCTGCTATGCCTGCTCCGTAGTGGTACCCGGGGGAAGCTATCCTTATGACGTG
CCTGACTATGCCAGCCTGGGAGGACCTTCTGAACTAGT
    
```

B



C



Supplementary figure 4. iSH2 DNA sequence and plasmid map of pAAV6-CMV-iSH2-SpA and pAAV6-cTnT-iSH2-SpA. A) The DNA sequence of iSH2 (grey) with a Kozak sequence (yellow), a PGG hinge (red) and HA-tag (blue) to be inserted into pAAV6-MCS-SpA plasmids. The sequence was flanked by HindIII (magenta) and SpeI (green) restriction sites for cloning into pAAV6-MCS-SpA plasmids to form (B) pAAV6-cTnT-iSH2-HA-SpA and (C) pAAV6-CMV-iSH2-HA-SpA. AMPr: ampicillin resistance gene, cTnT-477: cardiac troponin T promoter, ITR: inverted terminal repeat, SpA: synthetic polyadenylation sequence, iSH2: iSH2 sequence, CMV: Cytomeglovirus promoter.

Generation of AAV6-cTnT-IVS2-iSH2-HA-SpA & AAV6-CMV-IVS2-iSH2-HA-SpA from AAV-cTnT-MCS-SpA & AAV-CMV-MCS-SpA

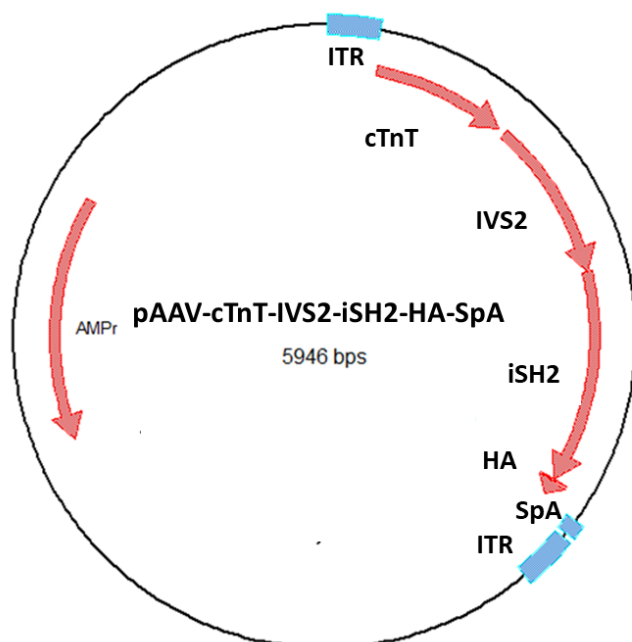
AAV6-cTnT-IVS2-iSH2-HA-SpA and AAV6-CMV-IVS2-iSH2-HA-SpA are identical to the constructs described in section 4.0 except for the addition of an IVS2.

A

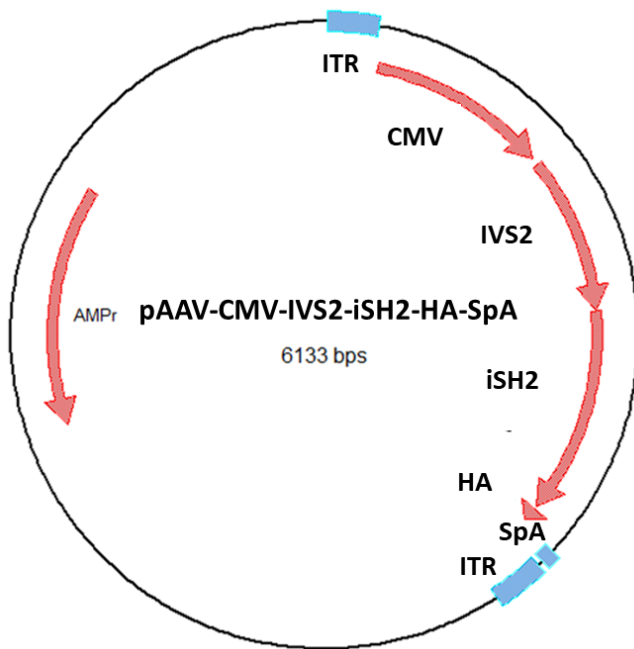
```

AAGCTTgtgagtttggggaccottgattgttctttctttttcgcotattgtaaaattcatggttatatggaggg
ggcaaagttttcaggggtgttgttttagaatgggaagatgtccottgtatcaccatggaccctcatgataattt
tgtttctttcactttctactctgttgacaaccattgtctcctcttattttctttttcattttctgtaactttt
tcgttaaacttttagcttgcaatttgaacgaatttttaaattcacttttgtttatttgtcagattgtaagtae
tttctctaatacactttttttcaaggcaatcagggatatattatattgtacttcagcacagtttttagagaaca
attgttataaataaatgataaggtagaataatttctgcatataaattctggctggcgtggaaatattcttatt
ggtagaacaactacatcctggtcacatcctgcctttctctttatggttacaatgatatacactgtttgag
atgaggataaaaatactctgagtccaaaccggggccctctgctaaccatgttcatgccttcttcttttttcta
cagGCCACCATGGCTCAGTACAACCCCAAGCTGGATGTGAAGTTGCTCTACCCAGTGTCCAAATACCAGCAG
GATCAAGTTGTCAAAGAAGATAATATTGAAGCTGTAGGGAAAAAATTACATGAATATAATACTCAATTTCAA
GAAAAAAGTCGGGAATATGATAGATTATATGAGGAGTACACCCGTACTIONCCAGGAAATCCAAATGAAAAGA
ACGGCTATCGAAGCATTTAATGAAACCATAAAAAATATTTGAAGAACAATGCCAAACCCAGGAGCGGTACAGC
AAAGAATACATAGAGAAGTTTAAACCGGAAGGCAACGAGAAAAGAAATTCAAAGGATTATGCATAACCATGAT
AAGCTGAAGTCGCGTATCAGTGAGATCATTGACAGTAGGAGGAGGTTGGAAGAAGACTTGAAGAAGCAGGCA
GCTGAGTACCGAGAGATCGACAAACGCATGAACAGTATTAAGCCGGACCTCATCCAGTTGAGAAAAGACAAGA
GACCAATACTTGATGTGGCTGACGCAGAAAGGTGTGCGGCAGAAGAAGCTGAACGAGTGGCTGGGGAATGAA
AATACCGAAGATCAATACTCCCTGGTAGAAGATGATGAGGATTTGCCCCACCATGACGAGAAGACGTGGAAT
GTCGGGAGCAGCAACCGAAACAAAGCGGAGAACCTATTGCGAGGGAAGCGAGACGGCACTTTCCTTGCCGG
GAGAGCAGTAAGCAGGGCTGCTATGCCTGCTCCGTAGTGGAACCCGGGGAAGCTATCCTTATGACGTGCCT
GACTATGCCAGCCTGGGAGGACCTTCCTGAAGTAGT
    
```

B

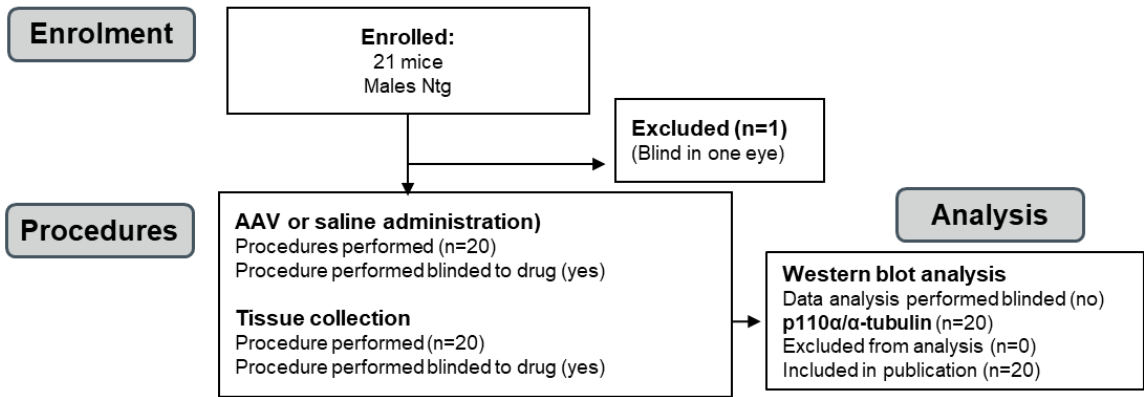


C

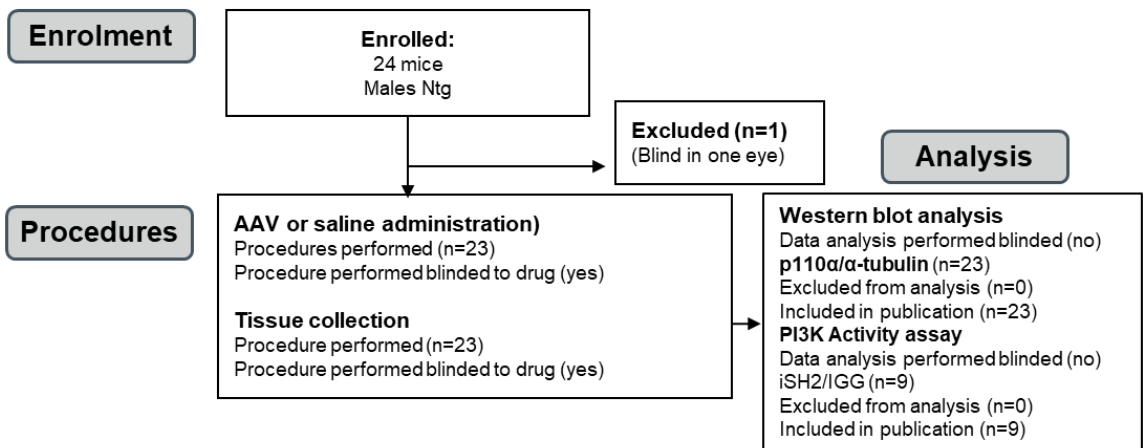


Supplementary figure 5. IVS2-iSH2 DNA sequence and plasmid map of pAAV6-CMV-IVS2-iSH2-SpA and pAAV6-cTnT-IVS2-iSH2-SpA. A) The DNA sequence of IVS2 (teal), iSH2 (grey) with a Kozak sequence (yellow), a PGG hinge (red) and HA-tag (blue) to be inserted into pAAV6-MCS-SpA plasmids. The sequence was flanked by HindIII (magenta) and SpeI (green) restriction sites for cloning into pAAV6-MCS-SpA plasmids to form (B) pAAV6-cTnT-iSH2-HA-SpA and (C) pAAV6-CMV-iSH2-HA-SpA. AMPr: ampicillin resistance gene, cTnT-477: cardiac troponin T promoter, ITR: inverted terminal repeat, SpA: synthetic polyadenylation sequence, iSH2: iSH2 sequence, CMV: Cytomeglovirus promoter.

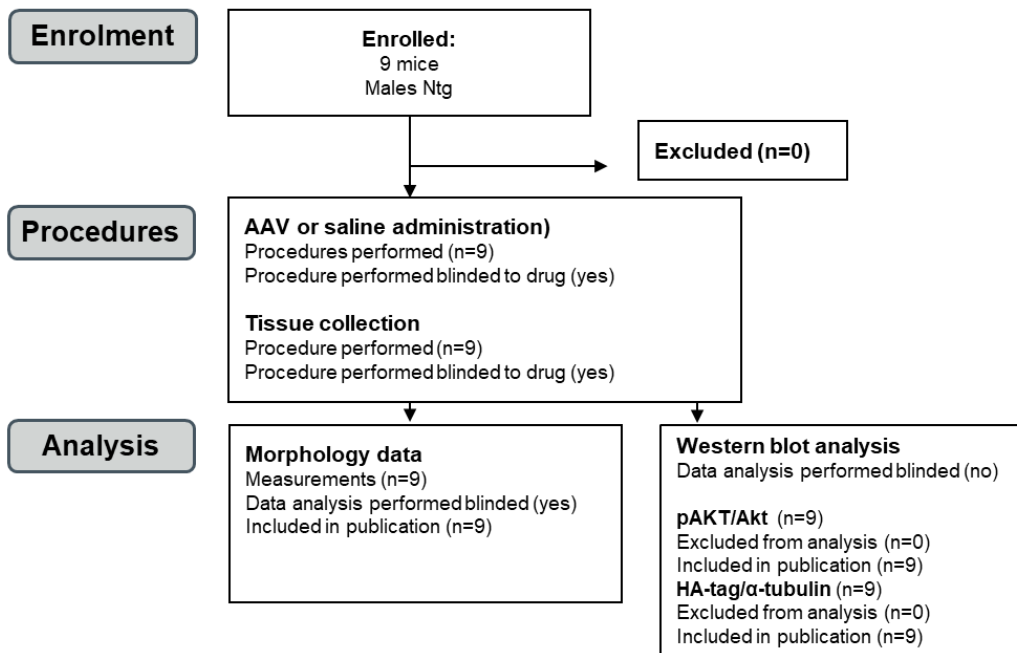
**Consolidated Standards of Animal Experiment Reporting (CONSAERT):
AAV6-cTnT-caPI3K Dose response cohort**



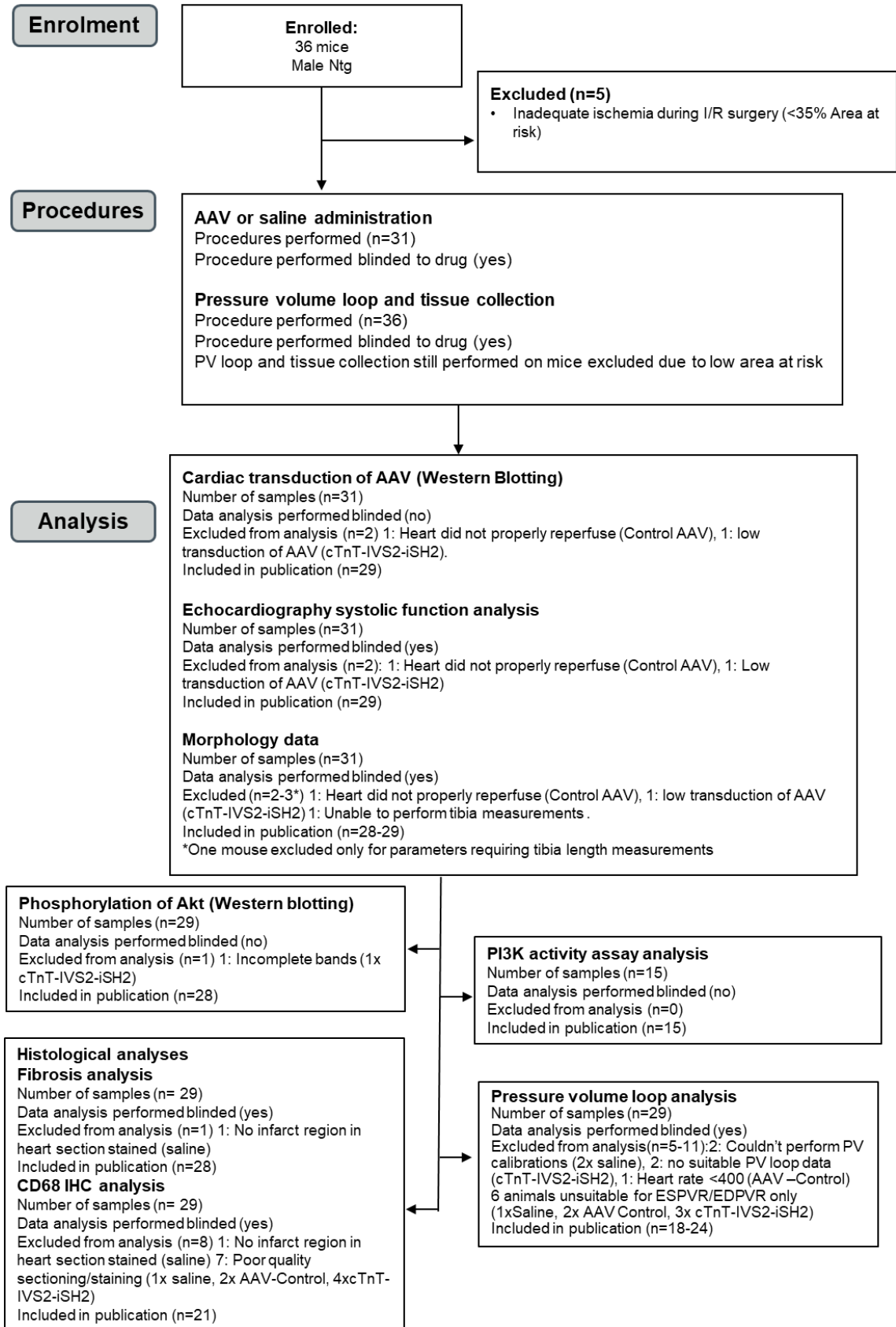
AAV6-CMV-IVS2-iSH2 Dose response cohort



AAV6-cTnT-IVS2-ISH2 healthy mouse cohort



AAV6-cTnT-IVS2-ISH2 I/R mouse cohort

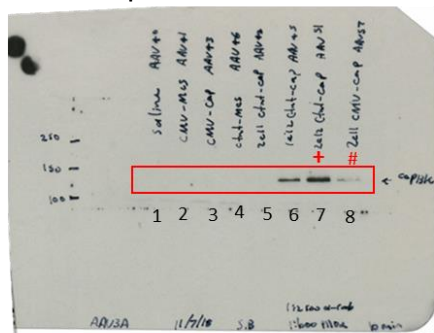


Western blotting raw blots

Supplementary figure 6

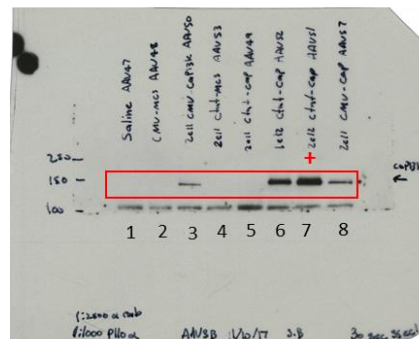
AAV6-cTnT-caPI3K Dose response cohort – Western Blots 1-4 p110α / α-tubulin probed for p110α

WB1 - p110α



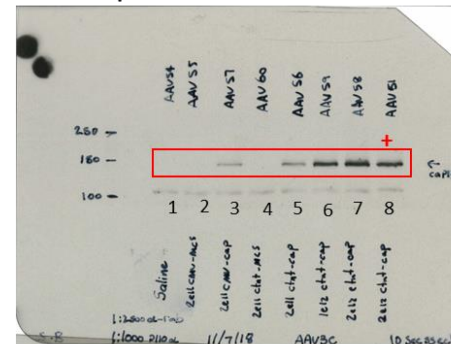
1	AAV40	Saline
2	AAV41	2 e11 CMV-MCS
3	AAV43	2e11 CMV_caPI3K
4	AAV46	2 e11 ctnt_MCS
5	AAV42	2e11 ctnt_caPI3K
6	AAV45	1e12 ctnt_caPI3K
7	AAV51	2e12 ctnt_caPI3K
8	AAV57	2e11 CMV_caPI3K

WB2 - p110α

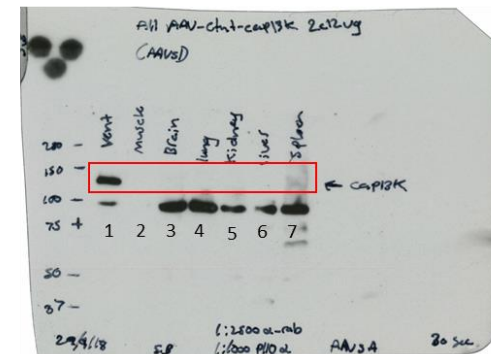


1	AAV47	Saline
2	AAV48	CMV-MCS
3	AAV50	2e11 CMV_caPI3K
4	AAV53	2e11 ctnt_MCS
5	AAV49	2e11 ctnt_caPI3K
6	AAV52	1e12 ctnt_caPI3K
7	AAV51	2e12 ctnt_caPI3K
8	AAV57	2e11 CMV_caPI3K

WB3 - p110α



1	AAV54	Saline
2	AAV55	CMV_MCS
3	AAV57	2e11 CMV_caPI3K
4	AAV60	2e11 ctnt_MCS
5	AAV56	2e11 ctnt_caPI3K
6	AAV59	1e12 ctnt_caPI3K
7	AAV58	2e12 ctnt_caPI3K
8	AAV51	2e12 ctnt_caPI3K



	AAV51	2e12 ctnt-caPI3K
1		Ventricle
2		Skeletal Muscle
3		Brain
4		Lung
5		Kidney
6		Liver
7		Spleen

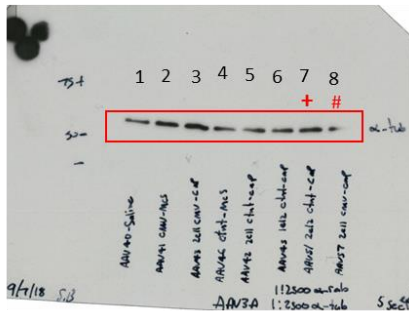
+ Common sample across blots

Sample excluded from blot due to incomplete band but repeated on WB2 & WB3 (only included once)

Supplementary figure 7

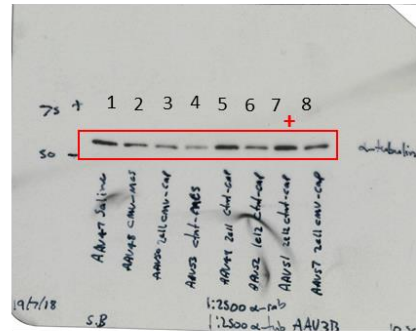
AAV6-cTnT-caPI3K Dose response cohort – Western Blots 1-4 p110 α / α -tubulin probed for α -tubulin

WB1 – α -tubulin



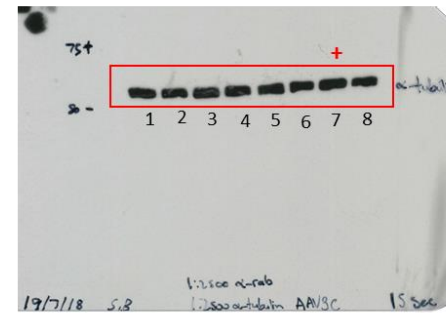
1	AAV40	Saline
2	AAV41	2e11 CMV-MCS
3	AAV43	2e11 CMV_caPI3K
4	AAV46	2e11 cntn_MCS
5	AAV42	2e11 cntn_caPI3K
6	AAV45	1e12 cntn_caPI3K
7	AAV51	2e12 cntn_caPI3K
8	AAV57	2e11 CMV_caPI3K

WB2 - α -tubulin



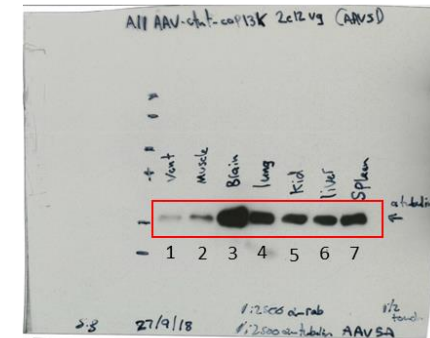
1	AAV47	Saline
2	AAV48	CMV-MCS
3	AAV50	2e11 CMV_caPI3K
4	AAV53	2e11 cntn_MCS
5	AAV49	2e11 cntn_caPI3K
6	AAV52	1e12 cntn_caPI3K
7	AAV51	2e12 cntn_caPI3K
8	AAV57	2e11 CMV_caPI3K

WB3 - α -tubulin



1	AAV54	Saline
2	AAV55	CMV_MCS
3	AAV57	2e11 CMV_caPI3K
4	AAV60	2e11 cntn_MCS
5	AAV56	2e11 cntn_caPI3K
6	AAV59	1e12 cntn_caPI3K
7	AAV58	2e12 cntn_caPI3K
8	AAV51	2e12 cntn_caPI3K

WB4 - α -tubulin
(non-cardiac tissue)



	AAV51	2e12 cntn-caPI3K
1		Ventricle
2		Skeletal Muscle
3		Brain
4		Lung
5		Kidney
6		Liver
7		Spleen

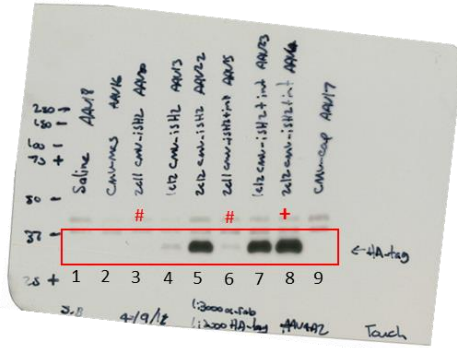
+ Common sample across blots

Sample excluded from blot due to incomplete band but repeated on WB2

Supplementary figure 8

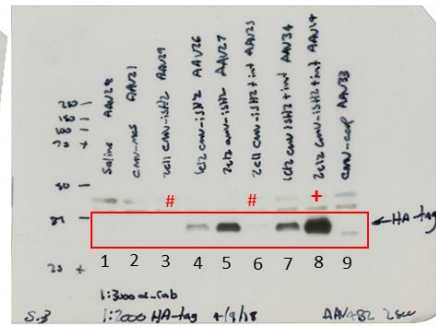
AAV6-CMV-iSH2/IVS2-iSH2 Dose response cohort (2x10¹¹ 1x10¹², 2x10¹²) - Western Blots 1-4 HA-tag (iSH2) / α-tubulin probed for HA-tag

WB1 – HA-Tag (iSH2)



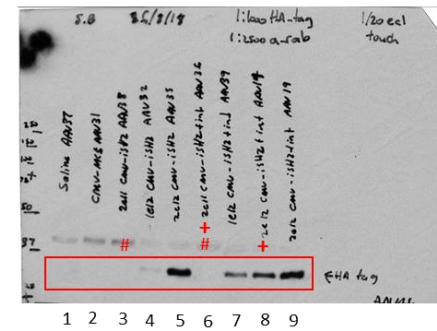
1	AAV18	Saline
2	AAV16	2e11 CMV_MCS
3	AAV20	2e11 CMV-iSH2
4	AAV13	1e12 CMV-iSH2
5	AAV22	2e12 CMV-iSH2
6	AAV15	2e11 CMV-IVS2-iSH2
7	AAV23	1e12 CMV-IVS2-iSH2
8	AAV14	2e12 CMV-IVS2-iSH2
9	AAV17	2e11 CMV-caPI3K

WB2 - HA-Tag (iSH2)



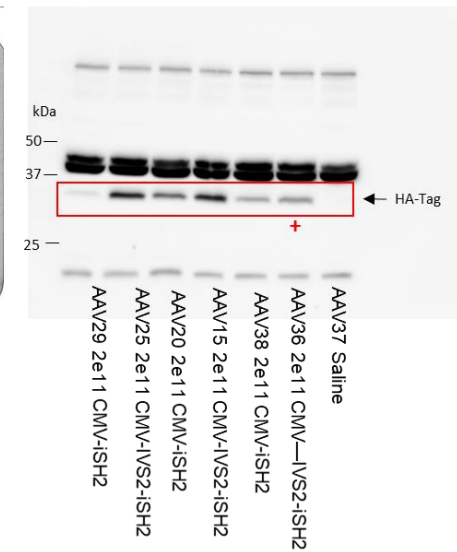
1	AAV28	Saline
2	AAV21	2e11 CMV_MCS
3	AAV29	2e11 CMV-iSH2
4	AAV26	1e12 CMV-iSH2
5	AAV27	2e12 CMV-iSH2
6	AAV25	2e11 CMV-IVS2-iSH2
7	AAV34	1e12 CMV-IVS2-iSH2
8	AAV14	2e12 CMV-IVS2-iSH2
9	AAV33	2e11 CMV-caPI3K

WB3 HA-Tag (iSH2)



1	AAV37	Saline
2	AAV31	2e11 CMV_MCS
3	AAV38	2e11 CMV-iSH2
4	AAV32	1e12 CMV-iSH2
5	AAV35	2e12 CMV-iSH2
6	AAV36	2e11 CMV-IVS2-iSH2
7	AAV39	1e12 CMV-IVS2-iSH2
8	AAV14	2e12 CMV-IVS2-iSH2
9	AAV19	2e12 CMV-IVS2-iSH2

WB4 HA-Tag (iSH2, low dose only)

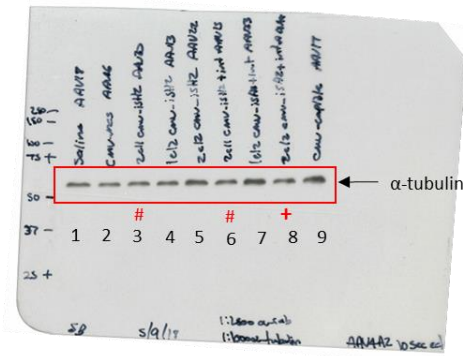


- + Common sample across blots
- # Sample excluded from blot due to low expression but repeated on WB4

Supplementary figure 9

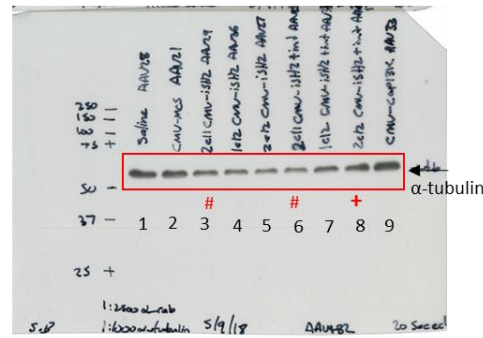
AAV6-CMV-iSH2/IVS2-iSH2 Dose response cohort (2×10^{11} 1×10^{12} , 2×10^{12}) – Western Blots 1-4 HA-tag (iSH2) / α -tubulin probed for α -tubulin

WB1 – α -tubulin



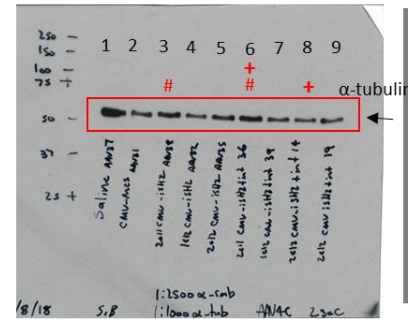
1	AAV18	Saline
2	AAV16	2e11 CMV_MCS
3	AAV20	2e11 CMV-iSH2
4	AAV13	1e12 CMV-iSH2
5	AAV22	2e12 CMV-iSH2
6	AAV15	2e11 CMV-IVS2-iSH2
7	AAV23	1e12 CMV-IVS2-iSH2
8	AAV14	2e12 CMV-IVS2-iSH2
9	AAV17	2e11 CMV-caPI3K

WB2 – α -tubulin



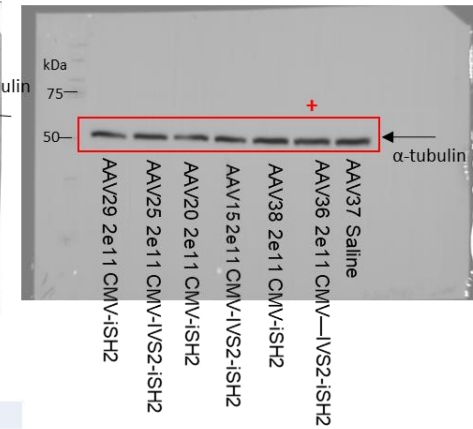
1	AAV28	Saline
2	AAV21	2e11 CMV_MCS
3	AAV29	2e11 CMV-iSH2
4	AAV26	1e12 CMV-iSH2
5	AAV27	2e12 CMV-iSH2
6	AAV25	2e11 CMV-IVS2-iSH2
7	AAV34	1e12 CMV-IVS2-iSH2
8	AAV14	2e12 CMV-IVS2-iSH2
9	AAV33	2e11 CMV-caPI3K

WB3 – α -tubulin



1	AAV37	Saline
2	AAV31	2e11 CMV_MCS
3	AAV38	2e11 CMV-iSH2
4	AAV32	1e12 CMV-iSH2
5	AAV35	2e12 CMV-iSH2
6	AAV36	2e11 CMV-IVS2-iSH2
7	AAV39	1e12 CMV-IVS2-iSH2
8	AAV14	2e12 CMV-IVS2-iSH2
9	AAV19	2e12 CMV-IVS2-iSH2

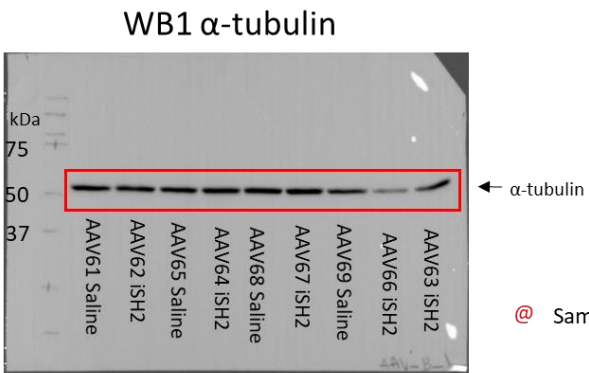
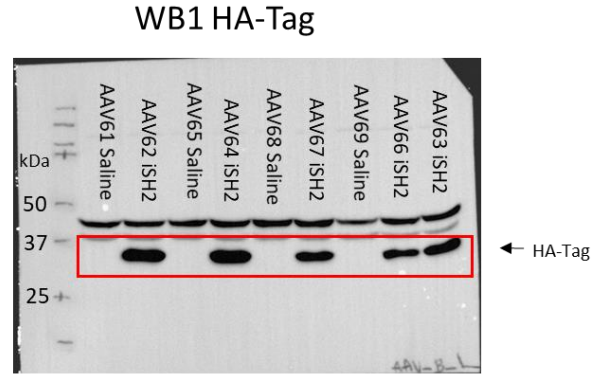
WB4 – α -tubulin (low dose only)



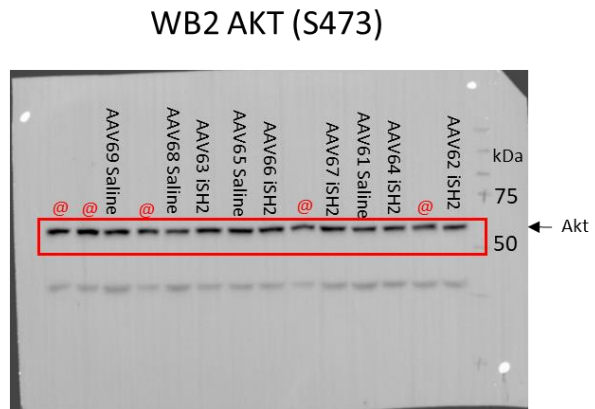
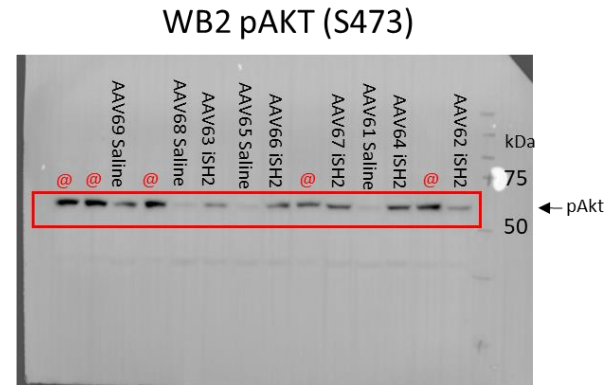
- + Common sample across blots
- # Sample excluded from blot due to low expression but repeated in WB4

Supplementary figure 10

**2x10¹² AAV6-cTnT-IVS2-iSH2 healthy cohort –
Western Blot 1 HA-tag (iSH2) / α -tubulin**



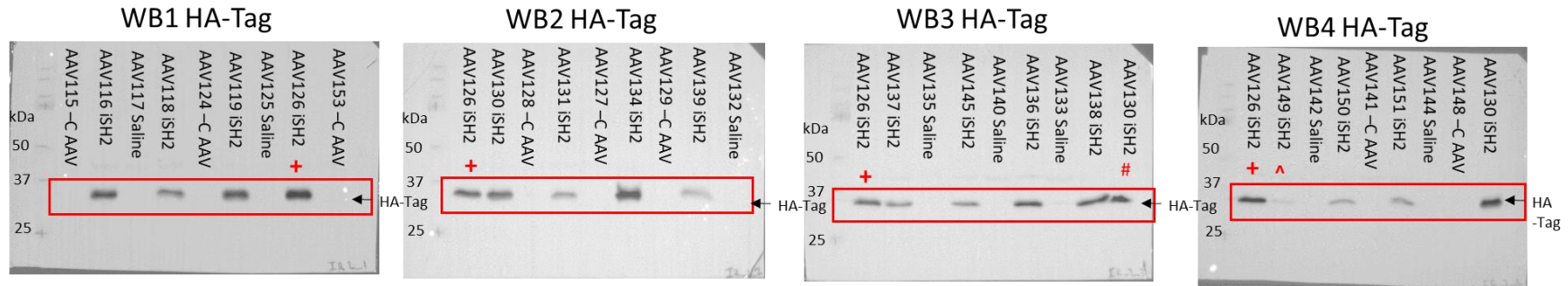
**2x10¹² AAV6-cTnT-IVS2-iSH2 healthy cohort –
Western Blot 2 pAkt/Akt**



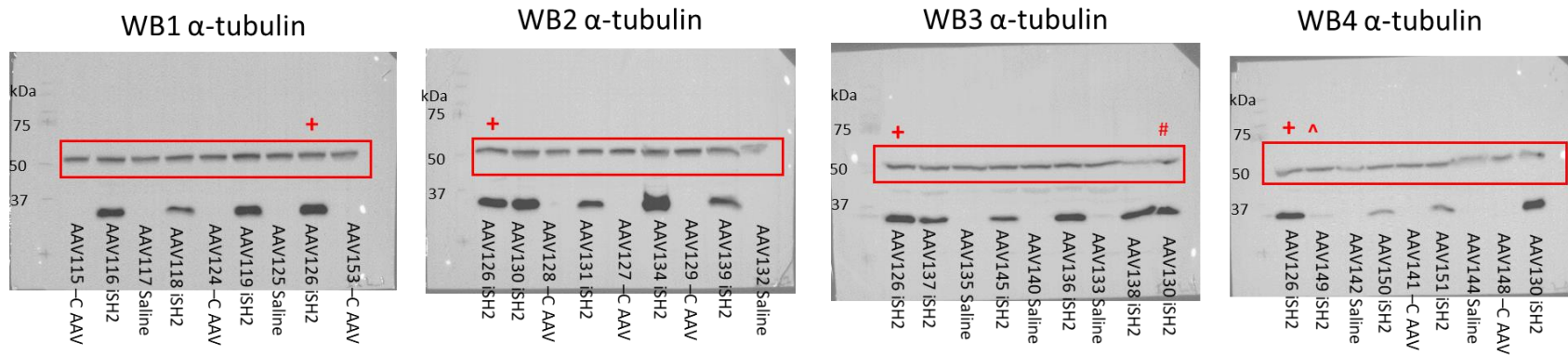
@ Sample not relevant to study

Supplementary figure 11

2x10¹² AAV6-cTnT-IVS2-iSH2 I/R cohort – Western Blots 1-4 HA-tag (iSH2) / α-tubulin probed for HA-tag



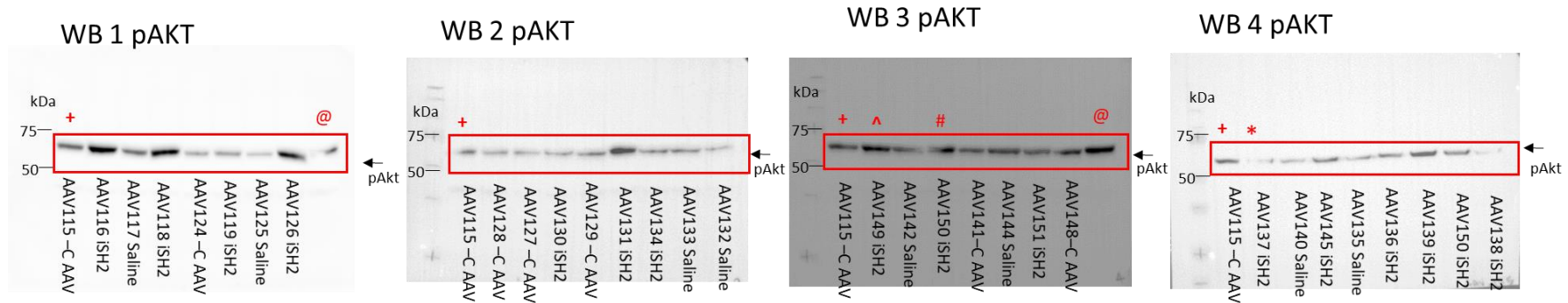
2x10¹² AAV6-cTnT-IVS2-iSH2 I/R cohort – Western Blots 1-4 HA-tag (iSH2) / α-tubulin probed for α-tubulin



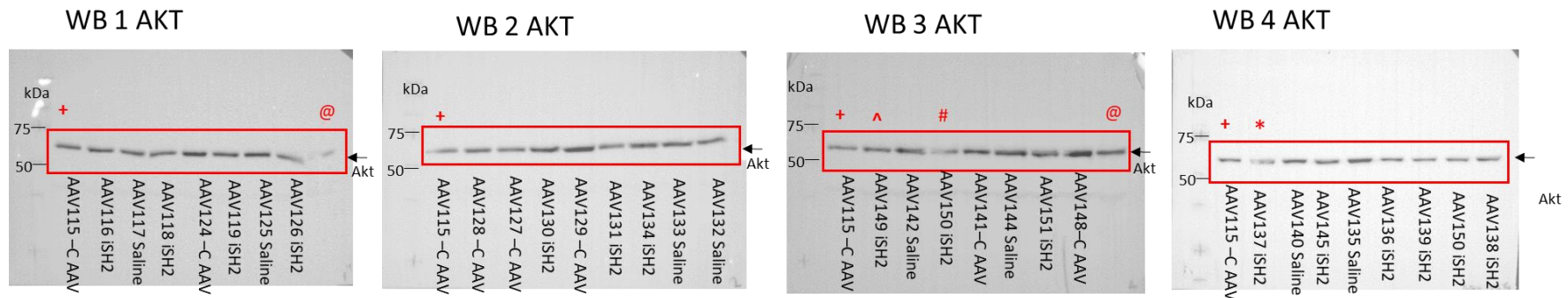
- # Sample excluded from blot but repeated on WB4
- + Common sample across blots
- ^ Mouse excluded from I/R study completely due to very low HA expression

Supplementary figure 12

2x10¹² AAV6-cTnT-IVS2-iSH2 I/R cohort – Western Blots 1-4 pAkt/ Akt probed for pAkt



2x10¹² AAV6-cTnT-IVS2-iSH2 I/R cohort – Western Blots 1-4 pAkt/Akt probed Akt

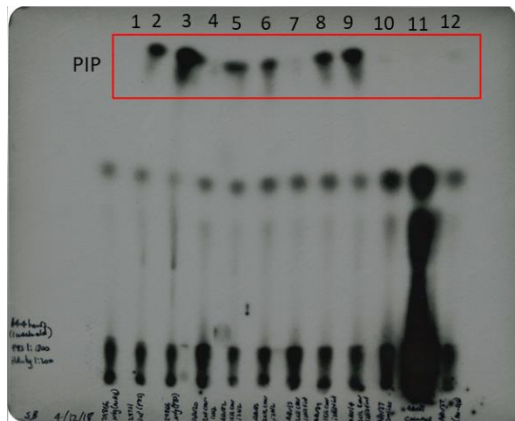


- * Sample excluded entirely due to incomplete band
- # Sample excluded from blot but repeated on WB 4
- @ Sample not relevant to study
- + Common sample across blots
- ^ Mouse excluded from I/R study completely due to very low HA expression

PI3K Activity assay raw blots

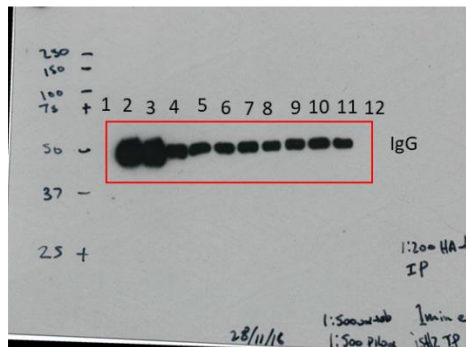
Supplementary figure 13

Dose response PI3K activity assay 1 – Probing with p85 in lanes 2-3 and Probing with HA-tag: lanes 4-11, No Ab controls: Lanes 1&12

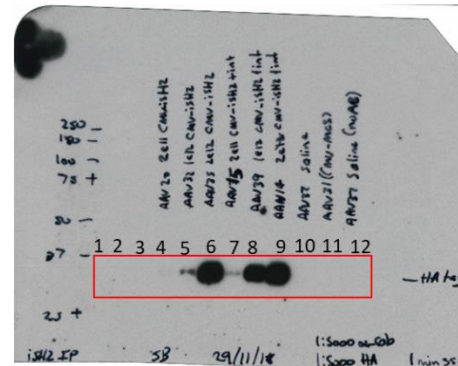


1	29866 (no AB)	Ntg control
2	29751 (P85)	dnP control
3	29866 (P85)	Ntg control
4	AAV20 (Ha-Tag)	2e11 CMV-iSH2
5	AAV32 (Ha-Tag)	1e12 CMV-iSH2
6	AAV35 (Ha-Tag)	2e12 CMV-iSH2
7	AAV15 (Ha-Tag)	2e11 CMV-IVS2-iSH2
8	AAV39 (Ha-Tag)	1e12 CMV-IVS2-iSH2
9	AAV14 (Ha-Tag)	2e12 CMV-IVS2-iSH2
10	AAV37 (Ha-Tag)	Saline
11	AAV31 (Ha-Tag)	CMV_Con
12	AAV37 (No AB)	Saline

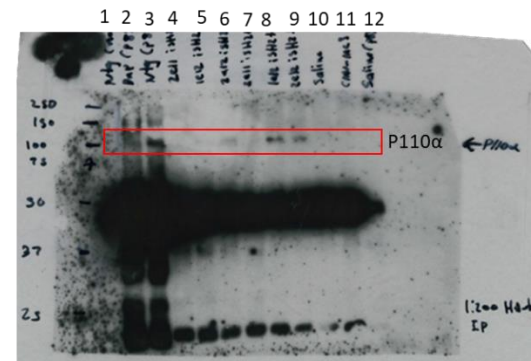
Dose response activity assay 1 – WB: IgG



Dose response activity assay 1 – WB: HA-tag

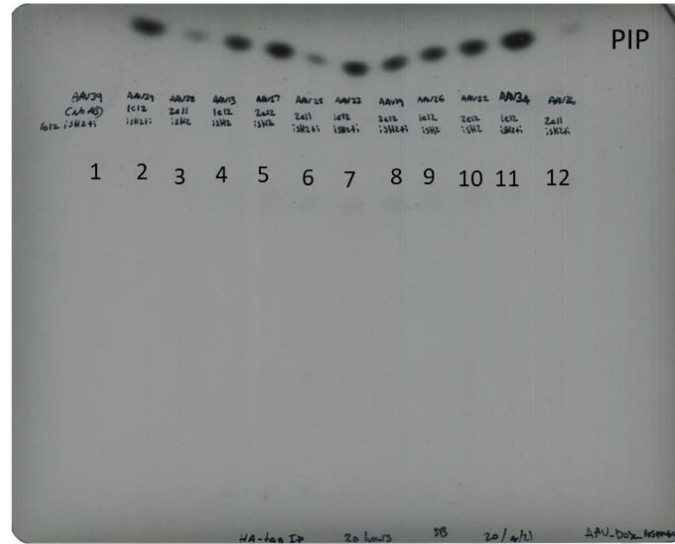


Dose response activity assay 1 – WB: p110α



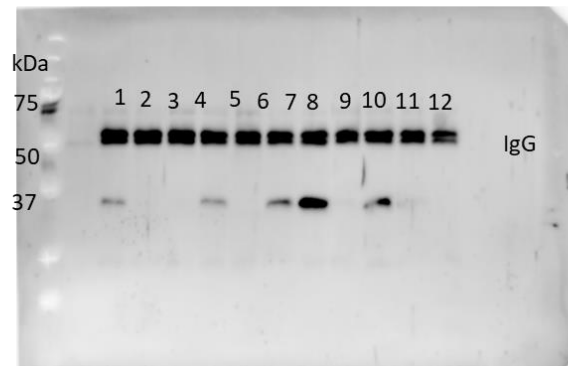
Supplementary figure 14

Dose response PI3K activity assay 2 –Probing with HA-tag: lanes 2-12, No AB control: lane 1



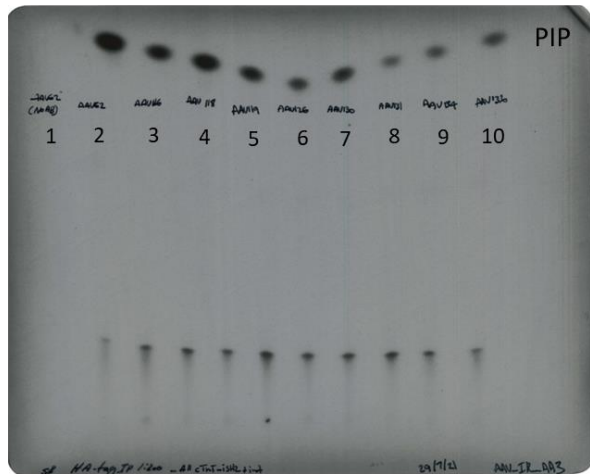
1	AAV39 (no AB)	1e12 CMV-IVS2-iSH2
2	AAV39 (HA-Tag)	1e12 CMV-IVS2-iSH2
3	AAV38 (HA-Tag)	2e11 CMV-iSH2
4	AAV13 (HA-Tag)	1e12 CMV-iSH2
5	AAV27 (HA-Tag)	2e12 CMV-iSH2
6	AAV25 (HA-Tag)	2e11 CMV-IVS2-iSH2
7	AAV23 (HA-Tag)	1e12 CMV-IVS2-iSH2
8	AAV19 (HA-Tag)	2e12 CMV-IVS2-iSH2
9	AAV26 (HA-Tag)	1e12 CMV-iSH2
10	AAV22 (HA-Tag)	2e12 CMV-iSH2
11	AAV34 (HA-Tag)	1e12 CMV-IVS2-iSH2
12	AAV36 (HA-Tag)	2e11 CMV-IVS2-iSH2

Dose response activity assay 2 – WB:IGG

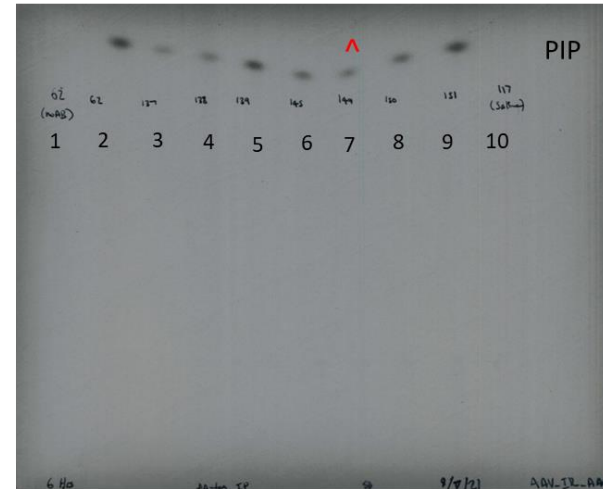


Supplementary figure 15

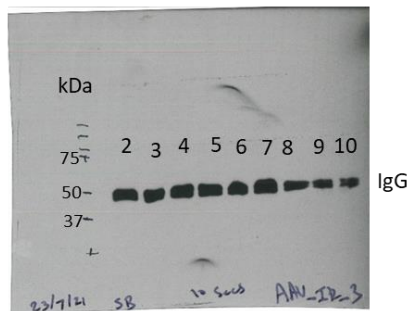
I/R cohort – Activity assay 1 – HA-tag



I/R cohort – Activity assay 2 – HA-tag



I/R cohort – Activity assay 1 – WB: IgG



1	AAV62	iSH2+i (no ab control)
2	AAV62	iSH2+i (common sample)
3	AAV116	cTnT-IVS2-iSH2
4	AAV118	cTnT-IVS2-iSH2
5	AAV119	cTnT-IVS2-iSH2
6	AAV126	cTnT-IVS2-iSH2
7	AAV130	cTnT-IVS2-iSH2
8	AAV131	cTnT-IVS2-iSH2
9	AAV134	cTnT-IVS2-iSH2
10	AAV136	cTnT-IVS2-iSH2

I/R cohort – Activity assay 2 – WB: IgG

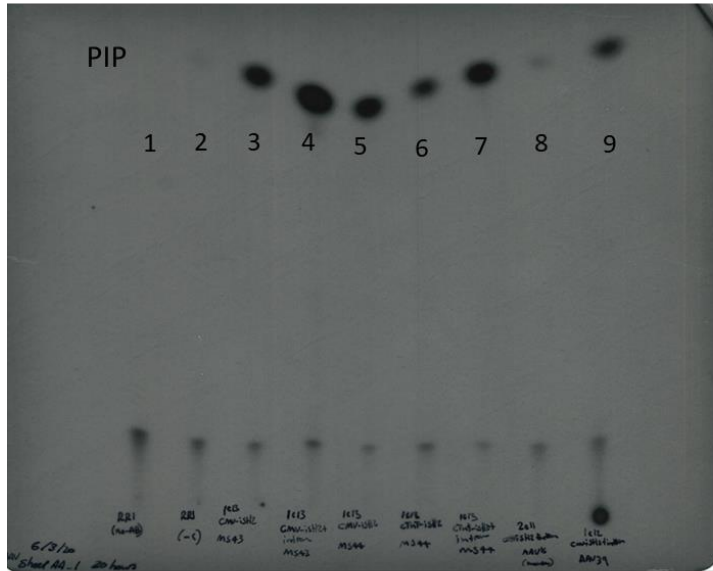


1	AAV62	iSH2+i (no ab control)
2	AAV62	iSH2+i (common sample)
3	AAV137	cTnT-IVS2-iSH2
4	AAV138	cTnT-IVS2-iSH2
5	AAV139	cTnT-IVS2-iSH2
6	AAV145	cTnT-IVS2-iSH2
7	AAV149	cTnT-IVS2-iSH2
8	AAV150	cTnT-IVS2-iSH2
9	AAV151	cTnT-IVS2-iSH2
10	AAV117	Saline

▲ Excluded due to low iSH2-HA expression

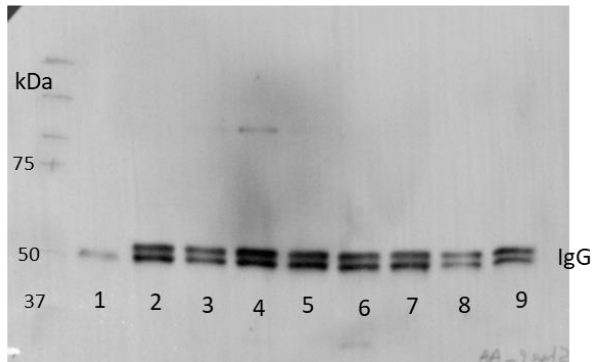
Supplementary figure 16

Sheep 2 and 3 – Activity assay – HA-tag



1	Sheep 2	Remote region1 (no AB)
2	Sheep 2	Remote region1
3	Sheep 2	1e13 AAV-CMV-iSH2
4	Sheep 2	1e13 AAV-CMV-IVS2-iSH2
5	Sheep 3	1e13 AAV-CMV-iSH2
6	Sheep 3	1e13 AAV-cTnT-iSH2
7	Sheep 3	1e13 AAV-cTnT-IVS2-iSH2
8	AAV15 (Mouse)	2e11 AAV-CMV-IVS2-iSH2
9	AAV39 (Mouse)	1e12 AAV-CMV-IVS2-iSH2

Sheep 2 and 3 – Activity assay –WB: IGG



References

1. Weeks KL, Gao X, Du XJ, et al. Phosphoinositide 3-Kinase p110alpha Is a Master Regulator of Exercise-Induced Cardioprotection and PI3K Gene Therapy Rescues Cardiac Dysfunction. *Circ Heart Fail*. Jul 1 2012;5(4):523-534.

Chapter 5

Clusterin is regulated by IGF1-PI3K signaling in the heart: implications for biomarker and drug target discovery, and cardiotoxicity

Chapter 5. Preface

Clusterin is regulated by IGF1–PI3K signaling in the heart: implications for biomarker and drug target discovery, and cardiotoxicity identifies a role of PI3K signalling to regulate clusterin expression. Given some cancer treatments aim to silence clusterin, this manuscript heeds warning of the potential cardiotoxic repercussion of cancer treatments that suppress the expression of genes aligned with the IGF1-PI3K signalling pathway and demonstrates the potential for large profiling data sets to identify if drug targets may have cardiotoxic side effects.

Chapter 5.

Clusterin is regulated by IGF1–PI3K signaling in the heart: implications for biomarker and drug target discovery, and cardiotoxicity

Published in ‘Archives of Toxicology’, March 2020 by S Bass-Stringer, JYY Ooi and JR McMullen.

Archives of Toxicology gives permission to reproduce this work as an academic thesis by the authors.

As equal first author, S Bass-Stringer contributed ~50% to this publication. This included contributions to the conception, experiments, drafting, design and editing.



Clusterin is regulated by IGF1–PI3K signaling in the heart: implications for biomarker and drug target discovery, and cardiotoxicity

Sebastian Bass-Stringer^{1,2} · Jenny Y. Y. Ooi^{1,3} · Julie R. McMullen^{1,2,3,4}

Received: 21 November 2019 / Accepted: 9 March 2020 / Published online: 14 March 2020
© Springer-Verlag GmbH Germany, part of Springer Nature 2020

Abstract

Open-access gene expression data sets provide a useful resource for identifying novel drug targets and biomarkers. The IGF1–PI3K pathway is a critical mediator of physiological cardiac enlargement/hypertrophy and protection. This study arose after mining a gene microarray data set from a previous study that compared heart tissue from cardiac-specific PI3K transgenic mouse models. The top-ranked candidate identified from the microarray data was clusterin. Clusterin has been proposed as a biomarker for multiple diseases including heart failure, and as a cancer drug target. Here, we show that clusterin gene expression is increased in hearts of transgenic mice with increased PI3K and decreased in mice with depressed cardiac PI3K. In vitro, clusterin secretion was elevated in media from neonatal rat ventricular myocytes treated with IGF1. Furthermore, by mining gene expression data from hearts during normal mouse postnatal growth, we also report an increase in clusterin expression with postnatal heart growth. Given we show that clusterin is regulated by the IGF1–PI3K pathway in the heart, and this pathway mediates physiological cardiac hypertrophy and cardioprotection, caution is required when considering clusterin as a biomarker for heart failure and as a cancer target. Mining pre-existing cardiac profiling data sets may be a useful approach to assess whether regulating new drug targets is likely to lead to cardiac damage/toxicity.

Keywords Cardiac hypertrophy · Cancer · Cardiotoxicity · Heart failure · Profiling · Biomarkers

Introduction

Mining profiling data sets can be a useful approach for identifying potential new drug targets and biomarkers. This communication arose after mining a gene microarray data set from a study that compared heart tissue of two cardiac-specific phosphoinositide 3-kinase (PI3K, p110 α) transgenic

mouse models: one with increased PI3K and one with decreased PI3K (Lin et al. 2010). We had previously used profiling data sets from the same study to identify and target PI3K-regulated mRNAs and microRNAs. This approach identified new therapeutic approaches for the failing heart (Bernardo et al. 2012, 2014, 2016, 2018).

In this report, we focus on clusterin. Clusterin is a highly conserved glycoprotein that functions as a molecular chaperone. The two main protein isoforms of clusterin include a secreted heterodimer (termed soluble clusterin, or apolipoprotein J when found associated with lipoproteins) or a truncated form found in intracellular compartments. Alterations in levels of clusterin have been implicated in a wide variety of diseases ranging from neurodegenerative (e.g. Alzheimer's disease) and developmental disorders, tumorigenesis and chemotherapy resistance, inflammatory disorders, and cardiac pathology such as myocardial infarction (MI) and heart failure (Trogakos 2013). Consequently, there has been interest in the use of clusterin as both a biomarker for a variety of diseases, and as a modifiable therapeutic tool.

The goal of this study was to assess whether clusterin is regulated by the insulin-like growth factor 1 (IGF1)–PI3K

Sebastian Bass-Stringer and Jenny Y. Y. Ooi have contributed equally to this work

✉ Julie R. McMullen
julie.mcmullen@baker.edu.au

¹ Cardiac Hypertrophy Laboratory, Baker Heart and Diabetes Institute, 75 Commercial Road, Melbourne, VIC 3004, Australia

² Department of Physiology, Anatomy and Microbiology, La Trobe University, Bundoora, VIC, Australia

³ Department of Diabetes, Central Clinical School, Monash University, VIC, Australia

⁴ Department of Physiology and Department of Medicine Alfred Hospital, Monash University, VIC, Australia

pathway in the heart. PI3K is cardioprotective and responsible for exercise-induced, physiological heart growth (McMullen et al. 2003). The findings described here have important implications when considering clusterin as a biomarker and/or therapeutic target.

Materials and methods

Animal ethics

All animal care and experimentation were conducted in accordance with protocols approved by the Alfred Research Alliance Animal Ethics Committee.

Transcriptomic analysis

Data were mined from our previous microarray data set (GEO accession #:GSE7487) from hearts (ventricles) of constitutively active PI3K (caPI3K) or dominant negative PI3K (dnPI3K) cardiac-specific female adult transgenic mice, and control non-transgenic (Ntg) mice (Lin et al. 2010). caPI3K mice have increased cardiac PI3K activity, larger hearts with preserved heart function (physiological cardiac hypertrophy), and are protected against cardiac pathology and failure in settings of stress (Weeks et al. 2012; Lin et al. 2010). In contrast, dnPI3K mice have reduced cardiac PI3K activity, and are more susceptible to cardiac pathology, dysfunction, heart failure and a common cardiac arrhythmia (i.e. atrial fibrillation, AF) (Lin et al. 2010; Pretorius et al. 2009). The microarray data were ranked by *P* value, and the most differentially expressed genes displaying an inverse relationship in caPI3K and dnPI3K hearts in comparison to Ntg were reviewed. The top candidate was also assessed in an independent published microarray dataset from hearts of female PI3K and IGF1 receptor (IGF1R) transgenic mice (McMullen et al. 2004).

Data were also mined from two independent RNA-sequencing data sets from isolated cardiac myocytes (GEO accession #:GSE95755), and ventricles (GEO accession #:GSE119530) comparing gene expression in myocytes/ventricles from wildtype mice at different time points of post-natal growth (Quaife-Ryan et al. 2017; Talman et al. 2018).

qPCR for validation of microarray data

Total RNA was extracted from mouse ventricles from male and female PI3K transgenic mice using TRIzol® Reagent (Thermo Fisher) according to the manufacturer's instructions. Complimentary DNA was obtained by reverse transcription using a High-Capacity cDNA Reverse Transcription Kit (Thermo Fisher) according to manufacturer's recommendations. Quantitative PCR was performed using

TaqMan Fast Advanced Master Mix and TaqMan probes for Clusterin (Mm01197002_m1) and Hypoxanthine phosphoribosyltransferase 1 (Hprt1, Mm03024075). Clusterin expression was normalized to Hprt1 using the $2^{(-\Delta\Delta Ct)}$ quantitation method.

Cell culture

Primary cultures of neonatal rat ventricular myocytes (NRVM) were prepared as described (Sapra et al. 2014). NRVM were treated with IGF1 (10 nM, Novozymes Biopharma AU Ltd, #Cm001, made at a concentration of 1 mg/ml in 10 mM HCl before dilution in media on the day of the experiment). Two independent isolated NRVM preparations were performed on different days and treated with IGF1 for 24 h and 48 h. At the end of the experiment, media were collected and stored for ELISA.

Clusterin ELISA

Clusterin concentration in conditioned media from NRVM was measured using a mouse Immunoassay Quantikine Clusterin ELISA kit (#MCLU00, R&D Systems Inc.)

Statistics

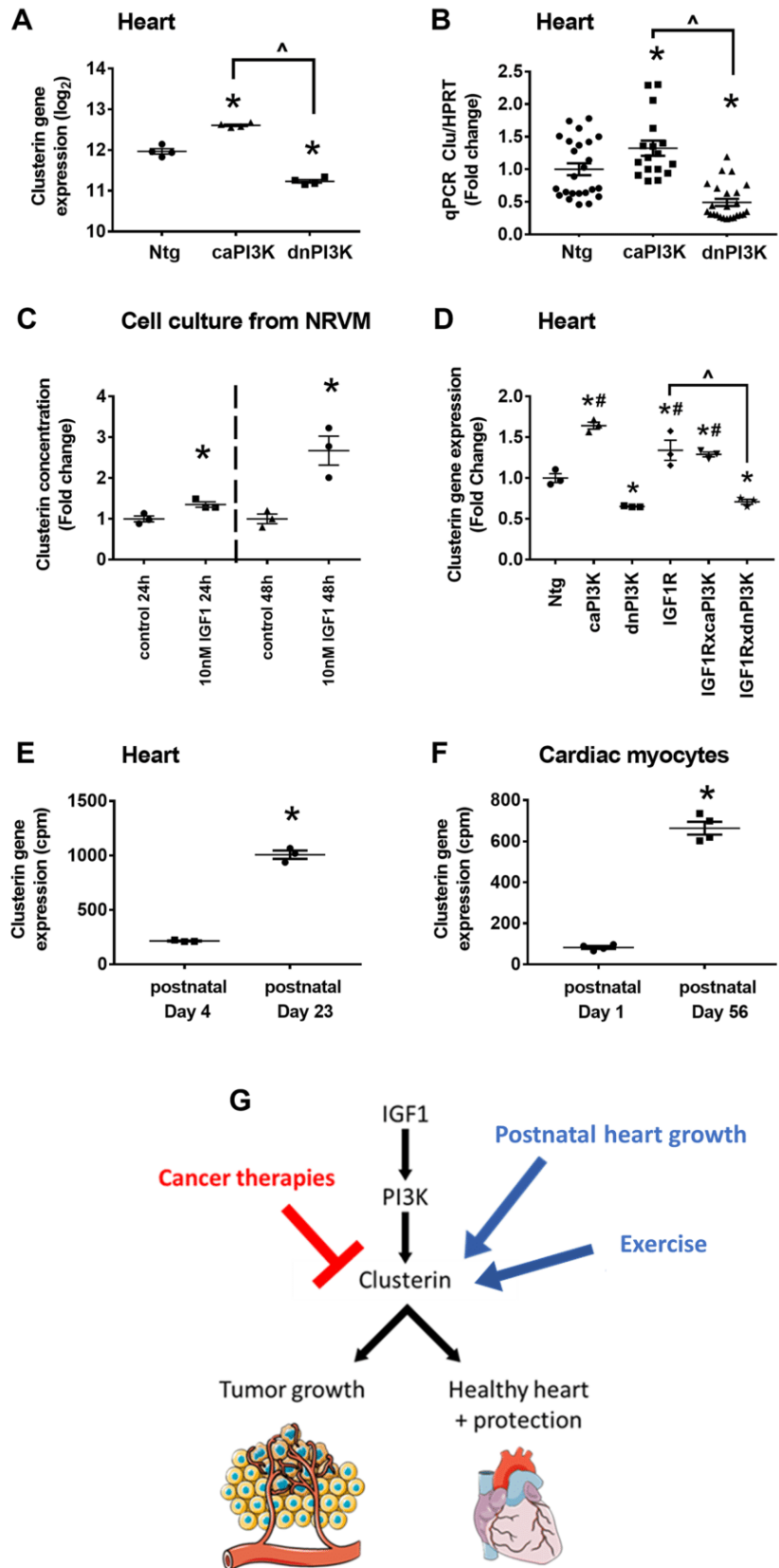
Results are displayed as mean \pm SEM. Graphpad Prism software v.7.03. was used for statistical analyses. Differences were assessed using one-way analysis followed by a Tukey's test. An unpaired *t* test was used when comparing two groups.

Results

The top-ranked gene from the microarray screen in hearts of PI3K transgenic mice was clusterin. Clusterin expression was increased in the hearts of caPI3K mice and reduced in dnPI3K mice (Fig. 1a). qPCR was performed in independent cohorts of mice to validate the microarray data. By qPCR, clusterin gene expression was elevated in hearts of caPI3K mice and decreased in hearts of dnPI3K mice (Fig. 1b).

To examine the regulation of clusterin in response to physiological and protective signaling further, we measured clusterin concentration in the media of NRVMs that had been treated with the growth factor, IGF1. IGF1 activates IGF1R and is upstream of the PI3K–Akt pathway. The concentration of secreted clusterin was higher in media from IGF1-treated NRVMs vs non-treated cells (Fig. 1c). Next, we reviewed a microarray data set from an independent study on hearts of caPI3K, dnPI3K, IGF1R, and double transgenic mice (IGF1RxcaPI3K, IGF1RxdnPI3K, Fig. 1d)(McMullen et al. 2004). Consistent with the earlier

Fig. 1 Clusterin is regulated by IGF1–PI3K signaling and during postnatal heart growth **a** Clusterin gene expression by microarray (GEO accession #:GSE7487), $n=4$ /group, $*P<0.0001$ vs Ntg; $^{\wedge}P<0.0001$. **b** Clusterin gene expression by qPCR, females $n=9–12$ /group and males $n=9–13$. $*P<0.05$ vs Ntg; $^{\wedge}P<0.0001$. Two data points greater than two standard deviations from the mean were excluded (i.e. one Ntg and one caPI3K). No difference was observed between males and females. **c** Each data point represents a single cell culture well ($*P<0.05$ vs control). The 24 h and 48 h treatments were performed on independent isolated NRVMs on different days. **d** Clusterin gene expression from an independent microarray data set. $n=3$ /group, $*P<0.05$ vs Ntg; $\#P<0.0001$ vs dnPI3K; $^{\wedge}P<0.0001$. **e** Clusterin gene expression from RNA-seq data set (GEO accession #:GSE119530), $n=3$ /group, $*P<0.0001$ vs postnatal day 4. **f** Clusterin gene expression from RNA-seq data set, (GEO accession #:GSE95755), $n=4$ /group, $*P<0.0001$ vs postnatal day 1. **g** Schematic depicting the regulation of clusterin by IGF1, PI3K, and links to healthy physiological heart growth and tumor growth



microarray data (Fig. 1a), clusterin gene expression was elevated in caPI3K hearts and reduced in dnPI3K hearts versus Ntg (Fig. 1d). Clusterin gene expression was also higher in hearts of IGF1R transgenic mice which display physiological heart growth, and are protected in cardiac stress settings (McMullen et al. 2004). Clusterin gene expression was comparably depressed in hearts of IGF1R-dnPI3K and dnPI3K hearts, suggesting clusterin is regulated by the IGF1R pathway in a PI3K-dependent manner.

To assess the regulation of clusterin in a different model of physiological heart growth, we mined gene expression data from mouse hearts and isolated cardiac myocytes from mouse hearts, during normal postnatal heart growth. On analyzing the data, clusterin gene expression was elevated during postnatal growth based on two independent data sets. Clusterin was increased approximately 4.6-fold in the mouse ventricle at postnatal day 23 vs postnatal day 4 (Fig. 1e); the mouse ventricle increased from approximately 10 mg to 70 mg between day 4 and 23 (Talman et al. 2018). Clusterin was also elevated approximately eightfold in mouse cardiac myocytes at postnatal day 56 vs postnatal day 1 (Fig. 1f) (Quaife-Ryan et al. 2017).

Discussion

To our knowledge, this is the first report to show that clusterin is regulated in a setting of IGF1–PI3K-induced physiological heart growth. Our results have important implications when considering clusterin, or any other candidate regulated in a setting of healthy heart growth, as a potential biomarker or drug target.

Previous work had shown increased cardiac and/or plasma clusterin in heart failure patients, elevated clusterin in rat hearts and plasma after MI, and increased secretion and expression of clusterin in isoproterenol-hypertrophied NRVM (isoproterenol used to mimic a pathological stimulus) (Koller et al. 2017; Turkieh et al. 2018). Consequently, it has been suggested that clusterin levels rise in a setting of cardiac stress and may be a predictor of premature death in patients with heart failure. This conclusion requires careful consideration given our current data and other previous work indicating that clusterin is also regulated in physiological and cardioprotective settings. First, our data indicate that clusterin expression is elevated in mice with physiological hypertrophy, i.e. caPI3K and IGF1R mice which are protected against cardiac disease. A limitation of the physiological transgenic mouse models (IGF1R and caPI3K) is that IGF1R expression and PI3K activity are chronically elevated in the heart. With genetic mouse models, there is the possibility for normal physiological processes to be disrupted. However, unlike other genetic models with > 50-fold increase in a protein/activity, our physiological genetic

models have altered activity/signaling within physiological ranges. For instance, PI3K activity is only elevated 6.5-fold in caPI3K mice and heart size is increased by about 20%. Furthermore, despite the chronic elevation in caPI3K or IGF1R, it is noteworthy that both the caPI3K and IGF1R cardiac-specific transgenic mice have normal or enhanced heart function (McMullen et al. 2004; Shioi et al. 2000). In addition, short-term IGF1 stimulation (24 h or 48 h) in cell culture led to increased release of clusterin from NRVM. Second, we also present data from two independent data sets to show that clusterin is increased in the heart during normal postnatal growth in mice (Quaife-Ryan et al. 2017; Talman et al. 2018). Third, another stimulus that induces physiological heart growth is exercise, and PI3K is a critical regulator of exercise-induced hypertrophy (McMullen et al. 2003). A recent study by Kurgan et al. (Kurgan et al. 2019) found an increased ratio of clusterin in blood spots from young healthy adult men 5 min and 1 h post-exercise (cycle ergometer) compared to pre-exercise levels (1.2–1.6-fold increase 5 min post-exercise; 1.3–1.7-fold increase 1 h post-exercise; $P < 0.01$ vs pre-exercise). Finally, clusterin has also been shown to provide protection against apoptosis in cardiomyocytes (Pereira et al. 2018; Jun et al. 2011). Collectively, this highlights the importance of taking caution when using multi-faceted proteins as biomarkers to identify disease states, as the very markers that are suggestive of disease can also be indicative of a protective state without pathology.

These findings are also important when considering targets for cancer therapeutics. Clusterin has been implicated in the pathogenesis and progression of numerous cancers (prostate, lung, breast, kidney, bladder and colon) (Shannan et al. 2006), and there have been 13 clinical trials with an antisense oligonucleotide that inhibits clusterin called Custirsen (<https://clinicaltrials.gov/ct2/results?cond=&term=custirsen&cntry=&state=&city=&dist=>). Phase 2 trials demonstrated a survival benefit in prostate cancer patients receiving Custirsen together with first-line chemotherapy. Despite two Phase 3 trials showing no survival benefit with Custirsen (Beer et al. 2017; Chi et al. 2017), research and reports proposing clusterin as a cancer target continue (Hoter et al. 2019; Wang et al. 2019).

Reduced PI3K in the mouse heart predisposes the heart to cardiac dysfunction, heart failure, and increased susceptibility to AF (Lin et al. 2010; McMullen et al. 2007; Pretorius et al. 2009). The results we present (Fig. 1a, b, d) provide evidence of a link between reduced cardiac PI3K activity and clusterin expression. Therapies that inhibit clusterin may, therefore, predispose individuals to cardiac vulnerability. This, in conjunction with the stress and long-term negative repercussions that chemotherapy and other cancer treatments have on cardiac function in an already compromised population, may pose an even greater risk

for cardiac damage during or following treatment. While no clear cardiac signal was identified in the two Phase 3 Custirsen trials, it is noteworthy there was a trend for atrial flutter and/or AF to be higher in the Custirsen arms (Beer et al. 2017; Chi et al. 2017). PI3K activity has also been shown to be lower in atrial appendages from patients with AF (Pretorius et al. 2009).

Here, we propose that IGF1R–PI3K signaling regulates clusterin (Fig. 1g). However, there is also evidence that the reverse can occur, i.e. clusterin modulating the PI3K–Akt pathway. In a cardiomyoblast cell line (H9c2 cells), it was reported that clusterin provided protection against oxidative stress (H₂O₂)-induced apoptosis. Oxidative stress was associated with a reduction in pAkt, and this was partially restored with clusterin. The clusterin-induced protection and pAkt was blunted with a PI3K inhibitor (LY294002), suggesting that clusterin can activate PI3K–Akt signaling (Jun et al. 2011). However LY294002 is not exclusively selective for PI3K (Gharbi et al. 2007). The interaction and regulation of clusterin and PI3K–Akt signaling is also complex in cancer cells. A study in the human cervical cancer cell line HeLa provided evidence that in a setting of cellular stress (serum starvation), secreted clusterin associated with IGF1, and inhibited IGF1 binding to IGF1R, which in turn reduced downstream PI3K–Akt signaling (Jo et al. 2008). In another study performed in a lung cancer cell line (A549 human non-small cell lung carcinoma), IGF1 treatment led to an increase in secreted clusterin which was required for activation of PI3K–Akt signaling (Ma and Bai 2012).

In conclusion, hundreds to thousands of candidate genes or proteins are proposed to represent novel drug targets and/or biomarkers for multiple diseases. Here, we highlight the complexity and precaution that should be taken when considering inhibition of a target that is regulated in a setting of physiological heart growth. Cardiotoxicity has emerged as one of the major reasons that drugs fail in phase 3 clinical trials or are later pulled from the market. Given we show that clusterin is regulated by the IGF1–PI3K pathway in the heart, and this pathway mediates physiological cardiac hypertrophy and cardioprotection (McMullen et al. 2003, 2007), caution is required considering clusterin as a biomarker for heart failure and as a cancer target (Fig. 1g). Mining pre-existing cardiac profiling data sets, may be a useful approach to assess whether regulating a novel drug target is likely to lead to cardiac toxicity.

Acknowledgements The authors wish to acknowledge Celeste MK Tai for assistance with figures, Esther Boey for assistance with cell culture. This work was supported by the Victorian Government's Operational Infrastructure Support Program. JRM is supported by a National Health and Medical Research Council Senior Research Fellowship (grant number 1078985). SBS is supported by a joint Baker Heart and Diabetes Institute-La Trobe University doctoral scholarship.

Compliance with ethical standards

Conflict of interest The authors declare that they have no conflict of interest.

References

- Beer TM, Hotte SJ, Saad F, Alekseev B, Matveev V, Flechon A, Gravis G, Joly F, Chi KN, Malik Z, Blumenstein B, Stewart PS, Jacobs CA, Fizazi K (2017) Custirsen (OGX-011) combined with cabazitaxel and prednisone versus cabazitaxel and prednisone alone in patients with metastatic castration-resistant prostate cancer previously treated with docetaxel (AFFINITY): a randomised, open-label, international, phase 3 trial. *Lancet Oncol* 18(11):1532–1542. [https://doi.org/10.1016/S1470-2045\(17\)30605-8](https://doi.org/10.1016/S1470-2045(17)30605-8)
- Bernardo BC, Gao XM, Winbanks CE, Boey EJ, Tham YK, Kiriazis H, Gregorevic P, Obad S, Kauppinen S, Du XJ, Lin RC, McMullen JR (2012) Therapeutic inhibition of the miR-34 family attenuates pathological cardiac remodeling and improves heart function. *Proc Natl Acad Sci USA* 109(43):17615–17620. <https://doi.org/10.1073/pnas.1206432109>
- Bernardo BC, Nguyen SS, Winbanks CE, Gao XM, Boey EJ, Tham YK, Kiriazis H, Ooi JY, Porrello ER, Igoor S, Thomas CJ, Gregorevic P, Lin RC, Du XJ, McMullen JR (2014) Therapeutic silencing of miR-652 restores heart function and attenuates adverse remodeling in a setting of established pathological hypertrophy. *FASEB J* 28(12):5097–5110. <https://doi.org/10.1096/fj.14-253856>
- Bernardo BC, Nguyen SS, Gao XM, Tham YK, Ooi JY, Patterson NL, Kiriazis H, Su Y, Thomas CJ, Lin RC, Du XJ, McMullen JR (2016) Inhibition of miR-154 protects against cardiac dysfunction and fibrosis in a mouse model of pressure overload. *Sci Rep* 6:22442. <https://doi.org/10.1038/srep22442>
- Bernardo BC, Weeks KL, Pongsukwechkul T, Gao X, Kiriazis H, Cemerlang N, Boey EJH, Tham YK, Johnson CJ, Qian H, Du XJ, Gregorevic P, McMullen JR (2018) Gene delivery of medium chain acyl-coenzyme A dehydrogenase induces physiological cardiac hypertrophy and protects against pathological remodeling. *Clin Sci (Lond)* 132(3):381–397. <https://doi.org/10.1042/CS20171269>
- Chi KN, Higano CS, Blumenstein B, Ferrero JM, Reeves J, Feyerabend S, Gravis G, Merseburger AS, Stenzl A, Bergman AM, Mukherjee SD, Zaleski P, Saad F, Jacobs C, Gleave M, de Bono JS (2017) Custirsen in combination with docetaxel and prednisone for patients with metastatic castration-resistant prostate cancer (SYNERGY trial): a phase 3, multicentre, open-label, randomised trial. *Lancet Oncol* 18(4):473–485. [https://doi.org/10.1016/S1470-2045\(17\)30168-7](https://doi.org/10.1016/S1470-2045(17)30168-7)
- Gharbi SI, Zvelebil MJ, Shuttleworth SJ, Hancox T, Saghri N, Timms JF, Waterfield MD (2007) Exploring the specificity of the PI3K family inhibitor LY294002. *Biochem J* 404(1):15–21. <https://doi.org/10.1042/BJ20061489>
- Hoter A, Rizk S, Naim HY (2019) The multiple roles and therapeutic potential of molecular chaperones in prostate cancer. *Cancers (Basel)*. <https://doi.org/10.3390/cancers11081194>
- Jo H, Jia Y, Subramanian KK, Hattori H, Luo HR (2008) Cancer cell-derived clusterin modulates the phosphatidylinositol 3'-kinase-Akt pathway through attenuation of insulin-like growth factor 1 during serum deprivation. *Mol Cell Biol* 28(13):4285–4299. <https://doi.org/10.1128/MCB.01240-07>
- Jun HO, Kim DH, Lee SW, Lee HS, Seo JH, Kim JH, Kim JH, Yu YS, Min BH, Kim KW (2011) Clusterin protects H9c2 cardiomyocytes from oxidative stress-induced apoptosis via Akt/

Chapter 6

General discussion and concluding
remarks

6.1 Summary of key findings

Heart failure (HF) is the final clinical presentation of a variety of cardiovascular diseases and is a leading cause of morbidity and mortality¹. Limited treatment options are available and current therapeutic interventions largely aim to delay progression and manage symptoms. As such, an urgent need for the development of novel therapeutics to improve outcomes in patients with HF is apparent.

PI3K is a key component of the IGF1-PI3K signalling pathway and has been demonstrated to be a master regulator of exercise-induced physiological cardiac hypertrophy², and its elevation protective in settings of cardiac disease^{3,4}. Aerobic exercise is one of the few interventions that is both safe and effective in improving outcomes following a diagnosis of stable HF⁵⁻⁷, but the physically debilitating nature of HF in addition to a lack of patient adherence can limit the capacity for exercise to be used as a form of treatment. Therapeutic strategies that aim to recapitulate the benefits of exercise on the heart through activation of PI3K are therefore of significant interest. In recent years, gene therapy has gained attention as a promising therapeutic avenue for HF treatment, with numerous studies reporting positive effects on cardiac function in animal models⁸. Given the aforementioned prospects of enhancing PI3K as a therapeutic intervention, a gene therapy aimed at increasing PI3K activity offers a promising approach for improving outcomes in patients with HF.

This thesis took steps in paving a translational bridge between basic research and therapeutic development by exploring the prospect of a PI3K-based therapy for the treatment of HF. Key studies and findings from each chapter are presented in Figure 6.1 and include:

- 1) improving current knowledge and understanding of the role of the PI3K signalling pathway in the heart by generating new PI3K transgenic models to study the safety profile of substantial inhibition and activation of PI3K (Chapter 2);
- 2) developing innovative techniques and tools with the potential to contribute to advances in the field of AAV gene therapy (Chapters 3 and 4);
- 3) trialling AAV-mediated PI3K gene therapies in healthy and HF animal models (Chapter 4); and
- 4) identifying PI3K-regulated targets which may lead to cardiotoxicity in the clinic if they are inhibited (Chapter 5).

Basic to Preclinical Research Pipeline

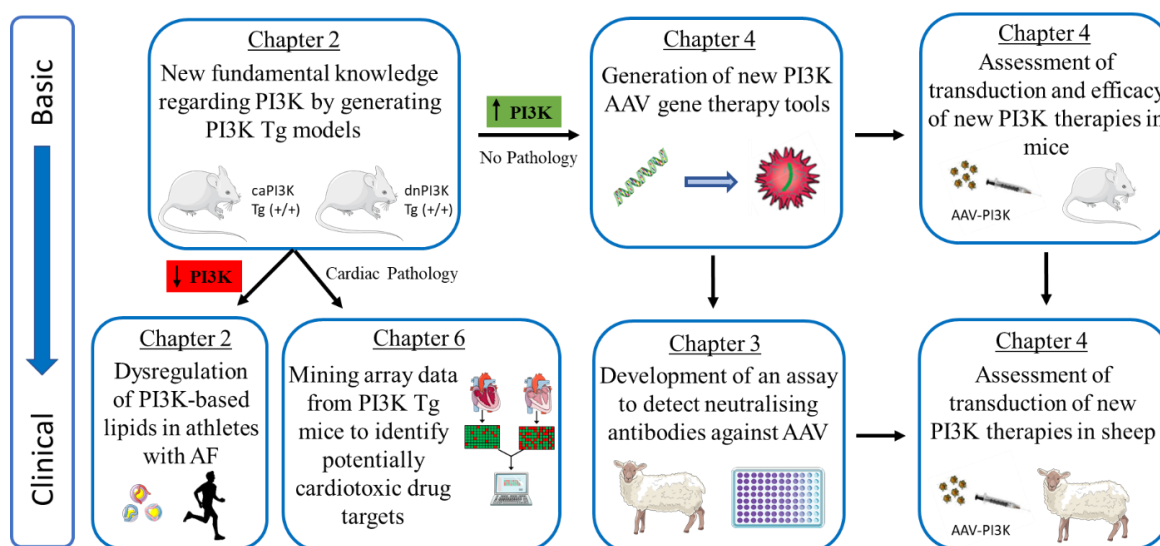


Figure 6.1 A schematic diagram summarising the core components and key findings of this thesis, and outlining how each chapter interconnects. A pipeline demonstrating the generation of basic research to preclinical/clinical outcomes within this thesis is presented.

6.2 Advancing knowledge of the PI3K signalling pathway and its protective role in the heart.

Chapter 2 comprised an in-depth interrogation of how changes in cardiac PI3K activity can alter cardiac physiology. Given how the dosage or degree of activation of any signalling pathway can significantly affect the phenotype, a comprehensive investigation is warranted in the development of any agent that acts to enhance or disrupt endogenous molecular signalling. This is particularly relevant in the context of targeting pathways to mimic the protective effects of exercise given the J-shaped relationship between exercise volume and intensity with cardiac risk. While it is well recognised that regular aerobic exercise reduces cardiac risk⁹, cardiac abnormalities and arrhythmias are observed in a subset of elite athletes undertaking extreme/endurance exercise training^{10, 11}. Since PI3K is a critical regulator of exercise-induced hypertrophy, it is important to investigate if cardiac abnormalities in athletes are potentially attributed to enhanced PI3K activity. In a similar vein, investigating the impact of substantially reduced PI3K activity on normal cardiac function is also important in the context of numerous cancer therapies designed to inhibit PI3K signalling and tumour growth. This chapter investigated firstly if a dose-dependent relationship exists between increased PI3K activity and adaptive physiological hypertrophy. Secondly, whether increases in PI3K activity in mice leads to cardiac

pathology and arrhythmia, as seen in some athletes undertaking extreme endurance exercise, and thirdly if reduced PI3K in transgenic mice is associated with cardiac pathology, dysfunction, arrhythmia or atrial thrombi.

Transgenic mice with varying degrees of cardiac PI3K activity were generated to assess these parameters (caPI3K & dnPI3K, heterozygote Tg(+/-) and homozygote Tg(+/+)). Given the known physiological differences between male and females, both sexes were evaluated independently. Increasing PI3K activity was associated with increasing heart weight in a dose-dependent manner in the absence of cardiac dysfunction, arrhythmia, fibrosis or atrial pathology. In contrast, reduced PI3K in homozygote dnPI3K Tg(+/+) was associated with clear evidence of cardiac dysfunction and fibrosis, as well as atrial enlargement and thrombi in a subset of mice.

Unexpectedly, the increase in heart weight and PI3K activity in caPI3K Tg(+/+) mice compared to caPI3K Tg (+/-) mice did not correspond to an increase in the phosphorylation of Akt in the heart. This observation and additional findings indicated that a component of PI3K-induced cardiac hypertrophy occurs independent of Akt phosphorylation, a finding not previously described in the Akt literature. Expression of calsequestrin-1 was found to be increased and decreased in a dose-dependent manner in the caPI3K and dnPI3K models, respectively, and represents a potential new mediator of PI3K-induced hypertrophy.

Chapter 2 also demonstrated that reduced PI3K leads to cardiac dysfunction and atrial pathology. This finding led to the hypothesis that extreme endurance exercise may be associated with defective PI3K signalling rather than increased PI3K signalling. This was assessed by mining data from a mouse model of extreme exercise training¹², and assessing lipid profiles of plasma samples from veteran athletes with and without AF. In endurance-trained mice there was evidence of dysregulation of the PI3K pathway, and in athletes with AF we identified dysregulation of PIP1, LPI and GM3 lipids (regulators within the PI3K signalling network). These lipids could be explored as markers to screen athletes who may be at risk of developing AF. There is also evidence to suggest that decreased PI3K could contribute to the association between physical inactivity and increased cardiovascular risk. Increased PI3K was able to restore abnormalities in the hearts of rats with low exercise capacity¹³.

Overall, these findings demonstrate the existence of a dose-dependent relationship between physiological hypertrophy and PI3K activity, with no evidence that elevated PI3K directly contributes to cardiac dysfunction and pathology. These findings strengthen

the rationale for pursuing a PI3K-based therapy for the treatment of HF as they demonstrate that such an approach is unlikely to have undesirable or adverse consequences to the heart.

6.3 Translation of fundamental PI3K cardiac research into therapeutic design and development

Having established the safety and efficacy of enhanced cardiac PI3K activity in mice, the preliminary ambition of this component of the thesis was to optimise a PI3K-based therapy to be trialled in healthy and cardiac disease mouse models of mice, and subsequently sheep. A previous study in my laboratory had administered the full-length caPI3K transgene to mice with established cardiac dysfunction due to chronic pressure overload induced by aortic banding⁴. They employed an AAV6 vector to administer caPI3K, and observed improved cardiac function in the mice 10 weeks post-AAV administration. Although this was a successful outcome, modifications to the initial AAV gene therapy construct were considered necessary to improve the clinical viability of the therapy. Furthermore translating from small to large animals is a crucial stepping-stone between the laboratory and the clinic given the physiological resemblance shared between large mammals and humans¹⁴. As such, initial plans involved trialling PI3K-based AAV constructs in healthy and heart disease models of sheep. Due to Melbourne, Australia recording the world's longest lockdown due to the COVID-19 pandemic, facilities available for large animal testing were unavailable for the last two years of my doctoral studies, and the majority of sheep studies were unable to proceed. Despite this, some initial sheep studies (prior to the pandemic), and a neutralising antibody method relevant to future sheep studies are presented.

A primary consideration that needs to be addressed when trialling AAV gene therapies on large animals or humans is the presence of neutralising antibodies (NAbs) against AAV. Multiple reports have found that a range of large animals and humans can harbour neutralising antibodies against many AAV serotypes^{15, 16}. This is problematic in a research setting because NAbs against AAV will prevent or severely diminish tissue transduction. Not only could this confound the results, but also both AAV generation and large animal/clinical trials come with substantial price tags, and therefore the potential loss of time, AAV and animals/housing due to NAbs is crucial to address. **Chapter 1 part 2** discusses the various methods in development to circumvent the challenges of NAbs, however performing preliminary screening of animals and patients for NAbs is

currently the most effective approach. **Chapter 3** addresses this through the development of an assay and comprehensive protocol for the detection of NABs against AAV6. The described assay evaluates the degree of AAV6 neutralisation in a given volume of serum through a colorimetric reaction that reflects the degree of *in vitro* viral transduction. The assay is based on the chromogenic reaction between the enzyme alkaline phosphatase and NBT/BCIP. The general premise of the assay was to determine the degree of NABs in a given animal by incubating a sample of serum in serial dilutions with a recombinant AAV that expresses an alkaline phosphatase reporter gene. Cells are infected with the serum/virus mixture and following addition of the NBT/BCIP substrate, the degree in which the expression of the reporter gene is inhibited reflects the amount of neutralising elements in a sample. NAb assays commonly employ light based reporter genes such as GFP or luciferase, however the development of this colorimetric assay proved to be advantageous due to it being cost effective, time efficient, and easy to set up without the need for specialised technical skills or equipment. Following development of this assay we were able to validate its efficacy using a monoclonal antibody against AAV6. The assay proved to be a valuable tool in the sheep studies described in **Chapter 4** and was further validated through comparison of the assay titers in sheep before and after receiving a direct cardiac injection of AAV.

The primary objective of **Chapter 4** was developing clinically viable therapeutic tools that could replicate some of the benefits of exercise by targeting and enhancing the PI3K signalling pathway. Novel constructs were developed with the intention of building upon and optimising aforementioned vector (AAV6-CMV-caPI3K) that showed promising results⁴. Key factors that were addressed included reducing costs of drug development by reducing the PI3K construct size (leading to significant improvements in AAV yield); improving cardiac specificity by employing a cardiac specific cTnT promoter; and improving transgene expression by adding an IVS2 enhancer element. An optimised PI3K construct was evaluated in healthy mice, an I/R injury HF mouse model, and preliminary assessment of the efficacy of PI3K constructs was trialled in healthy sheep to evaluate the translational potential. Use of the cTnT promoter provided cardiac specific expression following administration of AAV6 and we report preliminary data that IVS2 can enhance cardiac expression of AAV6 delivered constructs.

Due to the size of the caPI3K gene approaching the packaging capacity limit of AAV, production of this vector has proven to be inefficient and low yielding. However a substantially smaller PI3K(p85) fragment, iSH2, has previously been demonstrated to be

capable of binding to the p110 α catalytic subunit of PI3K and generating PI3K activity in cultured cells¹⁷. iSH2 was able to activate PI3K signalling *in vivo* in the rodent and ovine heart. This demonstrated that fragments of larger genes can still serve functional purposes, and in this study drastically improved the efficiency of AAV6 vector production and reduced the corresponding cost compared to an AAV6 containing a full length caPI3K transgene. Additionally, the AAV6 containing the full-length caPI3K transgene was unable to transduce the sheep heart, whereas administration of AAV6 containing iSH2 consistently provided a high degree of cardiac expression. Furthermore, the addition of IVS2 led to increased cardiac expression of AAV6-cTnT-iSH2 in an ovine model. Introducing AAV-mediated PI3K expression and activity into the hearts of large animals using iSH2 demonstrates its translational potential given the physiological similarities of the sheep and human heart^{8, 18}.

In contrast to previous reports using the AAV6-CMV-caPI3K construct, administering an AAV6 containing iSH2 did not induce physiological cardiac hypertrophy in healthy mice.⁴ However, we did observe iSH2-generated PI3K activity and a trend towards an increase in the phosphorylation of Akt ($p=0.08$), a downstream target of PI3K. Since PI3K activity and phosphorylation of Akt are cardioprotective^{3, 4, 19}, and our primary objective was to provide protection in a setting of cardiac injury, we proceeded to administer our AAV6-cTnT-IVS2-iSH2 construct to a larger cohort of mice with established cardiac damage due to a surgical myocardial ischemia/reperfusion (I/R) injury. Three months after I/R injury, phosphorylation of Akt was significantly increased in non-infarcted cardiac tissue from mice receiving AAV6 containing iSH2 compared to saline controls. Unexpectedly, this increase was not associated with improvements in cardiac function nor fibrosis. The lack of functional improvements in the I/R injury cohort may be attributed to several factors. The time of administration may have been too late for this type of cardiac injury. Given transduction of AAV has been demonstrated to peak 3-weeks after administration²⁰, the extent of cardiac damage from I/R may have been irreversible by the time PI3K was sufficiently activated. Administering the AAV at an earlier time point may therefore provide improved outcomes. The extent of Akt phosphorylation may have also been inadequate to significantly improve function. Although we observed a two-fold increase in phosphorylation of Akt following administration of AAV6-cTnT-IVS2-iSH2, the male caPI3K transgenic mouse models described in **Chapter 2** both exhibited close to a four-fold increase in Akt phosphorylation compared to their non-transgenic counterparts. Additionally, we observed a modest increase in spleen and kidney weights in mice that received AAV6

(AAV6-Control and AAV6-cTnT-IVS2-iSH2) compared to saline within the I/R study. This could reflect a systemic inflammatory response, suggesting 2×10^{12} vg may have been too high a dose in a setting of I/R injury, and potentially confounded the results. **Chapter 4** demonstrated the efficacy of a cardiomyocyte specific promoter, an enhancer element and the potential for AAV6-mediated gene therapy using a truncated PI3K transgene to activate PI3K signalling and cardioprotective downstream targets in both mice and sheep. Further optimisations may facilitate improvements in functional parameters in a setting of cardiac disease.

6.4 Detection of drug targets likely to cause cardiotoxicity using cardiac profiling data

Chapter 5 of this thesis demonstrated the potential value of mining profiling datasets as a preliminary process for identifying potential biomarkers of disease, or determining if altering a molecular target is likely to have deleterious side effects when developing novel therapeutics. This concept is showcased by demonstrating that the IGF1R-PI3K signalling pathway regulates clusterin, a molecular target that has been inhibited in numerous trials as a therapeutic approach for treating cancer²¹, and has been suggested as a predictor of premature death in patients with HF^{22, 23}. Gene microarray data sets from the hearts of dnPI3K Tg(+/-) and caPI3K Tg(+/-) mice described in **Chapter 2** were mined and a ranking system generated based on the inverse cardiac expression between the two mouse models with increased or decreased PI3K activity. Clusterin was demonstrated to be the most differentially regulated target in the hearts between the models of increased and decreased PI3K activity, suggesting a relationship with PI3K signalling. Subsequent analysis demonstrated that expression of clusterin was elevated during normal mouse postnatal growth. Moreover, *in vitro* treatment of neonatal rat ventricular cardiomyocytes with IGF1 led to increased secretion of clusterin. Given the importance of PI3K signalling in cardiac function and physiological growth, these findings highlight the potential cardiotoxic implications that could arise from therapies that inhibit signalling pathways responsible for cardioprotection. The detrimental cardiac phenotype identified in the homozygote dnPI3K Tg(+/+) model in **Chapter 2** also supports this conclusion.

6.5 Concluding remarks and future perspectives

In summary, HF is a debilitating and chronic disease with limited treatment options currently available. The potential development of cardiomyocyte-specific therapies represents a novel and innovative approach for its treatment. PI3K regulates physiological cardiac hypertrophy and increased cardiac PI3K activity is protective in a setting of HF. Development and optimisation of PI3K based gene therapies offers a therapeutic avenue for the treatment of HF. The use of AAV vectors for the transfer of genetic material continues to demonstrate popularity, safety and relevance in a clinical setting. In 2010 five AAV-based clinical trials were initiated and this has increased to 28 in 2019. The vast majority of the trials have targeted organ systems that can be accessed without surgical intervention, such as the CNS, eyes, liver or skeletal muscle²⁴. The implementation of tissue specific promoters is facilitating the capability of targeting organ systems such as the heart that are otherwise very challenging to access. Numerous challenges still need to be addressed to improve AAV technology: establishing and standardising efficacious methods of administration to inaccessible organ systems, improving transduction efficiency of target organs, reducing manufacturing cost by improving production yields and lastly performing life-long follow up studies.

In conclusion this research has 1) provided further knowledge and understanding of mechanistic properties of the IGF1-PI3K signalling pathway; 2) validated the safety and efficacy of PI3K as a therapeutic target; 3) highlighted the importance of PI3K signalling during drug and biomarker development; 4) led to the development of innovative AAV gene therapy techniques and tools which may facilitate further advances in the field of cardiac AAV gene therapy; and 5) trialled AAV-mediated PI3K gene therapies in healthy and HF animal models. The AAV-mediated truncated PI3K therapy did not lead to an improvement in cardiac function in a setting of myocardial ischemia/reperfusion injury but activation of PI3K and elevated phosphorylation of Akt was indicative of cardioprotective signalling, providing merit for additional evaluation. Future studies may benefit from using a lower dose of AAV, assessing a different model of cardiac injury, and administering the AAV at an earlier time point. Furthermore, considering cardiac function is governed by a multitude of signalling pathways, an approach that can simultaneously enhance PI3K signalling in addition to other protective pathways using a dual-therapy approach may confer greater functional improvements and demonstrate a promising approach for the treatment of heart failure.

6.6 References

1. Savarese G, Lund LH. Global Public Health Burden of Heart Failure. *Card Fail Rev.* Apr 2017;3(1):7-11. doi:10.15420/cfr.2016:25:2
2. McMullen JR, Shioi T, Zhang L, et al. Phosphoinositide 3-kinase(p110alpha) plays a critical role for the induction of physiological, but not pathological, cardiac hypertrophy. *Proc Natl Acad Sci U S A.* Oct 14 2003;100(21):12355-60. doi:10.1073/pnas.1934654100
3. McMullen JR, Amirahmadi F, Woodcock EA, et al. Protective effects of exercise and phosphoinositide 3-kinase(p110alpha) signaling in dilated and hypertrophic cardiomyopathy. *Proc Natl Acad Sci U S A.* Jan 9 2007;104(2):612-7. doi:10.1073/pnas.0606663104
4. Weeks KL, Gao X, Du XJ, et al. Phosphoinositide 3-kinase p110alpha is a master regulator of exercise-induced cardioprotection and PI3K gene therapy rescues cardiac dysfunction. *Circ Heart Fail.* Jul 1 2012;5(4):523-34. doi:10.1161/CIRCHEARTFAILURE.112.966622
5. Wisloff U, Stoylen A, Loennechen JP, et al. Superior cardiovascular effect of aerobic interval training versus moderate continuous training in heart failure patients: a randomized study. *Circulation.* Jun 19 2007;115(24):3086-94. doi:10.1161/CIRCULATIONAHA.106.675041
6. Giannuzzi P, Temporelli PL, Corra U, Tavazzi L, Group E-CS. Antiremodeling effect of long-term exercise training in patients with stable chronic heart failure: results of the Exercise in Left Ventricular Dysfunction and Chronic Heart Failure (ELVD-CHF) Trial. *Circulation.* Aug 5 2003;108(5):554-9. doi:10.1161/01.CIR.0000081780.38477.FA
7. O'Connor CM, Whellan DJ, Lee KL, et al. Efficacy and safety of exercise training in patients with chronic heart failure: HF-ACTION randomized controlled trial. *JAMA.* Apr 8 2009;301(14):1439-50. doi:10.1001/jama.2009.454
8. Bass-Stringer S, Bernardo BC, May CN, Thomas CJ, Weeks KL, McMullen JR. Adeno-Associated Virus Gene Therapy: Translational Progress and Future Prospects in the Treatment of Heart Failure. *Heart Lung Circ.* Nov 2018;27(11):1285-1300. doi:10.1016/j.hlc.2018.03.005
9. Kujala UM, Kaprio J, Sarna S, Koskenvuo M. Relationship of leisure-time physical activity and mortality: the Finnish twin cohort. *JAMA.* Feb 11 1998;279(6):440-4. doi:10.1001/jama.279.6.440
10. Galanti G, Stefani L, Mascherini G, Di Tante V, Toncelli L. Left ventricular remodeling and the athlete's heart, irrespective of quality load training. *Cardiovasc Ultrasound.* Nov 17 2016;14(1):46. doi:10.1186/s12947-016-0088-x
11. Buckley BJR, Lip GYH, Thijssen DHJ. The counterintuitive role of exercise in the prevention and cause of atrial fibrillation. *Am J Physiol Heart Circ Physiol.* Nov 1 2020;319(5):H1051-H1058. doi:10.1152/ajpheart.00509.2020
12. Aschar-Sobbi R, Izaddoustdar F, Korogyi AS, et al. Increased atrial arrhythmia susceptibility induced by intense endurance exercise in mice requires TNFalpha. *Nat Commun.* Jan 19 2015;6:6018. doi:10.1038/ncomms7018
13. Moreira JBN, Alves MNM, Britton SL, Koch LG, Wisloff U, Bye A. Pi3k modulates cardiomyocyte phenotype in rats selected for low aerobic capacity. *European Heart Journal.* 2013;34(suppl_1)doi:10.1093/eurheartj/eh309.P4202
14. Entrican G, Wattedgedera SR, Griffiths DJ. Exploiting ovine immunology to improve the relevance of biomedical models. *Mol Immunol.* Jul 2015;66(1):68-77. doi:10.1016/j.molimm.2014.09.002
15. Rapti K, Louis-Jeune V, Kohlbrenner E, et al. Neutralizing antibodies against AAV serotypes 1, 2, 6, and 9 in sera of commonly used animal models. *Mol Ther.* Jan 2012;20(1):73-83. doi:10.1038/mt.2011.177
16. Tellez J, Van Vliet K, Tseng YS, et al. Characterization of naturally-occurring humoral immunity to AAV in sheep. *PLoS One.* 2013;8(9):e75142. doi:10.1371/journal.pone.0075142
17. Klippel A, Escobedo JA, Hu Q, Williams LT. A region of the 85-kilodalton (kDa) subunit of phosphatidylinositol 3-kinase binds the 110-kDa catalytic subunit in vivo. *Mol Cell Biol.* Sep 1993;13(9):5560-6. doi:10.1128/mcb.13.9.5560-5566.1993
18. Camacho P, Fan H, Liu Z, He JQ. Large Mammalian Animal Models of Heart Disease. *J Cardiovasc Dev Dis.* Oct 5 2016;3(4)doi:10.3390/jcdd3040030

19. Bass-Stringer S, Tai CMK, McMullen JR. IGF1-PI3K-induced physiological cardiac hypertrophy: Implications for new heart failure therapies, biomarkers, and predicting cardiotoxicity. *J Sport Health Sci*. Nov 24 2020;doi:10.1016/j.jshs.2020.11.009
20. Zincarelli C, Soltys S, Rengo G, Koch WJ, Rabinowitz JE. Comparative cardiac gene delivery of adeno-associated virus serotypes 1-9 reveals that AAV6 mediates the most efficient transduction in mouse heart. *Clin Transl Sci*. Jun 2010;3(3):81-9. doi:10.1111/j.1752-8062.2010.00190.x
21. Shannan B, Seifert M, Leskov K, et al. Challenge and promise: roles for clusterin in pathogenesis, progression and therapy of cancer. *Cell Death Differ*. Jan 2006;13(1):12-9. doi:10.1038/sj.cdd.4401779
22. Turkieh A, Fertin M, Bouvet M, et al. Expression and Implication of Clusterin in Left Ventricular Remodeling After Myocardial Infarction. *Circ Heart Fail*. Jun 2018;11(6):e004838. doi:10.1161/CIRCHEARTFAILURE.117.004838
23. Koller L, Richter B, Winter MP, et al. Clusterin/apolipoprotein J is independently associated with survival in patients with chronic heart failure. *J Clin Lipidol*. Jan - Feb 2017;11(1):178-184. doi:10.1016/j.jacl.2016.11.009
24. Kuzmin DA, Shutova MV, Johnston NR, et al. The clinical landscape for AAV gene therapies. *Nat Rev Drug Discov*. Mar 2021;20(3):173-174. doi:10.1038/d41573-021-00017-7